Computational study of silicon clusters doped by some main group elements

Nguyen Minh Tam

Promotor:

Prof. Dr. Minh Tho Nguyen

Members of the Examination Committee:

Prof. Dr. Shaun Carl
Prof. Dr. Marc Hendrickx
Prof. Dr. Ewald Janssens
Prof. Dr. Minh Tho Nguyen
Prof. Dr. Szczepan Roszak
Prof. Dr. Thierry Verbiest

Dissertation presented in partial fulfilment of the requirements for the degree of Doctor of Science in Chemistry

September 2014

ISBN 978-90-8649-744-7
D/2014/10.705/52

To the memory of my grandmother,
For my father, my mother, and my sister

"You do not really understand something unless you can explain it to your grandmother."

– Albert Einstein –

Acknowledgments

First and foremost, I offer my utmost gratitude to my promotor, professor Minh Tho Nguyen. His guidance, support and encouragement, that I will never forget, helped me overcome a lot of difficulties not only in my study but also in my life through over the years in Leuven.

I would like to thank professor Peter Lievens and his coworkers, especially professor Ewald Janssens, who provided me with the valuable knowledge of experimental aspects of clusters. I am grateful for their critical reading of my manuscripts. I also thank Jorg de Haeck, Yejun Li for their fruitful collaboration.

I am especially thankful to the jury members: Prof. Thierry Verbiest, Prof. Marc Hendrickx, Prof. Shaun Carl, Prof. Szczepan Roszak, who have been very affable and generous with their time, ideas, and advices. I also thank Prof. Marc Hendrickx for his kindly help to translate the "Samenvatting".

I would like to thank Mrs. Rita Jungbluth and Dr. Hans Vansweevelt for their kindly help.

I am indebted to all my colleagues in Divison of Quantum Chemistry for their very fruitful cooperation and also for a pleasant atmosphere in the office. Especially, I am grateful to Dr. Vu Thi Ngan and Dr. Truong Ba Tai. Without their valuable help and guidance, I would finish neither my study nor my thesis. I also thank Dr. Tran Van Tan, Phung Manh Quan, Nguyen Thi Huyen for helpful discussion.

I am thankful to chị Vu Thi Ngan, anh Nguyen Tien Trung, chị Ho Phuong Hien, anh Ngo Tuan Cuong, chị Nguyen Bich Ngan, anh Nguyen Vinh Son, chị Nguyen Le Dung, anh Pham Vu Nhat, Le Hai Thuy, Nguyen Thi Huyen, Nguyen Thanh Tung, Phan Nguyen Trang, anh Dinh Thanh Viet, chị Mai Nga, Mai Tuan Dat, Pham Duc Hung, anh Phan Thanh Hai for many parties, pleasure trips and other events they let me enjoyed.

I will never forget the frenetic football matches and cheery glasses of beer after those with my friends in VINAKUL football team. I hope our team will achieve more successes in future.

I am indebted to the KU Leuven for the financial support through a GOA scholarship. I am grateful to the Institute for Computational Science and Technology at Ho Chi Minh city (ICST) for giving a long leave of absence. I thank my kindly

colleagues, especially Dr. Pham Ho My Phuong, Pham Quoc Buu, Pham Tan Hung, Duong Van Long for always welcoming me back.

I would like to thank my beloved parents and my young sister, who have been giving me their endless love and great care to me, that helped me overcome the discouragement to continue my way. I am grateful to Mrs. Le Mai Phuong for her care in Leuven.

Finally, I would like to thank everybody who helped and supported me complete this thesis as well as express my apologies that I could not mention personally one by one here.

List of abbreviations and acronyms

AIE	Adiabatic ionization energy
AO	Atomic orbital
CCSD(T)	Coupled clusters method including singly and doubly excited configurations and perturbative corrections for triple excitations
CBS	Complete basis set
DFT	Density functional theory
DOS	Density of states
EA	Electron affinity
ELI-D	Electron localizability indicator
ELF	Electron localization function
HOMO	Highest occupied molecular orbital
IE	Ionization energy
JSM	Jellium electron shell model
LUMO	Lowest unoccupied molecular orbital
MO	Molecular orbital
NBO	Natural bond orbital
PIE	Photo-ionization efficiency
TAE	Total atomization energy
VIE	Vertical ionization energy
ZPE	Zero-point energy
$\Delta_f H$	Heat of formation

List of publications

Used in this thesis

1. *Singly and doubly lithium doped silicon clusters: Geometrical and electronic structures and ionization energies.*
   N. M. Tam, V. T. Ngan, J. de Haeck, S. Bhattacharyya, H. T. Le, E. Janssens, P. Lievens and M. T. Nguyen.
   Journal of Chemical Physics **2012**, *136,* 024301.

2. *Thermochemical parameters and growth mechanism of the boron-doped silicon clusters, Si_nB^q with n = 1 – 10 and q = -1, 0, +1.*
   N. M. Tam, T. B. Tai and M. T. Nguyen.
   Journal Physical Chemistry C **2012**, *116*, 20086.

3. *Structure, thermochemical properties, and growth sequence of aluminum-doped silicon clusters Si_nAl_m (n = 1−11, m = 1−2) and their anions*.
   N. M. Tam, T. B. Tai, V. T. Ngan and M. T. Nguyen.
   Journal of Physical Chemistry A **2013**, *117*, 6867.

4. *Heats of formation and thermochemical parameters of small silicon clusters and their ions*, *$Si_n^{+/0/-}$ with n = 2 – 13*.
   N. M. Tam and M. T. Nguyen.
   Chemical Physics Letters **2013**, *584*, 147.

5. *Planar tetracoordinate carbon stabilized by heavier congener cages: The Si_9C and Ge_9C clusters*.
   N. M. Tam, V. T. Ngan and M. T. Nguyen.
   Chemical Physics Letters **2014**, *595-596*, 272.

6. *Ring Currents in Silicon Tetramer (Si_4, Si_4^{2+}) and Planar Tetracoordinate Carbon Doped Cluster Si_4C^{2+}: σ versus π Aromaticity.*
   N. M. Tam, H. T. Pham and M. T. Nguyen.
   Chemical Physics Letters, **2014**, *608*, 255.

7. *Effects of Protonation and Attachment of Alkali Metal Cations on the Singlet - Triplet Gap and Bonding of Silicon Trimer*.
   N. M. Tam, T. D. Hang, H. T. Pham, M. P. Pham-Ho and M. T. Nguyen.
   Journal of Computational Chemistry, submitted (August 2014).

8. *Theoretical Study of the Si_nMg_m Clusters and Ions: Toward Silicon Nanowires with Magnesium Linkers.*
   N. M. Tam, V. T. Ngan and M. T. Nguyen.
   Journal of Physical Chemistry A to be submitted (2014).

Others

9. *Evolution of Structures and Stabilities of Zinc-Doped Tin Clusters Sn_nZn, n = 1–12. Three-dimensional Aromaticity of the Magic Clusters $Sn_{10}Zn$ and $Sn_{12}Zn$.*
   T. B. Tai, **N. M. Tam** and M. T. Nguyen.
   *Chemical Phys*ics **2011**,*388,* 1.

10. *Structure of Boron Clusters Revisited, B_n with n = 14 -20.*
    T. B. Tai, **N. M. Tam** and M. T. Nguyen.
    Chemical Physics Letters **2012**, *530*, 71.

11. *Ionization energies and structures of lithium doped silicon clusters*.
    J. de Haeck, S. Bhattacharyya, H. T. Le, D. Debruyne, **N. M. Tam**, V. T. Ngan, E. Janssens, M. T. Nguyen and P. Lievens.
    Physical Chemistry Chemical Physics **2012***, 14,* 8542.

12. *The boron conundrum: the case of cationic clusters B_n^+ with n = 2 – 20.*
    T. B. Tai, **N. M. Tam** and M. T. Nguyen.
    Theoretical Chemistry Accounts **2012**, *131*, 1241.

13. *Heat of formation and thermochemical parameters of silole.*
    P. A. Denis, **N. M. Tam** and M. T. Nguyen.
    Chemical Physics Letters **2013**, *588*, 17.

14. *The boron conundrum: bonding in the bowl B_{30} and B_{36}, fullerene B_{40} and triple ring B_{42} clusters.*
    H. T. Pham, L. V. Duong, **N. M. Tam**, M. P. Pham-Ho and M. T. Nguyen.
    Chemical Physics Letters, **2014**, *608*, 295.

15. *Particle on a Hollow Cylinder: the Triple Ring Tubular Cluster B_{27}^+.*
    L. V. Duong, H. T. Pham, **N. M. Tam** and M. T. Nguyen.
    Physical Chemistry Chemical Physics, accepted (2014).

16. *Structure assignment, electronic properties, and magnetism quenching of endohedrally doped neutral silicon clusters, Si_nCo (n = 10 – 12).*
    Y. Li, **N. M. Tam**, P. Claes, A. Woodham, J. T. Lyon, V. T. Ngan, M. T. Nguyen, P. Lievens, A. Fielicke and E. Janssens.
    Journal of Physical Chemistry A, in press (2014).

17. *Influence of Cr doping on the stability and structure of small cobalt oxide clusters*.
    N. T. Tung, **N. M. Tam**, M. T. Nguyen, P. Lievens and E. Janssens.
    Journal of Chemical Physics, **2014**, *141*, 044311.

Samenvatting

Silicium speelt nog steeds een centrale rol in de halfgeleiderindustrie. In de wijdverspreide toepassingen die een grote invloed hebben op ons dagelijks leven, wordt silicium gebruikt in de vaste toestand. Echter bulksilicium dreigt niet langer te voldoen aan de huidige behoeften van miniaturisatie van de elektronische componenten. In de intensieve zoektocht naar apparaten van de toekomst, zijn pure siliciumclusters en siliciumclusters gedopeerdmet andere elementen naar voren gekomen als mogelijk alternatief. Dit perspectief heeft geleid tot een groot aantal studies betreffende binaire clusters van diverse elementen in het algemeen, en op silicium gebaseerde clusters in het bijzonder, omdat zij een groot aantal potentiële mogelijkheden bieden voor de ontwikkeling van nanoschaal materialen.

In deze context, voerden we in dit doctoraat theoretische onderzoek naar de geometrische en elektronische structuur van kleine siliciumclusters gedopeerd met enkele representatieve hoofdgroepelementen, waaronder Li, Mg, B, Al en ook C. Een dieper inzicht in hun geometrische en elektronische structuren, stabiliteit en bindingseigenschappen vormt een noodzakelijke stap in een uitgebreide en intensieve zoektocht naar veelbelovende clusters die kunnen worden beschouwd als bouwstenen voor verdere assemblage.

Onze zoektocht naar deminima op de potentiële energie-oppervlakken werd uitgevoerd met behulp van twee verschillende benaderingen. Voor de eerste, gebruikten we een stochastisch genetisch algoritme voor hetgenereren van een groot aantal potentieel interessante structuren. De corresponderende evenwichtsstructuren werden in eerste instantiegelokaliseerd met behulp van lage-kost-berekeningen,en vervolgens geheroptimaliseerdop een hoger niveau. In de tweede benadering, maakten we gebruik van onze chemische intuïtie, door voor deoorspronkelijke structuur van Si_nX_m-clusters ofwel Si-atomen te vervangen dooratomen van andere elementen, of door het toevoegen van doperingsatomen op verschillende posities. Het gebruik van het genetisch algoritme blijkt minder effectief te zijn voor het identificerenvan enkelvoudig gedopeerde clusters met een kleine grootte, omdat de meeste geometrische structuren in Si-clusters reeds vrij goed gekendzijn.

Daarentegen, multi-gedopeerde en grotere clusters impliceren een groot aantal structuren en dus is een genetische zoektocht nodig om de efficiëntie op te drijven. Dit belet niet dat een dergelijke zoektocht vaak moeilijk verloopt en bovendien veel rekencapaciteitvereist. Enkel door een combinatie van verschillende zoekstrategieën kon een samenhangende set van laag-energetische structuren verkregen worden. Wij zijn ervan overtuigd dat de isomeren beschreven in dit proefschrift ten minste overeenkomen met de daadwerkelijke meeste stabiele evenwichtsstructuren. Erisechter niet alleen een zorgvuldig onderzoek vereist, maar ook de nauwkeurigheid van de rekenkundige methoden isbelangrijk bij de bepaling van de globale minima.

De laaggelegen isomeren van de clusters werden geïdentificeerd op basis van theoretische resultaten verkregen met behulp van de hybride (U)B3LYP-functionaal in combinatie met de 6-311+G(d)-basisset (d-polarisatie plus sp-diffuse functies), en door vervolgens de grondtoestanden te identificerenmet behulp van hoge nauwkeurigheid computationele methoden, zoals G3B3 en G4, en waar mogelijk met het CCSD(T)/CBS protocol.

De energieën en verschillende fundamentele thermochemische parameters, waaronder de totale atomisatie-energieën (TAE), de standaardvormingsenthalpie (ΔH_f) , ionisatie-energieën (IE), elektronaffiniteiten (EA), bindingsenergieën (E_s) en dissociatie-energieën (D_e), werden bepaald met behulp van de Gn (G3B3 en G4) en CCSD(T)/CBS benaderingen. Voor de pure kationische en anionische Si_n-clusters, werd een uniforme set van standaardvormingswarmte bepaald tot n = 13. Soms zijn de verschillen tussen G4 en CBS TAE-waarden relatief groot. Deze verschillen in energetische eigenschappen tussen de G4 en CBS methoden kunnen worden begrepen aan hand van de wijze waarop de elektronische energie werd bekomen, alsook aan de hand van de gebruikte geometrie van de clusters. Bovendien blijkt de geometrische structuur een belangrijke factor voor het evalueren van de thermochemie.

Voor deze systemen worden experimentele resultaten in de huidige literatuur eveneens gekenmerkt door grote onzekerheden, waaronder de onzekerheid op de standaardvormingswarmte van het Si -atoom. Andere parameters daarentegen zoalsIE

en EAS, worden beter voorspeld, wat gedeeltelijk te wijten is aan een zekere wederzijdse annulering van fouten bij de beoordeling van de relatieve energieën. De bekomen G4 resultaten worden verondersteld ten minste nauwkeurig te zijn tot op ± 0,15 eV (Hoofdstuk 2).

Voor de lithium gedopeerd siliciumcluster, werden de adiabatische (AIEs) en verticale (VIEs) ionisatie-energieën van de Si_nLi_m clusters geëvalueerd. De op B3LYP/6/311+G(d) en CCSD(T)/aug-cc-pVDZ niveaus berekende AIE- en VIE-waarden voor Si_6Li_2, Si_7Li, $Si_{10}Li$, $Si_{11}Li$ vergelijken zich goed met de corresponderende experimentele resultaten zoals die verkregen werden uit foto-ionisatie efficiëntie-metingen (Hoofdstuk 3).

Voor boor-gedopeerd siliciumclusters, gaven de vormingswarmten zoals berekend met zowel de G4 als de CCSD(T)/CBS-methoden een goede overeenstemming met de beschikbare experimentele gegevens (Hoofdstuk 4).

Kortom, blijkt dat een nauwkeurige evaluatie van de TAEs en de standaard vormingswarmte van silicium gebaseerde clusters een grote uitdaging blijft voor ab-initio-berekeningen, teneinde de chemische nauwkeurigheid van ± 1,0 kcal / mol te bereiken. Vanwege de niet-klassieke binding in deze clusters kan het gebruik van andere thermochemische benaderingen (zoals reacties met bindingbreking) en berekeningen op een lager sofisticatieniveau niet worden toegepast. De enige optie is de kwaliteit van de golffuncties te verhogen tot boven CCSD(T). Echter, onze voorlopige berekeningen met behulp van de CCSDT-benadering wijzen erop dat dit veel meer computertijd vereist dan CCSD(T), veel meer dan de huidige beschikbare computercapaciteit.

Op basis van de geometrische eigenschappen van de grondtoestanden kon een groeimechanisme voor elke reeks van binaire siliciumclusters Si_nX_m worden voorgesteld. In het algemeen, verkiezen de alkali (Li) en aardalkali (Mg) de voorkeur voor een rand of een vlak van de Si_n-clusters, terwijl de boorgroepelementen (B, Al) de voorkeur geven aande substitutie in één van de Si-posities in de corresponderende Si_{n+1}-clusters. Door de kortere B-Si-bindingslengte ten opzichte van de Al-Si-analogen, kan de booronzuiverheid binnendringen in de overeenkomstige Si_n-kooi (tot

$n \geq 8$). De neutrale structuren van de dubbel gedopeerde siliciumclusters Si_nX_2 (X = Li, Mg , Al), hebben een soortgelijke groei: één doperingsatoomgesubstituteerd in een Si-positie van Si_{n+1}, terwijl het tweede doperingsatoomgewoonlijk wordt toegevoegd aan een rand of een vlak van de resulterende cluster.

Onze theoretische resultaten voorspellen ook dat sommige closed-shell systemen zoals Si_9B^-, $Si_{10}B^+$ (hoofdstuk 4), Si_9Al^- (hoofdstuk 5), en $Si_4C_2^+$ (hoofdstuk 7) worden gekenmerkt door verhoogde stabiliteiten. Hun hogere thermodynamische stabiliteit kan worden begrepen door hetJellium shell model (JSM). Volgens dit JSM, worden de valentie-elektronen verondersteld te bewegen in een eenvoudig gemiddeldpotentieelveld gevormd door de kernen en de kernelektronen, de valentie-elektronen vullen de waterstofachtige orbitalenop volgens het patroon $[1S^21P^61D^{10}2S^21F^{14}2P^61G^{18}2D^{10}...]$ enz... In dit model, komen het aantal valentie-elektronen van 8, 20, 34, 40, 56 en 68... te voorschijn als de magische getallen die overeenstemmen met een volledige vulling van de opeenvolgende schillen. Eerder typisch, deanionische structuren Si_9B^- en Si_9Al^- bevatten dezelfde Si_9-kooi waarin het boordoperingsatoomis ingekapseld, terwijl de Al-dopanteen vlak bedekt. Elk van hen heeft 40 valentie-elektronen en de DOS-eigenschappen zijn vergelijkbaar. Bijvoorbeeld, de elektronische structuur van beide deze anionen voldoendus aan de gesloten elektronenschilconfiguratie van $[1S^21P^61D^{10}2S^22P^61F^{14}]$, wat ze maakttot species met een verhoogde stabiliteit met een magisch aantal van 40 valentie-elektronen.

Wat betreft de bindingsverschijnselen, werden de elektronenlokalisatie-technieken (ELF en EDI-D) gebruikt om de positie van de elektronen te lokaliseren, en daardoor de chemische bindingskarakteristieken van een aantal specifieke clusters zoals Si_3, Si_4, Si_4^{2+}, Si_4C^{2+} en Si_9C te identificeren. Berekeningen van de ringstromen werden eveneens uitgevoerd om hun aromaticiteit (hoofdstuk7) te achterhalen. Dit onderzoek toonde aan, dat het bestaan van gedelokaliseerde bezette moleculaire orbitalen in een vlak molecule een noodzakelijke, maar niet voldoende,voorwaarde is om een bepaald aromatisch karakter (aromatische, niet-aromatische of anti-aromatisch) toe te wijzen aan dit specifiek type van elektronen. Verschillende criteria

moeten worden overwogen voor een meer consistente evaluatie van deze populaire en intrigerende moleculaire eigenschap.

Daarnaast vertonen zowel het Si_4C^{2+}dikation en hetneutrale Si_9C een vlakke tetra-gecoördineerd koolstofatoom (ptC) in hun laagst gelegen isomeer. Dit wordt veroorzaakt door de C-planarisatie, dat niet alleen de elektrondelokalisatiein het vierkante skelet omvat, maar ook de binding tussen de C-doperingsatoom en het Si-skelet van dit kleine dikation. In de grotere neutrale clusterkooi, heeft de Si_5 groep de neiging om de kooi elektronisch te stabiliseren door elektrontransfer en mechanisch door de geometrische beperkingen opgelegd door het handhaven van een PTC-configuratie.

In een poging om te zoeken naar potentiële linkers in het maken siliciumnanodraden, vonden we dat de dopeerstof Mg, vanwege de grote elektronenoverdrachtcapaciteit,zich gedraagt als kation $Mg^{\delta+}$ en daarbijeen ionische eenheid vormt met de $Si_n^{\delta-}$ anionische partner. Het resulterende Mg-kation kan worden gezien als een linker tussen de Si_n-blokken wat leidt tot gestabiliseerd lineaire $[(Si_k)Mg]_l$ structuren, die gedeeltelijk te wijten zijn aan elektrostatische aantrekkingskrachten. Dit liet ons toe om een aantal geschikte entiteiten te identificeren die kunnen gebruikt worden als superatomen voor verdereassemblage. Wij onderzochten de mogelijkheid van vijf-, zeven-, acht- en tien-atoom Si-bouwstenen, en de rol van Mg als linker die ze aaneensluit. De berekende gemiddelde assemblage-energie die een idee geeft betreffende de neiging tot vorming van de cluster $(Si_kMg)_l$ k = 5, 7, 8 en 10, toont dat siliciumclusters Si_kde neiging hebben tot ringvorm ($\mathbf{R}_l$) eerder dat tot het vormen lineaire structuren ($\mathbf{L}_l$), aangezien de assemblage-energie van $\mathbf{R}_l$ groter is dan die van $\mathbf{L}_l$.Een belangrijk feit is echter dat de gemiddelde assemblage-energie van de lineaire vorm toeneemt met de toenemende omvang (l), wat impliceert dat een (langere) nanodraad kan worden beschouwd als een plausibele mogelijkheid (hoofdstuk 6).

Table of Contents

Chapter 1

Introduction

Clusters have existed for centuries, even taking part in our day life, but they only became an object of scientific study since the detection of the carbon fullerene.[1] Clusters of the elements thus form a rapidly developing field of science whose ultimate aim is a contribution to modern technological developments.[2]

With the rapid progresses in nano-science, a new field, which is called cluster science, emerged around the early 1980s as a seperate domain of research. The studies of clusters have been carried out successively in order to achieve the main goals that are: i) to understand the bridge from molecular behavior to bulk condensed matter behavior,[3] and ii) to search for, and to bring into life, new kinds of materials with some fabulous properties, which can be produced by using clusters as building blocks.[1,4,5]

Atomic clusters can be defined as aggregates of typically a few to a few thousand atoms and thus represent a new form of matter between atoms and molecules, as well as between molecules and solids. An atomic cluster is in fact a group of atoms bound together by interatomic forces. The difference in characteristics between small clusters and molecules is thus insignificant, except for the fact that the structural arrangements and the inherent binding forces must be built up in such a way to permit the cluster system to grow much larger, with no upper limit to the size, by stacking more atoms of the same motif. As the number of atoms or basic units in the system increases, atomic clusters acquire more specific properties making them perhaps unique physical objects, which differ much from both single molecules and solid state. Thus the main differences between a cluster and a classical (organic or inorganic) molecule is their molecular structure and chemical bonding.

Concerning their size, clusters also lie between single molecules and bulk materials. There are different types of atomic clusters in nature as they possess a large variety of shapes (2D planar or quasi-planar, 3D cage, cube, sphere, tube, fullerene...) and symmetry. Clusters can exist in all forms of matter including solid state, liquid, gas phases and plasmas, depending on the nature and properties of the constituent components, and on the ways of generating them.

In this context, properties of clusters are strongly dependent on those of the elements involved. Clusters also attract significant interest from the point of view of chemical structure and bonding as they basically have non-classical features. Their physical and chemical properties are expected to be different from those of the bulk materials because of their physical size. Therefore, it is imperative to deeply understand the geometrical and electronic structures, as well the chemical properties of small elemental clusters.

In terms of dimension, the cluster size is in fact reaching the nanoscale range. However, clusters cannot just be considered as small solid particles, since their properties are typically size-dependent in a nontrivial, non-scalable way. Clusters with enhanced stability often behave as superatoms that can further be used as building blocks for new materials. Therefore, much effort has been invested in the search for clusters having interesting and novel properties, and can be tailored for self-assemblies. The presence of a dopant impurity usually alters the geometry and electronic structure of the cluster giving thus a new cluster, making it possible to modulate, among others, the optical or magnetic responses.

Silicon is extensively used in the semiconductor and optoelectronic industries.[6] In these important applications, silicon is often used in its bulk solid state. However bulk silicon can no longer satisfy the current needs of miniaturization of electronic devices. The demand for smaller and smaller devices has thus been stimulating a wealth of studies of silicon clusters, as they open up new avenues for development of nanoscaled materials.[7] A large number of experimental and theoretical studies recently reported in the literature leave no doubt for a considerable interest in silicon based clusters. The characteristics of electronic structure, spectroscopy and thermochemical properties of small silicon clusters in various charge states have carefully been studied in the literature.

More interestingly, since the first experimental observation for the existence of endohedral transition metal doped silicon clusters was reported,[8] in attempts to understand different aspects of the effect of mixing other elements on silicon clusters, a large number of studies on binary Si clusters in which many elements have been

considered as dopants including the main group elements, or transition metals, or lanthanide elements, etc… were performed with the aim to determine their stabilities, electronic and magnetic properties.[9-41,42,43,44,45,46,47]

Up to now, most of the reported investigations focused on binary silicon clusters with only one impure atom. Reports on impurity-rich mixed silicon clusters are rather scarce, despite the fact that it is of importance to gain a better understanding about materials having mixed elements. From the theory side, one of the main reasons for this relative lack of reports is that the search for their global minima is a tedious task, due to the huge number of local minima to be located on their potential energy surfaces. As a consequence, impurity-rich binary clusters present an urgent and necessary target for detailed studies.

Although many extensive and intensive examinations have been carried out, determination of the molecular and electronic structures of clusters, and the growth mechanisms of doped silicon clusters, that administrate the evolution of all physical and chemical properties, remains a great challenge. From a theoretical viewpoint, as stated above, one reason is that of a large number of possible geometric structures for a given cluster size, several energetically close-lying isomers often exist. The energy gaps between them are often lying within the current error margins of quantum chemical methods, in particular for density functional theory (DFT) methods.[48] Therefore, it is obvious that theory also faces many difficulties in accurately predicting the global energy minimum geometry of a cluster, and thereby in assigning different experimental spectra.

Due to the inherent deficiencies of popular computational methods in the determination of global minima (current DFT functionals were not constructed for clusters), several energetic parameters of silicon based clusters such as ionization energies (IE), electron affinities (EA), binding energies (E_b) and especially the standard enthalpies of formation ($\Delta_f H$, a key thermochemical parameter), are not well determined yet. In this context, it is necessary to use the high accuracy computational approaches combining with experimental spectroscopic techniques to investigate

structures, thermochemical parameters, and growth mechanisms of doped-silicon clusters.

Attempts to make silicon nanowires as assemblies of small silicon clusters were reported.[49] Previous studies showed the Si nanowires, in particular Al-doped derivatives, could be prepared.[50,51,52] However, relatively less is known about nanowires using other elements of the main groups as linkers. This type of material constitutes a promising area for theoretical explorations.

Recently, several combined experimental spectrometric and theoretical studies were carried out in our laboratory on silicon clusters doped by transition metal elements, Si_nM with M = V, Mn, Cu, Co...[53,54,55,56,57,58,59] Together with experimental investigations of the group of Professors Peter Lievens and Ewald Janssens at the Physics department, KU Leuven, using mass and free electron laser infrared spectrometric techniques, DFT computations allowed us to assign the experimental vibrational spectra, and thereby determine the most likely structures of the clusters observed. In some cases, energetic parameters such as ionization energies were also evaluated.

These extensive findings indicated that while Cu prefers to be absorbed on the surface of silicon hosts, V-doped clusters Si_nV^+ are built up by substituting one Si-atom of the Si_{n+1}^+ frameworks by one V-dopant. In addition, the endohedrally doped structures with encapsulated impurities were also found at some special sizes. For instance, Be was found to be located at the center of Si_8 and Si_{10} hosts[54,55] whereas some transition metals are also encapsulated into larger Si_n cages with n = 12, 14 and 16.[30,58]

Relatively much less is known on the binary silicon clusters containing other elements. In this context, we set out to extend our knowledge on binary silicon clusters. The main objective of the work carried out in the doctoral study, and reported in this thesis, was an investigation on the geometrical and electronic structures, thermochemical properties, and growth sequences of the silicon clusters doped with a few elements of the main groups. The elements considered are good representatives of the main groups in the Periodic Table including Li for the alkali

metals, Mg for the alkaline earth metals, B and Al for group 13. In addition, we also determined the molecular geometries and rationalize the chemical bonding of some small C-doped silicon clusters. We demonstrated that it is possible to achieve a planar tetracoordinate carbon (ptC) with enhanced stability by both electronic and mechanical effects within Si clusters.

On the basis of the relevant results obtained from our doctoral work, this thesis is divided into eight chapters as follows:

Chapter 1: General considerations,

Chapter 2: Computational determination of thermochemical parameters,

Chapters 3, 4, 5, and 6: Structures, thermochemical properties and growth mechanisms of silicon clusters doped by lithium (chapter 3), boron (chapter 4), aluminum (chapter 5) and magnesium (chapter 6). In chapter 6, we also considered the silicon nanowires with magnesium linkers,

Chapter 7: Chemical bonding in the small clusters Si_3 and Si_4 along with the carbon-doped Si clusters, and

Chapter 8: General conclusions and some perspectives.

Chapter 2 presents the computational methods currently used to study pure and doped clusters. DFT method was used to explore the lower-lying isomers of clusters whereas the energetics of the lowest-lying equilibrium structures and thereby to probe their growth pattern are determined by using the composite G4 protocol. Thermochemical properties of the clusters were calculated using both G4 and coupled-cluster theory CCSD(T)/CBS approaches.

Chapter 3 reports the study on singly and doubly lithium doped silicon clusters. Geometrical and electronic structures of neutral and cationic $Si_nLi_m^{0/+}$ cluster with n = 2-11 and m = 1, 2 were investigated using combined experimental and computational methods. Adiabatic (AIEs) and vertical (VIEs) ionization energies of Si_nLi_m clusters were determined using quantum chemical methods (B3LYP/6-311+G(d), G3B3 and CCSD(T)/aug-cc-pVxZ with x = D, T. Experimental values

were recently determined using threshold photoionization experiments in the 4.68 − 6.24 eV range for these systems.

Investigation of structures, growth mechanism of group 13 elements, including B and Al, doped silicon clusters in both neutral and ionic states is presented in Chapters 4 and 5, respectively. Lowest-energy minima of the clusters considered were identified on the basis of the B3LYP, G4 and CCSD(T) energies. Total atomization energies and thermochemical properties such as ionization energy, electron affinity and dissociation energies were obtained using the composite G4 and CCSD(T)/CBS (complete basis set up to n = 4) methods. Theoretical enthalpies of formation are used to assess available experimental values. We also rationalized the higher stability of the closed shells Si_9B^-, $Si_{10}B^+$ and Si_9Al^- in terms of the jellium electron shell model.

Chapter 6 report similar results on singly and doubly magnesium doped silicon clusters at neutral and cationic states $Si_nMg_m^{0/+}$ (n = 1-10, m =1, 2). The structural and stability patterns of magnesium doped silicon clusters using G4 results allowed us to identify the suitable members that can further be used as superatoms for assemblies. We thus probed the five-, seven-, eight-, and ten-Si atom building blocks, and the role of Mg as their linkers. This chapter includes some new aspects about the assemblage of Si clusters.

To obtain a deeper understanding of the chemical bonding phenomena of simple silicon clusters, we present in Chapter 7 an analysis of the silicon trimer Si_3, tetramer Si_4 and its doubly charged derivatives Si_4^{2+}. The pentatomic carbon-doped clusters having 18 valence electrons system Si_4C^{2+} (and its isoelectronic Al_4C^{2-} species) were also examined. Finally, we considered the Si_9C cluster which exhibits a ptC in a stable cage framework.

Finally, in the general conclusions of Chapter 8, we attempt to emphasize the main contributions of this doctoral work, and provide our points of view about some issues opened by the results, in particular the computational approaches, and the promising area of Si-based nanowires.

Due to the fact that the papers that form the basis of the thesis, were published in different journals, there is an inconsistence in the units used for energy (both kcal/mol and kJ/mol were used). I would apologize for any inconvenience.

References

1) H. W. Kroto, J. R. Heath, S. C. O'Brien R. F. Curl R. E. Smalley Nature 318 (1985) 162.

2) Reinhard P. G.; Suraud E. Introduction to Cluster Dynamics (2004) Wiley-VCH Verlag GmbH & Co. KGaA, Weiheim, Germany.

3) P. Jena, B. K. Rao, S. N. Khanna, Physics and Chemistry of Small Clusters (1987) Plenum, New York, USA.

4) W. Kratschmer, L. D. Lamb, K. Forstiropoulos, D. R. Huffman, Nature 347 (1990) 354.

5) a) S. N. Khanna, P. Jena, Phys. Rev. Lett. 69 (1992) 1664; b) S. N. Khanna, P. Jena, Phys. Rev. B 51 (1995) 13705.

6) K. D. Sattler, Handbook of Nanophysics. Clusters and Fullerenes (2011) CRC Press, London, U.K.

7) V. Kumar, Nanosilicon (2008) Elsevier, The Netherlands.

8) S. M. Beck, J. Chem. Phys. 87 (1987) 4233.

9) a) A. Grubisic, Y. J. Ko, H. Wang, K. H. Bowen, J. Am. Chem. Soc. 131 (2009) 10783; b) T. G. Liu, G. F. Zhao, Y. X. Wang, Phys. Lett. A 375 (2011) 1120; c) H. F. Li, X. Y. Kuang, H. Q. Wang, Phys. Lett. A 375 (2011) 2836; d) L. Guo, X. Zheng, Z. Zeng, C. Zhang, Chem. Phys. Lett. 550 (2012) 134.

10) a) A. Dkhissi, Int. J. Quant. Chem. 108 (2008) 996; b) D. Hossain, C. U. Pittman, S. R. Gwaltney, Chem. Phys. Lett. 451 (2008) 93; c) Y.-Z. Lan, Y.-L. Feng, Phys. Rev. A 79 (2009) 033201; d) G. L. Li, W. L. Ma, A. M. Gao, H. Y. Chen, D. Finlow, Q. S. Li, J. Theoret. Comput. Chem. 11 (2012) 185; e) H.G. Xu, M .M. Wu, Z. G. Zhang, J. Yuan, Q. Sun, W. J. Zheng, Chem. Phys. 136 (2012) 104308; f) P. Shao, X. Y. Kuang, L. P. Ding, M. M. Zhong, Z. H. Wang, Physica B 407 (2012) 4379.

11) a) D. H. Ziella, M. C. Caputo, P. F. Provasi, Int. J. Quant. Chem. 111 (2011) 1680; b) W. Ma, F. Chen, J. Mol. Model. 19 (2013) 4555; c) Y. Li, J. T. Lyon, A. P. Woodham, A. Fielicke, E. Janssens, Chem. Phys. Chem. 15 (2014) 1.

12) O. Cheshnovsky, S. J. Yang, C. L. Pettiette, M. J. Craycraft, Y. Liu, R. E. Smalley, Chem. Phys. Lett. 138 (1987) 119.

13) a) J. Z. Ye, B. X. Li, J. Phys. B 405 (2010) 1461; b) H. W. Fan, J. C. Yang, W. Lu, H. M. Ning, Q. C. Zhang, J. Phys. Chem. A 114 (2010) 1218.

14) a) H. G. Xu, Z. G. Zhang, Y. A. Feng, W. J. Zheng, Chem. Phys. Lett. 498 (2010) 22.

15) a) A. Gao, G. Li, Y. Chang, H. Chen, D. Finlow, Q. Li, Inorg. Chim. Acta. 367 (2011) 51; b) A. Kodlaa, S. El-Taher, Comp. Theor. Chem. 992 (2012) 134.

16) J. G. He, K. C. Wu, R. J. Sa, Q. H. Li, Y. Wei, Chem. Phys. Lett. 490 (2010) 132.

17) X. Kong, H. G. Xu, W. Zheng, J. Chem. Phys. 137 (2012) 064307.

18) a) A. D. Zdetsis, E. N. Koukaras, C. S. Garoufalis, J. Math.Chem. 46 (2009) 971; b) A. D. Zdetsis, J. Chem. Phys. 128 (2008) 184305; c) A. D. Zdetsis, J. Phys. Chem. A 112 (2008) 5712; d) A. D. Zdetsis, Phys. Rev. B 75 (2007) 085409.

19) a) R. Robles, S. N. Khanna, Phys. Rev. B 80 (2009) 115414; b) R. Robles, S. N. Khanna, J. Chem. Phys. 130 (2009) 164313.

20) a) J. R. Li, G. H. Wang, C. H. Yao, Y. W. Mu, J. G. Wan, M. J. Han, Chem. Phys. 130 (2009) 164514; b) B. X. Li, G. Y. Wang, W. F. Ding, X. J. Ren, J. Z. Ye, Phys. B-Cond. Mat. 404 (2009) 1679.

21) a) V. Quenau, E. Todorov, S. C. Sevov, J. Am. Chem. Soc. 120 (1998) 3263;b) S. A. Fischer, A. B. Madrid, C. M. Isborn, P. V. Prezhdo, J. Phys. Chem. Lett. 1 (2010) 232.

22) M. Savoca, A. Lagutschenkov, J. Langer, D. J. Harding, A. Fielicke, O. Dopfer, J. Phys. Chem. A 117 (2013) 1158.

23) M. Anafcheh, R. Ghafouri, N. L. Hadipour, Physica E 44 (2012) 2099.

24) a) Z. Shuai, J. H. Long, W. Ping, L. Cheng, L. G. Quan, Z. Ping, Chin. Phys. B 22 (2013) 123601; b) M. Anafcheh, R. Ghafouri, Physica E 48 (2013) 13.

25) D. Palagin, M. Gramzow, K. Reuter, J. Chem. Phys. 134 (2011) 244705.

26) X. Li, H. Wang, A. Grubisic, D. Wang, K. H. Bowen, M. Jackson, B. Kiran, J. Chem. Phys. 129 (2008) 134309.
27) K. Koyasu, J. Atobe, S. Furuse, A. Nakajima, J. Chem. Phys. 129 (2008) 214301.
28) H. C. Lopez, L. C. Balbas, G. Borstel, Phys. Rev. B 83 (2011) 075434.
29) a) W. J. Zhao, B. Xu, Z. X. Wang, Comput. Mater. Sci. 50 (2011) 2167; b) S. Jaiswal, V. P. Babar, V. Kumar, 88 (2013) 085412.
30) a) H. Kawamura, V. Kumar, Y. Kawazoe, Phys. Rev. B 71 (2005) 075423; b) L.-J. Guo, G.-F. Zhao, Y.-Z. Gu, X. Liu, Z. Zeng, Phys. Rev. B 77 (2008) 195417; c) H. G. Xu, Z. G. Zhang, Y. Feng, J. Y. Yuan, Y. C. Zhao, W. J. Zheng, Chem. Phys. Lett. 487 (2010) 204; d) W. Ji, C. Luo, Int. J. Quant. Chem. 112 (2012) 2525; e) T. Iwasa, A. Nakajima, J. Phys. Chem. C 116 (2012) 14071; f) C. L. Reis, J. M. Pacheco, J. Phys.: Condens. Mater. 22 (2010) 035501.
31) P. Gruene, A. Fielicke, G. Meijer, E. Janssens, V. T. Ngan, M. T. Nguyen, P. Lievens, ChemPhysChem 9 (2008) 811.
32) V. Z. Bayer, L. Leppert, K. Hirsch, A. Langenberg, J. Rittmann, M. Kossick, M. Vogel, R. Richter, A. Terasaki, T. Moller, B. V. Issendorff, S. Kummel, J. T. Lau, Phys. Rev. B 88 (2013) 115425.
33) Y. Cao, R. F. Hockendorf, M. K. Beyer, ChemPhysChem 9 (2008) 1383.
34) T. T. Cao, X. J. Feng, L. X. Zhao, X. Liang, Y. M. Lei, Y. H. Luo, Eur. Phys. J. D 49 (2008) 343.
35) a) C. Sporea, F. Rabilloud, J. Chem. Phys. 127 (2007) 164306; b) C. Sporea, F. Rabilloud, X. Cosson, A. R. Allouche, M. Frecon, J. Phys. Chem. A 110 (2006) 6032; c) C. Sporea, F. Rabilloud, A. R. Allouche, M. Frecon, J. Phys. Chem. A 110 (2006) 1046; d) L. H. Lin, J. C. Yang, H. M. Ning, D. S. Hao, H. W. Fan, J. Mol. Struct. THEOCHEM 851 (2008) 197; d) D. Hao, J. Liu, J.A. Yang, J. Phys. Chem. A 112 (2008) 10113; e) D. S. Hao, J. R. Liu, W. G. Wu, J. C. Yang, Theor. Chem. Acc. 124 (2009) 431; f) P. Karamanis, R. Marchal, P. Carbonniére, C. Pouchan, J. Chem. Phys. 135 (2011) 044511.
36) K. Koyasu, J. Atobe, M. Akutsu, M. Mitsui, A. Nakajima, J. Phys. Chem. A 111 (2007) 42.

37) E. Janssens, P. Gruene, G. Meijer, L. Woste, P. Lievens, A. Fielicke, Phys. Rev. Lett. 99 (2007) 063401.

38) A. Dmytruk, Y. S. Park, A. Kasuya, H. Kikuchi, M. Takahashi, Y. Kawazoe, A. Watanabe, J. Nanosci. Nanotechnol. 7 (2007) 3788.

39) a) S. Nigam, C. Majumder, S. K. Kulshreshtha, J. Chem. Phys. 121 (2004) 7756; b) C. Majumder, S. K. Kulshreshtha, Phys. Rev. B 69 (2004) 115432; c) S. Nigam, C. Majumder, S. K. Kulshreshtha, J. Chem. Phys. 125 (2006) 074303.

40) a) L. Ma, J. Zhao, J. Wang, B. Wang, Q. Lu, G. Wang, Phys. Rev. B 73 (2006) 125439; b) Y. Liu, G. L. Li, A. M. Gao, H. J. Chen, D. Finlow, Q. S. Li, Eur. Phys. J. D 64 (2011) 27; c) L. Ma, J. Wang, G. Wang, J. Chem. Phys. 138 (2013) 094304.

41) a) S. Nigam, C. Majumder, S. K. Kulshreshtha, J. Chem. Phys. 125 (2006) 074303; b) Y. Chang, G. Li, A. Gao, H. Chen, Q. Li, Theor. Chem. Acc. 130 (2011) 1009.

42) T. Bachels, R. Schafer, Chem. Phys. Lett. 324 (2000) 365.

43) F. Avaltroni, S. N. Steinmann, C. Corminboeuf, Phys. Chem. Chem. Phys. 14 (2012) 14842.

44) J. T. Lau, M. Vogel, A. Langenberg, K. Hirsch, J. Rittmann, V. Z. Bayer, T. Möller, B. V. Issendorff, J .Chem. Phys. 134 (2011) 041102.

45) S. A. Fischer, O. V. Prezhdo, J. Phys. Chem. C 115 (2011) 10006.

46) D. Palagin, T. Teufl, K. Reuter, J. Phys. Chem. C 117 (2013) 16182.

47) C. Majumder, S. K. Kulshreshtha, Phys. Rev. B 2004, 70, 245426.

48) T. Ziegler, J. Li, Can. J. Chem. 72 (1994) 783.

49) B. Mardsen, K. Sattler, Phys. Rev. B, 60 (1999) 11593.

50) U. Landman, R. N. Barnett, A. G. Scherbakov, P. Avouris, Phys. Rev. Lett. 85, (2000) 1958.

51) V. G. Kotlyar, A. V. Zotov, A. A. Saranin, T. V. Kasyanova, M. A. Cherevik, I. V. Pisarenko, V. G. Lifshits, Phys. Rev. B 66 (2002) 165401.

52) M. Paulose, C. A. Grimes, O. K. Varghese, E. C. Dickey, Appl. Phys. Lett. 81 (2002) 153.

53) N. M. Tam, V. T. Ngan, J. de Haeck, S. Bhattacharyya, H. T. Le, E. Janssens, P. Lievens, M. T. Nguyen, J. Chem. Phys. 136 (2012) 024301.
54) V. T. Ngan, M. T. Nguyen, J. Phys. Chem. A 114 (2010) 7609.
55) N. M. Tam, T. B. Tai, M. T. Nguyen, J. Phys. Chem. C 116 (2012) 20086.
56) N. M. Tam, T. B. Tai, V. T. Ngan, M. T. Nguyen, J. Phys. Chem. A 117 (2013) 6867.
57) a) V. T. Ngan, P. Gruene, P. Claes, E. Janssens, A. Fielicke, M. T. Nguyen, P. Lievens, J. Am. Chem. Soc. 132 (2010) 15589; b) P. Claes, E. Janssens, V. T. Ngan, P. Gruene, J. T. Lyon, D. J. Harding, A. Fielicke, M. T. Nguyen, P. Lievens, Phys. Rev. Lett. 107 (2011) 173401.
58) a) V. T. Ngan, E. Janssens, P. Claes, J. T. Lyon, A. Fielicke, M. T. Nguyen, P. Lievens, Chem. Eur. J. 18 (2012) 15788; b) V. T. Ngan, K. Pierloot, M. T. Nguyen, Phys. Chem. Chem. Phys. 15 (2013) 5493.
59) N. M. Tam, V. T. Ngan, M. T. Nguyen, Chem. Phys. Lett. 595-596 (2014) 272.

Chapter 2

Determination of Atomization Energies and Heats of Formation

This chapter is in part based on the following articles:

1) *Heats of formation and thermochemical parameters of small silicon clusters and their ions,* $Si_n^{+/0/-}$ *with* $n = 2 – 13$, N. M. Tam and M. T. Nguyen, *Chemical Physics Letters*, 584, 147 – 154 (2013).

2) *Effects of protonation and attachment of alkali metal cations on the singlet-triplet gap and bonding of silicon trimer,* N. M. Tam, T. D. Hang, H. T. Pham, M. P. Pham-Ho and M. T. Nguyen, *Journal of Computational Chemistry* (2014) submitted.

2.1 HEATS OF FORMATION AND TOTAL ATOMIZATION ENERGIES

The heat of formation (denoted as ΔH_f, $\Delta_f H$, $\Delta_f H^0$,… also called enthalpy of formation), which is a key and characteristic physico-chemical parameter of a molecular system, is of common use in many fields of chemistry. It is necessary for the evaluation of thermochemical quantities of a chemical system, or the energetic outcome of a chemical process. Knowledge of the heats of formation of the compounds involved is thus primordial in their thermodynamic and kinetic studies.

The standard heat (or enthalpy) of formation of a substance X, determined at given temperature and pressure, is the enthalpy of reaction accompanying the formation of of 1 mole of that substance from its constituent elements in their reference states. In the symbol of ΔH_f^0 or $\Delta_f H^0$, the superscript zero indicates that the process has occurred under standard conditions at the specified temperature.

Standard states are defined as follows: i) for a gas: the standard state is a pressure of exactly 1 atm (or 101.3 kPa); ii) for a solute present in an ideal solution: a concentration of exactly 1 M at a pressure of 1 atm, and iii) for an element: the form in which the element is the most stable under 1 atm of pressure.

As for example, the standard enthalpy of formation of CO_2 is the enthalpy of the following reaction under the conditions above at a certain temperature:

$$C_{(s,graphite)} + O_{2(g)} \rightarrow CO_{2(g)} \qquad (2.1)$$

$$\Delta H_r \text{ (reaction 2.1)} = \Delta H_f(CO_2)$$

All elements involved are in their standard states, and one mole of product is formed. The formation reaction is a constant pressure and constant temperature process. Since the pressure of the standard formation reaction is usually fixed at 1 atm, the standard enthalpy of formation or enthalpy of reaction is a function of temperature. Standard enthalpies of formation are often tabulated at a single temperature either 0K or 298 K (25 degree Celsius, represented by the symbol $\Delta H_{f,298}$).

For an element, the reference state is the thermodynamically most stable state of that element at the stated conditions. By convention, the standard conditions are set at temperature T = 298.15 K and pressure P = 1 atm, and the standard heats of formation of the elements in their reference states are equal to zero at all temperatures.[1] The standard states of the elements are gas for hydrogen, nitrogen and oxygen, solid for boron, carbon in the form of graphite, crystal for silicon etc... The standard enthalpy of formation of zero is due to the fact that there is no change involved in their formation. Thus, the standard heat of formation of molecular hydrogen, the reference state of hydrogen in whatever temperature, $\Delta_f H(H_2) = 0.0$ in whatever energy unit.

Due to their importance, determination of heats of formation has continuously been pursued using a variety of approaches and techniques by the physico-chemical community. The most common experimental measurements were based on the calorimetric and mass spectrometric techniques.[2] Among the latter, the Knudsen-effusion mass spectrometric measurements appear to be efficient for various types of elemental clusters.[3]

In general, from kinetic studies of chemical equilibrium carried out under different conditions of a reaction (2.2):

$$A + B \rightarrow C + D \qquad K_{eq} \qquad (2.2)$$

where $\Delta H_f(A)$ is unknown, the corresponding equilibrium constants ($K_{eq} = A \exp(-\Delta G_r/RT)$ can be determined, and subsequently the free (Gibbs) energies of reaction (ΔG_r) and thereby the enthalpy of reaction (ΔH_r) can be extracted if the variation of entropy ΔS is known ($\Delta H = \Delta G + T\Delta S$). Using the ΔH_r, the value $\Delta H_f(A)$ can thus be determined by a thermochemical cycle if the heats of formation of the other compounds (B, C and D in equation 2.2) are also well known.

$$\Delta H_r = \Delta H_f(C) + \Delta H_f(D) - [\Delta H_f(A) + \Delta H_f(B)] \qquad (2.3)$$

For a cluster M_n, the enthalpy of the dissociation reaction (2.4)

$$M_n(g) \rightarrow nM(g) \qquad (2.4)$$

corresponds to the *total atomization energy* (ΔH_r = TAE) of M_n, and this quantity can also be evaluated from the heats of formation of the cluster $\Delta_f H(M_n)$ and the element M $\Delta_f H(M)$.

The wealth of experimental results obtained for the heats of formation of chemical compounds in the gas phase have continuously been calibrated, evaluated and recommended in several books[4,5,6] and compilations.[7] Let us mention here the most known and employed compilations including the JANAF Thermochemical Tables,[8] JANAF-NIST Tables[9] and the open and large compilations of the USA National Institute of Standard and Technology (NIST) webpage.[10] For small and medium-sized stable organic and inorganic compounds, their heats of formation in the gas phase were determined with high accuracy, attaining the *chemical accuracy* of ± 1.0 kcal/mol (± 4 kJ/mol or ± 0.04 eV).[8,9,10] However, determination of thermochemical data for unstable species or short-lived transient intermediates whose productions are not straightforward, remains a challenge for experimental methods.

In this context, theoretical thermochemistry emerged in the last two decades as a convenient, effective, economic and reliable alternative to the speculative guess work. With the tremendous advances in computer technology, with the current generation of powerful teraflops and petaflops high-performance computers, quantum chemical computations can also nowadays achieve the *chemical accuracy* of ± 1.0 kcal/mol for thermochemical parameters.[11] The great advantage of theoretical approaches lies in the fact that they can predict with high accuracy parameters of unknown compounds.

In this chapter, we first briefly describe the current strategies for quantum chemical determination of heats of formation. Subsequently we apply these approaches to determine the heats of formation and thermochemical parameters of a series of small silicon clusters in three different charge states, $Si_n^{+/0/-}$ with n = 2-13.

The heats of formation cannot directly be derived from the total energies obtained from electronic structure computations. As in experiment, the use of thermochemical cycles involving the heat of a reaction such as (2.2) or (2.4) is necessary. This leads to two main approaches: while the first approach uses a working

reaction where only the heat of formation to be determined is unknown (reaction 2.2), the second approach involves a complete dissociation of the substance yielding atoms (reaction 2.4) for which the TAE needs to be determined.

1) *Approach using a working chemical reaction*: in this approach, the selection of a suitable reaction is of essential importance. When several working reactions are equally possible, the reaction having the largest similarity between both reactant and product sides should be considered. Such a similarity minimizes the importance of correlation effects by a mutual cancellation of errors. For example, exchange reactions and isodesmic (bond separation) reactions for larger species, are often preferred over other types of reaction.

An exchange reaction is that in which a bond from a partner in the reactants is interchanged giving the same bond in the products. An isodesmic reaction is a hypothetical chemical process in which the number of bonds of each formal type remains the same on each side of the equation but with changes occurring in their mutual relationships. For example, reaction (2.5) is an isodesmic reaction in which the bonds are separated but kept in both sides

$$H_2C{=}CH\text{-}CH{=}NH + 2CH_4 \rightarrow H_2C{=}CH_2 + H_3C\text{-}CH_3 + H_2C{=}NH \quad (2.5)$$

In other words, the heat of isodesmic reaction is a measure of deviations from the additivity of bond energies.[12] The main advantage of this approach is that it requires only a moderately high level of theory to obtain good reaction energies, in part due to cancellation of errors. It has been known that, for large compounds, economical quantum chemical methods can be used to obtain good results.[11,13] Its main problem turns out to be the accuracy of the experimental heats of formation of the compounds involved in the working reactions.

2) *Approach using the total atomization energy (TAE)*: this is a more direct way as it involves only the experimental heats of formation of the elements. However, the use of massively correlated wavefunctions is important, in particular for small molecules, and therefore evaluation of TAEs represents a challenge for computational methods.[13]

In both cases it is crucial to employ a quantum chemical method that is size consistent, that is E(A + B) = E(A) + E(B). Due to the fact that the chemical bonding in elemental clusters is of non-classical nature, reactions such as the isodesmic (bond separation) reactions… that are commonly used for organic compounds could not be applied to clusters. The reactions (2.6) provide us with an example. While the reaction (2.6a) could be used, the bond separation reactions (2.6b) and (2.6c) would be not suitable as the SiSi bonds in the tetramer Si_4 differ much from the single Si-Si bond in disilane and double Si=Si bonds in disilene. The number of Si-Si bonds in the tetramer is not recovered in the products. In addition, the experimental heat of formation of disilene is not known yet.

$$Si_4 + 8\ H_2 \rightarrow 4\ SiH_4 \qquad (2.6a)$$

$$Si_4 + 6\ H_2 \rightarrow 2\ H_3Si\text{-}SiH_3 \qquad (2.6b)$$

$$Si_4 + 5\ H_2 \rightarrow H_3Si\text{-}SiH_3 + H_2Si{=}SiH_2 \qquad (2.6c)$$

For this reason, we have chosen in the present study of clusters the approach involving first a theoretical determination of the TAEs. As stated above, this is a straightforward but challenging approach, due to the intrinsic differences of the electron correlation in the atoms and their molecules. Only a careful strategy for the treatment of electron correlation can give results attaining a chemical accuracy of ± 1.0 kcal/mol. Let us now briefly describe some important aspects of the strategies employed in this work for calculating the TAEs and then the heats of formation.

2.2 CHOICE OF QUANTUM CHEMICAL METHODS

2.2.1 The coupled-cluster theory

In this work we used the coupled-cluster (CC) theory which is known to provide massively correlated wavefunctions, and it is size consistent at all orders. Let us briefly mention the main points of the CC formalism for describing the electron correlation in many-body systems. In its single reference implementation, it essentially utilizes the Hartree–Fock molecular orbital wavefunctions as the references to generate the excited configurations to account for electron correlation.

The wavefunction of the coupled-cluster theory is written as an exponential ansatz (2.7):

$$|\Psi\rangle = e^{\hat{T}}|\Phi_0\rangle \qquad (2.7)$$

where $|\Phi_0\rangle$ is a Slater determinant usually constructed from Hartree–Fock molecular orbitals. $\hat{T}$ is an excitation operator which, when acting on $|\Phi_0\rangle$, produces a linear combination of excited Slater determinants.

The cluster operator is written in the form (2.8):

$$\hat{T} = \hat{T}_1 + \hat{T}_2 + \hat{T}_3 + \ldots \qquad (2.8)$$

in which $\hat{T}_1$ is the operator of all single excitations, $\hat{T}_2$ is the operator of all double excitations and so forth. The exponential operator $e^{\hat{T}}$ may be expanded into a Taylor series (2.9):

$$e^{\hat{T}} = 1 + \hat{T} + \frac{\hat{T}^2}{2!} + \ldots = 1 + \hat{T}_1 + \hat{T}_2 + \frac{\hat{T}_1^2}{2} + \hat{T}_1\hat{T}_2 + \frac{\hat{T}_2^2}{2} \qquad (2.9)$$

This series is however finite in practice because the number of occupied molecular orbitals is finite, as well the number of excitations. In order to simplify the task for finding the coefficients, the expansion of $\hat{T}$ into individual excitation operators is terminated at the second or slightly higher level of excitation (rarely exceeding four). Accordingly, there are various orders of the CC expansion, called CCSD, CCSDT, and so on. Advanced coupled-cluster methods such as the CCSDT and CCSDTQ can be used only for high-accuracy calculations of small molecules as they are very computer-time demanding. The most popular method is the CCSD(T) which includes all the single and double excitations of electrons plus a perturbative treatment of the triple excitations. The triple excitations are determined from MP4SDTQ perturbation theory calculations, rather than variationally evaluated as in the full CCSDT (with iterative convegence), and this is much less time consuming. The coupled-cluster CCSD(T) theory is used in the composite G4 method and the complete basis set (CBS) method.

2.2.2 The Composite G4 method.

The G4 approach is the latest version the Gaussian-X (GX) method initiated by Pople and coworkers.[14] This is also a composite technique in which a sequence of molecular orbital (MO) calculations is performed to arrive at an improved total electronic energy of a given molecular species. In the G4 protocol, the equilibrium structure is first determined at the (U)B3LYP/6-31G(2df,2p) level, instead of the (U)MP2/6-31G(d) as in the G3 method, or (U)B3LYP/6-31G(d) in the G3B3 method, and subsequently used to calculate harmonic vibrational frequencies at the same level. The frequencies are then scaled by a uniform factor of 0.9854 to take the known deficiencies at this level for this property into account. These scaled vibrational frequencies give also the zero-point energies E(ZPE) that are used to obtain the zero-point corrections to the total energies. Then, a series of single-point electronic energies calculations are subsequently carried out at higher levels of MO theory including the MP4(FC)/6-31G(d), MP4(FC)/6-31+G(d), MP4(FC)/6-31G(2df,p), CCSD(T,FC)/6-31G(d), MP2(FU)/G4Large to improve the accuracy of the total electronic energies. Generally, the G4 energy is given as (2.10):

$$E_0(\text{G4}) = E(\text{CCSD(T)/6-31G(d)} + E(\text{plus}) + E(\text{2df,p}) + E(\Delta\text{G3LXP}) + \Delta E(\text{HF}) + E(\text{SO}) + E(\text{HLC}) + E(\text{ZPE}) \quad (2.10)$$

The corrections are calculated as follows:

i) The correction for diffuse functions E(plus):

$$E(\text{plus}) = E(\text{MP4/6-31+G(d)}) - E(\text{MP4/6-31G(d)}) \quad (2.11)$$

ii) The correction for higher polarization functions E(2df,p):

$$E(\text{2df,p}) = E(\text{MP4/6-31+G(2df,p)}) - E(\text{MP4/6-31G(d)}) \quad (2.12)$$

iii) The E(ΔG3LXP) is a correction for larger basis set effects and for non-additivity caused by the assumption of separate basis set extensions for diffuse and higher polarization functions:

$$E(\Delta G3LXP) = E(MP2(full)/G3LargeXP) - E(MP2/6\text{-}31G(2df,p)) - E(MP2/6\text{-}31+G(d)) + E(MP2/6\text{-}31G(d)) \quad (2.13)$$

iv) The Hartree-Fock energy limit ΔE(HF/limit), the new step in G4 method, is calculated. The HF basis set limit is determined using a linear two point extrapolation scheme and the Dunning aug-cc-pVnZ basis set:

$$E(\text{HF/aug-cc-pV}nZ) = E(\text{HF/limit}) + B\exp(-\alpha n) \quad (2.14)$$

where n is number of contractions in valence shell of the basis set and α is an adjustable parameter. Then, the ΔE(HF) is calculated as difference between E(HF/limit) and E(HF/G3LargeXP):

$$\Delta E(\text{HF}) = E(\text{HF/limit}) - E(\text{HF/G3LargeXP}) \quad (2.15)$$

v) The spin-orbit correction E(SO), that is included for atomic species only, is also taken from either experiment or more accurate theoretical calculations.

vi) The empirical HLC term is added to take into account the remaining inherent deficiencies in the energy calculations:

For closed-shell molecules: $E(\text{HLC}) = -An_\beta$

For open-shell molecules: $E(\text{HLC}) = -A'n_\beta - B(n_\alpha - n_\beta)$

For atoms: $E(\text{HLC}) = -Cn_\beta - B(n_\alpha - n_\beta)$ (2.16)

where the A, A', B, C, D, values are chosen to give the smallest mean absolute deviation from experiment for the G3/05 test set. For G4 theory, A = 6.9471 mhartrees, A' = 7.1282 mhartrees, B = 2.4409 mhartrees, C = 7.1159 mhartrees and D = 1.4143 hartrees. The energy units are: 1 a.u. = 1 hartree = 627.5 kcal/mol = 2625 kJ/mol = 27.12 eV). The n_α and n_β are number of α and β valence electrons, respectively ($n_\alpha \geq n_\beta$). In addition, when molecular and atomic species only contain one pair of s electrons, and extra parameter is added to correct for the energy of pairs of electrons (E = 2.745 mhartrees), and,

vii) finally, E(ZPE), determined as above, is added.

Let us mention that the main difference between the earlier G3, G3B3... methods with G4 is that in G3 protocols, the quadratic configuration interaction QCISD(T) method is used to provide the basic total energies. A potential problem in this composite method concerns the evaluation of ZPEs. As stated above, the ZPE's are scaled using a uniform scaling factor (0.9854) which could be inadequate for some clusters. In a way, the ZPE values constitute a source of error in the TAE evaluation.

2.2.3 The Complete basis set approach (CCSD(T)/CBS)

In the complete basis set approach, electronic energies are calculated using the restricted/unrestricted coupled-cluster R/UCCSD(T) formalism (ROHF followed by UCCSD) with the correlation consistent aug-cc-pV*n*Z (aV*n*Z, *n* = D, T, Q, 5...) basis sets.[15] The CCSD(T) total energies are then extrapolated to the CBS limit energies using expression (2.17):

$$E(x) = E_{CBS} + B\exp[-(x-1)] + C\exp[-(x-1)^2] \qquad (2.17a)$$

where x = 2, 3 and 4 for the aV*n*Z basis, n = D, T and Q, respectively, and

$$E(x) = E_{CBS} + B/x^3 \qquad (2.17b)$$

where x = 4 and 5 for the aV*n*Z basis, n = Q and 5, respectively.

Depending on the size of molecules and computational resources, either equation 2.17a or 2.17b could be employed. Subsequently, a number of corrections should be included in the TAE evaluation. As in the G4 method, the most important corrections are the ZPEs, that are calculated from either CCSD(T)/aug-cc-pVnZ (n = D, T) at CCSD(T) optimize geometries when possible, or from DFT harmonic vibrational frequencies at corresponding equilibrium geometries.

Core-valence corrections (ΔE_{CV}) that are related to the correlation energies of core electrons, are obtained at the CCSD(T)/cc-pwCVTZ level[16] from the differences of total energies with full and frozen core electrons.

Douglas-Kroll-Hess (DKH) scalar relativistic corrections ($\Delta E_{DKH\text{-}SR}$), which account for changes in the relativistic contributions to the total energies of the

molecule and the constituent atoms, are calculated using the spin-free, one-electron DKH Hamiltonian.[17] $\Delta E_{DKH\text{-}SR}$ is defined as the difference in the atomization energy between the results obtained from basis sets re-contracted for DKH calculations and the atomization energy obtained with the normal valence basis set of the same quality. The DKH calculations are obtained as the differences of the results from the CCSD(T)/aug-cc-pVTZ and the CCSD(T)/aug-cc-pVTZ-DK levels of theory.

Finally, spin-orbit (SO) corrections of the atoms are obtained from the excitation energies of Moore[18] is used. For example, a value of 1.8 kJ/mol (0.43 kcal/mol) is taken for the Si atom. These corrections are relatively small but when taking their sum, they become non-negligible for a large cluster in the effort to attain a high accuracy of the TAEs.

2.2.4 Total Atomization Energies (TAE)

In the CCSD(T)/CBS protocol, the total atomization energy (ΣD_0 or TAE) of a compound is given by (2.18):

$$\Sigma D_0 = \Delta E_{elec}(CBS) + \Delta E_{CV} + \Delta E_{DKH\text{-}SR} + \Delta E_{SO} - \Delta E_{ZPE} \qquad (2.18)$$

By combining our computed ΣD_0 values from either the G4 and CCSD(T)/CBS calculations, with the experimental heat of formation at 0 K for the element Si, we can derive the enthalpy of formation $\Delta_f H°$ values at 0 K for the molecules in the gas phase (2.19):

$$TAE(M_n) = n.\Delta H_f(M) - \Delta H_f(M_n) \qquad (2.19)$$

It has been established that tight *d* functions (Gaussian functions with small exponents) can be necessary for calculating accurate atomization energies for second-row elements (cf. ref. 19 and references therein). Thus, for some systems, we also include a set of tight *d* functions for Si in the correlation consistent basis sets denoted as aug-cc-pV(n+*d*)Z, or in a simpler notation as aV(n+*d*)Z. Single-point CCSD(T) electronic energy calculations are carried out using the aV(n+*d*)Z basis sets, with n = 2, 3, 4 and/or 5, at optimized geometries. The final total valence electronic energies are again extrapolated to the complete basis set using equation (2.17).

As mentioned above, geometry optimizations and vibrational calculations of the structures located are performed using either DFT methods with the popular hybrid (U)B3LYP functional, or using the (U)CCSD(T)/aug-cc-pVnZ method where possible. B3LYP geometries and vibrational frequencies are also parts of the original composite G4 approach[20] but with the 6-31G(2df,p) basis set. It has been established that the B3LYP functional behaves well for Si clusters. CCSD(T)/CBS computations are only carried out for small clusters, simply due to the computational expenses that go beyond our actual computational resources.

2.3. TOTAL ATOMIZATION ENERGIES, HEATS OF FORMATION AND THERMOCHEMICAL PARAMETERS OF SMALL SILICON CLUSTERS AND THEIR IONS USING G4 AND CBS METHODS

Extensive investigations have been performed on Si clusters using various experimental methods[21,22,23,24,25,26,27,28,29,30,31,32,33,34,35] and quantum chemical computations.[36,37,38,39,40,41,42] The molecular structure and some spectroscopic signatures,[24,25] as well as the energetic parameters such as ionization energies (IE) and electron affinities (EA), of the small silicon clusters, Si_n with $n \leq 20$, have been relatively well determined.[23,26] On the contrary, their standard heats of formation ($\Delta_f H$), the key thermochemical parameters, are not established yet, even though total atomization energies (TAE) were determined for some small Si_n species (n up to 8),[28,29,30,31,32,33,34] because the heat of formation of the silicon element is not well determined yet.[34]

For the silicon element, an earlier value of $\Delta_f H_{298.15}(Si,g) = 455.6 \pm 4.2$ kJ/mol was tabulated in 1973 by Hultgren *et al.*[43] In their 1995 papers, Rocabois and coworkers[28,29] reviewed the values of $\Delta_f H(Si)$ reported from 1954 and according to their list, there have been not less than twelve different values determined using the second law of thermodynamics, and twenty one values from the third law, and these values range from 412.6 ± 5.9 to 468.6 ± 12.6 kJ/mol. These authors[28] proposed after careful evaluation a value of 445.3 ± 5 kJ/mol. In the 1998 JANAF database,[44] a value of $\Delta_f H_{298.15}(Si) = 450 \pm 8$ kJ/mol was selected, and the latter value, which is apparently the average of the two values given above, was chosen in the NIST

Chemistry Web Book.[45] Other theoretical values for the atomic heat of formation (0 K) include 452.3 ± 2.1 kJ/mol[46] and 449.3 ± 2.5 kJ/mol.[47]

When determining the heats of formation of Si_7 and Si_8 from their experimental TAEs, Meloni and Gingerich[34] pointed out the large difference (up to 73-83 kJ/mol) derived from two different values for $\Delta_f H$(Si), and summarized quite well the acute problem encountered: 'Evidently, the choice of the enthalpy of sublimation of silicon makes a significant difference on the $\Delta_f H_{298.15}(Si_n,g)$ values' (ref. 34, page 5474).

More recently, Karton and Martin[48] carefully re-examined the heat of formation of the Si element by means of high-accuracy quantum chemical computations on a few selected Si-compounds whose experimental data were well established, and accordingly proposed the value of 448.5 ± 0.8 kJ/mol (107.2 ± 0.2 kcal/mol). This value appeared fortuitously to be an average of the values of Rocabois *et al.*[28] and JANAF/CODATA[44] mentioned above. In this work, we used the latter value for the heat of formation for the atomic silicon.

In this work, we set out to determine first the TAEs using quantum chemical computations. Together with the atomic heat of formation, the values of the Si_n molecules, with n = 2 – 13, can subsequently be derived. We consider not only the neutral clusters but also their positive (Si_n^+) and negative (Si_n^-) ions. A consistent set of thermochemical parameters are thus determined using the composite G4 method, and for the smaller systems, a further calibration is also done using the coupled-cluster theory with complete basis set CCSD(T)/CBS protocol.

All electronic structure calculations are carried out using the Gaussian 09[49] and Molpro 2008[50] suites of programs. Geometries of the small Si_n, n = 2 – 13, clusters have been well established in the literature. However, we carry out additional searches for possible lower-lying isomers of each of the Si_n size considered, in particular for the ions, using a stochastic search algorithm.[51]

2.3.1 Shape of the lowest-lying isomers of Si_n clusters and their ions

n	Si_n^- a.*n*	Si_n n.*n*	Si_n^+ c.*n*
2	 $^2\Sigma_g$, $D_{\infty h}$	 $^3\Sigma_g^-$, $D_{\infty h}$	 $^4\Sigma_g^+$, $D_{\infty h}$
3	 $^2A_1$, C_{2v}	 $^1A_1$, C_{2v}	 $^2B_2$, C_{2v}
4	 $^2B_{2g}$, D_{2h}	 ^1A_g, D_{2h}	 $^2B_{2g}$, D_{2h}
5	 $^2A''_2$, D_{3h}	 $^1A'_1$, D_{3h}	 $^2A_1$, C_{2v}
6	 $^2B_2$, C_{2v}	 $^1A_1$, C_{2v}	 $^2B_1$, C_{2v}
7	 $^2A''_2$, D_{5h}	 $^1A'_1$, D_{5h}	 $^2A_1$, C_{2v}
8	 $^2B_1$, C_{2v}	 ^1A_g, C_{2h}	 $^2B_1$, C_{2v}
9	 ^2A, C_1	 $^1A'$, C_s	 $^2A_1$, C_{2v}
10	 $^2A_1$, C_{3v}	 $^1A_1$, C_{3v}	 ^2A, C_1
11	 $^2A'$, C_s	 $^1A'$, C_s	 $^2A'$, C_s
12	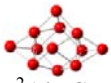 $^2A'$, C_s	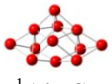 $^1A'$, C_s	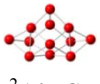 $^2A'$, C_s
13	 $^2A'$, C_s	 $^1A_1$, C_{2v}	 $^2B_2$, C_{2v}

Figure 2.1. Shapes of the lowest-lying isomers of Si_n in the neutral (**n.*n***, middle), cationic (**c.*n***, right) and anionic (**a.*n***, left) states.

Let us first briefly describe the geometries of the small Si_n clusters considered. Their positive and negative ions were well determined and abundantly discussed in the relevant literature,[36,37,38,39,40,41,42] and thus do not warrant additional description. In order to specify the structures actually computed in the present work, we display in Figure 2.1 the shapes of the equilibrium structures of the lowest-lying isomers of each size in the neutral, cationic and anionic states, together with their symmetry point group and electronic state. As for convention, each structure is labeled by **x.*n*** where **x** = **a** (anion), **n** (neutral) or **c** (cation) and ***n*** = the actual size of the cluster ranging from 2 to 13 (cf. Figure 2.1).

It is confirmed that for these sizes, no low-energy structure with endohedrally located Si atom within a Si cage is located. The neutral geometry is distorted, as expected, following electron attachment and detachment, in particular in the larger sizes. However, no structural rearrangement or disruption really occurs, except for n = 13. Each of the ionic structures is characterized by a low spin (doublet) ground state.

The shape of the neutral **n.13** remains unchanged following electron removal giving the cation **c.13**, but a strong geometrical relaxation however occurs upon electron attachment yielding the anion **a.13** (Figure 2.1). The anion shape in fact differs significantly from that of the neutral and cationic counterparts.

2.3.2 Total atomization energies (TAE)

Table 2.1 lists the different components obtained in the CCSD(T)/CBS protocol (referred hereafter as CBS) to predict the total atomization energies (ΣD_0, TAE) of Si_n clusters for n = 2 – 6, using the aVnZ (denoted as CBS(1)) and aV(n+d)Z (CBS(2)) basis sets. Table 2.2 summarizes the calculated TAE's of the neutrals, whereas Table 2.3 lists the heats of formation ($\Delta_f H^o$) at both 0 and 298 K derived from TAE's calculated using both G4 and CBS protocols. For the latter, computations for the cations and anions are also carried out using the computed ionization energies and electron affinities. For the purpose of comparison, available experimental values[28,29,30,31,32,33,34] for both quantities of the neutrals Si_n with n = 2 – 8 are also given in Tables 2.2 and 2.3.

The inclusion of the tight *d* functions causes some small reductions of the TAEs. The calculated CBS(1) TAEs without tight *d* polarization function differ up to 6 kJ/mol from the CBS(2) values including these functions (Table 2.2). This significant deviation demonstrates again the importance of tight polarisation functions in treatment of systems having multiple second-row atoms.

Table 2.1: Total atomization energy (TAE) (kJ/mol) for the neutral Si_n (n = 2 – 6) and different components of the CCSD(T)/CBS protocols.

n	CBS(1)[a]	CBS(2)[b]	E_{ZPE}[c]	ΔE_{CV}[d]	ΔE_{SR}[e]	ΔE_{SO}[f]	TAE(1)	TAE(2)
2	312.6	318.3	3.24	1.17	-0.39	-3.6	306.5	312.2
3	729.2	727.9	7.41	2.83	-1.35	-5.4	717.8	716.5
4	1177.7	1175.6	12.22	5.01	-2.22	-7.2	1161.1	1159.0
5	1577.7	1574.4	17.58	8.28	-2.50	-9.0	1556.9	1553.6
6	2023.8	2018.9	21.02	11.49	-3.44	-10.8	2000.0	1995.1

[a)] Based on CCSD(T) energies extrapolated using equation (2.15b) with aug-cc-pVQZ and aug-cc-pV5Z basis sets at CCSD(T)/aug-cc-pVTZ optimized geometries. This gives TAE(1) values.

[b)] Based on CCSD(T) energies extrapolated using equation (2.15b) with aug-cc-pV(Q+*d*)Z and aug-cc-pV(5+*d*)Z basis sets at CCSD(T)/aug-cc-pVTZ optimized geometries. This gives TAE(2) values.

[c)] Zero point energies taken from CCSD(T)/aug-cc-pVTZ harmonic vibrational frequencies.

[d)] Core-valence corrections obtained with the aug-cc-pwCVTZ basis sets at CCSD(T) geometries.

[e)] Scalar relativistic corrections based on CCSD(T)-DK/aug-cc-pVTZ-DK calculations and expressed relative to CCSD(T) results without the DK corrections.

[f)] Corrections due to the incorrect treatment of the atomic asymptote as an average of spin multiplets. Values based on C. Moore's Tables (ref.18).

Table 2.2: Total atomization energy (TAE) of the lowest-lying isomers of the neutral Si_n, (n = 2 – 13) using G4 and CCSD(T)/CBS approaches.

Structure	TAE (kJ/mol)			
	G4	**CBS(1)**	**CBS(2)**	**Exptl.** [a]
n.2 ($^3\sum_g^-$, $D_{\infty h}$)	311.6	306.5	312.2	319 ± 7
n.3 ($^1A_1$, C_{2v})	723.9	717.8	716.5	705 ± 16
n.4 (^1A_g, D_{2h})	1164.9	1161.1	1159.0	1151 ± 22
n.5 ($^1A'_1$, D_{3h})	1577.1	1556.9	1553.6	1559 ± 24
n.6 ($^1A_1$, C_{2v})	2021.7	2000.0	1995.1	1981 ± 32
n.7 ($^1A'_1$, D_{5h})	2446.2			2381 ± 36
n.8 (^1A_g, C_{2h})	2729.1			2735 ± 65
n.9 ($^1A'$, C_s)	3172.2			
n.10 ($^1A_1$, C_{3v})	3660.0			
n.11 ($^1A'$, C_s)	3946.7			
n.12 ($^1A'$, C_s)	4340.9			
n.13 ($^1A_1$, C_{2v})	4682.9			

[a] Experimental values taken from refs. 30 for Si_2, Si_3, and Si_4, 32 for Si_5, 33 for Si_6, and 34 for Si_7 and Si_8.

Of the G4 and CBS TAE values, the CBS(2) is the smaller one, except for Si_2 (Table 2.2). The G4 and CBS(1) TAE values for the neutral species differ by 5, 6 and 4 kJ/mol for Si_2, Si_3 and Si_4, respectively. The deviations are larger for Si_5 (20 kJ/mol) and Si_6 (22 kJ/mol) (Table 2.2). The deviations between G4 and CBS(2) TAEs are even larger. Such a difference can in part be attributed to the inherent treatment of the Si atom in each protocol and the one-electron basis sets used. All calculated TAEs compare relatively well with experimental data when the large error bars of the reported experimental data are taken into account (Table 2.2).

For small species where a comparison is possible, some relevant points can be presented as follows:

- **n.2**: Computed values are apparently underestimated, but the G4 and CBS(2) values of TAE(Si_2) = 312 kJ/mol is closer to the experimental one of 319 ± 7

kJ/mol [28,30] than the CBS(1) counterpart of 307 kJ/mol. The non-corrected (electronic) CBS(2) value of 318 kJ/mol for Si_2 listed in Table 2.1 is nearly identical with that reported earlier by Feller *et al.*[52] also using CCSD(T)/CBS but with basis set up to aug-cc-pV(6+*d*)Z. In fact, these authors derived a value of 314 kJ/mol for TAE(Si_2) including a correction of 2 kJ/mol for the higher-order correlation. If this correction of 2 kJ/mol is included, we thus obtain the same value as the latter authors in ref. 52 for TAE(Si_2).

- **n.3**: values TAE(Si_3) = 724 (G4) and 718 (CBS(1)) and 717 kJ/mol (CBS(2)) are overestimated with respect to the experimental result of 705 ± 16 kJ/mol [28,30] even though they are close to the upper limit of the error margin. Let us mention that for the triatomic neutral Si_3, our CBS results point out that both singlet ($^1A_1$) and triplet ($^3A'_2$) states are energetically degenerate. Previous studies[35] found a singlet ground state with a small singlet-triplet separation of about 4 kJ/mol.

- **n.4**: both computed values of 1165 (G4) and 1161 (CBS(1)) and 1159 kJ/mol (CBS(2)) for TAE(Si_4) are again overestimated but still within the upper error margin of the experimental of 1151 ± 22 kJ/mol.[28,31]

- **n.5**: the good agreement for TAE(Si_5), between 1557 kJ/mol by CBS(1) and 1559 ± 24 kJ/mol by experiment[28,32] appears to be fortuitous, in view of the fact that the values of 1577 (G4) and 1554 kJ/mol (CBS(2)) are further deviated, even though they still within the error bar of the experimental result.

- **n.6**: the TAE(Si_6) = 1995 kJ/mol derived by CBS(2) appears to be closer to the experimental data of 1981 ± 32 kJ/mol[28] than the G4 counterpart of 2022 kJ/mol.

- **n.7** and **n.8**. A disparate behavior of G4 values emerges. While the TAE(Si_7) = 2446 kJ/mol is not consistent with experiment, being 2381 ± 36 kJ/mol,[34] the TAE(Si_8) = 2729 kJ/mol compares better with the experimental result of 2735 ± 65 kJ/mol.[34] Note that both experimental values were determined using the same Knudsen cell mass spectrometric techniques. In view of the large error margin, the agreement for Si_8 appears again fortuitous.

For the larger Si_n with n = 9-13, the corresponding TAEs can now only be predicted by G4 results as summarized in Table 2.2 Overall, the CBS(2) results (Table 2.2) represent the best values we have obtained so far for this series. The large difference between G4 and CBS TAE values is disappointing. As the deviation tends to increase with increasing cluster size, a difference of at least 40 kJ/mol can be expected for the sizes n > 10. In this context, accurate determination of TAEs for small silicon clusters remains a challenge for quantum chemical computations. Protocols using appropriate working reactions, in which the errors of energies in both sides could mutually be cancelled, could provide more balanced results, but such reactions are not readily available.

2.3.3 Heats of formation ($\Delta_f H^o$)

Calculated results are summarized in Table 2.3. As this parameter of each species is directly derived from its TAE and the $\Delta_f H^o$(Si), the deviations discussed above for the TAEs will further be propagated. In addition, the discrepancy also arises from the value actually used for the element $\Delta_f H^o$(Si) (see above). Due to the involvement of the latter quantity, the deviation, as expected, increases with increasing cluster size. As a matter of fact, with an error of, for example, 5 kJ/mol, the atomic value $\Delta_f H^o$(Si) invariably induces an error of 5n kJ/mol on the molecular parameter of Si_n. We can however note some reasonable agreements between both CBS and experimental values, as for Si_3, Si_4 and Si_6, but the deviations turn out to be more substantial for Si_2 and Si_5.

As in the case for TAEs, the G4 values for Si_7 and Si_8 differ much from experiment for which the uncertainties reported are equally quite large (Table 2.3). Accordingly, the deviation for Si_7 amounts up to 45 kJ/mol, which is close to the upper bound of the error margin of ± 36 kJ/mol.[34]

Table 2.3: Heats of formation at 0K [$\Delta_f H$ (0 K)] and 298K [$\Delta_f H$ (298 K)] (kJ/mol) of the lowest-lying isomers of the neutral Si_n using G4 and CCSD(T)/CBS approaches

n	G4 (0K)	CBS(1) (0K)	CBS(2) (0K)	G4 (298K)	CBS(1) (298K)	CBS(2) (298K)	Exptl.[a] (298K)
2	585.5	590.5	584.8	588.3	593.4	587.7	575.5 ± 9.4
3	621.7	627.8	629.0	624.7	630.7	632.0	631.3 ± 7.9
4	629.3	633.0	635.1	632.8	636.5	638.7	634.8 ± 8.3
5	665.5	685.8	689.0	669.0	689.0	692.3	661.3 ± 10.3
6	669.4	691.1	696.05	674.6	696.3	701.2	702.8 ± 18.3
7	693.5			698.5			743 ± 36
8	859.1			866.0			837 ± 65
9	864.6			872.2			
10	825.3			832.7			
11	987.0			996.2			
12	1041.4			1050.9			
13	1148.2			1157.5			

[a] Experimental values taken from refs. 29 for Si_2 and Si_3, Si_4, Si_5, and Si_6, ref. 34 for Si_7 and Si_8.

2.3.4 Electron affinities (EA) and ionization energies (IE)

The adiabatic EA of each neutral Si_n is calculated as the difference between the heats of formation of both corresponding neutral and anionic clusters at the same computational method. Similarly, the adiabatic IE is derived calculated from the heats of formation of the corresponding neutral and cationic structures. Calculated results are given in Table 2.4, together with available experimental values.[21,26,53,54,55,56,57]

Results obtained for TAEs using both sets of CBS are similar. To simplify the presentation of data, only the CBS(1) values are listed in Table 2.4. Differences of a few hundredths of an eV (1 eV = 96.49 kJ/mol) between G4 and CBS(1) values can be noticed. Both sets of predictions are also in good agreement with available experimental data, with deviations < 0.1 eV (Table 2.4). Let us note that previous DFT/B3LYP computations also gave rise to reasonable IEs for Si_n clusters.[26] A

mutual cancellation of errors on the energies of both neutral and cationic forms is apparently occurred yielding better relative energetic quantities.

Table 2.4. Adiabatic electronic affinities (EA) and ionization energy (IE) of Si_n clusters, n = 2 – 13 (G4 and CCSD(T)/CBS(1)).

	EA, eV			IE, eV		
n	G4	CBS(1)	Exptl.[a)]	G4	CBS(1)	Exptl.[b)]
2	2.29	2.23	2.20 ± 0.01	7.89	7.85	7.92 ± 0.05
3	2.31	2.31	2.29 ±0.002	8.29	8.12	8.12 ± 0.05
4	2.18	2.14	2.13 ±0.001	8.00	7.95	8.20 ± 0.10
5	2.50	2.47	2.59 ± 0.02	8.17	8.09	7.96 ± 0.07
6	2.15	2.09	2.08 ± 0.14	7.76	7.71	7.80 ± 0.10
7	1.92		1.85 ± 0.02	8.02		7.80 ± 0.10
8	2.56		2.36 ± 0.10	7.11		
9	2.18		2.31 ± 0.25	7.72		
10	2.35		2.29 ± 0.05	7.95		
11	2.55		2.5	6.70		
12	2.49		2.6	7.39		
13	3.34			6.80		

[a)] Experimental values taken from refs. 53,54 for Si_2, 55 for Si_3, Si_4, Si_5, and Si_7, 56 for Si_6, Si_8, and Si_{10}, 57 for Si_9, 21 for Si_{11} and Si_{12}.

[b)] Experimental values taken from refs. 26 for Si_2, Si_3, Si_4, Si_5, Si_6, and Si_7.

Figure 2.2 schematically illustrates the comparison, and also the evolution of both EA and IE values with respect to the cluster size. Si_4, Si_5 and Si_7 are the cases bearing relatively large deviations (0.2 eV), and in opposite directions, between calculated and measured IEs. On the contrary, calculated EAs for these sizes appear to be more consistent with experiment. Therefore they warrant some additional evaluations.

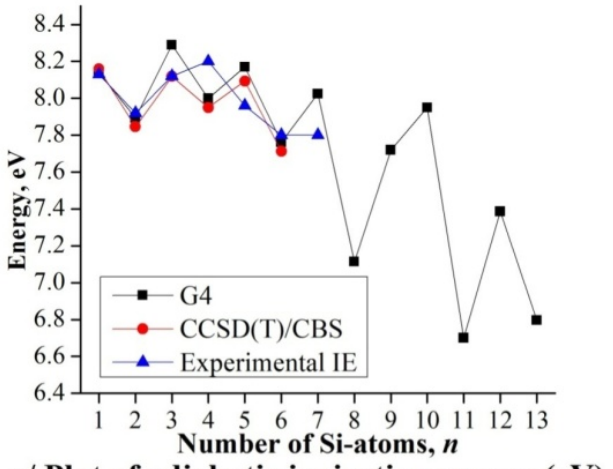

a/ Plot of adiabatic ionization energy (eV)

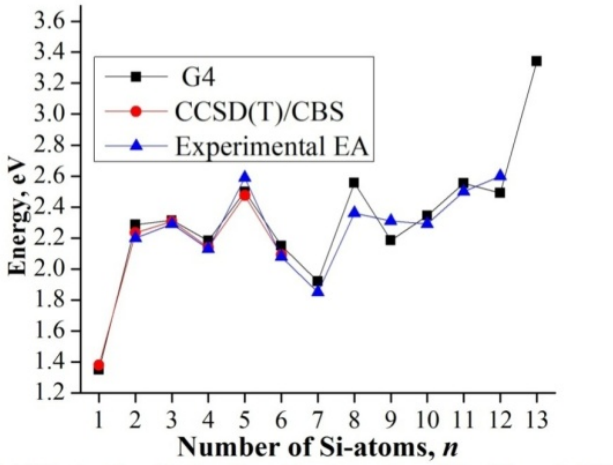

b/ Plot of adiabatic electronic affinities (eV)

Figure 2.2. Comparison and evolution of adiabatic ionization energies (IE) and electron affinities (EA) of Si_n clusters obtained using G4 and CCSD(T)/CBS approaches and experiment.

We point out above for Si_7 a large deviation of 45 kJ/mol of its G4 heat of formation relative to available experiment (Table 2.3). The G4 value for $EA(Si_7)$ = 1.92 eV turns out to be comparable to the experimental result of 1.85 ± 0.02 eV.[55] On

the contrary, the G4 value for IE(Si_7) = 8.02 eV represents the largest overestimation with respect to the experimental IE of 7.80 ± 0.10 eV.[26]

For the tetratomic system, a similar situation can be noted. Both calculated values of 2.18 (G4) and 2.14 eV (CBS) are close to the experimental EA of 2.13 eV[55] (Table 2.4). Again, the predictions of 8.00 (G4) and 7.95 eV (CBS) for IE(Si_4) correspond to the largest underestimation as compared to the experimental IE of 8.20 ± 0.10 eV.[26]

The EA and IE values for the pentatomic system follow a comparable pattern including a good G4 prediction for EA (2.50 *vs.* 2.59 eV), but a less good G4 IE (8.15 *vs.*7.96 eV). Overall, an error margin of, at most, ± 0.15 eV could be estimated on the G4 values for EAs and IEs of silicon clusters (Table 2.4). The EA of the element for which an experimental result is missing, can be predicted as EA(Si) = 1.35 ± 0.10 eV.

2.3.5 Average binding energies and dissociation energies of clusters

The relative stability of the Si_n clusters can be approached by using energetic parameters such as the average binding energy (E_b), and dissociation energy. The former properties can be defined as follows (equations 2.20, 2.21 and 2.22):

$$E_b(Si_n) = [(n)E(Si) - E(Si_n)]/n \quad (2.20)$$

$$E_b(Si_n^-) = [(n-1)E(Si) + E(Si^-) - E(Si_n^-)]/n \quad (2.21)$$

$$E_b(Si_n^+) = [(n-1)E(Si) + E(Si^+) - E(Si_n^+)]/n \quad (2.22)$$

where $E(Si)$, $E(Si_n)$, $E(Si_n^-)$, and $E(Si_n^+)$ are the G4 total energies of Si atom, neutral, anionic, and cationic Si_n cluster, respectively. The plots of their evolution are displayed in Figure 2.3.

The average binding energy (E_b) of cationic, neutral and anionic clusters uniformly increases with increasing size (Figure 2.3). The E_b values of smaller anionic clusters ($n \leq 6$) are slightly larger than those of corresponding neutral Si_n or cation Si_n^+. However, at larger sizes in ionic and neutral states, the E_b values are approximately close to each other, even though for $n \geq 13$, the E_b values of ions $Si_n^{+/-}$ tend to be somewhat larger than those of the neutral Si_n.

Table 2.5. Average binding energies (E_b) of Si_n^-, Si_n and Si_n^+, n = 2-13 (eV), using G4 and CCSD(T)/CBS(1) approaches.

n	$E_b(Si_n^-)$		$E_b(Si_n)$		$E_b(Si_n^+)$	
	G4	CBS	G4	CBS	G4	CBS
2	2.08	2.02	1.61	1.59	1.74	1.75
3	2.82	2.79	2.50	2.48	2.45	2.49
4	3.23	3.21	3.02	3.01	3.05	3.06
5	3.50	3.45	3.27	3.23	3.26	3.24
6	3.63	3.57	3.49	3.45	3.56	3.53
7	3.70		3.62		3.64	
8	3.69		3.54		3.66	
9	3.75		3.65		3.70	
10	3.89		3.79		3.81	
11	3.83		3.72		3.85	
12	3.84		3.75		3.81	
13	3.89		3.73		3.84	

In order to probe further the thermodynamic stability, dissociation energies (D_e) for various fragmentation channels of Si clusters are considered. The dissociation energy for the channel (2.23) of the cluster:

$$Si_n^{+/0/-} \rightarrow Si + Si_{n-1}^{+/0/-} \qquad (2.23)$$

is defined in equation (2.24) where $\Delta_f H^0$ are enthalpies of formation at 0 K of the relevant clusters, respectively:

$$D_e(Si_n^{+/0/-}) = \Delta_f H^0(Si) + \Delta_f H^0(Si_{n-1}^{+/0/-}) - \Delta_f H^0(Si_n^{+/0/-}) \qquad (2.24)$$

Table 2.6. Dissociation energies (D_e) of Si_n^-, Si_n and Si_n^+, n = 2-13 (eV), using G4 and CCSD(T)/CBS(1) approaches.

n	$D_e(Si_n^-)$		$D_e(Si_n)$			$D_e(Si_n^+)$	
	G4	CBS	G4	CBS	Exptl.[a)]	G4	CBS
2	4.17	4.03	3.23	3.18	3.21	3.48	3.49
3	4.30	4.34	4.27	4.26	4.09	3.88	3.99
4	4.44	4.43	4.57	4.59	4.60 ±0.15	4.86	4.76
5	4.59	4.44	4.27	4.10		4.10	3.96
6	4.26	4.21	4.61	4.59		5.02	4.97
7	4.17		4.40			4.14	
8	3.57		2.93			3.84	
9	4.22		4.59			3.99	
10	5.22		5.06			4.83	
11	3.18		2.97			4.22	
12	4.02		4.09			3.40	
13	4.39		3.54			4.13	

[a)] Experimental values taken from refs. 58 for $D_e(Si_2)$, 59 for $D_e(Si_3)$ and 60 for $D_e(Si_4)$.

The calculated and experimental results listed in Table 2.6 point out a good agreement. The smallest D_e values are found for the fragmentation channels (2.23). This indicates that a Si_n cluster, irrespective of its charge state, prefers to decompose forming the immediately smaller cluster Si_{n-1} plus the atomic Si counterpart. An odd-oven oscillation is not always found for the plots of these fragment channels (Figure 2.3). The Si_{10} system reveals maximum local peaks in all charge states, in agreement with previous findings. For both neutral and cationic clusters, the sizes of 4 and 6 are more stable than their neighbours.

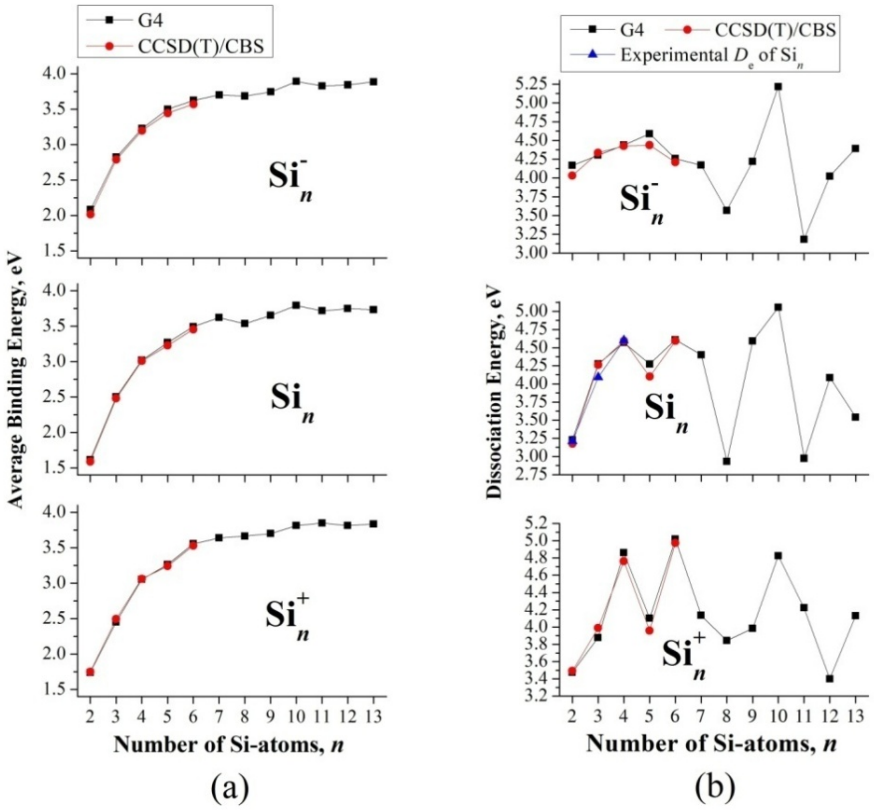

Figure 2.3. **a**) Evolution of average binding energies (E_b) of Si_n clusters; and **b**) Evolution of dissociation energy $D_e(Si_n^{+/0/-}) = \Delta H_f^0(Si) + \Delta H_f^0(Si_{n-1}^{+/0/-}) - \Delta H_f^0(Si_n^{+/0/-})$ of Si_n^+, Si_n and Si_n^- (n = 2 – 13). The values are illustrated as a function of size using G4 and CCSD(T)/CBS methods.

2.4. CONCLUDING REMARKS

In this theoretical study, we determined molecular structures and predicted a set of thermochemical properties of a series of small silicon clusters Si_n with n = 2-13 in the neutral, cationic and anionic states.

To establish the global minima we used a stochastic search method along with high accuracy quantum chemical calculations. Energetic parameters were

evaluated using both G4 and CCSD(T)/CBS energies. In the latter, calculations using basis sets without and with tight *d* polarization functions were carried out.

We determined a uniform set of standard heats of formation for the cationic and anionic Si clusters that are missing up to now, using the value for the element $\Delta_f H^o$(Si,298 K) = 451.5 kJ/mol. Differences between G4 and CBS TAE values are rather large. For these systems, experimental results in the current literature are also characterized by large uncertainties. This indicates that accurate evaluation of this basic parameter for either pure or doped silicon clusters, attaining the chemical accuracy of ± 1.0 kcal/mol or 4.0 kJ/mol, remains a great challenge for quantum chemical computations.

Relative parameters such as ionization energies and electron affinities were better predicted. The corresponding G4 results are expected to be accurate to, at most, ± 0.15 eV (± 3.0 kcal/mol or 12 kJ/mol).

Again, the average binding energy of Si cluster tends to increase with increasing size toward a certain limit. Fragmentation giving a Si atom constitutes the favoured dissociation channel. Relative to this reaction mode, an enhanced stability is found for the sizes 4, 6 and in particular 10.

References

1) P. W. Atkin, *Concepts in Physical Chemistry* (1995), Oxford University Press, U.K.

2) CODATA Task Group, *J. Chem. Thermodyn.* 10 (1978) 903.

3) K. A. Gingerich, *J. Phys. Chem.* 49 (1968) 14

4) R. Hultgren, P. D. Desai, D. T. Kawkins, M. Gleiser, K. K. Kelly, D. D. Wagman, Selected Values for the Thermodynamic Properties of the Elements, American Society of Metals, Metals Park, OH (1973).

5) J. D. Cox, G. Pilcher, Thermochemistry of Organic and Organometallic Compounds, Academic Press, London (1970).

6) L. V. Gurvic, I, V Veyts, C. B. Alcock, Thermodynamic Properties of Individual Substances, Hemisphere, New York (1991).

7) A large number of thermochemical data were compiled in the Journal of Physical Chemistry and Reference Data published by the American Chemical Society.

8) M. W. Chase, C. A. Davis, J. R. Downey, D. J. Frurip, R. A. McDonald, A. N. Syverud, JANAF Thermochemical Tables, *J. Phys. Chem. Ref. Data, Supplement 14* (1985).

9) M. W. Chase, NIST-JANAF Thermochemical Tables, J. *Phys. Chem. Ref. Data,* Monograph Nr. 9, 4th Edition, Supplement 1 (1998).

10) National Institute of Standard and Technology, Chemistry Web Book, http://webbook.nist.gov/chemistry/

11) M. Sana, M. T. Nguyen, Chem. Phys. Lett. 196 (1992) 390.

12) D. A. Ponomarev, V. V. Takhistov, J. Chem. Ed 74, (1997) 201.

13) K. A. Peterson, D. Feller, D. A. Dixon, Theor. Chem. Acc. 131 (2012) 1079.

14) a) J. A. Pople, M. Headgordon, D. J. Fox, K. Raghavachari, L. A. Curtiss, J. Chem. Phys. 90 (1989) 5622; b) L. A. Curtiss, C. Jones, G. W. Trucks, K. Raghavachari, J. A. Pople, J. Chem. Phys. 93 (1990) 2537; c) L. A. Curtiss, K. Raghavachari, G. W. Trucks, J. A. Pople J. Chem. Phys. 94 (1991) 7221; d) L. A. Curtiss, K. Raghavachari, P. C. Redfern, V. Rassolov, J. A. Pople J. Chem. Phys. 109 (1998) 7764.

15) R. A. Kendell, T. H. Dunning, R. J. Harrison, J. Chem. Phys. 96 (1992) 6796.

16) A. Halkier, T. Helgaker, P. Jørgensen, W. Klopper, H. Koch, J. Olsen, A. K. Wilson, Chem. Phys. Lett. 286 (1998) 243.

17 M. Douglas, N. M. Kroll, Ann. Phys. 82 (1974) 89.

18) C. E. Moore (1949) Atomic energy levels as derived from the analysis of optical spectra,Volume 1, H to V; U.S. National Bureau of Standards Circular 467, U.S. Department of Commerce, National Technical Information Service, COM-72-50282: Washington, D.C.

19) V. S. Nguyen, S. Swinnen, M. T. Nguyen, D. A. Dixon, J. Phys. Chem. C 113 (2009) 18914.

20) L. A. Curtiss, P. C. Redfern, K. Raghavachari, J. Chem. Phys. 126 (2007) 084108.

21) O. Cheshnovsky, S. H. Yang, C. L. Pettiette, M. J. Craycraft, Y. Liu, R. E. Smally, Chem. Phys. Lett. 138 (1987) 119.

22) A. A. Shvartsburg, B. Liu, M. F. Jarrold, K. M. Ho, J. Chem. Phys. 112 (2000) 4517.

23) A. A. Hoops, R. T. Bise, H. Choi, D. M. Neumark, Chem. Phys. Lett. 346 (2001) 89.

24) A. Fielicke, J. T. Lyon, M. Haertelt, G. Meijer, P. Claes, J. De Haeck, P. Lievens, J. Chem. Phys. 131 (2009) 171105.

25) J. T. Lyon, P. Gruene, A. Fielicke, G. Meijer, E. Janssens, P. Claes, P. Lievens, J. Am. Chem. Soc. 131 (2009) 1115.

26) O. Kostko, S. R. Leone, M. A. Duncan, M. Ahmed, J. Phys. Chem. A 114 (2010) 3176.

27) S. A. Fischer, A. B. Madrid, C. M. Isborn, O. V. Prezhdo, J. Chem. Phys. Lett. 1 (2010) 232.

28) P. Rocabois, C. Chatillon, C. Bernard, High Temp. High. Press. 27 (1995) 3.

29) P. Rocabois, C. Chatillon, C. Bernard, F. Genet, High Temp. High. Press. 27 (1995) 25.

30) R. W. Schmude, Q. Ran, K. A. Gingerich, J. E. Kingcade, J. Chem. Phys. 102 (1995) 2574.

31) R. W. Schmude, Q. Ran, K. A. Gingerich, J. Chem. Phys. 99 (1993) 7998.

32) Q. Ran, R. W. Schmude, M. Miller, K. A. Gingerich, Chem. Phys. Lett. 230 (1994) 337.

33) K. A. Gingerich, Q. Ran, R. W. Schmude, Chem. Phys. Lett. 256 (1996) 274.

34) M. Meloni, K. A. Gingerich, J. Chem. Phys. 115 (2001) 5470.

35) T. N. Kitsopoulos, C. J. Chick, Y. Zhao, D. M. Neumark, J. Chem. Phys. 95 (1991) 1441.

36) K. Raghavachari, L. A. Curtius, in Quantum Mechanical Electronic Structure Calculations With Chemical Accuracy, Ed: S. R. Langhoff, Kluwer, The Netherlands (1995).

37) C. Majumder, S. K. Kulshreshtha, Phys. Rev. B 70 (2004) 245426.

38) S. Nigam, C. Majumder, K. Kulshreshtha, J. Chem. Phys. 121 (2004) 7756; 125 (2006) 074303.

39) J. Yang, W. Xu, W. Xiao, J. Mol. Struct. Theochem, 719 (2005) 89.

40) S. Park, S. Lee, D. Neuhauser, J. Phys. Chem. A 110 (2006) 7173.

41) A. D. Zdetsis, J. Chem. Phys. 127 (2007) 244308.

42) H. u. Rehman, M. Springborg, Y. Dong, J. Phys. Chem. A 115 (2011) 2005.

43) R. Hultgren, P. D. Desai, D. T. Hawkins, M. Gleiser, K. K. Kelly, D. D. Wagman, Selected values for thermodynamic properties of the elements, American Society of Metals, Metals Park (1973).

44) M. W. Chase, Jr., NIST-JANAF Themochemical Tables, Fourth Edition, J. Phys. Chem. Ref. Data, Monograph 9 (1998), 1.

45) NIST Chemistry Web Book, http://webbook.nist.gov/chemistry/

46) R. S. Grev, H. F. Schaefer III, J. Chem. Phys. 97 (1992) 8389.

47) D. Feller, D. A. Dixon, J. Phys. Chem. A 103 (1999) 6413.

48) A. Karton, J. M. L. Martin, J. Phys. Chem. A 111 (2007) 5936.

49) M. J. Frisch, H. B. Schlegel, G. E. Scuseria, M. A. Robb, J. R. Cheeseman, J. A. Montgomery, T. Vreven, K. N. Kudin, J. C. Buran, J. M. Millam, *et al.* (2004) Gaussian 09 Revision: **B.01;** Gaussian, Inc.: Wallingford, CT, (2009).

50) H. J. Werner, P. J. Knowles, R. Lindh, F. R. Manby, M. Schütz, P. Celani, T. Korona, G. Rauhut, R. D. Amos, A. Bernhardsson, A. Berning, *et al.* (2006) MOLPRO, version 2006.1, a package of ab initio programs.

51) T. B. Tai, M. T. Nguyen, J. Chem. Theor. Comput. 7 (2011) 1119.

52) D. Feller, K. A. Peterson, D. A. Dixon, J. Chem. Phys. 129 (2008) 204105.

53) M. R. Nimlos, B. L. Harding, G. B. Ellison, J. Chem. Phys. 87 (1987) 5116.

54) C. C. Arnold, T. N. Kitsopoulos, D. M. Neumark, J. Chem. Phys. 99 (1993) 766.

55) C. Xu, T. R. Taylor, G. R. Burton, D. M. Neumark, J. Chem. Phys. 108 (1998) 1395.

56) H. Kawamata, Y. Negishi, R. Kishi, S. Iwata, A. Nakajima, K. Kaya, J. Chem. Phys. 105 (1996) 5369.

57) R. Kishi, H. Kawamata, Y. Negishi, S. Iwata, A. Nakajima, K. Kaya, J. Chem. Phys. 107 (1997) 10029.

58) K. P. Huber, G. Herzberg, Molecular Spectra and Molecular Structure, Constants of Diatomic Molecules, vol. IV, Van Nostrand Reinhold, New York, 1979.

59) D. R. Stull, H. Prophet, JANAF Thermochemical Tables, NSRDS Natl. Stand. Ref. Data Serv. Natl. Bur. Stand. No. 37 (U.S. GPO, Washington, DC, 1971)

60) A. A. Hoops, R. T. Bise, H. Choi, D. M. Neumark, Chem. Phys. Lett. 346 (2001) 89.

Chapter 3

Singly and doubly lithium doped silicon clusters: Geometrical and electronic structures and ionization energies

This chapter is adapted from the following article:

- *Singly and doubly lithium doped silicon clusters: Geometrical and electronic structures and ionization energies* by N. M. Tam, V. T. Ngan, J. de Haeck, S. Bhattacharyya, H. T. Le, E. Janssens, P. Lievens, and M. T. Nguyen, *Journal of Chemical Physics*, 136, 024301/11 (2012).

3.1. INTRODUCTION

Previous studies demonstrated that lithium (Li) behaves as an electron donor in neutral Si_nLi.[1,2,3,4] Hence, the Li atom favors adsorption on a bridge site of the corresponding Si_n cluster and the silicon framework in Si_nLi species is basically similar to that of the Si_n^- anion.[1] For the $Si_nLi^{0/-}$ (n = 1−8) series, Yang *et al*.[5] used the G3 method and found that the ground state structures of neutral Si_nLi are of adsorptive type in which Li is simply added to the Si_n clusters, whereas Si_nLi^- anions are of substitutional type. Logically, one adsorptive Li atom and one substitutional Li atom could be expected in the doubly doped neutral Si_nLi_2 clusters. However, Sporea *et al*. [2,4] did not agree with that conclusion in a subsequent theoretical study on structures of small Si_nLi and Si_nLi_2 (n = 1–6). The latter authors deduced that even in Si_nLi_2, the bare Si_n frames remain and both Li atoms act as electron donors. A similar behavior was found for sodium doped Si_nNa_m clusters ($n \leq 6$; $m \leq 2$).[6] This finding may not be generalized because the authors only considered small-sized silicon clusters.

It is apparent that larger singly and doubly lithium-doped silicon cluster sizes should be carefully investigated before a general growth pattern can be established. A few small mixed lithium-silicon clusters with more than two Li atoms were also studied theoretically.[7] Interestingly, the multi-lithium doped silicon cluster $Si_5Li_7^+$ was predicted to have a perfect seven-peak star-like structure due to the electron donation behavior of Li atoms.[8] Although some experimental data on sodium doped silicon clusters, including threshold photoionization and photoelectron spectroscopy studies, are available,[9,10,11,12] experiments reported for the lithium congener are rather scarce.

In the present chapter, geometrical and electronic structures and energetics of the singly and doubly lithium doped silicon clusters in both neutral and cationic states, $Si_nLi_m^{0/+}$ with n = 2-11 and m = 1-2, are further discussed. Our theoretical investigation was carried out in concert with experimental threshold photoionization measurements. However, among the investigated species only Si_6Li_2, Si_7Li, $Si_{10}Li$, and $Si_{11}Li$ have sufficiently low ionization thresholds allowing experimental

determination of their ionization energies. Our ultimate goal is to identify the ground-state structure of the clusters and to derive their growth mechanisms in comparison with the bare silicon clusters.

3.2. EXPERIMENTAL RESULTS

These experiments were carried out by the group of professors Peter Lievens and Ewald Janssens at the Department of Physics and Astronomy, KU Leuven. For the sake of comparison and discussion, we briefly mention the main experimental results. We sincerely thank our co-authors for allowing us to report their results here.

Of all singly and doubly lithium doped silicon clusters in the considered mass range, i.e., $Si_nLi_{1,2}$ with $n \leq 11$, only Si_7Li, $Si_{10}Li$, $Si_{11}Li$, and Si_6Li_2 have ionization energies in the studied energy range ($\leq$ 6.24 eV) (Figure 3.1(a)). The ionization threshold of the other $Si_nLi_{1,2}$ ($n \leq 11$) species is above 6.24 eV. All of them show up intensely in the mass spectrum measured using 7.89 eV photons (Figure 3.1(b)), which puts an upper limit on their ionization threshold.

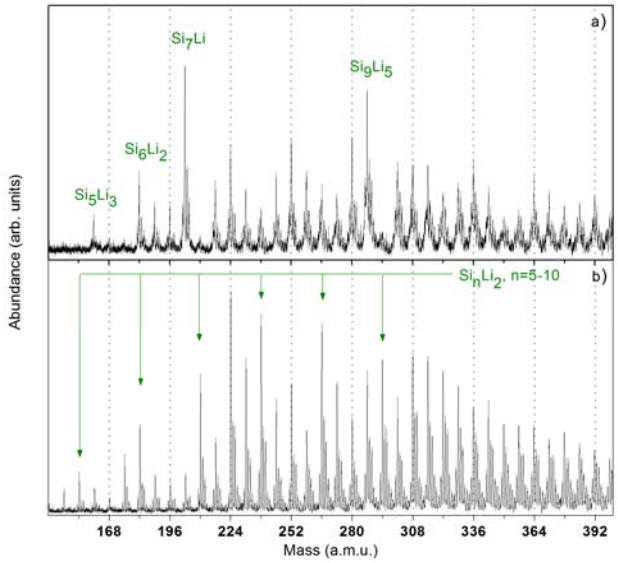

Figure 3.1 Mass abundance spectra of neutral Si_nLi_m clusters produced at 100 K and post-ionized using either a) 6.42 eV photons or b) 7.89 eV photons. The arrows mark Si_nLi_2 and dotted lines the pure Si_n clusters.

Figure 3.2 shows the photo-ionization efficiency (PIE) curves of Si_7Li, $Si_{10}Li$, $Si_{11}Li$, and Si_6Li_2. The open squares represent the experimental data, while the solid (red) lines are the smeared out step functions fitted to the data. The scatter at the baseline is mainly due to the low signal to noise ratio. The scatter above the VIE is intrinsic. The experimental VIE and the ionization thresholds are both indicated in the figures with a (red) dot. The positions of the VIEs and AIEs calculated in this work (described in section 3.4) are indicated by green arrows. The small features in front of the ionization thresholds are parts of the PIE curves of $Si_{n-1}Li_{1,2+4}$ species which have the same mass as $Si_nLi_{1,2}$ and are probed at slightly higher lithium contents in the source.

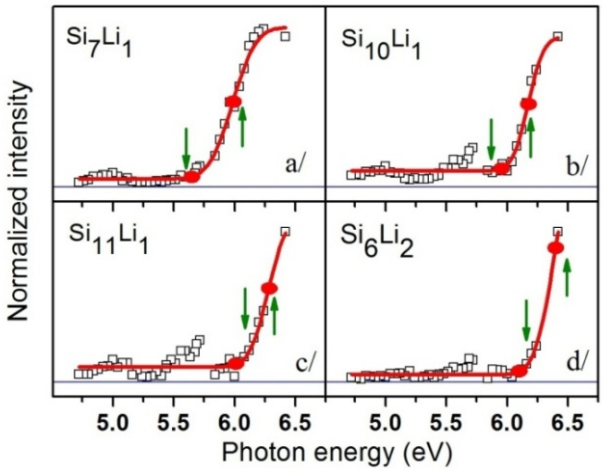

Figure 3.2 PIE curves of the Si_nLi_m clusters ($n \leq 11$, $m = 1, 2$) with an AIE below 6.25 eV; Si_7Li, $Si_{10}Li$, $Si_{11}Li$, and Si_6Li_2. The open squares represent the experimental data, while the solid red lines represent smeared-out step functions fitted to the data. The experimental VIE and the ionization threshold are both indicated by a red dot. The positions of the calculated vertical and adiabatic energies (VIE and AIE, respectively) are indicated by green arrows.

3.3. COMPUTATIONS

The popular hybrid B3LYP functional in combination with the 6-311+G(d) basis set is used for optimizing the geometries and computing harmonic vibrational

frequencies and thereby evaluating zero-point energy corrections. The B3LYP functional has been shown to be good in predicting IEs of bare silicon clusters.[13,14,15,16] To obtain more accurate energetic parameters, higher levels of theory such as the composite G3B3 method and coupled-cluster theory are used. Let us mention again that G3B3 total energy is based on quadratic configuration interaction QCISD(T) energy. The coupled-cluster CCSD(T) theory is used in conjunction with the correlation consistent aug-cc-pVTZ basis set for the small Si_nLi_m (n = 2-5 and m = 1-2) clusters. For larger Si_nLi_2 clusters (n = 6-11), single point electronic energies are calculated at the CCSD(T)/aug-cc-pVDZ level for selected isomers using the B3LYP optimized geometries.

In this study, generation of new structures for each Si_nLi_m cluster system is initially based on the structures previously reported in the literature. Wang et al.[1] showed that the Si_nLi geometric structures are similar to those of corresponding anionic Si_n^- clusters, if one neglects the Li atom. On this basis, we generate structures of Si_nLi by adding a Li atom at different positions around the well-known geometric structures of the pure anionic silicon Si_n^- clusters (of Chapter 2) and then optimize their geometries. Similarly, we create the initial new structures of Si_nLi_2 by adding the second Li atom around the different isomeric structures of Si_nLi. Besides, we also carry out systematic exchanges of the Si atoms by Li atoms in order to derive additional structures for both series of Si_nLi and Si_nLi_2 clusters.

3.4. RESULTS AND DISCUSSION

This part is organized in three sections. In the first section we discuss the structures and energetics of lower-lying isomers of each cluster size for both neutral and cationic $Si_nLi_m^{0/+}$ with $n = 2 - 11$ and $m = 1 - 2$. The second and third sections are devoted to their growth mechanism and their dissociation energies, respectively. Conventionally, the **n-mX$^{0/+}$** label is used for the isomers of the $Si_nLi_m^{0/+}$ cluster, with **X** = **A**, **B**, **C**... referring to the different isomers with increasing relative energy.

3.4.1. Structures of $Si_nLi_m^{0/+}$ with n = 2 – 11 and m = 1,2

3.4.1.1. $Si_nLi_m^{0/+}$ with n = 2 –5 and m = 1, 2

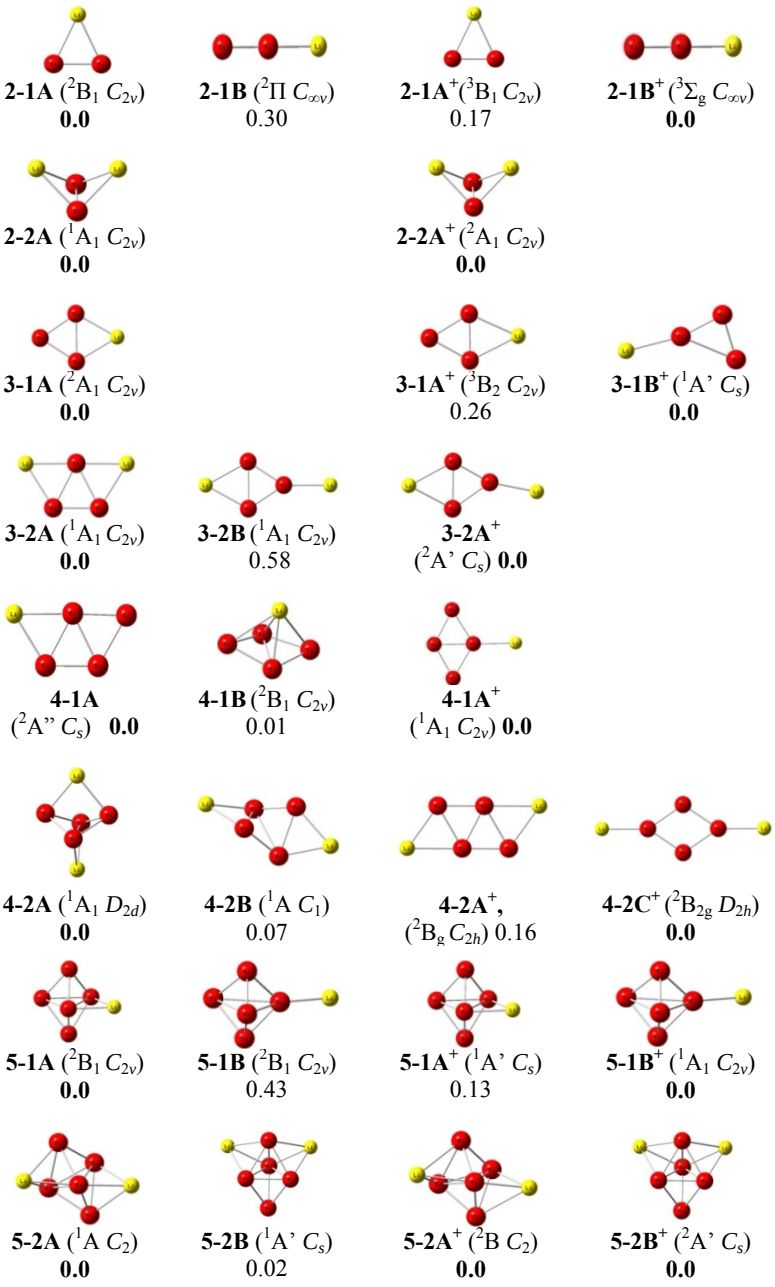

Figure 3.3 Low-lying isomers of neutral and cationic $Si_nLi_m^{0/+}$ with $n = 2 - 6$ and $m = 1, 2$. The entries are electronic state, point group and relative energy (in eV, calculated at the B3LYP/6-311+G(d) + ZPE level)

Shapes of the optimized geometries of the smallest lithium doped silicon clusters, Si_nLi_m with $n = 2 - 5$ and $m = 1, 2$, are displayed in Figure 3.3. The lowest energy isomers agree well with the results reported in previous theoretical studies.[1,2,3,4] In particular, Sporea *et al*.[6] investigated their structures and IEs at the B3LYP/6-31+G(d) level. Wang *et al*.[1] performed calculations using the quadratic configuration interaction method, QCISD/6-311+G(d)//MP2/6-31G(d) for the small neutral clusters Si_nLi ($n = 2 – 7$) and found a correlation between vertical IEs of Si_nLi and electron affinities of the corresponding Si_n clusters.

Table 3.1. AIE and VIE (eV) of the lowest energy isomers of Si_nLi_m clusters with n = 2-5, m = 1-2 calculated at three different levels of theory.

Ionization Transition	B3LYP/6-311+G(d)		G3B3		CCSD(T)/aug-cc-pVTZ	
	AIE	VIE	AIE	VIE	AIE	VIE
2-1A→ 2-1A$^+$	6.79	6.89	6.83	6.93	6.85	6.96
3-1A→ 3-1A$^+$	6.95	7.27	6.96	7.22	6.85	7.18
4-1A→ 4-1A$^+$	6.09	6.24	6.21	6.29	6.09	6.22
5-1A→ 5-1A$^+$	6.62	7.41	6.73	7.25	6.62	7.40
2-2A→ 2-2A$^+$	6.01	6.18	6.08	6.23	5.94	6.14
3-2A→ 3-2A$^+$	6.29	6.61	6.37	6.69	6.27	6.60
4-2A→ 4-2A$^+$	5.79	6.83	6.13	7.05	5.85	6.86
5-2A→ 5-2A$^+$	6.37	6.83	6.46	6.93	6.37	6.86

Table 3.1 presents calculated AIEs and VIEs of the lowest-energy isomers found for Si_nLi_m at three different levels of theory including B3LYP/6-311+G(d), G3B3 and CCSD(T)/aug-cc-pVTZ. For these small clusters, the lowest-energy isomers in both neutral and cationic forms are characterized the same shape (labeled by the letter **A**). The AIE and VIE values obtained using B3LYP slightly differ from those derived using CCSD(T) but the deviations are about ± 0.1 eV. Also the differences with the G3B3 values are less than ± 0.1 eV, except for **4-2A** where differences between B3LYP and G3B3 of more than 0.3 and 0.2 eV are found for the AIE and VIE values, respectively. Accordingly, the B3LYP approach is considered to

be reliable to investigate the ionization energies of the larger Si_nLi_m clusters, with an error margin of about ± 0.1 eV relative to CCSD(T) values.

3.4.1.2. $Si_6Li_m^{0/+}$ with m = 1, 2

Isomeric structures of Si_6Li and Si_6Li_2 and their cations are illustrated in Figure 3.4. The C_{2v} pentagonal bipyramid **6-1A** in a $^2B_2$ state is the lowest-lying form of the neutral Si_6Li. This is in agreement with the results of Yang *et al.*[3] The cation **6-1A**$^+$ with a similar shape to the neutral, is a local minimum lying 0.18 eV above the lowest-lying C_s isomer **6-1B**$^+$. The Li atom in the cationic isomer **6-1B**$^+$ binds with a Si atom, whereas in the neutral **6-1A** the dopant adds on the surface of the silicon framework.

The mass spectra shown in Figure 3.1 indicate that the ionization threshold of Si_6Li is higher than 6.42 eV, which is closer to the computed AIE value for isomer **6-1A** (6.41/6.12 eV at B3LYP / CCSD(T)) than that for isomer **6-1B** (AIE of 5.59/5.45 eV from B3LYP / CCSD(T)).

For Si_6Li_2, both lowest-lying isomers **6-2A** and **6-2B** are energetically degenerate according to B3LYP results. CCSD(T) results show a marginal preference for **6-2B** by only by 0.01 eV. The degeneracy of both isomers can be related to the similar silicon framework in which the Li atoms play the role of charge donor. They both have one Li atom situated on a pentagon and the other Li capped on different Si−Si edges.

The experimental PIE curve of Si_6Li_2 (see Figure 3.2) yields an ionization threshold energy of 6.10 ± 0.26 eV and a VIE of 6.40 ± 0.15 eV, in good agreement with the calculated values of **6-2A,** being 6.15/6.00 eV and 6.47/6.34 eV for the AIE and VIE at the B3LYP / CCSD(T) level, respectively. The AIE and VIE values of **6-2B** are somewhat lower than the experimental values, being 6.01 / 5.90 eV and 6.22/6.12 eV for the AIE and VIE at B3LYP / CCSD(T). But, given the experimental and theoretical uncertainties on the derived values, the presence of isomer **6-2B** in the cluster beam cannot definitely be excluded.

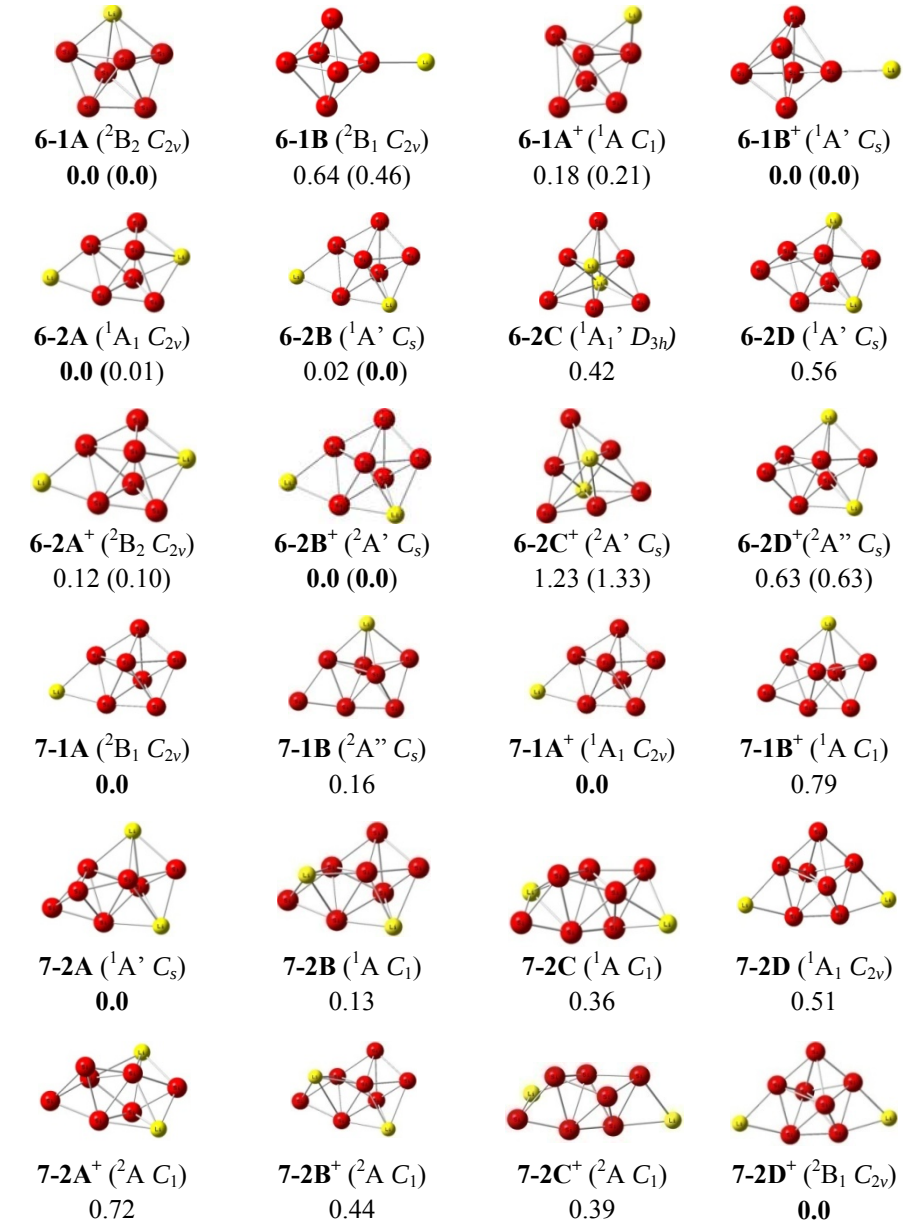

Figure 3.4 Low-lying isomers of the neutral and cationic $Si_6Li_m^{0/+}$ and $Si_7Li_m^{0/+}$ with m = 1, 2. Relative energies (in eV) are calculated at the B3LYP/6-311+G(d) + ZPE. Value given in parentheses are from CCSD(T)/aug-cc-pVDZ + ZPE level.

3.4.1.3. $Si_7Li_m^{0/+}$ with m = 1, 2

For these systems, our results concur with previous studies[1,3] that the most stable structure of Si_7Li is an edge-capped pentagonal bipyramid where the Li takes a capping position. Other isomers of this cluster have not been discussed in earlier studies. Figure 3.4 illustrates the lower-lying isomers of $Si_7Li^{0/+}$ and $Si_7Li_2^{0/+}$. Of particular interest is the observation that the substitutive isomer **7-1B** in which the Li atom substitutes a Si atom of the pentagon, is only 0.16 eV higher in energy than **7-1A**.

The most stable cation of Si_7Li^+, **7-1A**$^+$, exhibits a structure similar to the neutral ground state. The substitutive isomer **7-1B**$^+$, however, becomes much less stable than **7-1A**$^+$.

The doubly lithium doped neutral Si_7Li_2 cluster adopts **7-2A**, a bicapped pentagonal bipyramid, as its lowest-energy form. In this isomer, both Li atoms substitute Si atoms of the pentagon. **7-2D**, where both Li atoms adsorb to edges of the pentagon, is 0.51 eV higher in energy than **7-2A**. However, there is again a reversed energy ordering for the $Si_7Li_2^+$ cation, namely, **7-2D**$^+$ becomes the lowest-lying isomer being 0.72 eV more stable than **7-2A**$^+$.

The experimental PIE curve of Si_7Li (Figure 3.2a) yields an ionization threshold energy of 5.65 ± 0.04 eV and a VIE of 5.98 ± 0.01 eV. The calculated B3LYP values for **7-1A** of 5.60 and 6.06 eV, respectively, agree well with experiment. Calculated AIE and VIE for isomer **7-1B** are significantly higher than the experimental values (see Table 3.2). Accordingly, **7-1A** is likely the isomer present in the experiment. No accurate value for the ionization threshold could be determined in experiment for Si_7Li_2, but the mass spectra obtained by ionization with 6.42 eV laser light show that the ionization threshold must be between 6.24 and 6.42 eV (cf. Figure 3.1). This result supports **7-2A** and excludes **7-2D** as the global minimum of this size.

3.4.1.4. $Si_8Li_m^{0/+}$ with m = 1, 2

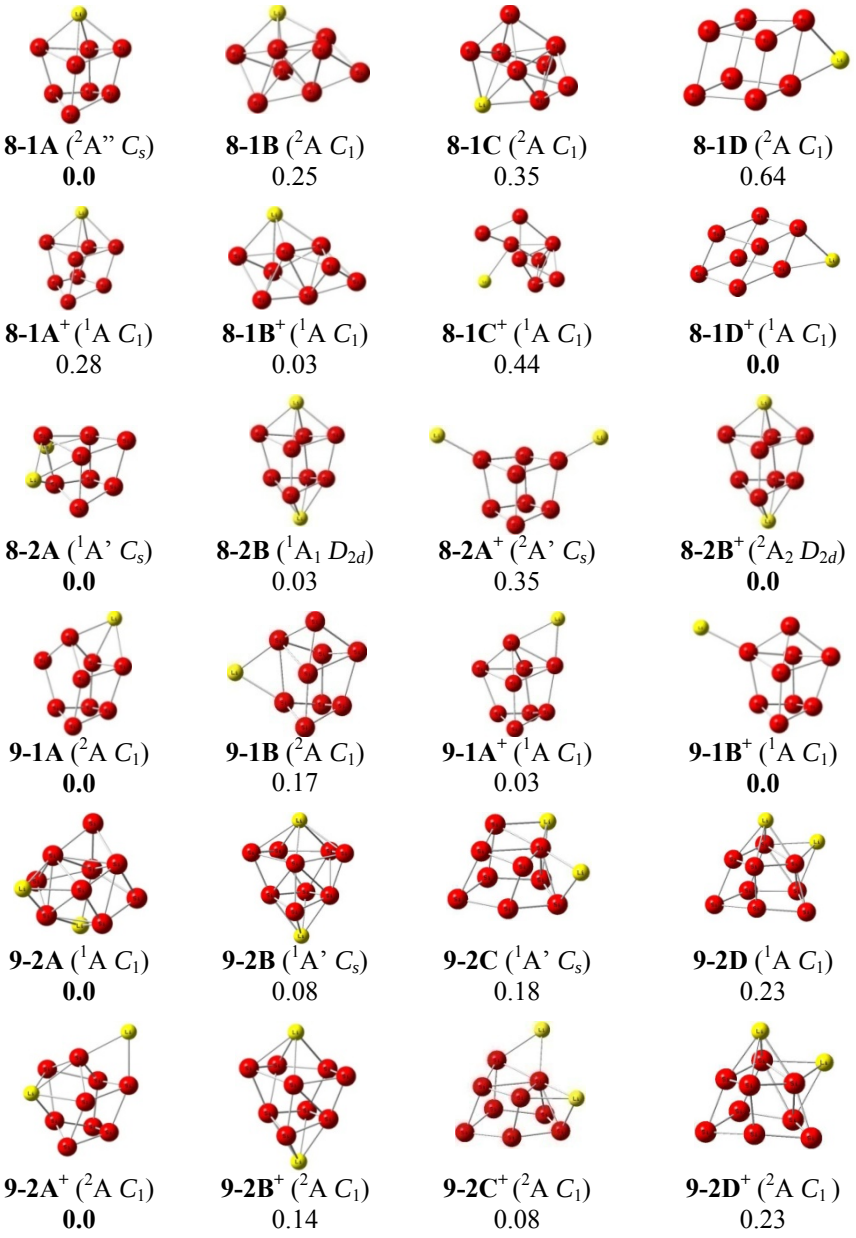

Figure 3.5 Low-lying isomers of the neutral and cationic $Si_8Li_m^{0/+}$ and $Si_9Li_m^{0/+}$ with m = 1, 2. Relative energies are calculated at the B3LYP/6-311+G(d) + ZPE level.

TABLE 3.2. Calculated and experimental values of AIEs and VIEs of Si_nLi and Si_nLi_2 neutral clusters with $n = 6-11$.[a)]

Ionization Process	AIE (eV)			VIE (eV)		
	B3LYP	CCSD(T)	Exptl.	B3LYP	CCSD(T)	Exptl.
6-1A→ 6-1A$^+$	6.41	6.12	**6.42–**	6.94	6.70	
6-1B→ 6-1B$^+$	5.59	5.45	**7.89**	6.44	6.19	
6-2A→ 6-2A$^+$	6.15	6.00		6.47	6.34	
6-2B→ 6-2B$^+$	6.01	5.90	**6.10**	6.22	6.12	**6.40**
6-2C→ 6-2C$^+$	6.84	6.80	**± 0.26**	7.08	7.13	**± 0.15**
6-2D→ 6-2D$^+$	6.09	5.89		6.48	6.38	
7-1A)→ 7-1A$^+$	5.60	5.45	**5.65**	6.06	5.87	**5.98**
7-1B→ 7-1B$^+$	6.24	6.05	**± 0.04**	6.57	6.45	**± 0.01**
7-2A→ 7-2A$^+$	6.48	6.41		6.72	6.71	
7-2B→ 7-2B$^+$	6.07	5.98	**6.20–**	6.33	6.31	
7-2C→ 7-2C$^+$	5.95	5.91	**6.42**	6.35	6.33	
7-2D→ 7-2D$^+$	5.25	5.20		5.74	5.65	
8-1A→ 8-1A$^+$	6.60	6.42		7.12	6.95	
8-1B→ 8-1B$^+$	6.10	5.94	**< 6.42**	6.43	6.33	
8-1C→ 8-1C$^+$	6.41	6.29		6.83	6.67	
8-1D→ 8-1D$^+$	5.68	5.43		6.05	5.88	
8-2A→ 8-2A$^+$	6.87	6.89	**6.42–**	7.03	6.99	
8-2B→ 8-2B$^+$	6.49	6.41	**7.89**	6.74	6.70	
9-1A→ 9-1A$^+$	5.91	5.68	**< 7.89**	6.53	6.38	
9-1B→ 9-1B$^+$	5.71	5.42		6.28	6.07	
9-2A→ 9-2A$^+$	6.36	6.27		6.72	6.73	
9-2B→ 9-2B$^+$	6.43	6.37	**6.42–**	6.76	6.80	
9-2C→ 9-2C$^+$	6.26	6.21	**7.89**	6.53	6.52	
9-2D→ 9-2D$^+$	6.36	6.25		6.72	6.70	
10-1A→ 10-1A$^+$	5.86	5.61		6.19	6.00	
10-1B→ 10-1B$^+$	5.80	5.53	**5.95**	6.24	6.06	**6.17**
10-1C→ 10-1C$^+$	5.84	5.64	**± 0.05**	6.36	6.20	**± 0.01**
10-1D→ 10-1D$^+$	5.82	5.56		6.18	6.00	

10-2A→ 10-2A$^+$	6.01	6.07		6.77	6.66	
10-2B→ 10-2B$^+$	5.95	6.09	**< 7.89**	6.75	6.63	
10-2C→ 10-2C$^+$	5.99	6.01		6.74	6.61	
10-2D→ 10-2D$^+$	5.81	5.73		6.29	6.27	
11-1A→ 11-1A$^+$	5.96	5.79		6.89	6.76	
11-1B→ 11-1B$^+$	6.10	5.87	**6.01**	6.47	6.27	**> 6.20**
11-1C→ 11-1C$^+$	5.83	5.83	**± 0.16**	6.46	6.26	
11-1D→ 11-1D$^+$	5.63	5.47		6.38	6.17	

[a)] Calculated AIEs are corrected by ZPEs obtained at the B3LYP/6-311+ G(d) level.

The global minimum **8-1A** of Si_8Li (Figure 3.5) can on the one hand be considered as a substitutive derivative of the C_{2v} symmetric bicapped pentagonal bipyramid Si_9 [cf. refs.14,15] and keeps the C_{2v} symmetry of Si_9. On the other hand, **8-1A** can be formed by adding Li^+ on Si_8^-.[15] **8-1D**, which is composed of bicapped Si_8^- and Li^+, is 0.64 eV higher in energy than **8-1A**. Conversely, the cationic system Si_8Li^+ favors the additive isomer **8-1D$^+$** which becomes the lowest-lying isomer. Again, a reversed energy ordering is found following electron removal at the expense of substitutive derivatives such as **8-1A$^+$**.

Si_8Li_2 has two very close-lying isomers **8-2A** and **8-2B**, both have a Si framework similar to that of the dianion Si_8^{2-}.[17] The position of the Li atoms in **8-2A** and **8-2B** are also of substitutive type as compared to the bare Si_9 cluster. The cationic isomer **8-2B$^+$** turns out to be the ground state of $Si_8Li_2^+$. In the cation, the Li atoms stay further from the Si framework than in the neutral.

No accurate experimental value for the ionization threshold could be determined either for the monolithiated or dilithiated cluster of this size. However, the recorded mass spectra indicate that the ionization threshold of Si_8Li is below 6.42 eV, whereas that of Si_8Li_2 is between 6.42 and 7.89 eV (cf. Figure 3.1) This is in agreement with the higher calculated AIE of Si_8Li_2 as compared to Si_8Li, but does not allow us to make a definite assignment of their ground state structures.

3.4.1.5. $Si_9Li_m^{0/+}$ with m = 1, 2

The neutral Si_9Li system (Figure 3.5) has **9-1A** as the global minimum. In this isomer, the Li atom adds on a face of the bicapped pentagonal bipyramid Si_9.[14,15] **9-1B**, an edge-capped derivative of Si_9, is located only 0.17 eV higher in energy than **9-1A**. This means that face-capping is slightly preferred over edge-capping for the neutral state of this cluster. In the cationic Si_9Li^+, three close-lying isomers are generated by capping Li at different positions on a silicon framework similar to the ground state of the anionic Si_9^-.[15] This suggests that the Li^+ cation loosely moves around a silicon frame. Among these isomers, **9-1B**$^+$ where Li^+ only binds to one Si atom constitutes the most stable isomer.

For the doubly lithium doped system, the lowest-lying isomer **9-2A** is a penta-capped trigonal prism in which one Li atom substitutes a Si position of the trigonal prism of Si_{10} [14,15] and the other Li atom adds on a side face. **9-2B**, being only 0.08 eV less stable than **9-2A**, is also based on the tetra-capped triagonal prism shape of Si_{10}, but one Li atom now takes a substitutive position and the other takes a bridging position. Both Li atoms in **9-2C** and **9-2D** have additive positions. For the $Si_9Li_2^+$ cation, we find **9-2A**$^+$ as the lowest-lying isomer. However, **9-2C**$^+$, which becomes quasi-degenerate with **9-2A**$^+$, still has the bicapped pentagonal bipyramidal shape of Si_9,[14] and both Li atoms are added around the silicon framework. **9-2D**$^+$ remains characterized by the shape of Si_9 with Li atoms circulating around, but this isomer lies energetically higher than the former.

Due to the presence of Si_8Li_5 in the cluster beam, of which the maximum in the isotopic distribution (259 amu) coincides with that of Si_9Li, it was hard to experimentally determine an ionization threshold for Si_9Li. At least no sharp photo-ionization curve could be recorded. Also for Si_9Li_2, no accurate experimental value for the ionization threshold could be determined. Based on the mass spectra collected by ionization with 6.42 and 7.89 eV laser light (cf. Figures 3.1 and 3.2), it is known that the ionization threshold must be larger than 6.42 and below 7.89 eV. Of the four lowest-energy isomers for Si_9Li_2, this result does only exclude **9-2C**.

3.4.1.6. $Si_{10}Li_m^{0/+}$ with m = 1, 2

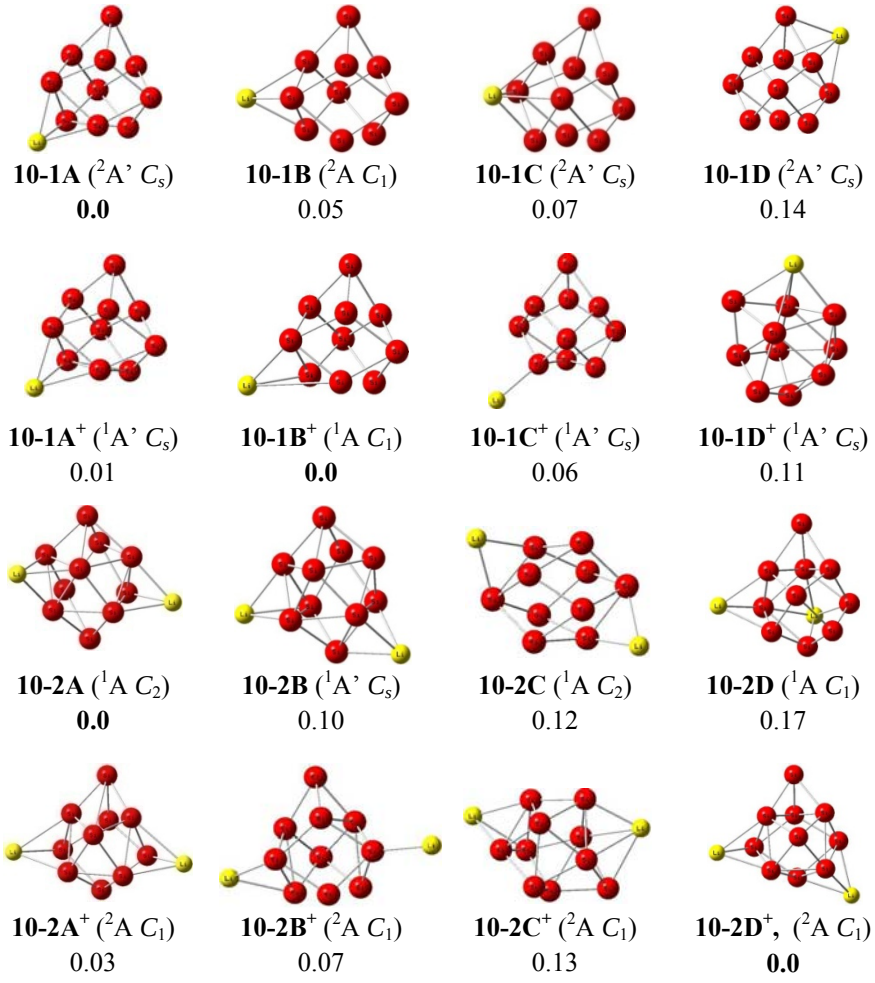

Figure 3.6. Low-lying isomers of the neutral and cationic clusters $Si_{10}Li_m^{0/+}$ with m = 1, 2. Relative energies are calculated at the B3LYP/6-311+G(d) + ZPE level.

Figure 3.6 illustrates the shape, symmetry and energetics of the lower-lying structures of $Si_{10}Li_{1,2}^{0/+}$. All the four lower-lying isomers of $Si_{10}Li$ have the tetra-capped trigonal prism framework of Si_{10}[14,15] where the Li atom exohedrally adds on different positions. In a previous paper, Sporea *et al.*[18] found that a Li atom can be encapsulated in the silicon cage Si_{10}. The lowest-lying isomer c-Li@Si_{10}, which possesses D_{4d} symmetry of lithium-doped cage-like silicon clusters, however, is

calculated to be 1.5 eV higher in energy than **10-1A**. This shows that lithium prefers to expose on the surface of the silicon cores.

A similar structure to the global minimum of neutral **10-1A** is found for the cationic $Si_{10}Li^+$ **10-1A**$^+$, but it is slightly less stable than **10-1B**$^+$ which has an edge-capped lithium on the Si_{10} tetra-capped trigonal prism. The face-capped **10-1A**$^+$ (+0.01 eV) and top-capped **10-1C**$^+$ (+0.06 eV) isomers are nearly degenerate.

Regarding the doubly doped species, the lowest-lying isomer **10-2A** contains a bicapped square antiprism Si_{10} framework, similar to the ground state structure of the dianionic Ge_{10}^{2-} as found by King *et al*,[19] and has two face-capping Li atoms. The higher-energy isomers **10-2B** and **10-2C** differ from **10-2A** only by the positions of the capping Li atoms. It seems that the bicapped square antiprism Si_{10}^{2-} is rather stable, and Li atoms mainly are electron donors interacting by electrostatic forces and moving as Li^+ cations around the silicon dianion. The **10-2D** isomer, where the tetra-capped trigonal prism remains and the Li atoms add on different faces is also energetically close to **10-2A**. It should be noted that for this size, more isomers are found to be close in energy, which implies a large spectrum of isomers having similar energy content. Different from the neutral $Si_{10}Li_2$, the cationic $Si_{10}Li_2^+$ clusters prefer the tetra-capped trigonal prism framework of Si_{10}. The three lowest-lying isomers including **10-2D**$^+$ (0.0 eV), **10-2A**$^+$ (+0.03 eV), and **10-2B**$^+$ (+0.07 eV) have the Li atoms at different positions around that silicon frame.

Figure 3.2b shows the PIE curve of $Si_{10}Li$. The experiment yields an ionization threshold energy of 5.95 ± 0.05 eV and a VIE of 6.17 ± 0.01 eV. The B3LYP values for **10-1A** of 5.86 and 6.19 eV, respectively, compare favorably with experiment. However, the other isomers shown in Figure 3.6 cannot fully be excluded. No ionization threshold could be measured for the dilithiated system. But based on the appearance of the $Si_{10}Li_2$ in the mass spectrum taken after ionization with 7.89 eV photons it is clear that the ionization threshold must be lower than this value.

3.4.1.7. $Si_{11}Li_m^{0/+}$ with m = 1, 2

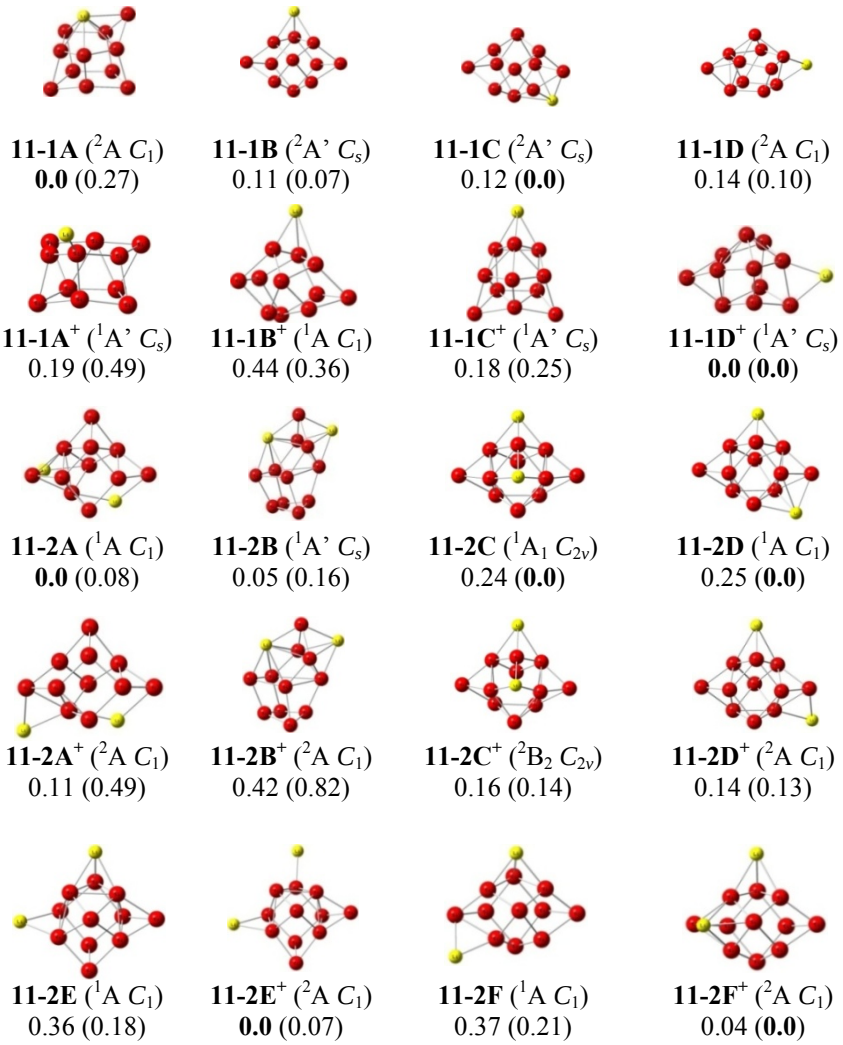

Figure 3.7 Low-lying isomers of the neutral and cationic clusters $Si_{11}Li_m^{0/+}$ with m = 1 – 2. Relative energies (in eV) are calculated at the B3LYP/6-311+G(d) + ZPE. Value given in parentheses are from CCSD(T)/aug-cc-pVDZ + ZPE computations.

Calculated results for this system are summarized in Figure 3.7. **11-1A**, which is a substitutive derivative of a pentacapped trigonal prism structure, is the lowest-lying isomer of $Si_{11}Li$ using B3LYP. However, CCSD(T) suggests that **11-1C**

is the most stable structure and its geometric shape of silicon framework is similar to that of the most stable Si_{11}^- anionic isomer.[20] This agrees with a previous finding that the geometric shapes of Si_nLi are similar to those of the corresponding Si_n^- anions if we neglect the Li atom in Si_nLi.[1]

11-1B and **11-1C** are formed by adding Li on different positions of the penta-capped trigonal prism Si_{11}. The cationic isomer **11-1D**$^+$, which is found to be the most stable form of the $Si_{11}Li^+$, is in fact an edge-capped Si_{11}. The Si_{11} framework of this isomer is geometrically similar to the ground state of the neutral Si_{11} cluster.[14,16]

Figure 3.2c shows the PIE curve of $Si_{11}Li$. The experiment yields an ionization threshold energy of 6.01 ± 0.16 eV and a VIE above 6.20 eV. Accordingly, our B3LYP values for **11-1A** of 5.96 and 6.89 eV, respectively, are comparable with experiment. Calculated AIE values for isomers **11-1C** and **11-1D** are significantly below 6.01 eV, excluding them as ground state structures. However, based on the calculated ionization energies, isomer **11-1B** cannot be ruled out.

Based on B3LYP calculations, the lowest-energy isomer **11-2A** of $Si_{11}Li_2$ has the shape of hexa-capped trigonal prism and one Li atom substitutes a Si position of the trigonal prism of Si_{12}[14] whereas the other Li atom adds on different face. According to CCSD(T) results, however, both isomers **11-2C** and **11-2D** which are energetically degenerate, are the most stable isomers and they both are only 0.08 eV lower in energy than **11-2A**.

Structurally, both **11-2C** and **11-2D** also have the hexa-capped trigonal prism framework of Si_{12}[14] in which one Li atom substitutes a capped Si position and the other Li atom adds on different positions. In contrast, B3LYP results predict that the cation $Si_{11}Li_2^+$ adopts **11-2E**$^+$ as its most preferred form where both Li atoms bind on the surface of the silicon framework. However, **11-2F**$^+$ becomes the most stable isomer at the CCSD(T) level. **11-2F**$^+$ has both Li atoms added on two surfaces of silicon core of the most stable Si_{11}^- anion.[20]

3.4.2. Growth Mechanisms of $Si_nLi_m^{0/+}$

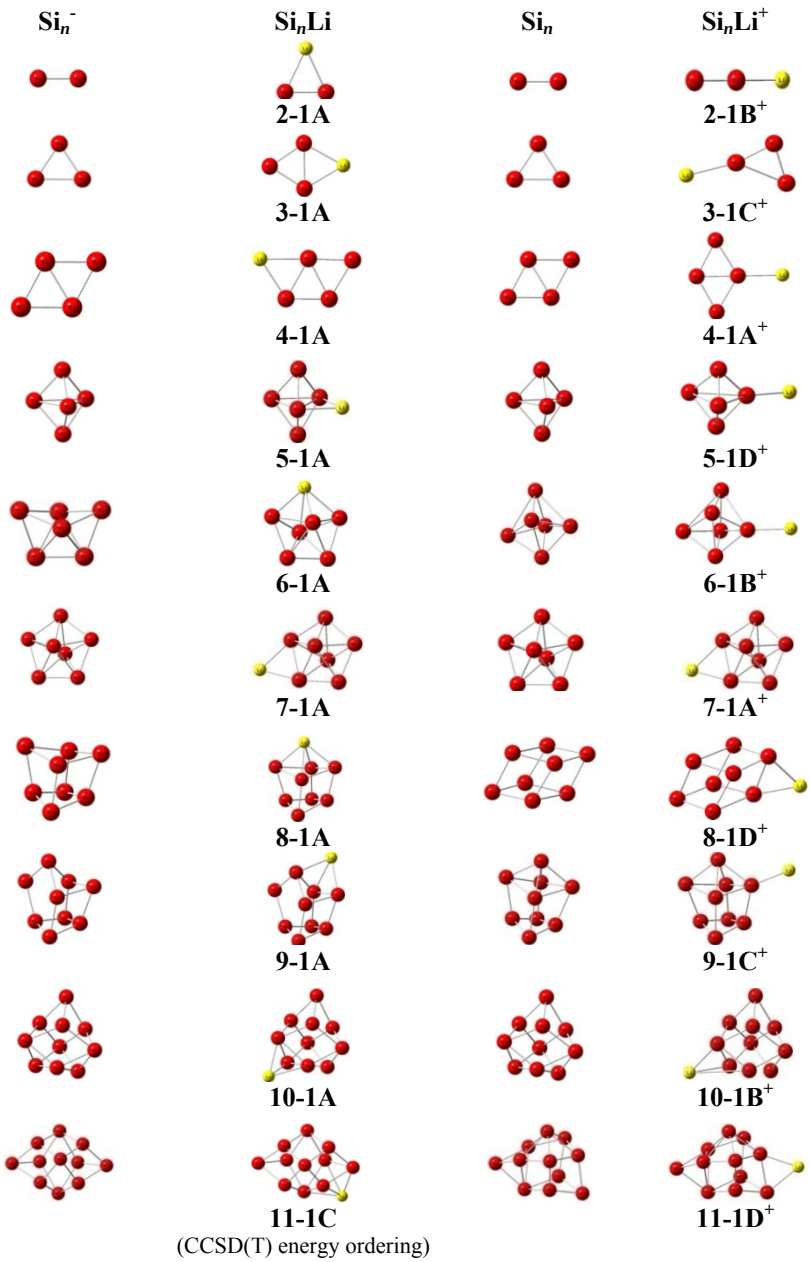

Figure 3.8 The growth pattern of the neutral and cationic Si_nLi systems compared with Si_n^- and Si_n ground state structures. Geometries of the bare Si clusters are taken from refs. 13 and 14 and reoptimized at the B3LYP/6-311+G(d) level.

Based on a comparison between the available experimental ionization energies and the calculated values for $Si_nLi_{1,2}$, it is reasonable to assume that the lowest-energy isomers located at the B3LYP level are actually the isomers that are present in the experiment (at least none of the lowest-energy isomers found could be excluded on the basis of this comparison). From here on, we therefore focus on the lowest energy isomers found for $Si_nLi_{1,2}^{0/+}$ and analyze their growth patterns.

To facilitate the comparison, Figures 3.8 and 3.9 summarize the ground state structures of Si_nLi, Si_nLi^+, Si_nLi_2, and $Si_nLi_2^+$ with n = 2-11 and compare them with those of the bare clusters Si_n^-, Si_n, and Si_{n+1} whose structures are taken from previous studies[14,15,20] and reoptimized at the B3LYP/6-311+G(d) level. We find that the Li dopant atoms adopt quite different behaviors depending on the number of Li atoms and on the charge state.

In the singly doped neutral Si_nLi clusters, the Li atom favors addition on either an edge or a face of a Si_n framework that is similar to the ground state structure of the anionic Si_n^-. In some cases, the additive position can alternatively be described as substituting a silicon atom in Si_{n+1}, such as in Si_5Li, Si_6Li, Si_8Li and $Si_{10}Li$. Generally, if the Li atom is located at the additive position, it preferentially chooses a position which is also a substitution to the corresponding Si_{n+1} framework.

For the cations Si_nLi^+, Li seems to either bind with one Si atom of the bare Si_n cluster or adds on one of its edges. There is no exception on this empirical rule in the size range $n = 2-11$. In the positively charged state, the Li atom moves more freely due to the less negative charge distribution on the silicon frame, therefore it has fewer bonds with the silicon atoms than in the neutral.

Figure 3.9 shows that the doubly doped Si_nLi_2 species bear the shape of the Si_{n+1} counterparts. One Li atom actually substitutes into a Si position of Si_{n+1}, whereas the other Li atom is adding on an edge or a face. $Si_{10}Li_2$ is an exception on this observation. The ground state of $Si_{10}Li_2$ has both Li atoms added on the surface of the dianionic Si_{10}^{2-} [cf. ref. 21]. This is due to the high stability of the dianion counterpart. The substitution mechanism appears to persist in the doubly doped system, in particular for the larger sizes.

In contrast to the neutrals, the $Si_nLi_2^+$ cations have both Li atoms being added on an edge or a face of the Si_n^- framework. Again the substitution is disfavored in this charged state.

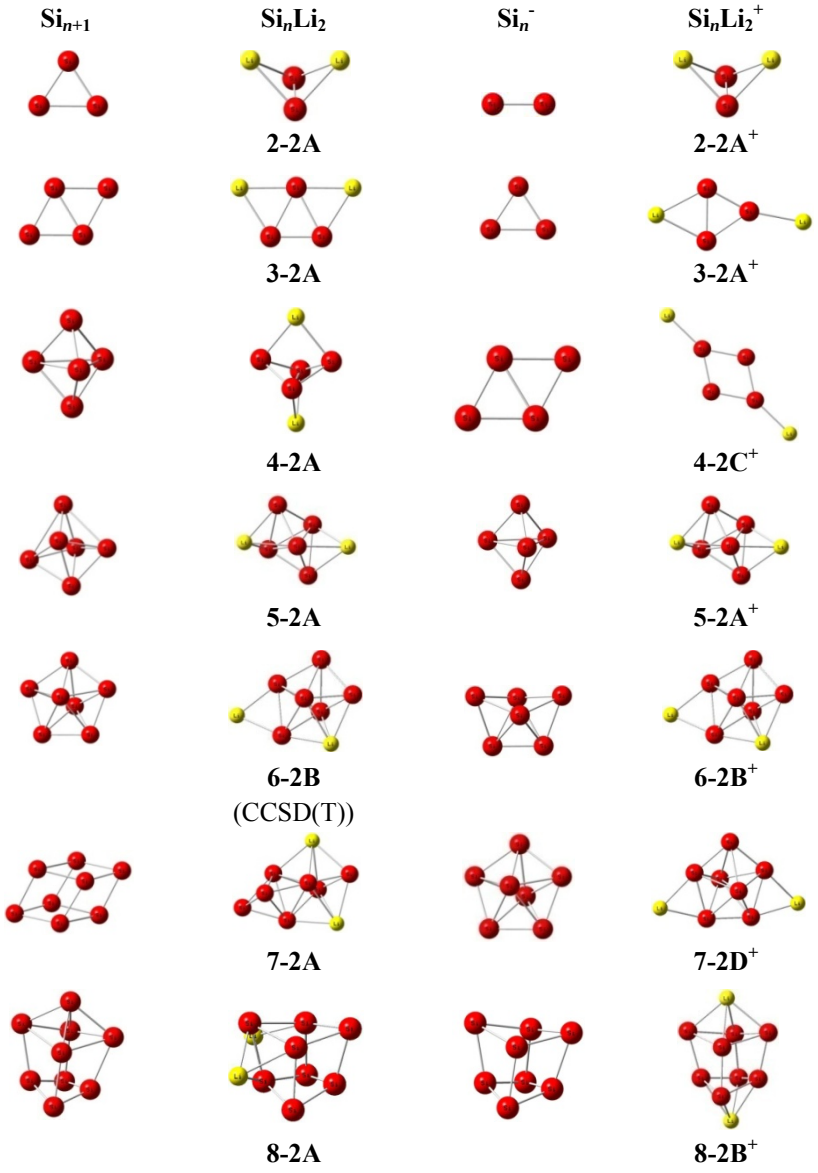

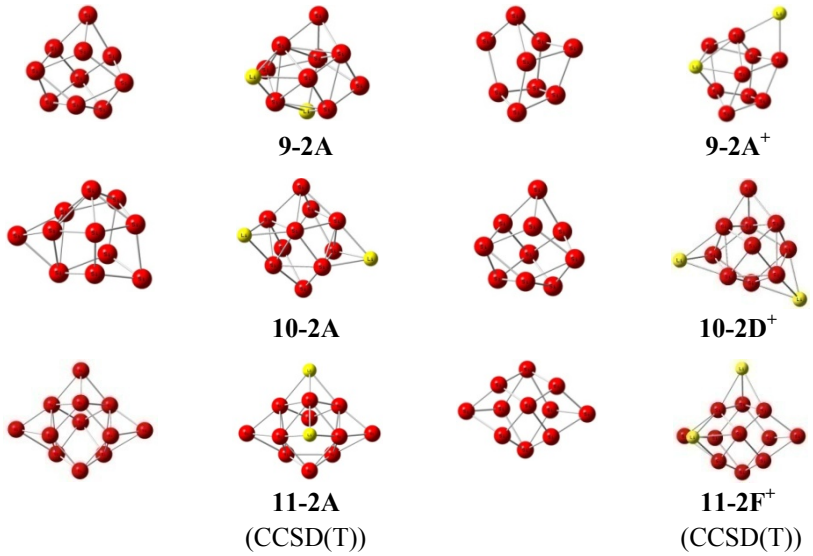

Figure 3.9. The growth pattern of the neutral and cationic Si_nLi_2 systems. Geometries of the bare Si clusters are taken from refs. 13 and 14, and reoptimized at the B3LYP/6-311+G(d) level.

3.4.3. Dissociation Energies

Dissociation energies of the Si_nLi and Si_nLi^+ with $n = 1–11$ clusters are calculated using the B3LYP/6-311+G(d) method for different fragmentation paths and illustrated in Figure 3.10.

The dissociation energy D_{e1} is defined as the energy required in the reaction $Si_nLi \rightarrow Si_n + Li$. This quantity has local minima for $n = 1$, 4 and 7 and is maximal for $n = 2$, 5 and 8. This means that SiLi, Si_4Li and Si_7Li are relatively less stable and the Si_2Li, Si_5Li, and Si_8Li are relatively more stable Si_nLi clusters. It is interesting to note a remarkable similarity between the evolution of the dissociation energy D_{e1} of binary Si_nLi clusters and the electron affinity (EA) of pure Si_n with the size ($n = 1 – 11$). Both curves show local minima for $n = 1$, 4 and 7 and local maxima for $n = 5$ and 8 (see Figure 3.10). This parallelism, which can be understood by the correspondence between the HOMO of Si_nLi and the LUMO of Si_n, was already noticed by Kishi *et al.*[9] and verified by Sporea *et al.*[2] for small Si_nLi ($n = 3 – 6$). While the energy of the

LUMO is relevant for the EA, the HOMO energy scales not only with the VIE but also with the bond dissociation energy.

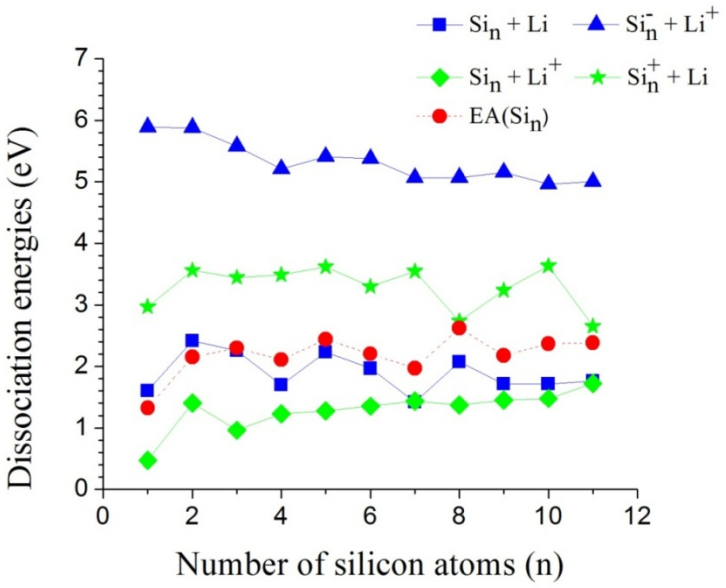

Figure 3.10. Dissociation energies (corrected by ZPE) of Si_nLi ($Si_nLi \rightarrow Si_n + Li$ and $Si_nLi \rightarrow Si_n^- + Li^+$) and Si_nLi^+ ($Si_nLi^+ \rightarrow Si_n + Li^+$ and $Si_nLi^+ \rightarrow Si_n^+ + Li$) and the electron affinity of Si_n calculated using the B3LYP/6-311+G(d) method as function of the number of Si atoms.

The D_{e2} values, which are defined as the energy required in the heterolytic bond cleavage reaction $Si_nLi \rightarrow Si_n^- + Li^+$, are also calculated. The size dependence of this heterolytic reaction path is less pronounced. Figure 3.10 shows that all dissociation energies according to the $Si_nLi \rightarrow Si_n^- + Li^+$ process are much larger than those of the corresponding homolytic dissociation energies in the reaction $Si_nLi \rightarrow Si_n + Li$. This means that the homolytic bond cleavage is largely favored over the heterolytic processes.

D_{e3} and D_{e4} are defined as the energy required for the $Si_nLi^+ \rightarrow Si_n + Li^+$ and $Si_nLi^+ \rightarrow Si_n^+ + Li$ reactions, respectively. D_{e3} has a local minimum for $n = 3$ and local maxima for $n = 2$ and 11. The D_{e4} is local minima for $n = 6$, 8, and 11 and local

maxima for n = 2, 7, and 10. The D_{e4} values are larger than D_{e3} for all Si_nLi^+ sizes. Accordingly the Si_nLi^+ cations favor cationic Li^+ ejection over neutral Li elimination.

Proceeding in the opposite directions, namely $Si_n^- + Li^+ \rightarrow Si_nLi$ and $Si_n + Li^+ \rightarrow Si_nLi^+$, the corresponding D_{e2} and D_{e3} values represent the lithium cation affinities (LiCA) of the anionic and neutral pure Si clusters, respectively. It is obvious from Figure 3.10 that the LiCA of the charged species are much larger than those of the neutral counterparts. Similarly, the D_{e1} and D_{e4} values define the Li atom affinities (LiA) of the neutral and cationic pure Si clusters, respectively. In this case, the charged species have consistently larger LiA's than the neutrals. This suggests that the electrostatic attraction plays an important role in the addition process of the dopant.

Figure 3.10 suggests that the different dissociation energies tend to converge to certain limit values. However the size considered, being up to n = 12, is too small to allow an extrapolation.

3.5. CONCLUDING REMARKS

In the present theoretical study in concert with experiment, the geometric and electronic structures of both neutral and cationic Si_nLi_m clusters, with n = 2–11 and m = 1, 2, were determined using quantum chemical methods including the B3LYP/6-311+G(d), G3B3, and CCSD(T)/aug-cc-pVnZ (n = D,T) levels. It is found that the shape of the cationic isomers does not differ much from their corresponding neutrals isomers following ionization. However, in a number of cases, a reversed energy ordering between isomeric forms occurs.

We also determined the adiabatic (AIEs) and vertical (VIEs) ionization energies of the Si_nLi_m clusters. The calculated AIE and VIE values at the B3LYP/6/311+G(d) level of Si_6Li_2, Si_7Li, $Si_{10}Li$, $Si_{11}Li$ compare relatively well with the corresponding experimental results obtained using the photo-ionization efficiency measurements carried out by our collaborators in the department of Physics and Astronomy, KU Leuven.

These are the only clusters of the investigated Si_nLi_m (n = 2–11 and m = 1, 2) series for which the experimental ionization energies were found to be lower than 6.25 eV.

The growth mechanism of the singly and doubly lithium doped silicon clusters can be understood on the basis of the following observations. Let us however emphasize that the results summarized here are mainly valid for gas phase clusters:

i) in the neutral Si_nLi, the Li atom favors addition on either an edge or a face of the anionic Si_n^- while in the cationic Si_nLi^+, it connects one Si atom of the bare Si_n cluster or adds on one of its edges;

ii) the neutral Si_nLi_2 clusters have the shape of the Si_{n+1} counterparts. One Li atom adds on an edge or a face of it, whereas the other Li substitutes into a Si position of Si_{n+1}. This differs from the growth pattern of the cationic $Si_nLi_2^+$, where both Li atoms add on an edge or a face, and

iii) the neutral $Si_{11}Li$ and $Si_{10}Li_2$ and cationic $Si_9Li_2^+$ clusters represent exceptions with Li atoms behaving differently. Their different structures can in part be understood from the stability of the relevant core Si clusters.

References

1) H. Wang, W. C Lu, Z. S. Li, Ch. C. Sun, J. Mol. Struct. (THEOCHEM) 730 (2005) 263.

2) C. Sporea, F. Rabilloud, X. Cosson, A. R. Allouche, M. Aubert-Frécon, J. Phys. Chem. A 110 (2006) 6032.

3) J. C. Yang, L. Lin, Y. Zhang, A. F. Jalbout, Theor. Chem. Account. 121 (2008) 83.

4) C. Sporea, F. Rabilloud, M. Aubert-Frécon, J. Mol. Struct. (Theochem) 802 (2007) 85.

5) D. Hao, J. Liu, J. Yang, J. Phys. Chem. A 112, 10113 (2008).

6) C. Sporea, F. Rabilloud, A. R. Allouche, M. Frécon, J. Phys. Chem. A 110, 1046 (2006).

7) B. H. Boo, S. J. Kim, M. H. Lee, N. Nishi, Chem. Phys. Lett. 453 (2008) 150.

8) W. Tiznado, N. Perez-Peralta, R. Islas, A. Toro-Labbe, J. M. Ugalde, G. Merino, J. Am. Chem. Soc. 131 (2009) 9426.

9) R. Kishi, S. Iwata, A. Nakajima, K. Kaya, J. Chem. Phys. 107 (1997) 3056.

10) R. Kishi, H. Kawamata, Y. Negishi, S. Iwata, A. Nakajima, K. Kaya, J. Chem. Phys. 107 (1997) 10029.

11) D. Y. Zubarev, A. I. Bolydrev, X. Li, L. F. Cui, L. S. Wang, J. Phys. Chem. A 109 (2005) 11385.

12) D. Y. Zubarev, N. Alexandrova, A. I. Boldyrev, X. Li, L. F. Cui, L. S. Wang, J. Chem. Phys. 124 (2006) 124305.

13) C. Bauschlicher, Chem. Phys. Lett. 246, (1995) 40.

14) S. Nigam, C. Majumder, S. K. Kulshreshtha, J. Chem. Phys. 121 (2004) 7756.

15) J. C. Yang, W. G. Xu, W. S. Xiao, J. Mol. Struct. (THEOCHEM) 719 (2005) 89.

16) W. Qin, W. C. Lu, L. Z. Zhao, Q. J. Zang, C. Z. Wang, K. M. Ho, J. Phys. 21 (2009) 455501.

17) V. T. Ngan, M. T. Nguyen, J. Phys. Chem. A 114 (2010) 7609.

18) C. Sporea, F. Rabilloud, J. Chem. Phys. 127 (2007) 164306.

19) R. B. King, I. Silaghi-Dumitrescu, M. M. Uta, Inorg. Chem. 45 (2006) 4974.

20) B. Li, Q. Xu, Phys. Stat. Sol. 241 (2004) 990.

21) A. D. Zdetsis, J. Chem. Phys. 127 (2007) 244308.

Chapter 4

Thermochemical Parameters and Growth Mechanism of the Boron Doped Silicon Clusters

This chapter is adapted from the following article:

- *Thermochemical parameters and growth mechanism of the boron-doped silicon clusters, Si_nB^q with n = 1 – 10 and q = -1, 0, +1* by N. M. Tam, T. B. Tai and M. T. Nguyen, *Journal Physical Chemistry C*, *116*, 20086-20098 (2012).

4.1. INTRODUCTION

Recently, our group[1] found that the species $M@Si_8^q$ containing 34 valence electrons possess the perfect octahedral structures in which the impurities M (Be, B, C, N… with appropriate positive charge) are located at the center of the Si_8 cube. These species apparently exhibit the intriguing features of a cubic aromaticity with 8 valence electrons that satisfy the electronic shell model. However, due to the lack of results on the other sizes, the thermodynamical stability of these systems has not been examined. Closed shell impure clusters with compact and high symmetry structures are of current interest because they can be used as building-blocks for self-assembling nano-materials. Such endohedral structures were recently observed for the group IVA doped clusters such as $M@Ge_n$, $M@Sn_n$ and $M@Pb_n$ with n = 10, 12 and 14.[2,3,4] However, endohedral $M@Si_n$ clusters are rather scarce, in part due to the fact that the size of similar Si_n cages remains too small to enclose the M impurities. The existence of the $M@Si_8$ species prompts us to find more evidence for stable $M@Si_n$ clusters containing the light dopants such as Be, B, C...

Boron-silicon compounds have also attracted much attention in part due to their important applications in micro-electronic industries. Boron is the most important element widely used to date as a p-type dopant in crystalline silicon. Earlier studies showed that when the concentration of boron is increased, formation of either a silicon boride phase or Si-B clusters occurs in crystalline Si.[5,6] These solid materials are also known for their mechanical hardness. However, in spite of the demonstrated importance of the boron-silicon compounds, an understanding of their electronic and thermodynamic properties is still limited. According to our best knowledge, only a few studies on small Si_nB clusters were reported. Heats of formation of gas phase small Si_nB clusters with n = 1-3 were measured by Viswanathan *et al.*[7] Davy *et al.*[8] performed a theoretical study on structure, energy and vibration spectra of the small mixed species B_2Si, B_2Si_2 and BSi_2 using MO calculations.

More recently, a combined experimental and theoretical study on small anionic Si_nB^- and Si_nAl^- clusters with n = 1-6 were carried out by Sun *et al.*[9] using time-of-flight mass spectrometry and DFT calculations. In this context, an

investigation on Si_nB clusters in various charge states appears necessary to gain more insights into the structural features and fundamental properties of these intriguing systems.

Motivated by the above reasons, we set out to carry out a systematic investigation on a series of small boron doped silicon clusters Si_nB with n = 1-10 in the cationic, neutral and anionic states using both DFT and MO methods. Our theoretical predictions on the growth pattern point out that the closed shell systems $Si_{10}B^+$ and Si_9B^- are characterized by an enhanced stability. Their high thermodynamic stabilities can consistently be rationalized in terms of the electron shell model.

4.2. COMPUTATIONAL METHODS

Thermochemical properties of clusters considered are calculated using the composite G4 and CCSD(T)/CBS (complete basis set) approaches that were effectively used in our recent studies on silicon doped boron clusters B_nSi.[10]

Previous investigations on mixed Si_nM clusters indicated that the dopant M either adsorbs on the surface or substitutes one of the Si-atoms of a Si_{n+1} cluster. On this basis, the trial structures of Si_nB are generated by two ways: i) addition of a B-atom at different positions around the well-known geometric structures of the bare anionic, cationic and neutral silicon $Si_n^{-/0/+}$ clusters, and ii) substitution by a B-atom at a Si position of the Si_{n+1}parents. Then, their geometries are fully optimized. In addition, alternative structures of the doped silicon clusters previously reported are also used as initial structures for geometry optimizations at the B3LYP/6-31G(d) level.[11,12] Thanks to the fact that the structures of small pure and impure silicon clusters were well established (cf. previous chapters), our simple but careful and extensive search method allows us to find most, if not all, of the stable equilibrium structures of the Si_nB clusters considered. Geometries and vibrational frequencies of the converged equilibrium structures Si_nB and their anions and cations are subsequently reoptimized using again the hybrid B3LYP functional but in conjunction with the larger 6-311+G(d) atomic basis set.[13,14,15]

Standard enthalpies of formation of the global minima are evaluated from the corresponding total atomization energies (TAE)[16] using both G4[17] and CCSD(T)/CBS methods. These approaches are described in Chapter 2. Then, the calculated heats of formation at 0 K are used to evaluate the adiabatic ionization energy (IE), electron affinity (EA) and other energetic quantities. Due to our limited computational resources, CBS calculations are performed only for the smallest molecules Si_nB with n = 1-4. The G4 approach is therefore used for the entire series considered.

4.3. RESULTS AND DISCUSSION

The shapes of the equilibrium structures of the neutral Si_nB, cationic Si_nB^+ and anionic Si_nB^- systems and their relative energies obtained using both B3LYP and G4 methods, symmetry point groups are shown on Figures 4.1, 4.2, 4.3 and 4.4. The different components obtained in the CCSD(T)/CBS protocol (referred to hereafter as CBS) for evaluating their total atomization energies (ΣD_0) are given in Table 4.1. The heats of formation of the clusters derived using the ΣD_0 obtained from both CBS and G4 methods are given in Table 4.2. The computed adiabatic ionization energies (IEs) and adiabatic electron affinities (EAs) of Si_nB clusters are listed in Table 4.3. The average binding energies (E_b) and embedded energy (EE) are tabulated in Table 4.4.

4.3.1. Thermochemical properties of clusters

At the first glance, there is a reasonable agreement between both sets of CBS and G4 results. The heats of formation at 0K (ΔH^0_f) obtained by the CBS method are larger than those obtained applying the composite G4 approach (Table 4.2). The difference varies in the range of 0.9 − 5.8 kcal/mol. The adiabatic IE is obtained from the energy difference between the neutral Si_nB and its corresponding Si_nB^+ cation, whereas the adiabatic EA corresponds to the energy difference between the neutral Si_nB and its Si_nB^- anion. As expected, values given in Table 4.3 also reveal a better agreement between both theoretical approaches. The maximum difference between both sets of values is 0.11 eV for EA's and 0.12 eV for IE's. These differences of energetic values between both G4 and CBS methods can be understood from the ways of computing single point electronic energies, as well as the geometries of clusters

used (cf. Chapter 2). While geometries are obtained, as mentioned above, at the CCSD(T)/aug-cc-pVTZ level for the CBS method, the G4 approach actually uses geometries obtained at the B3LYP/6-31G(2df,p) level.

Table 4.1. Total atomization energies (ΣD_0, TAE, kcal/mol) for Si_nB clusters (n = 1-4) and different components of CCSD(T)/CBS computations

Structure[a]	ΔCBS[b]	E_{ZPE}[c]	ΔE_{CV}[d]	ΔE_{SR}[e]	ΔE_{SO}[f]	ΣD_0 (TAE)
1a.1	114.13	1.12	0.60	-0.26	-0.46	112.88
1n.1	75.37	1.05	0.63	-0.11	-0.46	74.37
1c.1	-132.83	1.00	0.31	0.04	-0.46	-133.94
2a.1	243.88	2.74	1.27	-0.55	-0.89	240.97
2n.1	187.55	2.52	1.41	-0.39	-0.89	185.17
2c.1	-10.37	2.22	0.90	0.24	-0.89	-12.34
3a.1	350.73	3.98	1.80	-0.80	-1.32	346.43
3n.1	284.17	3.78	1.88	-0.64	-1.32	280.31
3c.1	108.76	3.87	1.57	-0.32	-1.32	104.82
4a.1	449.37	5.34	2.44	-0.93	-1.75	443.79
4n.1	386.46	5.25	2.83	-0.75	-1.75	381.55
4c.1	216.14	4.63	3.00	-0.25	-1.75	212.52

[a] Shape of the optimized structures are given in Figure 4.1.

[b] Extrapolated by using eq. (1) with the aVQZ and aV5Z basis sets.

[c] Zero point energies taken from the CCSD(T) harmonic frequencies.

[d] Core-valence corrections obtained with the aug-cc-pwCVTZ basis set at the optimized CCSD(T) geometries.

[e] Scalar relativistic corrections based on CCSD(T)-DK/cc-pVTZ-DK calculations and expressed relative to the CCSD(T) results without DK corrections.

[f] Corrections due to the incorrect treatment of the atomic asymptotes as an average of spin multiplets. Values based on Moore's Tables, ref. 18.

Table 4.2. Heats of formation at 0K [ΔH_f (0 K)] and 298K [ΔH_f (298 K)] (kcal/mol) of Si_nB in neutral, cationic and anionic states obtained (G4 and CCSD(T)/CBS) in their lowest-energy forms.

	ΔH_f (0K)			ΔH_f (298K)		
	G4	**CBS**	**Exptl.[a]**	**G4**	**CBS**	**Exptl.[a]**
1a.1	128.11	129.42		129.19	130.49	
1n.1	167.06	167.93	165.87 ± 3.35	168.15	169.01	166.82±3.35
1c.1	378.12	376.24		379.22	377.34	
2a.1	105.80	108.53		106.78	109.50	
2n.1	162.92	164.33	163.72 ± 4.78	163.87	165.28	164.43±4.78
2c.1	360.25	361.84		361.26	362.84	
3a.1	107.10	110.27		108.13	111.29	
3n.1	174.80	176.39	167.06 ± 7.41	175.85	177.43	167.54±7.41
3c.1	350.56	351.88		351.59	352.88	
4a.1	114.29	120.11		115.25	121.01	
4n.1	178.99	182.35		180.20	183.45	
4c.1	348.46	351.38		350.20	352.58	
5a.1	96.49			97.69		
5n.1	174.11			175.38		
5c.1	350.56			351.77		
6a.1	105.22			106.40		
6n.1	188.32			189.91		
6c.1	353.20			354.56		
7a.1	138.94			140.49		
7n.1	206.48			208.03		
7c.1	358.62			360.16		
8a.1	147.61			149.35		
8n.1	222.52			224.54		
8c.1	363.72			365.02		

9a.1	126.07	128.22
9n.1	210.21	212.57
9c.1	369.09	371.26
10a.1	164.52	166.73
10n.1	235.70	238.06
10c.1	358.01	360.38

[a] Experimental values taken from ref. 7.

Table 4.3. Adiabatic ionization energies (IE, eV) and electronic affinity (EA, eV) of neutral Si_nB using G4 and CCSD(T)/CBS calculations.

Neutrals	Cations	IE		Anions	EA	
		G4	CBS		G4	CBS
1n.1 ($C_{\infty v}$ $^4\Sigma^-$)	**1c.1** ($C_{\infty v}$ $^3\Sigma^+$)	9.15	9.03	**1a.1** ($C_{\infty v}$ $^3\Pi$)	1.69	1.67
2n.1 (C_{2v} $^2B_2$)	**2c.1** (C_{2v} $^1A_1$)	8.56	8.56	**2a.1** (C_{2v} $^1A_1$)	2.48	2.42
3n.1 (C_{2v} $^2A_1$)	**3c.1** (C_{3v} $^1A_1$)	7.62	7.61	**3a.1** (C_{2v} $^1A_1$)	2.94	2.87
4n.1 (C_{2v} $^2B_2$)	**4c.1** (D_{4h} $^1A_{1g}$)	7.35	7.33	**4a.1** (C_{3v} $^1A_1$)	2.81	2.70
5n.1 (C_s ^{2}A")	**5c.1** (C_s ^{1}A')	7.65		**5a.1** (C_{4v} $^1A_1$)	3.37	
6n.1 (C_s ^{2}A")	**6c.1** (C_{2v} $^1A_1$)	7.15		**6a.1** (C_{5v} $^1A_1$)	3.60	
7n.1 (C_s ^{1}A')	**7c.1**(C_s ^{1}A')	6.60		**7a.1** (C_s ^{1}A')	2.93	
8n.1(C_1 ^{2}A)	**8c.1**(O_h $^1A_{1g}$)	6.12		**8a.1**(C_s ^{1}A')	3.25	
9n.1(C_s ^{2}A')	**9c.1**(C_{3v} $^1A_1$)	6.89		**9a.1**(D_{3h} $^1A_1$')	3.65	
10n.1(C_s ^{2}A')	**10c.1**(C_{4v} $^1A_1$)	5.30		**10a.1**(C_1 ^{1}A)	3.09	

More importantly, both methods show a good agreement with available experimental data. The heats of formation of diatomic SiB obtained from the G4 and CBS methods amount to 167.1 and 167.9 kcal/mol, respectively, that agree well with the experimental value of 165.87 ± 3.35 kcal/mol[7] which was determined by using

Knudsen cell mass spectrometry and thermal functions. Similar observation is found for the triatomic Si_2B whose experimental heat of formation of 163.72 ± 4.78 kcal/mol[7] is somewhat larger than the G4 value of 162.9 kcal/mol but slightly smaller than the CBS value of 164.3 kcal/mol. The computed heats of formation of 174.8 (G4) and 176.4 (CBS) kcal/mol for Si_3B are significantly larger than its available experimental value of 167.06 ± 7.41,[7] but they are also situated within the error margin of ± 7.41 kcal/mol. This agreement lends us confidence in thermochemical parameters predicted for the remaining clusters. The G4 values thus provide us with a consistent set of heats of formation for the whole series of Si_nB clusters in three charge states, and they can be used for the systems whose experimental data are not determined yet.

4.3.2. Lower-lying isomers of Si_nB clusters and their growth mechanism

As mentioned above, a large number of isomeric equilibrium structures are located for each of the clusters considered. In this chapter, we only present some lower-lying isomers whose relative energies are close to the ground states (within 1.0 eV). As for a convention, each structure described hereafter is defined by the label **nX.Y** in which **n** is the size of Si_n, **X = n, c, a** stands for a neutral, cation or anion, respectively, and **Y** = **1, 2**… indicates the energy ordering of the isomer considered. We first describe briefly the situation in each size, followed by an analysis of their growth pattern.

n = 1: SiB, SiB^+ and SiB^-. In good agreement with earlier reports,[19] our calculations show that the diatomic SiB is characterized by the high spin **1n.1** with the $^4\sum^-$: $[1\sigma^2 2\sigma^2 1\pi^2 3\sigma^1]$ valence electronic configuration. Following attachment of one excess electron into π bonding orbital, the high spin state **1a.1** $^3\Pi$: $[1\sigma^2 2\sigma^2 1\pi^2 2\pi^1 3\sigma^1]$ becomes the ground state of SiB^-. The cationic diatomic SiB^+ is found to be the triplet **1c.1** with valence electronic configuration of $^3\sum^+$: $[1\sigma^2 2\sigma^2 1\pi^2 3\sigma^0]$.

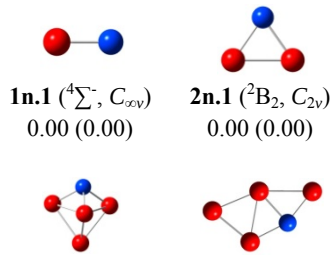

1n.1 ($^4\Sigma^-$, $C_{\infty v}$) 0.00 (0.00) **2n.1** ($^2B_2$, C_{2v}) 0.00 (0.00) **3n.1** ($^2A_1$, C_{2v}) 0.00 (0.00) **3n.2** ($^2A_1$, C_{2v}) 0.47 (0.56) **4n.1** ($^2B_2$, C_{2v}) 0.00 (0.00)

4n.2 ($^2A'$ C_s) 0.45 (0.70) **4n.3** ($^2A''$ C_s) 0.57 (0.38)

a) The neutral Si_nB clusters

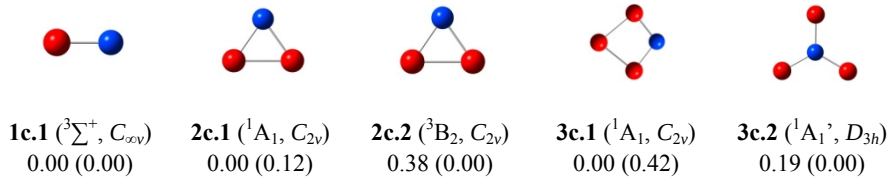

1c.1 ($^3\Sigma^+$, $C_{\infty v}$) 0.00 (0.00) **2c.1** ($^1A_1$, C_{2v}) 0.00 (0.12) **2c.2** ($^3B_2$, C_{2v}) 0.38 (0.00) **3c.1** ($^1A_1$, C_{2v}) 0.00 (0.42) **3c.2** ($^1A_1'$, D_{3h}) 0.19 (0.00)

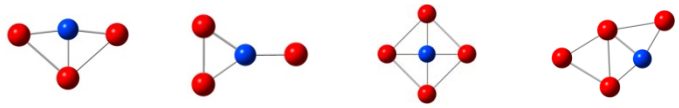

3c.3 ($^3B_2$, C_{2v}) 0.71 (0.69) **3c.4** ($^3B_2$, C_{2v}) 1.13 (0.83) **4c.1** ($^1A_{1g}$, D_{4h}) 0.00 (0.00) **4c.2** ($^1A'$, C_s) 0.67 (0.70)

b) The cationic Si_nB^+ clusters

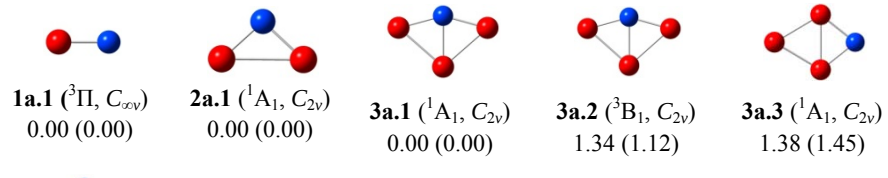

1a.1 ($^3\Pi$, $C_{\infty v}$) 0.00 (0.00) **2a.1** ($^1A_1$, C_{2v}) 0.00 (0.00) **3a.1** ($^1A_1$, C_{2v}) 0.00 (0.00) **3a.2** ($^3B_1$, C_{2v}) 1.34 (1.12) **3a.3** ($^1A_1$, C_{2v}) 1.38 (1.45)

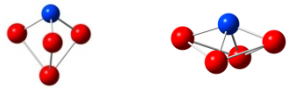

4a.1 ($^1A_1$, C_{3v}) 0.00 (0.11) **4a.2** ($^1A_1$, C_{2v}) 0.04 (0.00)

c) The anionic Si_nB^- clusters

Figure 4.1. Shapes, electronic states and relative energies (ΔE, eV) of the lower-lying isomers Si_nB with n = 1-4 at the **a**) neutral, **b**) cationic, and **c**) anionic states. ΔE values are obtained at the G4 and B3LYP/6-311+G(d)+ZPE (in parentheses) levels.

n = 2: Si_2B, Si_2B^+ and Si_2B^-. Si_2B has a triangular ground state **2n.1** (C_{2v}, $^2B_2$) in which the B atom connects with two Si-atoms. Following either attachment or detachment of one electron to form the charge species, the shape of the resulting ions remains almost unchanged. Both the cation Si_2B^+ and anion Si_2B^- exhibit the C_{2v} ($^1A_1$) structures **2c.1** and **2a.2** with closed-shell electronic configurations (Figure 4.1).

n = 3: Si_3B, Si_3B^+ and Si_3B^- (Figure 4.1). Si_3B has a C_{2v} ($^2A_1$) ground state **3n.1** in which the third Si atom is connected with a Si-B edge of **2n.1** rather than with a Si-Si edge. The next isomer is another C_{2v} ($^2A_1$) structure **3n.2** with a relative energy of 0.47 eV, which is formed from the latter motif where the third Si-atom is connected with the Si-Si edge of **2n.1**. There is a negligible difference in geometries of the anion Si_3B^- and cation Si_3B^+ as compared to their neutral counterpart. The structure **3a.1** (C_{2v}, $^1A_1$) is found to be the global minimum of Si_3B^-. The remaining isomers are at least 1.34 eV less stable than **3a.1** (Figure 4.1).

At the B3LYP/6-311+G(d) level, a high symmetry structure **3c.2** (D_{3h}, $^1A_1$') in which the B-impurity is located at the center of a Si_3 triangle is calculated to be the lowest-energy isomer for the cation Si_3B^+. The next isomer is a C_{2v} $^1A_1$ structure **3c.1** that has the shape of the corresponding neutral **3n.1**. However, G4 calculations point out a reversed energy ordering that **3c.1** is now the most stable isomer with energy gap of 0.19 eV below **3c.2**. Two triplet states **3c.3** and **3c.4** are also located as local minima with 0.71 and 1.13 eV higher in energy as compared to **3c.1** (Figure 4.1).

n = 4: Si_4B, Si_4B^+ and Si_4B^- (Figure 4.1). Interestingly, the Si_4B^+ cation exhibits a perfect squared form **4c.1** (D_{4h}, $^1A_1$') in which B-atom is located at the center of a Si_4 square. This isomer can be formed by directly binding one Si atom to the B atom of **3n.1**. The shape of MOs of **4c.1** reveals that its LUMO and LUMO+1 are degenerate. Consequently, following attachment of one excess electron, geometry of the corresponding neutral is distorted under a Jahn-Teller effect. Structure **4n.1** (C_{2v}, $^2B_2$) in which the B atom is distorted out of the structural plane of **4c.1**, is found to be the global minimum for Si_4B. Based on G4 results, the 3D form **4n.2** is the next isomer which is 0.45 eV less stable than the global minimum. A planar form **4n.3**

which is formed by connecting the fourth Si atom with the Si-Si edge of **3n.1** is also located with a relative energy of 0.57 eV.

In the anionic state, there is an interesting competition in energy between both isomers **4a.1** and **4a.2**. At the B3LYP/6-311+G(d) level, **4a.2** is the lowest-lying isomer being 0.11 eV more stable than **4a.1**. However, our G4 results show a reversed energy ordering in that **4a.1** is now the most stable isomer, but being only 0.04 eV lower in energy than **4a.2**. This gap is decreased to 0.026 eV from CCSD(T)/aug-cc-pVTZ calculated results. Thus, we can conclude that both structures likely exist as degenerate equilibrium ground states for the anion Si_4B^-.

n = 5: Si_5B, Si_5B^+ and Si_5B^- (Figure 4.2). The most stable form of Si_5B is a 3D structure **5n.1** (C_s, $^2A''$) in which the new Si atom is located on the C_4 axis and bound to four Si-atoms of **4n.1**. The second isomer is a C_s structure **5n.2** that is 0.41 eV higher in energy. Remaining structures are much less stable being at least 0.64 eV higher in energy.

Following attachment of one excess electron, the anion Si_5B^- turns out to have a high symmetry C_{4v} ($^1A_1$) structure **5a.1** that is similar to its neutral counterpart. Other isomeric anions are found to be at least 0.63 eV higher in energy as compared to **5a.1**. Interestingly, **5c.3** is calculated as the lowest-energy isomer of the cation Si_5B^+ by B3LYP/6-311+G(d). Again, G4 results give rise to a reversed energy ordering in which **5c.1** is now the most stable isomer and located at 0.52 eV below **5c.3**. Thus, we establish that **5c.1** is the lowest-energy form of the cation Si_5B^+.

n = 6: Si_6B, Si_6B^+ and Si_6B^- (Figure 4.2). The Si_6B ground state is a low symmetry C_s ($^2A''$) structure **6n.1** which is formed by either adding one Si atom into the plane containing the four-membered ring of **5n.1**, or by adsorbing one Si-atom on the C5 axis of **5n.4**. A C_{2v} structure **6n.2** which is formed by substituting a Si atom of the pentagon Si_7 framework by a B, is found to be the second-lying isomer with a large relative energy of 0.39 eV. Two other isomers **6n.3** and **6n.4** that can be derived by adding one Si atom on a different triangular faces of **5n.1** are the next isomers with relative energies of ~0.45 eV.

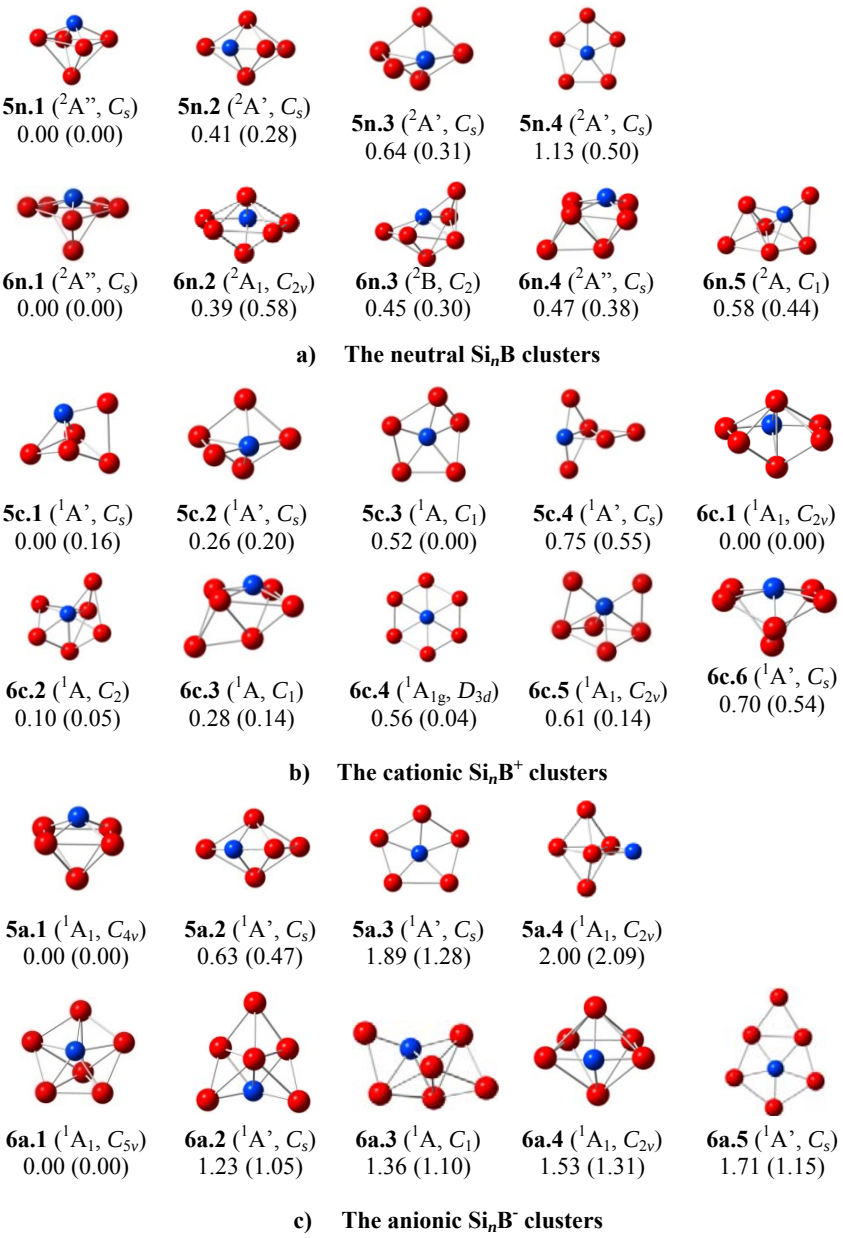

Figure 4.2. Shapes, electronic states and relative energies (ΔE, eV) of the lower-lying isomers Si_nB with n = 5 and 6 at the **a**) neutral, **b**) cationic, and **c**) anionic states. ΔE values are from G4 and B3LYP/6-311+G(d)+ZPE (in parentheses) computations.

There is a structural competition for Si_6B^+ cations. Accordingly, two structures including the C_{2v} **6c.1** which is a distorted form of **6n.2,** and the C_2 **6c.2** which is actually the cationic state of **6n.3**, are almost degenerate within an energy gap of 0.1 eV. The next isomer is the C_1 **6c.3** that corresponds to a **6n.4** cation. Although the high symmetry **6c.4** (D_{3d}) has a tiny energy gap of 0.04 eV at the B3LYP/6-311+G(d) level, G4 results point out that it is much less stable with a relative energy of 0.56 eV. The corresponding cationic species of **6n.1** is found to be much less stable with energy gap of 0.70 eV.

The anion Si_6B^- is a perfect bipyramid pentagonal **6a.1**. Although some other isomers **6a.2** – **6a.5** are also located, they are at least 1.23 eV higher in energy.

n = 7: Si_7B, Si_7B^+ and Si_7B^- (Figure 4.3). G4 results emphasize two degenerate structures **7n.1** and **7n.2** for the neutral Si_7B. They are formed by adding one Si on different triangular faces of the neutral **6n.1** (Figure 4.2). The isomer **7n.3** is also found to be quite stable being at 0.11 (G4) and 0.12 (B3LYP) eV.

Following either an attachment or a detachment of one electron, the shape of the resulting charged species Si_7B^+ and Si_7B^- are slightly distorted with respect to their neutral form. The ions **7c.1** and **7a.1**, that are distorted forms of **7n.1**, are the structures of the cation Si_7B^+ and anion Si_7B^-, respectively. The following isomers **7c.2** and **7a.2** are basically the cationic and anionic forms of **7n.2**. Other isomers are much less stable relative to their global minima.

n = 8: Si_8B, Si_8B^+ and Si_8B^- (Figure 4.3). There is again a strong competition in bonding motifs for the Si_8B clusters. Two structures including **8n.1** which is formed by adding the new Si on a triangular Si_3 face of **7n.2**, and a packing form **8n.2** in which B is located at the center of the cubic Si_8 form are almost degenerate in energy. The energy difference between them is only 0.08 eV (B3LYP/6-311+G(d)), and this gap is slightly increased to 0.14 eV in favor of **8n.1** by G4 calculations.

For anionic clusters, B3LYP calculations result in two degenerate structures **8a.1** and **8a.4** with an energy gap of only 0.05 eV. However, G4 results show that **8a.1** is the most stable isomer as this gap is increased up to 0.42 eV. The structure

8a.2 which is formed by substituting one Si-atom of the bicapped pentagonal bipyramid Si_9 structure by one B, is rather stable being only 0.26 eV higher in energy.

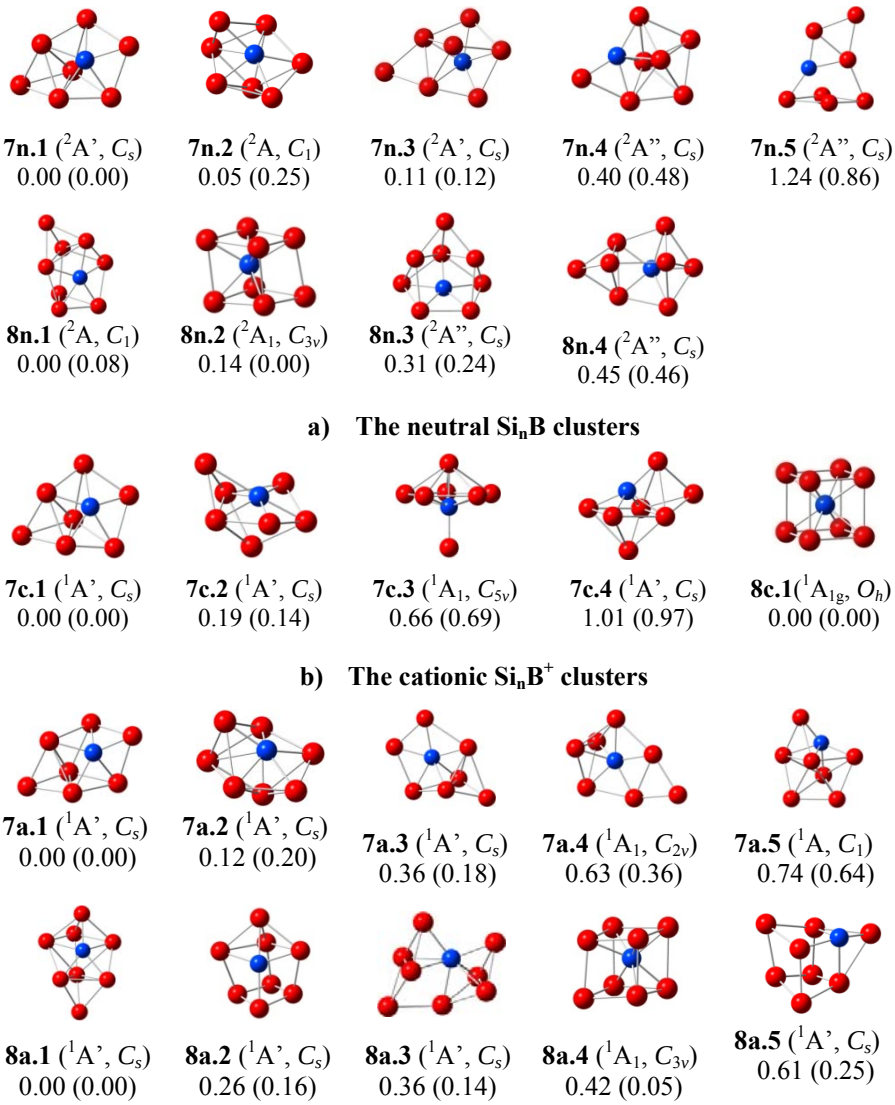

Figure 4.3 Shapes, electronic states and relative energies (ΔE, eV) of the lower-lying isomers Si_nB with n = 7-8 at the **a**) neutral, **b**) cationic, and **c**) anionic states. ΔE values are G4 and B3LYP/6-311+G(d) + ZPE (in parentheses) levels.

Present computations thus confirm that in the cationic state, the perfect octahedral cube **8c.1** is the global minimum of Si_8B^+.[1] Other isomers are found to be much less stable than **8c.1**. We would refer to the previous paper[1] for a detailed analysis of the chemical bonding phenomenon and the special aromatic character of the cubic Si_8B^+.

n = 9: Si_9B, Si_9B^+ and Si_9B^- (Figure 4.4). Our G4 results indicate that the C_s ^{2}A' **9n.1** that is constructed by adding the entering Si on top of **8n.2** is the most stable isomer of Si_9B. This structure is similar to that of the Si_9Be reported by Kumar and Kawazoe.[20] The C_s ^{2}A' **9n.2** in which B is situated inside of the Si_9 cage is almost degenerate at the B3LYP/6-311+G(d) level. Again, G4 calculations place the latter at 0.42 eV higher in energy relative to **9n.1**. The charged species **9a.1** and **9c.1** possess the same shape as their neutral, but with a higher symmetry.

n = 10: $Si_{10}B$, $Si_{10}B^+$ and $Si_{10}B^-$ (Figure 4.4). B3LYP/6-311+G(d) energies show that **10n.3** in which B is located inside a Si_{10} cage composed of two five-membered rings, is the lowest-energy isomer. The next isomer is the C_s **10n.1** that is formed by attaching the additional Si on a triangular face of **9n.2** with 0.16 eV higher in energy than **10n.3**, and the C_1 **10n.2** is located with relative energy of 0.36 eV. As in the previous case, G4 results however indicate that **10n.1** is actually the most stable isomer of $Si_{10}B$ and **10n.2** is a quasi-degenerate being only 0.02 eV higher in energy than **10n.1**. For its part, **10n.3** is now at 0.16 eV higher in energy (G4). **10n.4** is formed by adding one Si on a triangular face of **9n.3** and also low-energy being 0.16 eV above **10n.1** (G4).

The C_{4v} $^1A_1$ **10c.1** in which B is located at the center of a Si_{10} cage is the lowest-energy $Si_{10}B^+$. Interestingly, **10c.1** is again found to be similar to its isoelectronic species $Si_{10}Be$ reported earlier.[20a] Structures **10c.2** and **10c.5** that are the cationic forms of **10n.1** and **10n.2**, respectively, are now much less stable with relative energy of 0.82 and 1.22 eV (G4).

For the anions $Si_{10}B^-$, five structures, namely **10a.1** – **10a.5**, are almost degenerate in energy within an energy separation of only 0.09 eV at B3LYP/6-

311+G(d) (Figure 4.4). On the contrary, G4 computations suggest that the two structures **10a.1** and **10a.2** are the more stable among the isomers located.

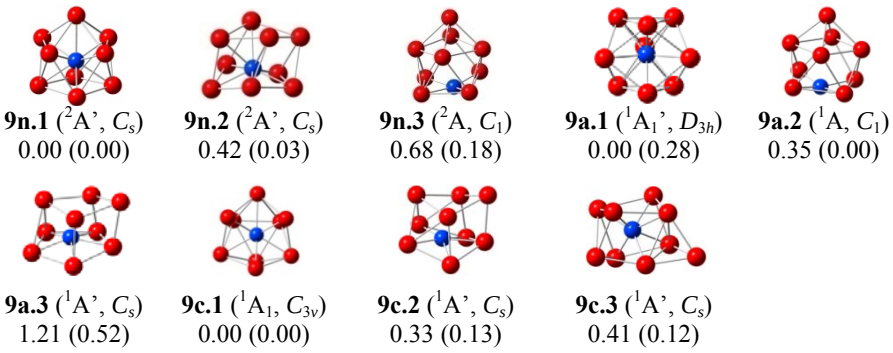

a) The Si_9B clusters

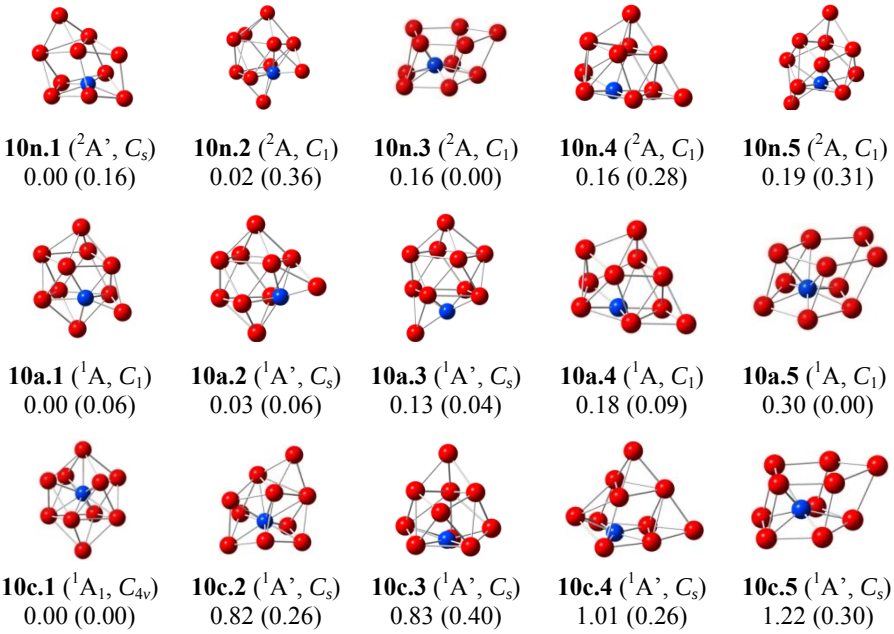

b) The $Si_{10}B$ clusters

Figure 4.4 Shapes, electronic states and relative energies (ΔE, eV) of the lower-lying isomers of **a**) Si_9B and **b**) $Si_{10}B$. ΔE values are from G4 and B3LYP/6-311+G(d) + ZPE (in parentheses) levels.

Growth Pattern. On the basis of the structural features of the most stable forms identified above, the growth mechanism for the clusters Si_nB with n = 1-10 emerge as follows:

i) each boron doped silicon cluster Si_nB is formed by adding the new Si atom into the smaller sized but doped cluster $Si_{n-1}B$. This motif appears to be more favoured over the alternative in which the B atom attaches to the Si_n core;

ii) a competition between the exposed (exohedral) and the enclosed (endohedral) structures appears to occur from the size n = 8 (Si_8B) where the exposed **8n.1** remains energetically preferred over the enclosed counterpart **8n.2** even though the energy separation is getting small, and

iii) the larger size clusters Si_9B and $Si_{10}B$ definitely prefer an enclosed structure where the B-impurity is now doped inside the corresponding Si_n cage.

4.3.3. Relative stability of clusters considered

In order to probe the inherent thermodynamic stability of the clusters considered, the average binding energies (E_b) and embedded energies (EE) of clusters are examined. The average binding energies (E_b) can be defined as follows:

$$E_b(Si_nB) = [nE(Si) + E(B) - E(Si_nB)]/(n+1) \quad (4.1)$$

$$E_b(Si_nB^-) = [(n-1)E(Si) + E(Si^-) + E(B) - E(Si_nB^-)]/(n+1) \quad (4.2)$$

$$E_b(Si_nB^+) = [(n-1)E(Si) + E(Si^+) + E(B) - E(Si_nB^+)]/(n+1) \quad (4.3)$$

where E(B), E(Si), $E(Si^+)$, $E(Si^-)$ are total energies of the B-atom, Si-atom and the charged Si^+ and Si^-, respectively. $E(Si_nB)$, $E(Si_nB^+)$ and $E(Si_nB^-)$ are total energies of the clusters Si_nB at the neutral, cationic and anionic states, respectively. All these values are obtained from G4 calculations.

The E_b values are summarized in Table 4.4, while their plots are depicted in Figure 4.5a. It can be seen that the E_b values tend to be increased with increasing cluster sizes. The $Si_{10}B^+$ cluster reveals the highest E_b value as compared to the smaller cationic Si_nB^+ species. At the neutral state, Si_9B presents the highest E_b value

that indicates its high thermodynamical stability. Similarly, in the series of anions considered, it is Si_9B^- which gets a maximum peak in the E_b plot (Figure 4.5).

Table 4.4. Average inding energies (E_b, eV) and embedded energies (*EE*, eV) of Si_nB^-, Si_nB and Si_nB^+ clusters (G4 calculations)

n	***E*_b**			***EE***		
	Si_nB^-	Si_nB	Si_nB^+	Si_nB^-	Si_nB	Si_nB^+
1	1.80	1.63	1.13	3.60	3.26	2.25
2	3.07	2.70	2.56	5.05	4.86	4.20
3	3.45	3.06	3.19	5.34	4.72	5.39
4	3.63	3.34	3.50	5.24	4.62	5.27
5	3.93	3.59	3.67	6.07	5.21	5.72
6	3.98	3.65	3.80	6.08	4.63	5.24
7	3.88	3.68	3.87	5.10	4.09	5.52
8	3.92	3.71	3.94	5.80	5.11	6.10
9	4.09	3.86	3.98	7.17	5.70	6.53
10	3.99	3.83	4.09	4.93	4.19	6.84

To confirm our above findings, the embedded energy (*EE*) of clusters is further examined. Embedded energy is the energy gain in incorporating B-impurity into the Si_n hosts and defined as follows (equation 4.4):

$$EE(Si_nB^{-/0/+}) = E(Si_n^{-/0/+}) + E(B) - E(Si_nB^{-/0/+}) \qquad (4.\ 4)$$

where $E(Si_n^{-/0/+})$ are the total G4 energies of the anionic, neutral and cationic Si_n clusters, respectively. These total G4 energies are previously calculated for the global minima of the pure clusters $Si_n^{0/-/+}$ reported in Chapter 2.

Table 4.4 and Figure 4.5b show that Si_9B and Si_9B^- are indeed characterized by the highest *EE* values among of the neutral Si_nB and anionic Si_nB^- clusters, respectively. These predictions agree well with the findings for the E_b values. Similarly, the cation $Si_{10}B^+$ again possesses the highest EE value as compared to other

cationic species within the series. From these observations, we conclude that an enhanced thermodynamic stability is established for the species $Si_{10}B^+$, Si_9B, and Si_9B^-.

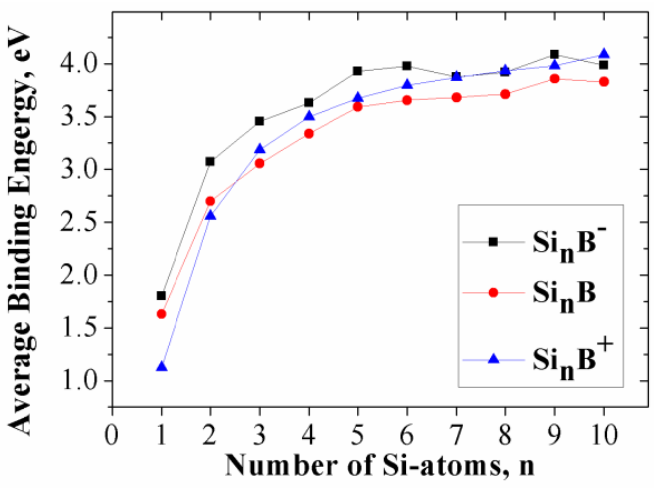

a) Plots of average binding energy (eV)

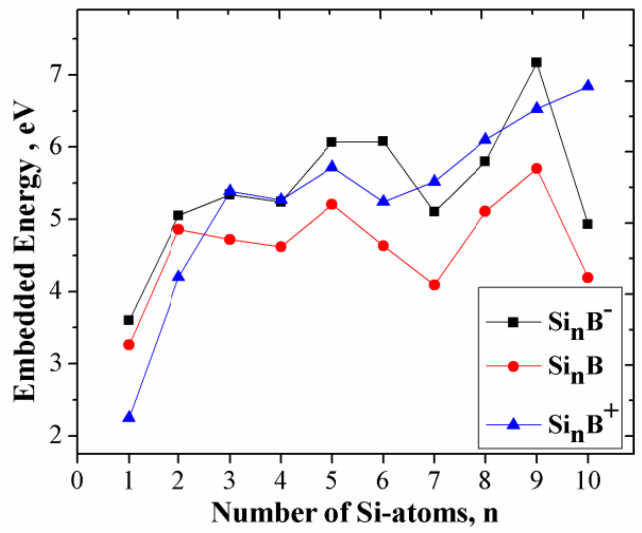

b) Plots of embedded energies (eV)

Figure 4.5. Average binding energy (E_b, eV) and embedded energies (*EE*, eV) of the $Si_nB^{+/0/-}$ clusters using the composite G4 method.

4.3.4. Dissociation energies

In order to evaluate further the thermodynamic stability, the dissociation energies (D_e) for the various fragmentation channels of the clusters considered are determined. Results calculated from total G4 energies are shown in Table 4.5.

Table 4.5. Dissociation energies (D_e, kcal/mol) for various fragmentation channels of Si_nB in neutral, cationic and anionic states (G4 calculations).

n	***D*e , kcal/mol**									
	(1)	**(2)**	**(3)**	**(4)**	**(5)**	**(6)**	**(7)**	**(8)**	**(9)**	**(10)**
1	75.2	75.2	108.5	83.1	83.1	108.5	54.6	51.9	51.9	54.6
2	111.3	112.1	129.5	137.4	116.5	163.6	125.1	101.7	96.8	105.2
3	95.3	108.9	105.9	131.9	123.2	170.9	116.9	107.3	124.3	123.5
4	103.0	106.5	100.0	136.6	120.8	165.5	109.3	121.3	121.5	127.4
5	112.1	120.0	125.0	158.6	140.0	192.0	105.1	123.3	132.0	134.0
6	93.0	106.8	98.5	145.0	140.3	184.2	104.6	115.8	120.9	132.3
7	89.0	94.4	73.5	125.5	117.6	156.2	101.8	124.6	127.3	132.6
8	91.2	117.9	98.5	135.0	133.9	187.1	102.1	137.7	140.7	167.1
9	119.5	131.5	128.7	172.6	165.3	210.0	101.8	148.3	150.7	163.0
10	81.7	96.7	68.7	121.8	113.7	162.1	118.3	147.1	157.7	164.7

(1) $Si_nB \rightarrow Si_{n-1}B+Si$; (2) $Si_nB \rightarrow Si_n+B$; (3) $Si_nB^- \rightarrow Si_{n-1}B^- +Si$; (4) $Si_nB^- \rightarrow Si_{n-1}B + Si^-$;
(5) $Si_nB^- \rightarrow Si_n^- + B$; (6) $Si_nB^- \rightarrow Si_n + B^-$; (7) $Si_nB^+ \rightarrow Si_{n-1}B^+ +Si$;
(8) $Si_nB^+ \rightarrow Si_{n-1}B + Si^+$; (9) $Si_nB^+ \rightarrow Si_n^+ + B$; (10) $Si_nB^+ \rightarrow Si_n + B^+$

Dissociation energies of the neutrals Si_nB for the Si-elimination channel (**1**) $Si_nB \rightarrow Si_{n-1}B + Si$ turn out to be smaller than those for the B-loss channel (**2**) $Si_nB \rightarrow Si_n + B$. This observation is consistent with the growth mechanism established above that a neutral Si_nB tends to be formed by attaching one extra Si into the smaller size $Si_{n-1}B$, rather than the alternative motif where the B-impurity is doped into the Si_n host. Similar observations are found for the charged species that the anionic Si_nB^- and cationic Si_nB^+ clusters tend to be fragmented to form one Si atom plus a smaller anion

$Si_{n-1}B^-$ along the fragmentation channel (**3**) and the cation $Si_{n-1}B^+$ along the channel (**7**), respectively.

More importantly, our calculations reveal that the clusters Si_9B, Si_9B^- and $Si_{10}B^+$ exhibit the highest D_e values within the series of neutral, anionic and cationic clusters, respectively. These results are internally consistent with the above discussion that these species constitute the enhanced stability systems among the clusters considered.

4.3.5. Enhanced stability and Jellium electron shell model (JSM)

As for a rationalization of the relative stability of Si_nB clusters, we re-examine their MO pictures under the viewpoint of the Jellium electron shell model (JSM),[21] which was successfully applied to interpret the stability motif of different types of atomic clusters in our recent reports.[1,2,3,4,22] According to this simple model in which the valence electrons are assumed to be itinerant in a simple mean-field potential formed by the nuclei of atoms, the valence electrons fill the spherical orbitals following the pattern of orbitals as $[1S^21P^61D^{10}2S^21F^{14}2P^61G^{18}2D^{10}\ldots]$ etc… Within this model, the number of electrons of 2, 8, 18, 20, 34, 40, 58 and 68… emerge as the magic numbers that simply correspond to a complete filling of the successive shell electrons.

We should note that the observed number of closed shell electrons of a simple JSM is predicted on the basis of a spherical background. Thus, these magic numbers can eventually be changed due to a lowering of the molecular symmetry which induces a slight perturbation of the mean-field potential. For instance, based on a mass spectroscopic study, Lievens and coworkers found that the $Pb_{12}Al^+$ cluster containing 50 valence electrons is a species with enhanced stability.[23] This special stability can be rationalized by considering the fact that a splitting of the $l = 4$ (F) shells in an icosahedral symmetry invariably lowers the energy level under crystal field effects.[24] This assumption was subsequently applied to rationalize the high stability of the doped group IVA clusters such as the clusters $X_{10}M^-$ (X = Ge, Sn, Pb and M = Cu, Ag, Au),[2,3] $Ge_{12}M^q$ (M = Li, Be, Mg, B, Al), and $Sn_{12}Zn$.[4]

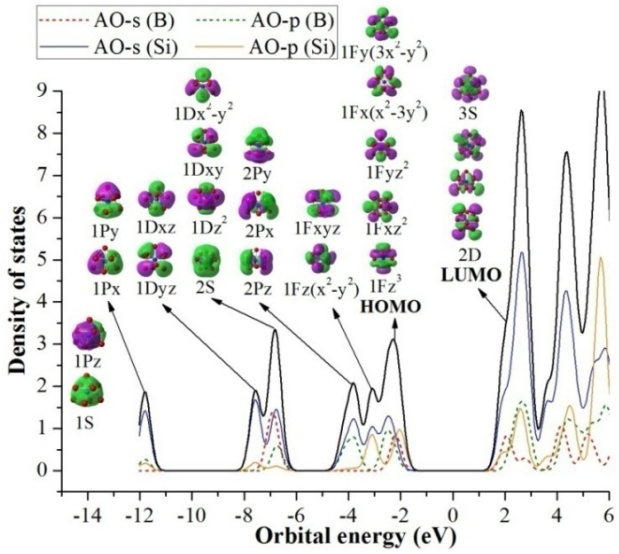

a) Total (black solid line) and partial (colored lines) DOSs of the lowest-lying Si_9B^-

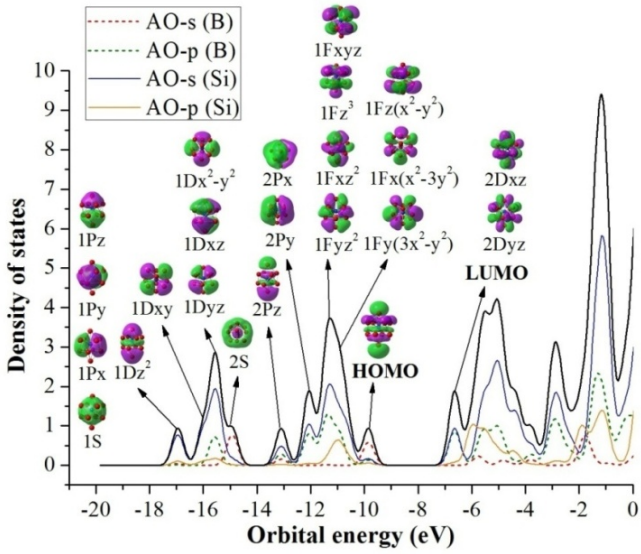

b) Total (black solid line) and partial (colored lines) DOSs of the lowest-lying $Si_{10}B^+$

Figure 4.6. Total (DOS) and partial (pDOS) densities of state of **a**) Si_9B^- and **b**) $Si_{10}B^+$. The shapes of orbitals of clusters are obtained from B3LYP/6-311+G(d) calculations.

The shape of the MOs and their energy levels of the Si_9B^- anion displayed in Figure 4.6a indicate that its 40 valence electrons are distributed in the following electron configuration of Si_9B^-:

$[1(A_1')^2 1(A_2'')^2 1(E')^4 1(E'')^4 2(A_1')^4 2(E')^4 2(A_2'')^2 3(E')^4 2(E'')^4 4(E')^4 3(A'')^2 3(A')^2 1(A_2')^2]$.

The lowest MO is an *s*-type valence orbital, being followed by three *p*-type orbitals of the $1P^6$ subshell. Our analysis shows that the 1S-orbital is constructed by interaction between *s*-AO of B-atom and *s*-AOs of Si-atoms, while MOs of 1P subshells are mainly composed of *s*-AO(Si) and *p*-AOs of B-atom with much smaller contribution. The partial densities of states (pDOS) plots also reveal that s-orbital of the 2S subshell is formed by a symmetric combination of 3*s*-AOs of Si and 2*s*-AO of B. This combination stabilizes the 2S subshell in pushing it deeper into the 1D subshell. More interestingly, the significant contributions of 2*p*-AOs of B and 3*s*-AOs of Si are also observed for the MOs of the 2P subshell. An analysis of MOs indicates that while the MOs of the P-subshells contribute to both chemical bonds between B-impurity and Si_9 host, and also to those of Si-atoms of the Si_9 host. The remaining MOs are only responsible for chemical bonding within the Si_9 host framework. Generally, although the 1D-subshell is split into the 2S-subshell due to the effect of B-impurity, the electronic configuration of the anion Si_9B^- basically satisfies the electron shell model of Si_9B^-: $[1S^2 1P^6 1D^{10} 2S^2 2P^6 1F^{14} 1G^0]$ and makes it an enhanced stability species with a magic number of 40 valence electrons.

Similar observation is also found for the cationic clusters $Si_{10}B^+$ (Figure 4.6b) containing 42 valence electrons with electronic configuration of $Si_{10}B^+$:

$[(1A_1)^2 (1E)^4 (2A_1)^2 (3A_1)^2 (1B_1)^2 (2E)^4 (1B_2)^2 (4A_1)^2 (5A_1)^2 (3E)^4 (6A_1)^2 (4E)^4 (2B_1)^2 (4E)^4 (2B_2)^2 (7A_1)^2 (5E)^0]$.

This corresponds to the energy sequence of electronic shell model as:

$[1S^2 1P^6 1D^{10} 2S^2 1F^2 2P^6 1F^{12} 1G^2]$.

Similar to the cases of the clusters doped by elements of group IVA previously reported, due to a symmetry lowering of the $Si_{10}B^+$ (C_{4v}) geometry, the G-subshell is now split and results in a large energy gap of 3.16 eV between the frontier orbitals, that ultimately leads to a large stabilization and high thermodynamic stability for the cation $Si_{10}B^+$.

The numbers of valence electrons of Si_4B^- and Si_8B^+ are 20 and 34, respectively, that are also magic numbers in JSM. However, our theoretical predictions point out that they are not emerged with an enhanced stability as the cases of Si_9B^- and $Si_{10}B^+$. Experimental studies that could be performed in near future are expected to give more insights into the stability of these interesting motifs.

4.4. CONCLUDING REMARKS

In this study, we reported on a systematic investigation of the boron doped silicon clusters Si_nB (n = 1-10) in the neutral, anionic and cationic states using quantum chemical MO calculations. The global minima of the clusters considered were identified on the basis of the G4 energies. Total atomization energies, heats of formation and the thermochemical derivatives such as ionization energy, electron affinity, dissociation energies… were obtained using G4 and CCSD(T)/CBS methods. Some available experimental thermochemical values can be assessed. We thus determined for the first time a consistent and reliable set of values for the standard enthalpies of formation for the whole series of Si_nB.

The growth mechanism for boron doped silicon clusters Si_nB with n = 1 -10 can be established as follows:

i) Each boron doped silicon cluster Si_nB is formed by attaching the additional Si atom into the smaller size and doped $Si_{n-1}B$;

ii) A competition between the exposed and the enclosed structures begins to occur at the size n = 8 (Si_8B), and

iii) The larger size clusters such as Si_9B and $Si_{10}B$, exhibit the enclosed structures where the B-impurity is doped at the center of the corresponding Si_n host cage.

Our calculations also predicted that the species Si_9B^-, Si_9B and $Si_{10}B^+$ are characterized by an enhanced stability with high average binding energies and embedded energies. The higher stability of the closed shells Si_9B^- and $Si_{10}B^+$ can be rationalized in terms of the Jellium electron shell model.

References

1) V. T. Ngan, M. T. Nguyen, J. Phys. Chem. A 114 (2010) 7609.

2) (a) T. B. Tai, M. T. Nguyen J. Phys. Chem. A 115 (2011) 9993 and references therein; (b) T. B. Tai, M. T. Nguyen, Chem. Phys. Lett. 492 (2010) 290.

3) T. B. Tai, H. M. T. Nguyen, M. T. Nguyen, Chem. Phys. Lett. 502 (2011) 187.

4) T. B. Tai, N. M. Tam, M. T. Nguyen, Chem. Phys. 388 (2011) 1.

5) (a) J. Yamauchi, N. Aoki, I. Mizushima, Phys. Rev. B 55 (1997) R10245; (b) Y. Yoshimoto, Y. Suwa, App. Phys. Lett. 99 (2011) 191901 and references there in.

6) K. Ohmori, N. Esashi, M. Takao, D. Sato, Y. Hayafuji, App. Phys. Lett. 87 (2005) 112101.

7) R. Viswanathan, R. W. Schmude, K. A. Gingerich, J. Phys. Chem. 100 (1996) 10784.

8) R. Davy, E. Skoumbourdis, D. Dinsmore, Mol. Phys. 103 (2005) 611.

9) Z. Sun, Z. Yang, Z. Gao, Z. C. Tang, Rapid. Comm. Mass. Spect. 21 (2007) 792-798.

10) T. B. Tai, P. Kadlubanski, S. Roszak, D. Majumdar, J. Leszczynski, M. T. Nguyen, ChemPhysChem. 12 (2011) 2948.

11) A. D. Becke, J. Chem. Phys. 98 (1993) 5648.

12) J. P. Perdew, J. A. Chevary, S. H. Vosko, K. A. Jackson, M. R. Pederson, D. J. Singh, C. Fiolhais, Phys. Rev. B 46 (1992) 6671.

13) T. Clark, J. Chandrasekhar, G. W. Spitznagel, P. V. Schleyer, J. Comp. Chem. 4 (1983) 294.

14) A. D. Mclean, G. S. Chandler, J. Chem. Phys., 72 (1980) 5639.

15) M. J. Frisch, J. A. Pople, J. S. Binkley, J. Chem. Phys. 80 (1984) 3265.

16) K. A. Peterson, S. S. Xantheas, D. A. Dixon, T. H. Dunning J. Phys. Chem. A 102 (1998) 2449.
17) L. A. Curtiss, P. C. Redfern, K. Raghavachari, J. Chem. Phys. 126 (2007) 084108.
18) C. E. Moore. Atomic energy levels as derived from the analysis of optical spectra, Volume 1, H to V; U.S. National Bureau of Standards Circular 467, U.S. Department of Commerce, National Technical Information Service, COM-72-50282: Washington, D.C. 1949.
19) A. I. Boldyrev, J. Simons, J. Phys. Chem. 97 (1993) 1526.
20) (a) V. Kumar, Y. Kawazoe, Appl. Phys. Lett. 83 (2003) 2677; (b) V. Kumar, Y. Kawazoe, Phys. Rev. Lett. 87 (2001) 045503; (c) V. Kumar, A. K. Singh, Y. Kawazoe Phys. Rev. B 74 (2006) 125411; (d) V. Kumar, Y. Kawazoe, Phys. Rev. B 65 (2002) 073404.
21) M. Brack, Rev. Mod. Phys. 65 (1993) 677.
22) (a) T. B. Tai, M. T. Nguyen, J. Comp. Chem. 33 (2012) 800; (b) T. B. Tai, M. T. Nguyen, J. Chem. Theoret. Comput. 7 (2011) 1119; (c) T. B. Tai, M. T. Nguyen, Chem. Phys. Lett. 489 (2010) 75; (d) T. B. Tai, P. V. Nhat, M. T. Nguyen, S. G. Li, D. A. Dixon, J. Phys. Chem. A 115 (2011) 7673; (e) T. B. Tai, P. V. Nhat, M. T. Nguyen, Phys. Chem. Chem. Phys. 12 (2010) 11477.
23) S. Neukermans, E. Janssens, Z. F. Chen, R. E. Silverans, P. v. R. Schleyer, P. Lievens, Phys. Rev. Lett. 92 (2004) 163401.
24) K. E. Schriver, J. L. Persson, E. C. Honea, R. L. Whetten, Phys. Rev. Lett. 64 (1990) 2539.

Chapter 5

Structure, Thermochemical Properties and Growth Sequence of Aluminum Doped Silicon Clusters and Their Anions

This chapter is adapted from the following article:

- *Structure, thermochemical properties, and growth sequence of aluminum-doped silicon clusters Si_nAl_m (n = 1-11, m = 1-2) and their anions* by N. M. Tam, T. B. Tai, V. T. Ngan, and M. T. Nguyen, *Journal of Physical Chemistry A*, 117, 6867-6882 (2013).

5.1. INTRODUCTION

Among impure silicon materials, the aluminum-silicon mixture gives rise to quite intriguing compounds. Previous studies showed considerable significance of aluminum–silicon compounds in the field of nano-materials.[1,2,3] The Si nanowire doped by one Al-atom has been found to enhance electrical conductivity as compared to pristine Si-nanowire.[1] Kotlyar *et al.*[2] found that Al atoms form an ordered array of magic clusters on the surfaces of Si(111). Paulose and co-workers[3] also reported the persistent formation of Al-Si nanowires. In this context, some studies on small binary Al-Si clusters were previously performed. Sun *et al.*[4] carried out an experimental study on Si_nB^- and Si_nAl^- anionic clusters (with n = 1-6) using a laser ablation technique and time-of-flight mass spectrometry. Geometric structures of these clusters were also investigated theoretically using DFT method. Subsequently, geometrical features and stabilities of the $Si_nAl^{-/0/+}$ clusters with n = 2-21 were examined by Li *et al.*[5] using molecular dynamics (MD) method. However, according to our best knowledge, investigations on multiple aluminum doped silicon clusters are not available yet. In addition, thermochemical properties of the Si_nAl clusters have not been determined in earlier reports.

In view of the lack of reliable information on these systems, we set out to perform a systematic investigation on a series of small singly and doubly aluminum doped silicon cluster Si_nAl_m with n = 1-11 and m = 1,2, in both neutral and anionic states including their geometrical structures and thermochemical properties, and thereby to probe their growth pattern.

5.2. COMPUTATIONAL METHODS

We first use a stochastic genetic algorithm to generate all possible structures.[6] The equilibrium structures that are initially detected using low-level computations, are reoptimized using a higher level method. Initial structures of clusters Si_nAl are also manually constructed by either substituting one Si-atom of the Si_{n+1}frameworks by one Al-atom, or adding one Al-atom at various positions on surfaces of the Si_n clusters. Similarly, initial structures of Si_nAl_2 clusters are generated from known structures of pure silicon clusters and singly aluminum doped silicon

clusters Si_nAl. In addition, the local energy minima of Si_nX_m clusters previously reported are also used as initial guess structures.

While low-level computations on initial geometries are carried out using the hybrid B3LYP functional along with the 6-31G(d) basis set, all selected equilibrium geometries of Si_nAl_m (n = 1-11, m = 1-2) are fully optimized using the same functional but with the larger 6-311+G(d) basis set.[7,8,9] Their harmonic vibrational frequencies are also calculated at the same level to characterize the optimized structures and to evaluate their ZPEs.

The G4 approach is used for the entire series considered, while the CCSD(T)/CBS calculations (CBS) are performed only for the smaller molecules Si_nAl and Si_nAl_2 with n = 1-3 due to the limited computer resources.

5.3. RESULT AND DISCUSSION

Shapes of equilibrium structures of the $Si_nAl_m^{0/-}$ clusters detected, their symmetry point groups and G4 relative energies are shown in Figures 5.1, 5.2, 5.3, 5.4, 5.5 and 5.6. The different components obtained in the CBS protocol for evaluating total atomization energies (TAE, ΣD_0) of the smaller clusters $Si_nAl_m^{0/-}$ (n = 1-3, m = 1-2) are given in Table 5.1. The values for heats of formation of the clusters derived from their ΣD_0 values are given in Table 5.2. Computed adiabatic electron affinities (EAs) of Si_nAl_m clusters are given in Table 5.3, and average binding energies (E_b) tabulated in Table 5.4.

5.3.1. Lower-lying isomers of Si_nAl_m clusters in both neutral and anionic states

We present some lower-lying isomers whose relative energies are close to each ground state structure (within ~1.0 eV). As for a convention, each structure described hereafter is defined by the label **x**.**n.m.Y** in which **x** = **n** and **a** stands for a neutral and anionic state, respectively, **n** the size of Si_n, **m** the size of Al_m, and finally **Y** = **A, B, C**… refers to the different isomers with increasing relative energy ordering. Concerning the energy ordering within a system, the structure labeled with the letter **A** (**x**.**n.m.A**) invariably refers to the lowest-lying isomer obtained from G4 calculations.

5.3.1.1. The singly aluminum doped $Si_nAl^{0/-}$

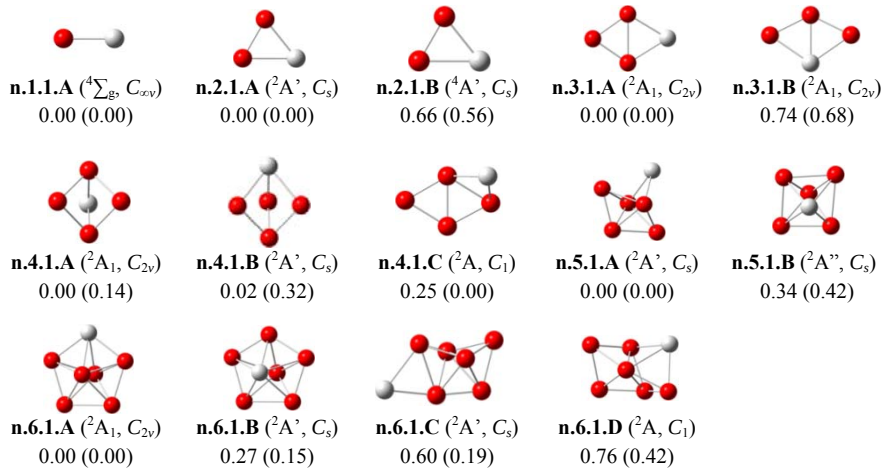

a) The neutral Si_nAl clusters

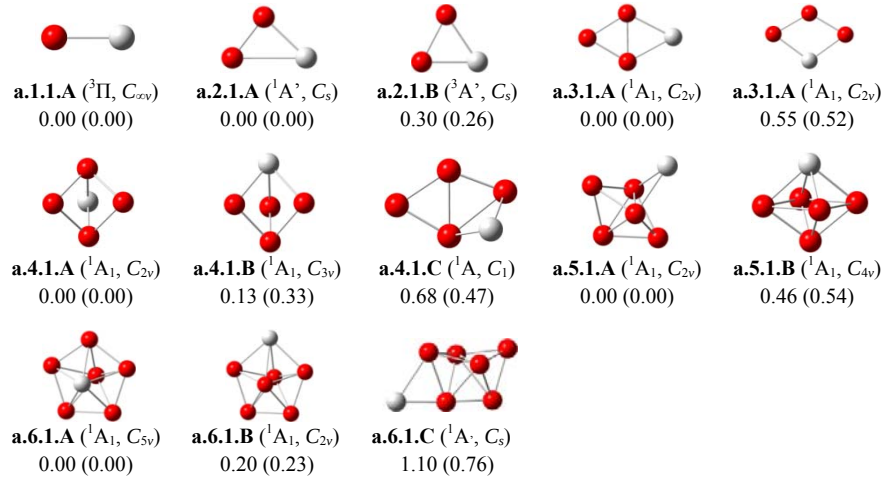

b) The anionic Si_nAl^- clusters

Figure 5.1. Shapes, electronic states and relative energies (ΔE, eV) of the lower-lying isomers Si_nAl with n = 1-6 at the **a**) neutral and **b**) anionic states. ΔE values are obtained using the G4 approach. Values given in parentheses are from B3LYP/6-311+G(d) + ZPE computations.

The main structures are displayed in Figures 5.1 - 5.3. There is a good agreement between our predictions and earlier reports[5,10] on the identification of the

global minima of small-sized Si_nAl with n = 1-6 (Figure 5.1). Their main characteristics can be summarized as follows:

SiAl. The high spin state **n.1.1.A** ($^4\sum$) with an electronic configuration of $[1\delta^2 2\delta^2 1\pi^2 3\delta^1]$ is confirmed as the ground state of the neutral diatomic, with a doublet-quartet separation gap of 1.0 eV. This electronic configuration is similar to that of Si_2^+ (Figure 5.1).

Si_2Al – Si_6Al (Figure 5.1). Structure **n.2.1.A** is an isoceles triangle, and **n.3.1.A** is planar. The smallest three-dimensional global minimum is found for Si_4Al where both structures **n.4.1.A** and **n.4.1.B** are almost degenerate with an energy gap of only 0.02 eV. Both structures are formed by replacing one Si-atom of the trigonal bipyramid Si_5 by one Al-atom. Similarly, both Si_5Al **n.5.1.A** and Si_6Al **n.6.1.A** are formed by substituting one Si-atom of the edge-capped trigonal bipyramid Si_6 and pentagonal bipyramid Si_7 hosts by one Al-atom, respectively.

Following attachment of one excess electron, the resulting anionic clusters Si_nAl^- with n = 1-5 have geometries similar to their neutral counterparts (Figure 5.1b). Interestingly, the anionic cluster Si_6Al^- has high symmetrical C_{5v} structure **a.6.1.A** which is an anionic species of **n.6.1.B**. Structure **a.6.1.B** which corresponds to an anionic state of the neutral **n.6.1.A**, turns out to be less stable with relative energy of 0.20 eV.

Si_7Al. There is a discrepancy between our predictions and previous reports on the identity of the Si_7Al ground state. Earlier studies[5,11] showed that **n.7.1.E** (C_s, ^{2}A") which is formed by substituting one Si atom of the bicapped octahedral Si_8 framework by Al impurity is the most stable isomer of Si_7Al. That differs from our G4 calculations that reveal the C_s structure **n.7.1.A** (Figure 5.2).

Another C_s structure **n.7.1.B** is the second isomer with only 0.07 eV higher in energy. Both isomers are formed by replacing one Si atom of the edge-capped pentagonal bipyramid of the cation Si_8^+ by one Al impurity.[12] Our computed results agree well with a more recent result obtained by Karamanis *et al*.[13]

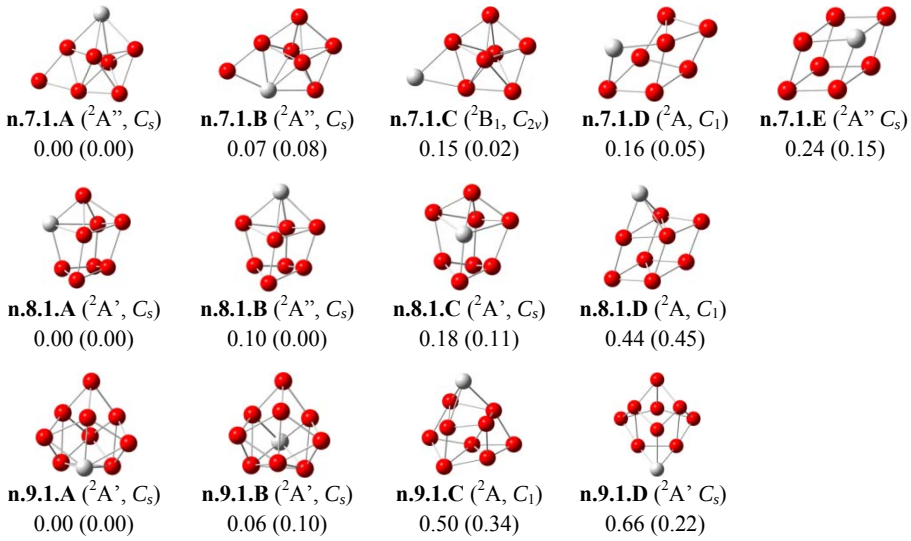

a) The neutral Si_nAl clusters

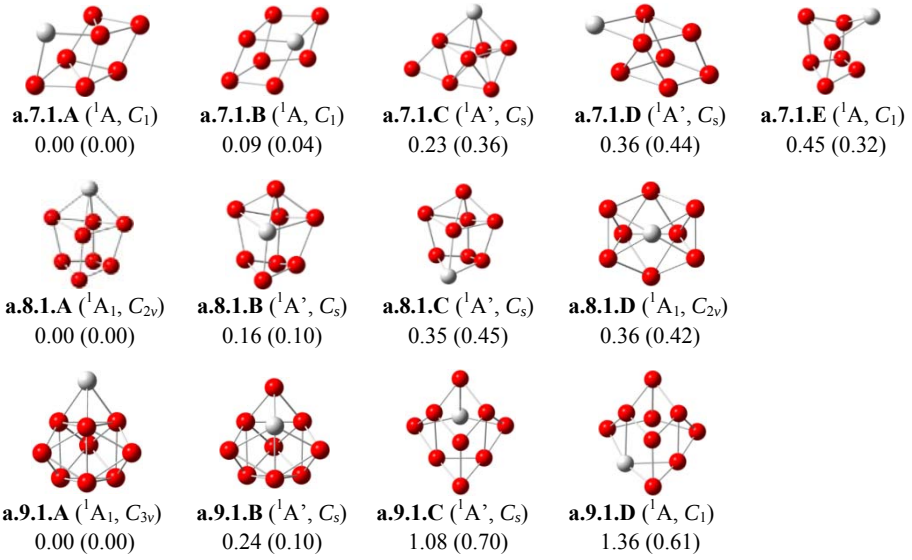

b) The anionic Si_nAl^- clusters

Figure 5.2. Shapes, electronic states and relative energies (ΔE, eV) of the lower-lying isomers Si_nAl with n = 7-9 at the **a**) neutral and **b**) anionic states. ΔE values are obtained using the G4 approach. Values given in parentheses are from B3LYP/6-311+G(d) + ZPE computations.

In the anionic state, Li *et al.*[5] reported that **a.7.1.B** is the most stable isomer for Si_7Al^-. However, we found that both isomers **a.7.1.A** and **a.7.1.B** are almost degenerate with energy gap of only 0.09 eV. The first isomer was missed in earlier studies. Both isomers are again formed by substituting one Si atom in bicapped octahedral of the Si_8 host by Al dopant.

Si_8Al. Nigam *et al.*[11] showed that **n.8.1.B** is the most stable isomer. Our G4 calculations emphasize the global minimum character of **n.8.1.A**, being 0.10 eV below the second stable isomer **n.8.1.B**. Both isomers **n.8.1.A** and **n.8.1.B** are also formed by replacing one of Si atoms of the bicapped pentagonal bipyramid Si_9^+ framework[12] by Al (Figure 5.2).

In the negatively charged state, our G4 results indicate that **a.8.1.A** is the corresponding anion of **n.8.1.B**, whereas its isomer **a.8.1.B**, being the corresponding anion of **n.8.1.A**, is a local minimum lying 0.16 eV above **a.8.1.A**. There is thus a reversed energy ordering between isomers upon electron attachment. These results agree well with recent studies of Li *et al.*[5] and Karamanis *et al.*[13]

Si_9Al. The ground state **n.9.1.A** (C_s, $^2A'$) is formed by substituting one Si atom of trigonal prism of the tetra-capped trigonal prism cage of Si_{10}[14] by Al dopant. G4 calculations result in a near degeneracy of both **n.9.1.B** and **n.9.1.B** with a gap of only 0.06 eV (Figure 5.2).

In the anionic state, a higher symmetry structure **a.9.1.A** (C_{3v}, $^1A_1$) is determined. Both lowest-lying isomers **a.9.1.A** and **a.9.1.B** (at 0.24 eV above **a.9.1.A**) have a tetra-capped trigonal prism Si_{10} framework. Other anionic structures are much less stable (Figure 5.2).

$Si_{10}Al$. According to B3LYP calculations, four neutral isomers **n.10.1.A**, **n.10.1.B**, **n.10.1.C** and **n.10.1.E** that exhibit the same penta-capped trigonal prism framework of pure Si_{11},[11] are energetically degenerate within an energy range of 0.06 eV. At the G4 level, however, the isomers **n.10.1.C** and **n.10.1.E** are now 0.18 and 0.29 eV higher in energy than **n.10.1.A**, respectively. For their part, **n.10.1.A** and **n.10.1.B** have the same energy content (a tiny gap of 0.02 eV) and both thus

constitute the dual global minima of $Si_{10}Al$ (Figure 5.3). These predictions are in good agreement with those of Karamanis *et al*.[13]

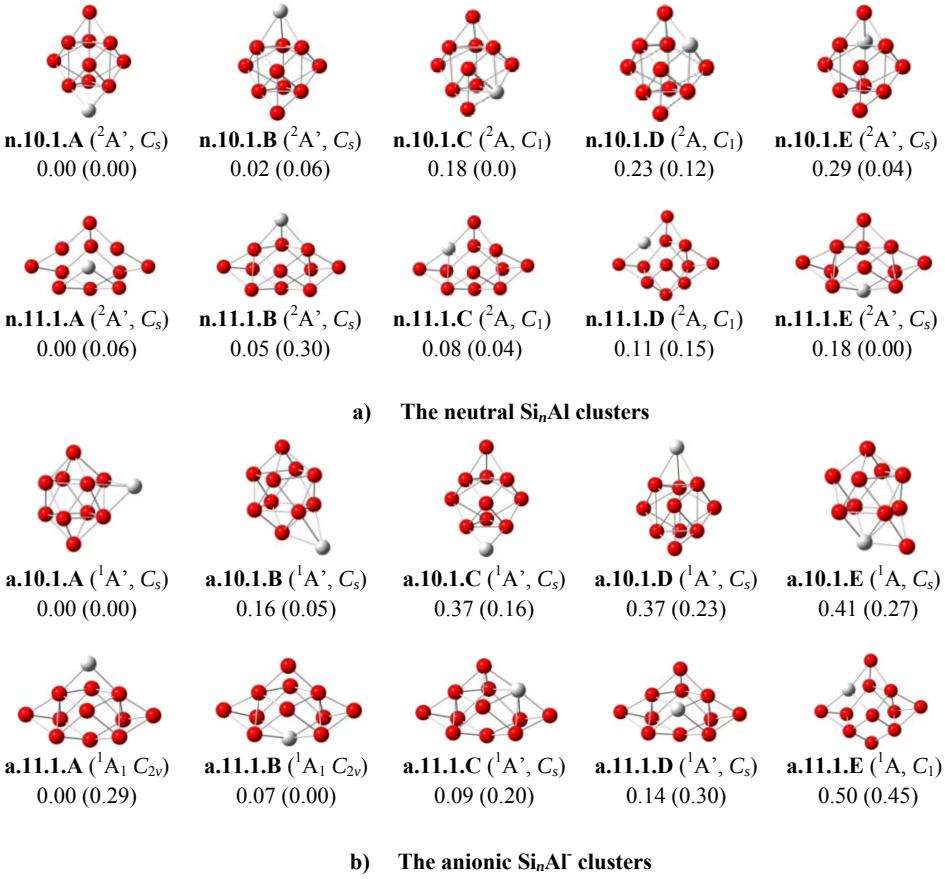

Figure 5.3. Shapes, electronic states and relative energies (ΔE, eV) of the lower-lying isomers Si_nAl with n = 10-11 at the **a**) neutral and **b**) anionic states. ΔE values are obtained using the G4 approach. Values given in parentheses are from B3LYP/6-311+G(d) +ZPE computations.

There is again a discrepancy between our predictions and previous studies for the ground state of the anion $Si_{10}Al^-$. A previous study[5] showed that **a.10.1.D**, which is the corresponding anion of **n.10.1.B**, is the most stable form. Our G4

calculations indicate that **a.10.1.A** is at 0.16 eV below **a.10.1.B**. Both lowest-lying isomers are formed by capping an Al atom on a face of a bicapped squared anti-prism cage of the pure Si_{10}^{-2} dianion.[15]

$Si_{11}Al$. Our B3LYP calculations agree with Li *et al.*[5] that **n.11.1.E** is the most stable form, while both isomers **n.11.1.C** and **n.11.1.A** are energetically degenerate with only 0.04 and 0.06 eV less stable than **n.11.1.E**, respectively. Conversely, taking G4 results, **n.11.1.A** is now 0.18 eV more stable than **n.11.1.E**. Both **n.11.1.B** and **n.11.1.C** are again energetically degenerate with only 0.05 and 0.08 eV higher than the lowest-energy isomer, respectively (Figure 5.3). A reason for such a close energy is that these low-lying isomers can all be formed by replacement of one Si atom of hexa-capped trigonal prism Si_{12}^{+} cage[11] by the Al dopant.

For the anions, Li *et al.*[5] reported **a.11.1.C** as the most stable $Si_{11}Al^{-}$ shape. Our G4 results do not concur with this finding, and instead favour **a.11.1.A** which is the corresponding anion of **n.11.1.B**. Again, the anionic forms **a.11.1.B** and **a.11.1.C** are only 0.07 and 0.09 eV higher in energy, respectively.

It is apparent that substitution by Al at different Si centers of a pure Si cluster leads to multiple mixed isomers with comparable energy content. Such a pattern is in particular reinforced in the anions where both Al^{-} anion and Si atom are isoelectronic.

5.3.1.2. The doubly aluminum doped $Si_nAl_m^{0/-}$ with n = 1-11 and m = 2

Their structural evolution can be viewed in Figures 5.4 (n = 1-5), 5.5 (n = 6-8) and 5.6 (n = 9-11).

$SiAl_2$. For this triatomic species (Figure 5.4), at the B3LYP level, the high spin triangle **n.1.2.B** ($^3A_2$, C_{2v}) is the neutral ground state being 0.12 eV lower in energy than the same shape isomer but with a closed-shell electronic configuration **n.1.2.A** ($^1A_1$, C_{2v}). This is at variance with our G4 calculations that point out a reversed energy ordering in favor of **n.1.2.A**, with energy gap of 0.24 eV below **n.1.2.B**. For the charged state, both B3LYP and G4 methods agree with each other confirming the doublet triangle **a.1.2.A** ($^2B_2$, C_{2v}) as the ground state. The higher spin

isomer **a.1.2.B** ($^4B_2$, C_{2v}) is significantly less stable than **a.1.2.A,** being at 0.55 (G4) and 0.60 eV (B3LYP) higher in energy than **a.1.2.A**.

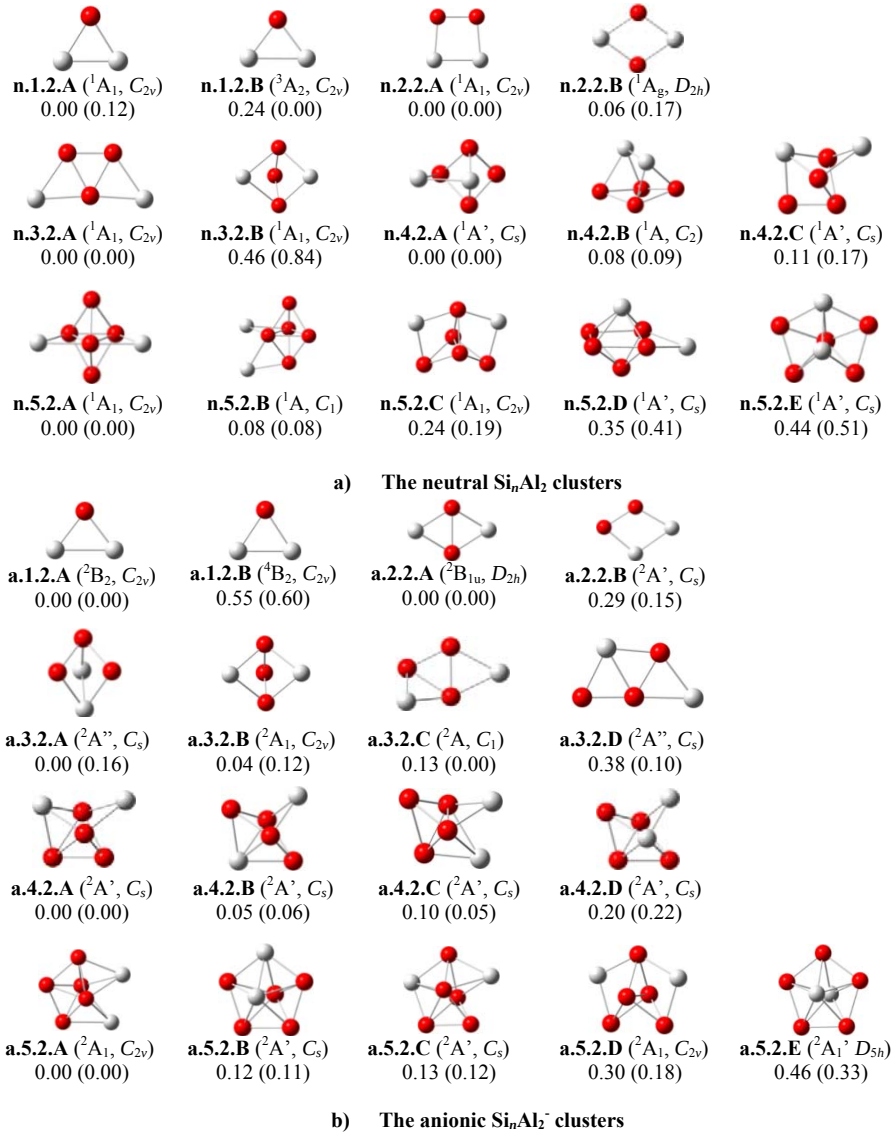

Figure 5.4. Shapes, electronic states and relative energies (ΔE, eV) of the lower-lying isomers Si_nAl_2 with n = 1 – 5 at the **a**) neutral and **b**) anionic states. ΔE values are obtained using the G4 method. Values given in parentheses are from B3LYP/6-311+G(d) +ZPE computations.

Si_2Al_2. For this tetratomic cluster (Figure 5.4), the lowest-lying isomers in both neutral and anionic states possess planar structure. The low spin **n.2.2.A** ($^1A_1$, C_{2v}) and the higher symmetry **n.2.2.B** (^1A_g, D_{2h}) are again energetically quasi-degenerate with a gap of only 0.06 eV (this energy gap being 0.17 eV at the B3LYP level). **a.2.2.A**, which is actually the anionic state of **n.2.2.B**, becomes the ground state with 0.29 eV (G4) more stable than **a.2.2.B** as a consequence of energy ordering reversal upon electron attachment.

Si_3Al_2. For the pentatomic molecules (Figure 5.4), the neutral isomer **n.3.2.A** ($^1A_1$, C_{2v}) in which two Al atoms add on two edges of the Si_3 triangle, is the lowest-lying isomer and the second isomer **n.3.2.B** lies at 0.46 eV higher in energy.

In the anion state, **a.3.2.C**, the corresponding anion of **n.3.2.A**, is the lowest-lying isomer at the B3LYP level. Our G4 results show a higher stability for **a.3.2.A**, being 0.16 eV lower than **a.3.2.C**, but **a.3.2.B** is found at only 0.04 eV below **a.3.2.A**. Both **a.3.2.A** and **a.3.2.B** have a trigonal bipyramid shape of the pure Si_5 cluster in which two Si positions are now occupied by two Al atoms.

Si_4Al_2. **n.4.2.A** ($^1A'$, C_s) is formed by substituting one Si atom of the trigonal bipyramid framework of Si_5 by an Al dopant, whereas the other Al is added on an edge of it (Figure 5.4). The singlet **n.4.2.B** (^1A, C_2), formed by a similar way, has an energy separation of only 0.09 eV.

In the anionic state, two lowest-lying isomers **a.4.2.A** and **a.4.2.B** also have a tiny energy gap of 0.05 eV. The isomer **a.4.2.C** is also a stable structure being only 0.1 eV below **a.4.2.A**. Interestingly, all lower-lying anions $Si_4Al_2^-$ possess an edge-capped trigonal bipyramid Si_6 host in which both Al atoms differently occupy two Si positions of the pure cluster.

Si_5Al_2. The low spin neutral **n.5.2.A** ($^1A_1$, C_{2v}) and the next isomer **n.5.2.B** (^1A, C_1) are formed by adding two Al atoms on two edges of the pure trigonal bipyramid Si_5 framework. In other words, they both have the shape of the pure Si_6 counterpart in which one Si position is changed by an Al atom whereas the other Al

adds on one of its edges (Figure 5.4). As a consequence, both structures are close in energy (0.08 eV).

In the charged state, **a.5.2.A** arises from swapping of two Si atoms by two Al atoms in a pentagonal bipyramid Si_7 form. The other local minima are located in this case at most 0.5 eV above **a.5.2.A**.

Si_6Al_2. The same degeneracy pattern is again verified for this system, either in the neutral or the charged state (Figure 5.5). The neutrals **n.6.2.A** (^{1}A', C_s), **n.6.2.B** (^{1}A', C_s) and **n.6.2.C** ($^1A_1$, C_{2v}) are separated from each other by only 0.06 - 0.08 eV (G4). Remarkably, the four lowest-lying isomers of neutral Si_6Al_2 have all a pentagonal bipyramid Si_7 form in which the first Al atom replaces one Si, and the second Al is capping on a pentagon edge.

In the anionic state, a competition emerges between **a.6.2.A** (^{2}A", C_s) and **a.6.2.B** (^2A_u, C_i) (Figure 5.5). According to B3LYP results, **a.6.2.B** is 0.08 eV lower in energy than **a.6.2.A,** but G4 results indicate a reversed energy ordering even though **a.6.2.A** is only 0.05 eV below **a.6.2.B**. Both structures practically exist as the degenerate ground state of the anion $Si_6Al_2^-$. The isomer **a.6.2.A** possesses a capped pentagonal bipyramid structure of the Si_8^+ cation,[12] produced by a double Al substitution, whereas **a.6.2.B** exhibits the bicapped octahedral shape of neutral Si_8[11] in which two Si atoms are also substituted by two Al. Isomer **a.6.2.C**, being the corresponding anion of **n.6.2.B**, is again at 0.07 eV above **a.6.2.A** (G4 values).

Si_7Al_2. The singlet neutral **n.7.2.A** (^{1}A, C_1) is characterized by the capped pentagonal bipyramid of the cation Si_8^+ in which the first Al atom substitutes a Si atom in the pentagon and the remaining Al caps on its face (Figure 5.5). Besides, G4 results also point out a similar energy locations for **n.7.2.A**, **n.7.2.B** (^{1}A', C_s) and **n.7.2.C** (^{1}A', C_s) (a gap of 0.02 – 0.05 eV, G4 and B3LYP levels).

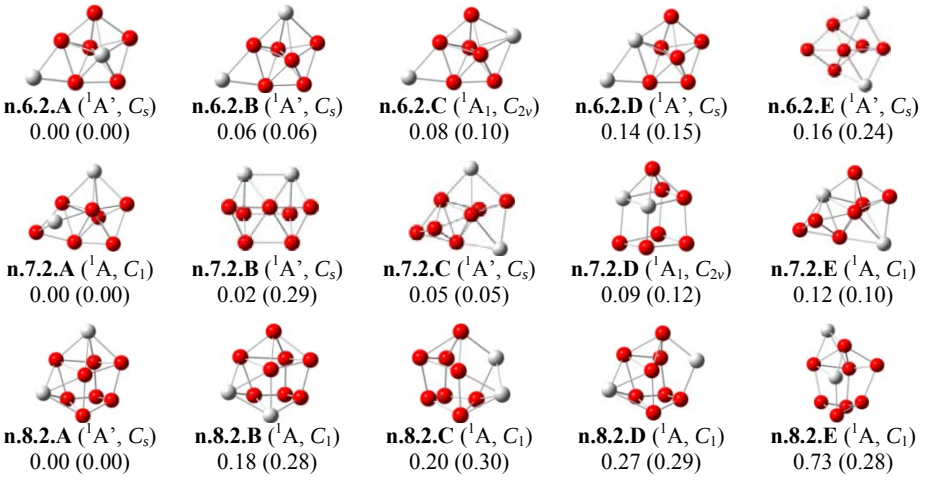

a) The neutral Si_nAl_2 clusters

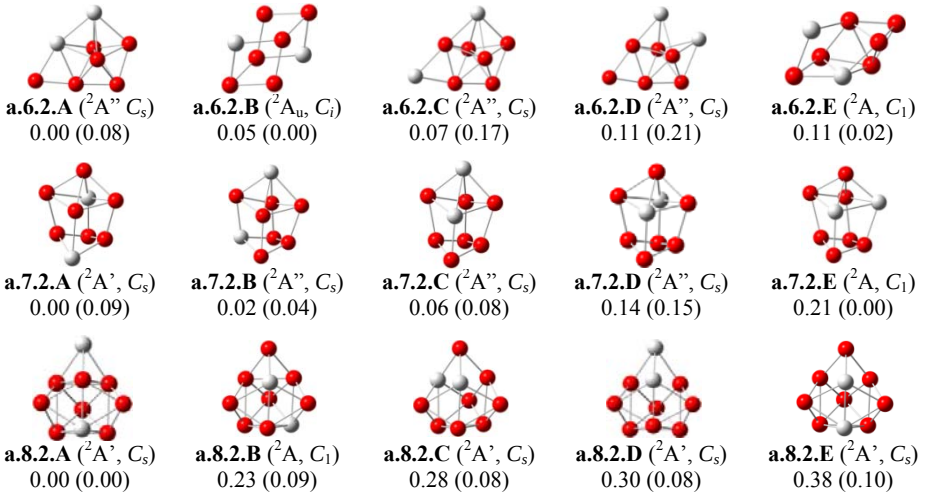

b) The anionic $Si_nAl_2^-$ clusters

Figure 5.5. Shapes, electronic states and relative energies (ΔE, eV) of the lower-lying isomers Si_nAl_2 with n = 6-8 at the **a**) neutral and **b**) anionic states. ΔE values are obtained using the G4 approach. Values given in parentheses are from B3LYP/6-311+G(d) + ZPE computations.

All the five lower-lying isomeric anions $Si_7Al_2^-$ derived from the same bicapped pentagonal bipyramidal block of the bare Si_9 cluster, and thus possess

similar energy content. According to G4 results, three isomers **a.7.2.A** (^{2}A', C_s), **a.7.2.B** (^{2}A", C_s) and **a.7.2.C** (^{2}A", C_s) are located within a tiny gap of only 0.02 and 0.06 eV. Although **a.7.2.E** is found to be the lowest-lying structure at the B3LYP level, it becomes now at 0.21 eV above **a.7.2.A** using the G4 method. There is thus a spectrum of global minima that feature the same 3D shape but with different positions of the dopants.

Si_8Al_2. The neutral **n.8.2.A** (^{1}A', C_s) involves an Al capping on a surface of the pure neutral Si_9 and a substitution of the remaining Al atom (Figure 5.5). In this system, the usual degeneracy is removed. Three isomers **n.8.2.B**, **n.8.2.C** and **n.8.2.D**, formed by the same way, are now 0.30 eV above **n.8.2.A**. In the same vein, the energy gap between anionic isomers equally tends to increase, with **a.8.2.A** (^{2}A', C_s) being 0.23 eV (G4) more stable than the second isomer **a.8.2.B** (^{2}A, C_1). All lower-lying anionic isomers of $Si_8Al_2^-$ are constructed from a tetra-capped trigonal prism structure of the pure Si_{10} with both Al atoms substituting two Si ones.

Si_9Al_2. The high symmetry neutral **n.9.2.A** ($^1A_1$', D_{3h}) is apparently stabilized, being now 0.43 eV below than the second isomer **n.9.2.B** (^{1}A', C_s). Nevertheless, both structures are generated by a similar way: by capping an Al atom at different faces of the tetra-capped trigonal prism Si_{10} and by substituting a Si atom by the other Al atom at different positions (Figure 5.6). The remaining isomers are now much less stable, being at least 0.60 eV (G4) higher in energy than **n.9.2.A**.

In contrast to the neutrals, an energetic degeneracy persists in the charged state. The two lowest-lying anionic forms **a.9.2.A** (^{2}A', C_s) and **a.9.2.B** (^{2}A', C_s) are in fact separated by only 0.02 eV in favor of the latter (B3LYP). G4 results however point out a reversed energy ordering at the expense of **a.9.2.B,** but with a small gap of 0.09 eV with respect to **a.9.2.A**. The latter contains a bicapped squared anti-prism Si skeleton of the pure dianionic Si_{10}^{2-} structure.[15] As usual, one capped Si atom is substituted by an Al dopant, whereas the other Al caps on a face of the cage. The second stable **a.9.2.B** and the remaining lower-lying isomers are, as expected, generated by substituting two Si positions in the pure Si_{11} framework by both Al dopants (Figure 5.6).

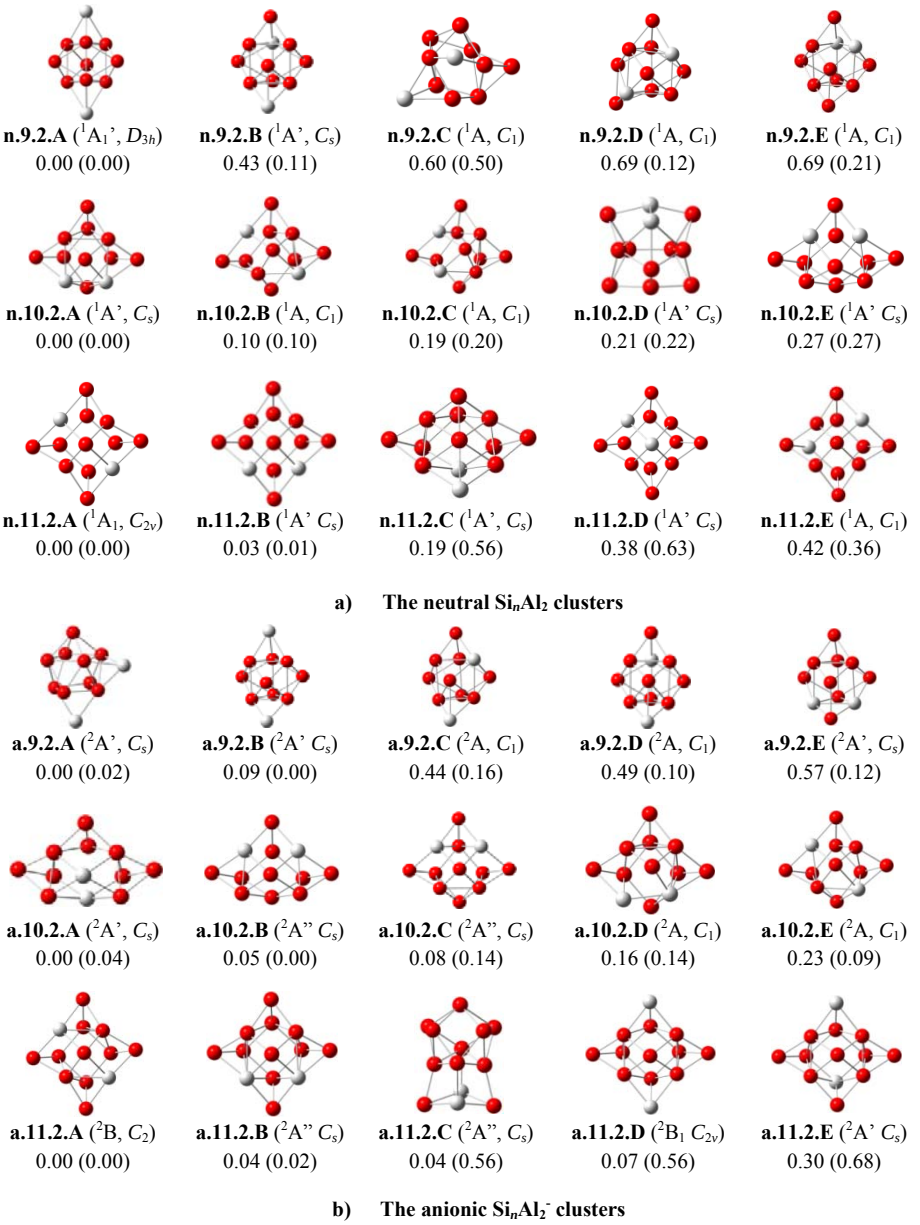

Figure 5.6. Shapes, electronic states and relative energies (ΔE, eV) of the lower-lying isomers Si_nAl_2 with n = 9-11 at the **a**) neutral, and **b**) anionic states. ΔE values are obtained using the composite G4 method. Values given in parentheses are from B3LYP/6-311+G(d) + ZPE computations.

$Si_{10}Al_2$. **n.10.2.A** (^{1}A', C_s) is calculated at 0.10 and 0.20 eV lower than **n.10.2.B** and **n.10.2.C**, respectively (Figure 5.6). These lowest-lying isomers are all generated by a double substitution of two Si positions from the ground state of the hexa-capped trigonal prism of the pure Si_{12}^+ cation.[11]

A competition in relative stability apparently occurs between both anionic isomers **a.10.2.A** and **a.10.2.B**. At the B3LYP/6-311+G(d) level, **a.10.2.B** (^{2}A", C_s) is 0.04 eV more stable than **a.10.2.A** (^{2}A', C_s). G4 results again show a reversed energy ordering in that **a.10.2.A** is 0.05 eV lower in energy than **a.10.2.B**. As in the $Si_9Al_2^-$ case, the energetic degeneracy is not lifted yet for the anions $Si_{10}Al_2^-$. In both global minima structures, two Si atoms on the Si_{12}^+ skeleton are substituted by two Al dopants. G4 calculations also indicate that the third isomer **a.10.2.C** is only 0.08 eV higher in energy than **a.10.2.A**, being thus practically competing with the former (Figure 5.6).

$Si_{11}Al_2$. Surprisingly, an energetic degeneracy comes back for this system (Figure 5.6). The separation between both isomers **n.11.2.A** ($^1A_1$, C_{2v}) and **n.11.2.B**(^{1}A', C_s) amounts now only to 0.03 eV (G4). Both isomers contain a Si hepta-capped trigonal prism similar to the ground state of the Si_{13}^+ cation,[11] with substitution of both Al atoms at different Si positions. The isomer **n.11.2.C**, formed by adding an Al atom on the Si_{12}^+ stable geometry and substituting one Si atom in it by the other Al, is a low-energy local minimum at 0.19 eV above **n.11.2.A**.

The anion $Si_{11}Al_2^-$ holds the energetic trend in having two very close-lying isomers **a.11.2.A** (having the shape of the neutral **n.11.2.A**) and **a.11.2.B** (having the shape of **n.11.2.B**) in which the former is only 0.05 eV below the latter (Figure 5.6). Calculated G4 results also emphasize two other energetically higher but degenerate structures **a.11.2.C** and **a.11.2.D**.

5.3.2. Equilibrium growth sequence of the Si_nAl_m clusters

On the basis of the structural features of the most stable isomers identified above, the growth pattern of the clusters Si_nAl_m with n = 1-11 and m = 1-2 can be established considering the following findings.

Because the Al element has one valence electron less than the Si, Al is isoelectronic with Si^+, and Al^- with Si. Thus in a singly doped neutral Si_nAl, the Al atom favors substitution at a Si position of silicon framework of the isoelectronic cation Si_{n+1}^+. In other words, the ground state structure of a neutral Si_nAl cluster can be derived from the pure cation Si_{n+1}^+.

Similarly, a Si_nAl^- anion has the Al atom substituted into a Si position of the ground state structure of the neutral Si_{n+1}. The most stable structure of the anion $Si_{10}Al^-$, however, has an Al atom being added on the face of the dianionic Si_{10}^{2-} framework. This can be understood by the high thermodynamic stability of the latter dianion.

The growth patterns of both neutral Si_nAl and anionic Si_nAl^- systems are found to be comparable to those of the isovalent Si_nB and Si_nB^-, respectively, reported in our earlier study[16] (Chapter 4) with n = 1-7. The essential difference between Si_nAl and Si_nB clusters resides in the fact that the Al-Si bond lengths in the mixed framework are much longer than the B-Si counterparts. Due to the shorter bond length, the B-impurity can be more easily encapsulated into a Si_n cage, even at a smaller size ($n \geq 8$) than the Al-dopant. Endohedral doping thus occurs much earlier in the boron series.

In the doubly doped neutral Si_nAl_2 clusters, with n = 1-9, each mixed cluster can be regarded as a direct derivative of a Si_{n+1} counterpart in which one Si atom is actually substituted by an Al dopant. Such an operation leads to a ground state structure similar to the cation Si_{n+1}^+. The other Al atom is usually added on an edge, or a face, of the existing cluster. In the larger neutral $Si_{10}Al_2$ and $Si_{11}Al_2$ ground states, they are basically made by simple substitution of two Si atoms in the corresponding cation Si_{12}^+ and Si_{13}^+ cages, respectively, by two Al dopants.

For the negatively charged state, the $Si_nAl_2^-$ anions also contain the cationic Si_{n+2}^+ skeletons in which two Si positions are substituted by two Al dopants. Again, such a similarity in growth pattern can be rationalized by the lack of one electron in the outermost orbital of Al atom, which makes them isoelectronic. However, the anion $Si_9Al_2^-$ represents an exception to this sequence. The lowest-lying structure of

$Si_9Al_2^-$ includes one Al atom substituting a Si position of the dianionic Si_{10}^{2-} cage, and the other Al capping on its face, due to the high thermodynamic stability of the dianion counterpart.

It can be seen that the $Si_nAl_m^q$ clusters tend to be formed by a substituting motif rather than a capping motif. As a matter of fact, geometries of $Si_nAl_m^q$ and Si_{n+m}^{q+m} are similar, due to the smaller valence electron number, by one unit, of each Al atom. For singly doped silicon clusters Si_nAl^q, the Al dopant looks to avoid high coordination position. Except for the anion Si_6Al^- where Al has a maximum coordination number of 5, the Al atom in other stable species prefers occupation of positions having lower coordination numbers.

5.3.3. Thermochemical properties

Calculated results are summarized in Table 5.1 and Table 5.2. The enthalpies of formation at 0K (Δ_fH^0) obtained using G4 are found to be slightly smaller than those obtained by the CCSD(T)/CBS, except for the diatomic SiAl. The difference varies in the range of 1.6 – 5.3 kcal/mol for the species considered (Table 5.2). Such deviations are significant. Computed adiabatic electron affinities (EAs) of Si_nAl_m clusters are given in Table 5.3.

Table 5.1. Total atomization energies (ΣD_0, TAE, kcal/mol) of Si_nAl_m clusters (n = 1-3, m = 1-2) and different components of CCSD(T)/CBS computations (CBS).

Struct.	ΔCBS[a]	E_{ZPE}[b]	ΔE_{CV}[c]	ΔE_{SR}[d]	ΔE_{SO}[e]	ΣD_0 (TAE)
a.1.1.A	90.30	0.60	-0.14	-0.34	-0.64	88.57
n.1.1.A	58.80	0.54	0.19	-0.15	-0.64	57.66
a.2.1.A	200.42	1.41	0.16	-0.65	-1.07	197.45
n.2.1.A	148.25	1.29	0.38	-0.52	-1.07	145.76
a.3.1.A	306.50	2.69	0.68	-0.90	-1.50	302.08
n.3.1.A	249.02	2.73	0.90	-0.67	-1.50	245.02
a.1.2.A	165.27	1.22	-0.09	-0.63	-0.85	162.47
n.1.2.A	119.09	1.40	-0.06	-0.55	-0.85	116.23
a.2.2.A	268.30	2.50	0.36	-0.87	-1.28	264.00

n.2.2.A	221.92	2.56	0.79	-0.56	-1.28	218.30
a.3.2.A	356.67	3.39	1.02	-1.08	-1.71	351.51
n.3.2.A	307.91	3.12	1.39	-0.77	-1.71	303.71

[a)] Extrapolated by using eq. (1) with the aVQZ and aV5Z basis sets.

[b)] Zero point energies taken from CCSD(T) harmonic vibrational frequencies.

[c)] Core-valence corrections obtained with the aug-cc-pwCVTZ basis set at CCSD(T) optimized geometries.

[d)] Scalar relativistic corrections based on CCSD(T)-DK/aug-cc-pVTZ-DK calculations and expressed relative to the CCSD(T) results without DK corrections.

[e)] Corrections due to the incorrect treatment of the atomic asymptotes as an average of spin multiplets. Values based on Moore's Tables in ref. 17.

Table 5.2. Heats of formation at 0K [$\Delta_f H$ (0 K)] and 298K [$\Delta_f H$ (298 K)] (kcal/mol) of Si_nAl_m(n = 1-11, m = 1- 2) in both neutral and anionic states obtained using G4 and CCSD(T)/CBS calculations

Structure	**ΔH_f (0 K)**		**ΔH_f (298 K)**	
	G4	CBS	G4	CBS
a.1.1.A	100.8	98.8	101.2	99.2
n.1.1.A	127.9	129.7	128.3	130.1
a.2.1.A	94.3	97.2	94.9	97.7
n.2.1.A	146.6	148.8	147.3	149.5
a.3.1.A	96.6	99.7	97.3	100.4
n.3.1.A	155.2	156.8	155.8	157.4
a.4.1.A	106.2		106.6	
n.4.1.A	178.1		179.1	
a.5.1.A	97.4		98.3	
n.5.1.A	165.5		166.5	
a.6.1.A	106.0		106.9	
n.6.1.A	181.7		182.7	
a.7.1.A	140.4		141.7	

n.7.1.A	206.0		207.5	
a.8.1.A	138.6		140.1	
n.8.1.A	219.9		221.4	
a.9.1.A	126.6		128.1	
n.9.1.A	217.8		219.5	
a.10.1.A	155.8		157.9	
n.10.1.A	229.0		231.1	
a.11.1.A	177.1		179.2	
n.11.1.A	259.5		261.5	
a.1.2.A	103.4	105.1	103.7	105.4
n.1.2.A	147.3	151.4	147.5	151.6
a.2.2.A	107.0	110.8	107.4	111.2
n.2.2.A	153.8	156.5	154.2	156.9
a.3.2.A	125.2	130.5	126.0	130.6
n.3.2.A	175.6	178.3	176.6	178.7
a.4.2.A	110.7		111.4	
n.4.2.A	169.7		170.5	
a.5.2.A	121.6		122.8	
n.5.2.A	181.9		183.2	
a.6.2.A	143.9		145.1	
n.6.2.A	193.2		194.3	
a.7.2.A	156.3		157.8	
n.7.2.A	215.5		217.0	
a.8.2.A	148.8		150.3	
n.8.2.A	209.7		211.3	
a.9.2.A	152.7		154.6	
n.9.2.A	205.9		207.7	
a.10.2.A	186.9		188.7	
n.10.2.A	248.0		249.6	
a.11.2.A	197.9		199.6	
n.11.2.A	259.0		260.6	

Table 5.3. Adiabatic electronic affinities (EA, eV) of Si_nAl_m (n = 1-11, m = 1-2) using G4 and CCSD(T)/CBS calculations

n	Si_nAl		Si_nAl_2	
	G4	CBS	G4	CBS
1	1.17	1.34	1.90	2.00
2	2.27	2.24	2.03	1.98
3	2.54	2.47	2.18	2.07
4	3.11		2.56	
5	2.95		2.61	
6	3.28		2.14	
7	2.85		2.57	
8	3.52		2.64	
9	3.96		2.31	
10	3.17		2.65	
11	3.57		2.65	

5.3.4. Thermodynamic stability of clusters

To probe the inherent thermodynamic stability of the clusters considered, the average binding energies (E_b) of clusters are again examined. The average binding energies (E_b) can conventionally be defined as follows (equations 6.1 - 6.4):

$$E_b(Si_nAl) = [nE(Si) + E(Al) - E(Si_nAl)]/(n+1) \quad (6.1)$$

$$E_b(Si_nAl^-) = [(n-1)E(Si) + E(Si^-) + E(Al) - E(Si_nAl^-)]/(n+1) \quad (6.2)$$

$$E_b(Si_nAl_2) = [nE(Si) + 2xE(Al) - E(Si_nAl_2)]/(n+2) \quad (6.3)$$

$$E_b(Si_nAl_2^-) = [(n-1)E(Si) + E(Si^-) + 2xE(Al) - E(Si_nAl_2^-)]/(n+2) \quad (6.4)$$

where E(Al), E(Si), $E(Si^-)$ are the total energies of the Al-atom, Si-atom and the anion Si^-, respectively. For their part, $E(Si_nAl)$, $E(Si_nAl^-)$, $E(Si_nAl_2)$, and $E(Si_nAl_2^-)$ are total energies of the neutral Si_nAl, anionic Si_nAl^-, neutral Si_nAl_2 and anionic $Si_nAl_2^-$ structures, respectively. All these energies are obtained from G4 calculations. While

the E_b values are given in Table 5.4, plots illustrating their evolution are depicted in Figure 5.7.

The E_b values increase with increasing cluster sizes. For neutral Si_nAl clusters, the $Si_{10}Al$ reveals the highest E_b value as compared to those of the remaining singly doped species. At the anionic state, Si_9Al^- presents with the highest E_b value that indicates its high thermodynamical stability. This finding is in agreement with the fact that the isoelectronic Si_{10} is a quite stable pure Si clusters. For Si_nAl_2 clusters, the Si_9Al_2 in both neutral and anionic states consistently attain the maximum peaks in the E_b plots.

Table 5.4. Average binding energies (E_b, eV) of Si_nAl_m (n = 1-11, m = 1-2) using G4 calculations

n	**Si_nAl**	**Si_nAl^-**	**Si_nAl_2**	**$Si_nAl_2^-$**
1	1.29	1.20	1.74	1.92
2	2.14	2.45	2.40	2.57
3	2.67	2.97	2.66	2.82
4	2.87	3.22	3.03	3.23
5	3.26	3.52	3.19	3.37
6	3.36	3.63	3.31	3.41
7	3.39	3.57	3.35	3.49
8	3.46	3.70	3.51	3.63
9	3.59	3.85	3.62	3.71
10	3.64	3.81	3.56	3.67
11	3.61	3.80	3.60	3.70

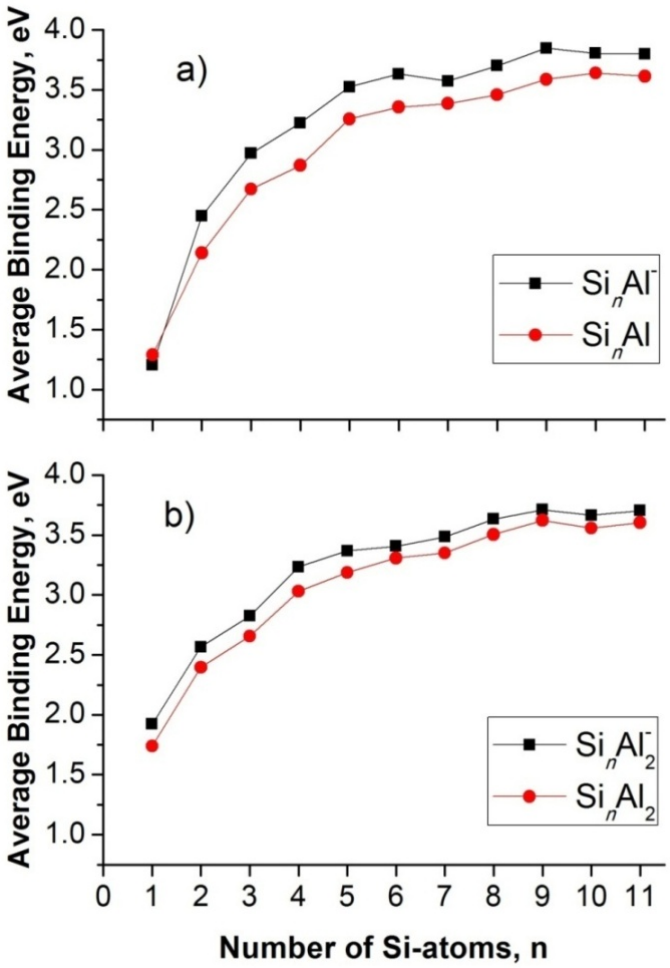

Figure 5.7. Average binding energy (E_b, eV) of the $Si_nAl_m^{/0/-}$ (n = 1- 11, m = 1- 2) clusters using the composite G4 method.

5.3.5. Dissociation energies

To evaluate further the thermodynamic stability, dissociation energies (D_e) for the various fragmentation channels of both singly and doubly aluminum doped silicon clusters considered are determined. Results calculated from total G4 energies are listed in Table 5.5.

Table 5.5. Dissociation energies (D_e, kcal/mol) for various fragmentation channels of Si_nAl_m (n = 1- 11, m = 1- 2) from G4 calculations.

a) Si_nAl

n	D_e(1)	D_e (2)	D_e (3)	D_e (4)	D_e (5)	D_e (6)
1	59.5	59.5	77.3	55.5	55.5	77.3
2	88.4	73.5	113.7	109.7	73.1	116.5
3	98.6	73.6	104.8	126.1	78.7	122.8
4	84.3	52.5	97.6	125.1	74.0	115.0
5	119.8	73.7	116.1	156.8	84.2	132.5
6	91.1	58.5	98.6	135.7	84.6	124.9
7	82.9	40.0	72.9	117.4	61.3	96.3
8	93.3	65.7	108.9	143.5	87.9	137.6
9	109.3	69.1	119.3	169.4	109.9	151.0
10	96.0	48.5	77.9	138.1	67.5	112.3
11	76.7	56.6	85.9	128.0	80.1	129.7

(1) $Si_nAl \rightarrow Si_{n-1}Al + Si$; (2) $Si_nAl \rightarrow Si_n + Al$; (3) $Si_nAl^- \rightarrow Si_{n-1}Al^- + Si$;
(4) $Si_nAl^- \rightarrow Si_{n-1}Al + Si^-$; (5) $Si_nAl^- \rightarrow Si_n^- + Al$; (6) $Si_nAl^- \rightarrow Si_n + Al^-$;

b) Si_nAl_2

n	D_e (7)	D_e (8)	D_e (9)	D_e (10)	D_e (11)	D_e (12)	D_e (13)	D_e (14)	D_e (15)
1	88.1	60.8	88.1	63.8	100.9	77.6	95.3	100.9	94.8
2	100.7	73.1	114.4	72.6	116.5	67.5	110.6	108.4	124.0
3	85.4	59.9	101.2	57.9	104.7	51.6	100.9	98.2	114.4
4	113.1	88.6	108.9	90.6	141.0	75.8	138.3	117.5	130.8
5	95.0	63.9	105.4	65.2	124.2	56.0	114.8	108.0	128.5
6	95.9	68.7	95.0	53.9	114.1	42.3	108.7	94.7	107.2
7	84.9	70.7	78.4	63.7	112.9	64.2	120.5	93.3	100.5
8	113.0	90.4	123.8	83.6	142.8	70.0	141.9	125.7	147.6
9	110.9	92.1	128.9	72.3	133.1	54.1	136.0	131.8	145.0
10	65.2	61.2	77.5	41.9	95.2	49.2	113.0	84.5	101.4

11	96.2	80.7	105.1	65.1	126.2	59.4	132.4	107.3	129.0

(7) $Si_nAl_2 \rightarrow Si_{n-1}Al_2 + Si$; (8) $Si_nAl_2 \rightarrow Si_nAl + Al$; (9) $Si_nAl_2 \rightarrow Si_n + Al_2$;
(10)$Si_nAl_2^- \rightarrow Si_{n-1}Al_2^- + Si$; (11)$Si_nAl_2^- \rightarrow Si_{n-1}Al_2 + Si^-$; (12) $Si_nAl_2^- \rightarrow Si_nAl^- + Al$;
(13) $Si_nAl_2^- \rightarrow Si_nAl + Al^-$; (14) $Si_nAl_2^- \rightarrow Si_n^- + Al_2$; (15) $Si_nAl_2^- \rightarrow Si_n + Al_2^-$.

The dissociation energies of the neutrals Si_nAl for the Si-elimination channel (**1**) $Si_nAl \rightarrow Si_{n-1}Al + Si$ turn out to be larger than those for the Al-loss channel (**2**) $Si_nAl \rightarrow Si_n + Al$.

Similar observations are found for the negatively charged species that the anionic Si_nAl^- clusters tend to be fragmented generating one Al element plus a smaller anion Si_n^- along the fragmentation channel (**5**).

For doubly doped neutral Si_nAl_2 clusters, dissociation energies for Al-loss channels (**8**) $Si_nAl_2 \rightarrow Si_nAl + Al$ are invariably smaller than those for Si-elimination pathways (**7**) $Si_nAl_2 \rightarrow Si_{n-1}Al_2 + Si$, and for the diatomic aluminum Al_2-loss route (**9**) $Si_nAl_2 \rightarrow Si_n + Al_2$.

Similarly, the anions $Si_nAl_2^-$ follow preferential fragmentation to form one Al plus a smaller anion Si_nAl^- along the channel (**12**) $Si_nAl_2^- \rightarrow Si_nAl^- + Al$.

5.3.6. Jelium electron shell model (JSM)

As for a rationalization of the relative stabilities of Si_nAl clusters, we reexamine their MO pictures under the viewpoint of the Jellium electron shell model (JSM).[18] The total density of states (DOS) of a molecular system can be considered as an energy spectrum of its molecular orbitals (MOs). The partial density of states (pDOS) is computed only from relevant atomic orbitals and thereby shows the composition of the MOs involved.

This simple model was successfully applied to interpret the stability motif of different types of doped silicon clusters in our recent studies.[19] To facilitate the reading, let us remind again that in this model the valence electrons are supposed to be freely itinerant in a simple mean-field potential formed by the nuclei of atoms and core electrons, the valence electrons fill the hydrogen-like orbitals following the

pattern of orbitals as [$1S^2 1P^6 1D^{10} 2S^2 1F^{14} 2P^6 1G^{18} 2D^{10}$…] etc… Within this model, the number of electrons of 8, 20, 34, 40, 56 and 68… emerge as the *magic numbers* that actually correspond to a complete filling of the successive shell electrons.

In this context and as for a typical example, we examine the valence electronic configuration of the anionic cluster Si_9Al^- (cf. Figure 5.8a) due to its enhanced stability. In search for an answer to the question of why Si_9Al^- is getting higher stability, the neutral cluster Si_{10} ($^1A_1$, C_{3v}), which is known for its high thermodynamic stability, is taken as a reference (cf. Figure 5.8b).

Both structures in fact contain 40 valence electrons. The Si_9Al^- anion possesses an orbital configuration of:

Si_9Al: $(1a_1)^2(1e)^4(2a_1)^2(2e)^4(3a_1)^2(3e)^4(4a_1)^2(4e)^4(1a_2)^2(5a_1)^2(5e)^4(6a_1)^2(6e)^4(7a_1)^2$

and the neutral Si_{10} ($^1A_1$, C_{3v}) pure cluster has an orbital configuration of :

Si_{10}: $(1a_1)^4(1e)^4(2a_1)^2(2e)^8(3a_1)^4(3e)^4(1a_2)^2(4a_1)^2(5e)^8(6a_1)^2$.

Both orbital configurations effectively correspond to the same energy sequence of the electronic shell model: [$1S^2 1P^6 1D^{10} 2S^2 1F^{14} 2P^6$].

In this case, the DOS's of both Si_9Al^- and Si_{10} structures show many similarities as they have the same C_{3v} point group. The pDOS plots also reveal that the MOs of Si_9Al^- are mainly composed of the *s*-AOs and *p*-AOs of Si-atoms, whereas the contribution of *s*-AOs and *p*-AOs is negligible to split the sub-shells (Figure 5.8).

Let us note a relationship between the DOS of Si_9Al^- and the DOS of the isovalent Si_9B^- ($^1A_1$', D_{3h}) which was reported in Chapter 4. Both anionic structures contain the same silicon Si_9 cage in which the B dopant is encapsulated but the Al dopant caps on its face. The boron anion Si_9B^- also has 40 valence electrons and its DOS features are quite similar to that of Si_9Al^- (Figure 5.8) and generally, the electronic structure of both anions Si_9Al^- and Si_9B^- satisfies the electron shell configuration of [$1S^2 1P^6 1D^{10} 2S^2 2P^6 1F^{14}$], and this basically makes them enhanced stability species with a *magic number of 40 valence electrons*.

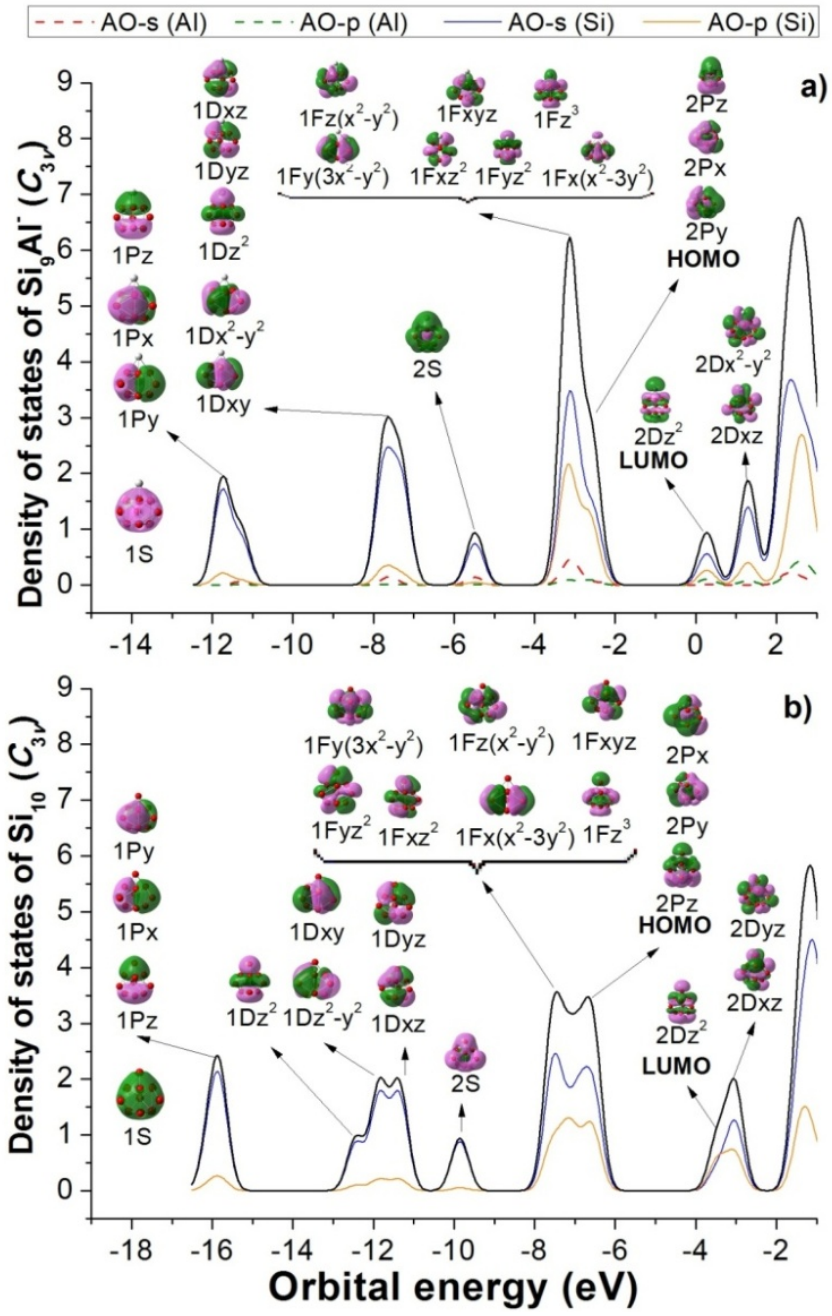

Figure 5.8. Total (DOS) and partial (pDOS) densities of state of **a**) Si_9Al^-, and **b**) Si_{10}. (B3LYP/6-311+G(d))

5.4. CONCLUDING REMARKS

In this chapter we reported on geometrical and electronic structures of the aluminum doped silicon Si_nAl_m clusters, with n = 1-11 and m = 1-2, in both neutral and anionic states. The global energy minima of the clusters considered are identified on the basis of G4 energies. Total atomization energies, enthalpies of formation and thermochemical properties including electron affinity, average binding energy, and dissociation energies are predicted for the first time using the G4 and CCSD(T)/CBS methods.

In most of the sizes investigated, two or more lowest-lying isomers of each size are calculated to be energetically degenerate (G4 values). Substitution of Si atoms at different positions of a corresponding pure silicon clusters by Al dopants invariably leads to a spectrum of distinct binary structures but with similar shape and comparable energy content. Such an energetic degeneracy persists in the larger cluster sizes, in particular for the anions. Within the expected accuracy of the methods employed, it is not possible to clearly identify the most stable structure for each size.

The growth sequence for singly and doubly aluminum doped silicon clusters can be established as follows:

i) in the neutral Si_nAl, the Al dopant prefers substitution into one of the Si positions the pure cation Si_{n+1}^+. Formally, an anion Si_nAl^- can formally be produced from the neutral Si_{n+1} by substitution of any Si atom by the Al impurity,

ii) the growth pattern of both neutrals Si_nAl and anions Si_nAl^- is similar to the structural evolution of their isovalent counterparts, namely the neutrals Si_nB and anions Si_nB^-, respectively. Having longer Al-Si bond lengths than the B-Si distances, the Al impurity cannot easily intrude inside the corresponding Si_n cage (for up to $n \geq 8$) such as the specific characteristic of the B dopant,

iii) the doubly doped neutral Si_nAl_2 clusters possess the shape of their pure Si_{n+1}^+ counterparts. One Al dopant replaces a Si atom of the latter, and the other Al dopant adds on an edge or a face. This differs from the growth pattern of the anions

$Si_nAl_2^-$ where both Al atoms simply substitute two Si centres of a Si_{n+2}^+ framework, and

iv) the neutral $Si_{10}Al_2$ and $Si_{11}Al_2$ clusters and their anions emerge as interesting exceptions in which the Al dopants behave differently. This can be understood from characteristics and stability of the relevant pure Si clusters.

References

1) U. Landman, R. N. Barnett, A. G. Scherbakov, P. Avouris, Phys. Rev. Lett. 85 (2000) 1958.

2) V. G. Kotlyar, A. V. Zotov, A. A. Saranin, T. V. Kasyanova, M. A. Cherevik, I. V. Pisarenko, V. G. Lifshits, Phys. Rev. B 66 (2002) 165401.

3) M. Paulose, C. A. Grimes, O. K. Varghese, E. C. Dickey, Appl. Phys. Lett. 81 (2002) 153.

4) Z. Sun, Z. Yang, Z. Gao, Z. C. Tang, Rapid. Comm. Mass. Spectrom. 21 (2007) 792.

5) B. Li, G. Wang, M. Ye, G. Yang, C. Yao, J. Mol. Struct. THEOCHEM 820 (2007) 128.

6) T. B. Tai, M. T. Nguyen, J. Chem. Theo. Comput. 7 (2011) 1119.

7) T. Clark, J. Chandrasekhar, G. W. Spitznagel, P. V. Schleyer, J. Comput. Chem. 4 (1983) 294.

8) A. D. McLean, G. S. Chandler, J. Chem. Phys. 72 (1980) 5639.

9) M. J. Frisch, J. A. Pople, J. S. Binkley, J. Chem. Phys. 80 (1984) 3265.

10) L. B. Knight, A. J. McKinley, R. M. Babb, M. D. Morse, C. A. Arrington, J. Chem. Phys. 98 (1993) 6749.

11) a) S. Nigam, C. Majumder, S. K. Kulshreshtha, J. Chem. Phys. 121 (2004) 7756; b) Majumder, S. K. Kulshreshtha, Phys. Rev. B 69 (2004) 115432; c) S. Nigam, Majumder, S. K. Kulshreshtha, J. Chem. Phys. 125 (2006) 074303.

12) a) J. T. Lyon, P. Gruene, A. Fielicke, G. Meijer, E. Janssens, P. Claes, P. Lievens, J. Am. Chem. Soc. 131 (2009) 1115; b) A. Fielicke, J. T. Lyon, M. Haertelt, G. Meijer, P. Claes, J. De Haeck, P. Lievens, J. Chem. Phys. 131 (2009) 171105.

13) P. Karamanis, R. Marchal, P. Carbonniére, C. Pouchan, Chem. Phys. Lett. 500 (2010) 59.

14) J. C. Yang, W. G. Xu, W. S. Xiao, J. Mol. Struct. THEOCHEM 719 (2005) 89.

15) A. D. Zdetsis, J. Chem. Phys. 127 (2007) 244308.

16) N. M. Tam, T. B. Tai, M. T. Nguyen, J. Phys. Chem. C 116 (2012) 20086.

17) C. E. Moore. Atomic energy levels as derived from the analysis of optical spectra, Volume 1, H to V; U.S. National Bureau of Standards Circular 467, U.S. Department of Commerce, National Technical Information Service, COM-72-50282: Washington, D.C. 1949.

18) M. Brack, Rev. Mod. Phys. 65 (1993) 677.

19) a) N. M. Tam, T. B. Tai, M. T. Nguyen, J. Phys. Chem. C 116 (2012) 20086; b) V. T. Ngan, M. T. Nguyen, J. Phys. Chem. A, 114 (2010) 7609; c) V. T. Ngan, E. Janssens, P. Claes, J. T. Lyon, A. Fielicke, M. T. Nguyen, P. Lievens, Chem. Eur. J. 18 (2012) 15788.

Chapter 6

Si_nMg_m: Toward Silicon Nanowires with Magnesium Linkers

This chapter is adapted from the following article:

Theoretical Study of the Si_nMg_m Clusters and Ions: Toward Silicon Nanowires with Magnesium Linkers, by N. M. Tam, V. T. Ngan, and M. T. Nguyen, *Journal of Physical Chemistry A* (2014) to be submitted.

6.1 INTRODUCTION

Clusters with enhanced stability often behave as superatoms that can further be considered as building blocks for new materials. Some previous attempts to prepare silicon nanowires as assemblies of small silicon clusters have been reported.[1] Previous studies showed the Si nanowire modified by one Al atom has been found to enhance electrical conductivity as compared to pristine Si-nanowire.[2] Kotlyar *et al.*[3] found that Al atoms form an ordered array of magic clusters on the surfaces of Si(111). Paulose and co-workers[4] also reported the persistent formation of Al-Si nanowires. Relatively much less is known about nanowires or assemblies using other elements as linkers. Recent work in our laboratory pointed out that the Li and Mn elements emerge as possible linkers. While Li linkers give rise to low spin assemblies,[5] Mn turns out to lead to high spin adducts.[6]

In a further attempt to search for potential linkers for Si nanowires, a simple form of nano-assemblies, we set out to perform a systematic investigation on a series of small singly and doubly doped Si_nM_m, in which M is an earth-alkali element M = Be, Mg and Ca. It turns out that the magnesium doped silicon clusters emerge as the most promising candidates for this purpose. Therefore we report in this chapter the calculated results on Si_nMg_m with n = 1-10 and m = 1-2, in both neutral and cationic states. Perhaps more promising, we also find that the magnesium element behaves as good linkers for silicon blocks giving rise to a variety of oligomers having different shapes. Of the latter, the linear oligomers constitute the first step for preparing potential 1D nanowires.

The present chapter is organized in the following way. As in previous chapter, a systematic analysis of the computational results of Mg-doped Si clusters Si_nMg_m (n = 1-10; m = 1-2) will first but briefly be described. The structural and stability patterns allow us to identify the suitable members that can further be used as superatoms for assemblies. We thus probe the five-, seven-, eight- and ten-atom Si building blocks, and the role of the Mg element as the linkers connecting them.

The searches for energy minima of both Si_nMg and Si_nMg_2 are conducted using the same approaches described in Chapters 3, 4 and 5. While low-level computations on initial geometries are carried out using the hybrid B3LYP functional in conjunction with the 6-31G basis set, all selected equilibrium geometries of Si_nMg_m (n = 1-10, m = 1-2) are fully optimized using the same functional but with the larger 6-311+G(d) basis set.[5,6,7] Their harmonic vibrational frequencies are also calculated at the same level of theory.

Standard enthalpies of formation of the global minima are subsequently evaluated from the corresponding total atomization energies (ΣD_0, TAE)[8] performed using the composite G4 approach.[9] By combining our computed ΣD_0 values determined from G4 calculations with the known experimental heats of formation at 0 K for the Mg and Si elements, we can derive $\Delta_f H°$ values at 0K for the molecules in the gas phase. In this work, we use the values at 0K $\Delta_f H°(Mg) = 34.87 \pm 0.2$ kcal/mol, and $\Delta_f H°(Si) = 107.2 \pm 0.2$ kcal/mol.[10] We subsequently obtain the heats of formation at 298K by following the classical thermochemical procedure.[11] The calculated heats of formation at 0K are used to evaluate the adiabatic ionization energies (IE) and other energetic quantities.

6.2 LOWER-LYING ISOMERS OF Si_nMg_m CLUSTERS IN BOTH NEUTRAL AND CATIONIC STATES

Shapes of equilibrium structures of the $Si_nMg_m^{0/+}$ clusters located, their symmetry point groups and G4 relative energies are shown in Figures 6.1, 6.2, 6.3 and 6.4. The calculated heats of formation are given in Table 6.1. Computed adiabatic ionization energies (IEs) of Si_nMg_m clusters are given in Table 6.2, and average binding energies (E_b) tabulated in Table 6.3.

To simplify the presentation of data, we only display some lower-lying isomers whose relative energies are close to each ground state structure (within ~1.0 eV). As for a convention, each structure described hereafter is defined by the label **x**.***n.m.*****Y** in which **x** = **n** and **c** stands for a neutral and cationic state, respectively, ***n*** the size of Si_n, ***m*** the size of Al_m, and finally **Y** = **A, B, C**… refers to the different isomers with increasing relative energy ordering. Concerning the energy ordering

within a system, the structure labeled with the letter **A** (**x.*n.m*.A**) invariably refers to the lowest-lying isomer obtained from G4 calculations. In the following section, we briefly describe the main characteristics of the singly and doubly doped clusters, in terms of their geometry, symmetry, spin state and relative energy.

6.2.1 The singly magnesium doped $Si_nMg^{0/+}$

The main structures are displayed in Figures 6.1 and 6.2. The geometrical features of neutral Si_nMg are in line with a previous study[12] on the identification of the global minima of small-sized neutral Si_nMg with $n = 1 – 10$. However, for Si_8Mg, Fan *et al.*[12] reported that isomer **n.8.1.D** (C_{2v}, $^1A_1$) is the most stable structure whereas our G4 results indicate that two energetically degenerate lowest-lying isomers are **n.8.1.A** (C_s, $^1A'$) and **n.8.1.B** (C_1, ^1A) which are 0.30 eV lower in energy than **n.8.1.D**. Both isomers are formed by substituting one of Si atoms of the bicapped pentagonal bipyramid Si_9 framework.[13]

A main property of the Si_nMg species is, as expected, an electron transfer from the dopant to Si_n. The positive charges on Mg in Si_5Mg, Si_6Mg, Si_7Mg, Si_8Mg, and $Si_{10}Mg$ amount to 1.1, 1.4, 0.3, 1.3 and 0.7 electron, respectively (NBO charges using B3LYP/6-311+G(d)). Each cluster is thus polarized as an ionic entity $(Si_n)^{\delta-}.Mg^{\delta+}$.

As far as we are aware, there is no previous study on cationic Si_nMg clusters. Their main characteristics can be summarized as follow:

i) The doublet spin state isomer **c.1.1.A** ($^2\Pi$) is confirmed as the ground state of cationic dimer $SiMg^+$.

ii) The global minimum of cations Si_2Mg and Si_3Mg is isoceles triangle **c.2.1.A** (C_{2v}, $^2A_1$) and planar quadrilateral **c.3.1.A** (C_s, $^2A'$), respectively.

iii) For Si_4Mg^+, three isomers **c.4.1.A** (C_{2v}, $^2A_1$), **c.4.1.B** (C_s, $^2A'$), **c.4.1.C** (C_1, ^2A) which are generated by capping Li at different positions on the rhombus framework of Si_4, are the lowest-lying structures. The planar structure **c.4.1.A**, being 0.10 eV and 0.12 eV lower in energy than **c.4.1.B** and **c.4.1.C**, respectively, is the most stable isomer.

iv) The cationic ground state of Si_5Mg^+ is a 3D isomer **c.5.1.A** (C_{2v}, $^2B_1$). It has the shape of the corresponding neutral **n.5.1.A** in which a Mg-atom caps on an edge of the trigonal bipyramid Si_5.[13]

v) For Si_6Mg^+, our G4 results indicate that both lowest-lying isomers **c.6.1.A** (C_{2v}, $^2B_2$) and **c.6.1.B** (C_s, $^2A'$), formed by capping a Mg-dopant on the edge-capped trigonal bipyramid Si_6 framework,[13] are almost degenerate with energy gap of only 0.09 eV.

vi) Similarly, the most stable structure Si_7Mg^+ **c.7.1.A** (C_{2v}, $^2A_1$) is generated by adding a Mg-atom on the edge of pentagonal bipyramid Si_7 host.[13]

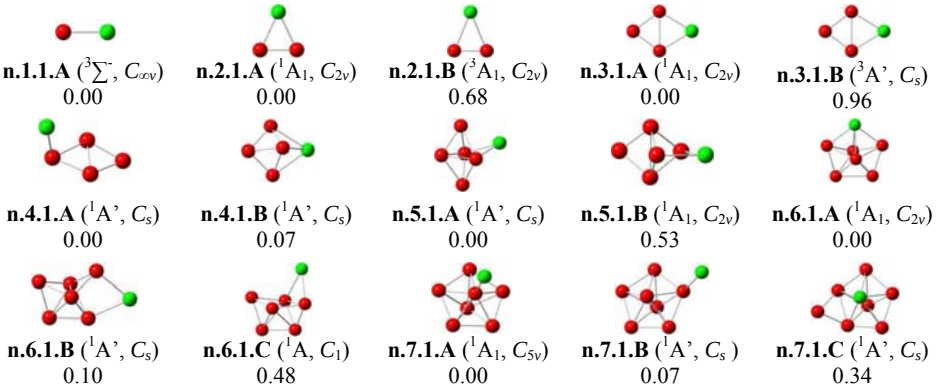

a/ The neutral Si_nMg clusters

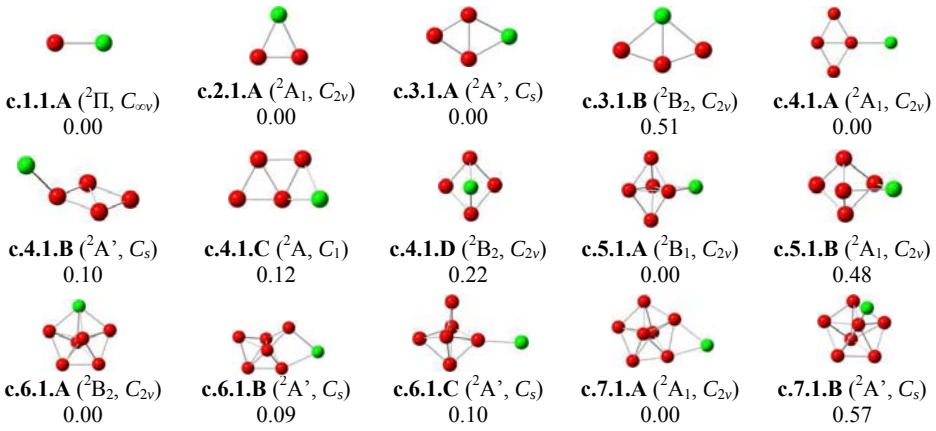

b/ The cationic Si_nMg^+ clusters

Figure 6.1 Shapes, electronic states, point groups, and relative energies (G4 values, eV) of lower-lying isomers of the neutral Si_nMg and Si_nMg^+ with n = 1-7.

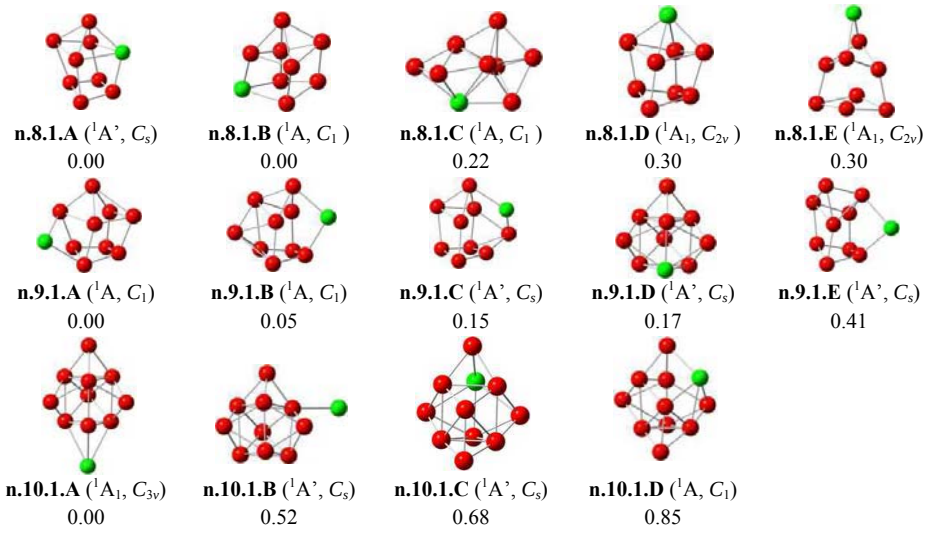

a/ The neutral Si_nMg clusters

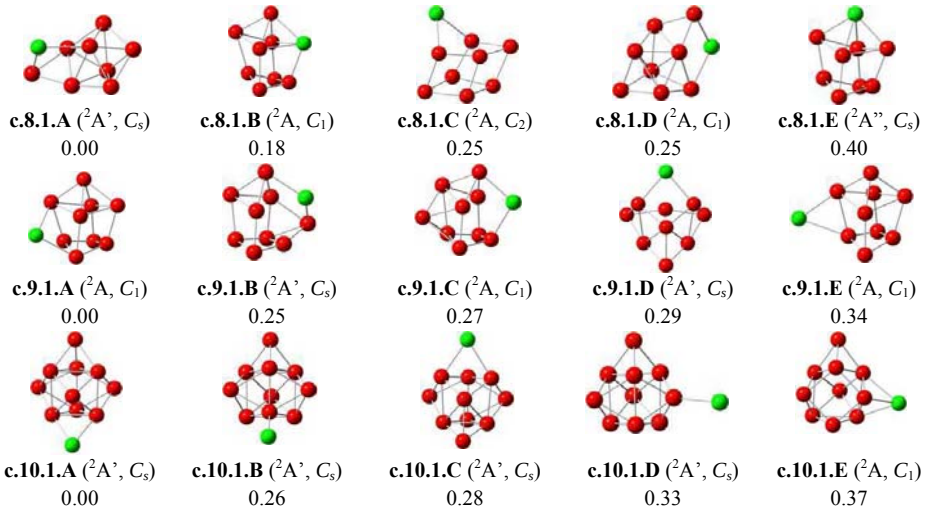

b/ The cationic Si_nMg^+ clusters

Figure 6.2 Shapes, electronic states, point groups, and relative energies (G4 values, eV) of lower-ling isomers of neutral Si_nMg and Si_nMg^+ with n = 8-10.

vii) For Si_8Mg^+, the isomer **c.8.1.A** (C_s, ^{2}A') formed by capping the Mg-impurity on the surfaces of Si_8^+ framework[14] is the lowest-lying isomer with energy gap of 0.18 eV below the next isomer, **c.8.1.B** (C_1, ^{2}A), that has the shape of the corresponding neutral **n.8.1.A**.

viii) The most stable structure of Si_9Mg^+ **c.9.1.A** (C_1, ^2A) has the same shape with the ground state of the neutral Si_9Mg **n.9.1.A** in which the Mg-atom is exposed on the surface of the bicapped pentagonal bipyramid Si_9^+ skeleton, and

ix) For $Si_{10}Mg^+$, most of lower-lying isomers have the tetra-capped trigonal prism framework of Si_{10}[14] from which the Mg-atom exohedrally adds on different positions. According to our G4 calculations, **c.10.1.A** (C_s, $^2A'$), being around 0.3 eV lower in energy than the remaining stable structures, is the lowest-lying isomer of cationic $Si_{10}Mg^+$.

6.2.2 The doubly magnesium doped $Si_nMg_m^{0/+}$ with n = 1-10 and m = 2

Their structural evolution is illustrated in Figures 6.3 for n = 1-7 and 6.4 for n = 8-11. Some main points can be noted:

i) **$SiMg_2$.** The triangular isomer **n.1.2.A** (C_{2v}, $^1A_1$) possesses a closed shell electronic configuration in which the Si-atom connects with two Mg-atoms. This is confirmed as the ground state of the neutral $SiMg_2$ with a small singlet-triplet separation gap of 0.12 eV. Following detachment of one electron, the resulting cationic cluster $SiMg_2^+$ **c.1.2.A** (C_{2v}, $^2B_1$) has the shape almost unchanged with respect to its neutral counterpart.

ii) **Si_2Mg_2**. All lowest-lying structures in both neutral and cationic states have the planar geometries. The parallelogram neutral **n.2.2.A** (C_{2h}, ^1A_g), being 0.11 eV lower in energy than the planar quadrilateral isomer **n.2.2.B** (C_s, $^1A'$), is the global minimum. A D_{2h} structure is located as a first-order saddle point having one imaginary frequency. The latter is a transition structure connecting two C_{2h} **n.2.2.A** structures, but the energy barrier is small indicating a floppy character of this cluster size.

In the cationic state, our G4 calculation results in a near degeneracy of both **c.2.2.A** (C_s, $^2A'$) and **c.2.2.B** (C_{2v}, $^2A_1$). The isomer **c.2.2.A** in which one Mg-atom connects with two Si-atoms whereas the other Mg bonds with only one Si-atom is the most stable isomer with an energy gap of only 0.07 eV below **c.2.2.B**.

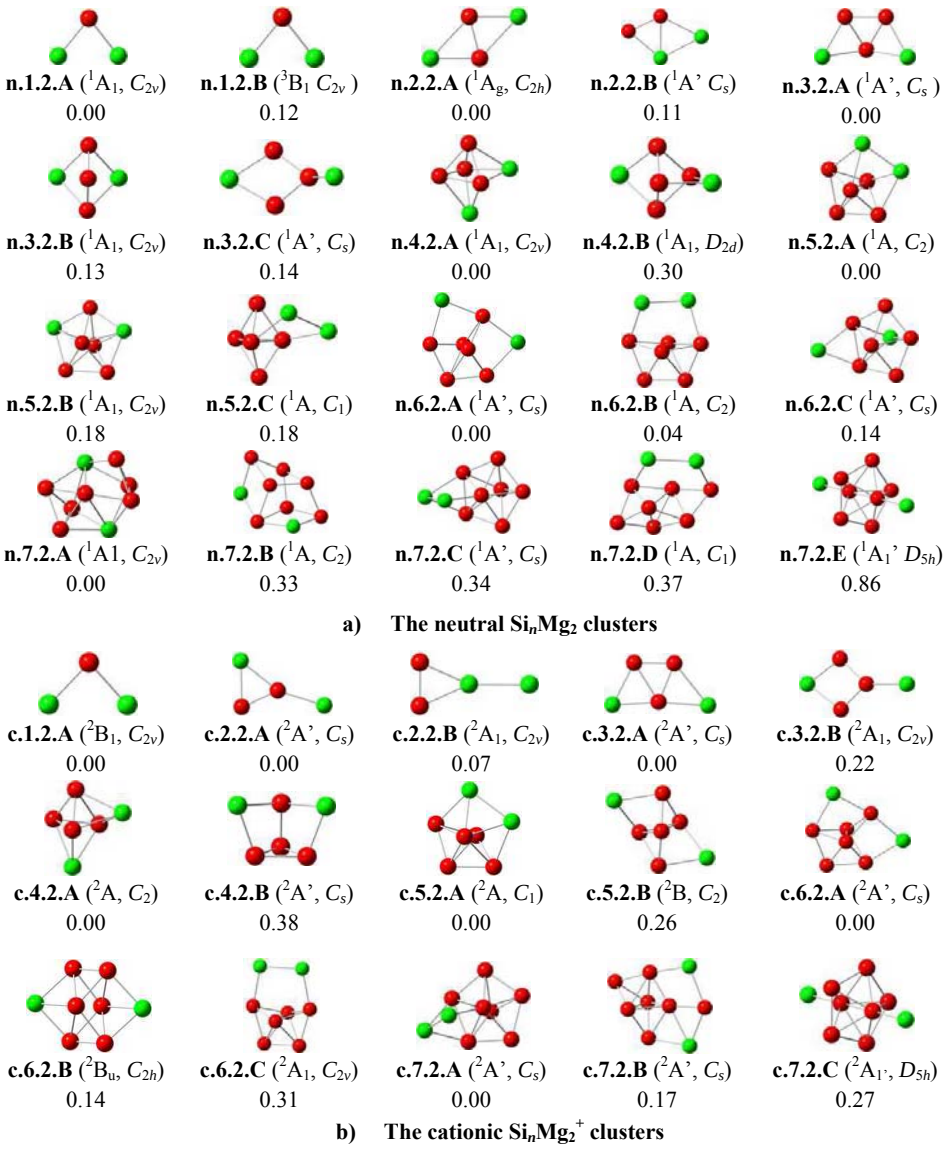

Figure 6.3 Shapes, electronic states, point groups, and relative energies (G4 values, eV) of lower-ling isomers of neutral Si_nMg_m and cationic $Si_nMg_m^+$ with n = 1-7 and m=2.

iii) **Si_3Mg_2.** For the pentatomic molecules, the neutral isomer **n.3.2.A** (C_s, ^{1}A'), formed by adding two Mg-atom on two edges of the Si_3 triangle, is the lowest-lying isomer. The second isomer **n.3.2.B**, which is generated by replacing two positions of Si atoms in Si_5 framework by two Mg-dopants, lies at 0.13 eV above **n.3.2.A**. In the cationic state, the corresponding cation of **n.3.2.A,** the planar structure **c.3.2.A** (C_s, ^{2}A'), being 0.22 eV lower in energy than next isomer **c.3.2.B**, is the ground state of cation $Si_3Mg_2^+$.

iv) **Si_4Mg_2**. The most stable isomer of neutral Si_4Mg_2, **n.4.2.A** (C_{2v}, $^1A_1$), can be considered as a substitution of two Si-atoms of the Si_6 counterpart by two Mg-atoms. In other words, it can be formed by replacing one Si-atom of the trigonal bipyramid Si_5 by one Mg-atom whereas the remaining Mg-atom caps on a face of it. The higher symmetry **n.4.2.B** (D_{2d}, $^1A_1$), being 0.30 eV higher in energy than **n.4.2.A**, becomes the second stable isomer. In the cationic state, the corresponding cation of **n.4.2.A**, **c.4.2.A** (C_2, ^{2}A), is also the lowest-lying structure being 0.38 eV more stable than next isomer **c.4.2.B**.

v) **Si_5Mg_2**. The lowest-lying neutral isomer **n.5.2.A** (C_2, ^{1}A) possesses the form of the pure Si_6 skeleton in which a Mg atom replaces one Si position whereas the other Mg caps on one of its faces. The two next isomers, **n.5.2.B** and **n.5.2.C**, being 0.18 eV higher in energy than **n.5.2.A**, exist as degenerate equilibrium structures. In the shape of **n.5.2.B**, both Mg atoms substitute two positions of Si atoms in pentagonal bipyramid Si_7, while **n.5.2.C** is formed by adding both Mg atoms on trigonal bipyramid Si_5.

In the cationic state, similar to Si_3Mg_2 and Si_4Mg_2, the corresponding cation of the most stable neutral Si_5Mg_2 **c.5.2.A** (C_1, ^{2}A), which lies at 0.26 eV lower in energy than **c.5.2.B**, becomes the most stable structure.

vi) **Si_6Mg_2**. Our G4 results emphasize two degenerate structures **n.6.2.A** (C_s, ^{1}A') and **n.6.2.B** (C_2, ^{1}A) for the neutral Si_6Mg with an energetic gap of only 0.04 eV. Both of them are generated by capping two Mg atoms on different positions of the Si_6 framework. However, it can also be considered that **n.6.2.A** is formed by replacing a Si atom in pentagonal bipyramid Si_7 skeleton by a Mg atom whereas the

other Mg add on a face of it. **n.6.2.C** is also quite stable, being at 0.14 eV above **n.6.2.A**.

In the cationic state, again, the most stable isomer **c.6.2.A** (C_s, ^{1}A') is the corresponding cation of the lowest-lying neutral **n.6.2.A**. However, **c.6.2.C**, the corresponding cation of the lowest-lying neutral **n.6.2.B**, is much less stable than **c.6.2.A** with a separation gap of 0.31 eV. The second isomer **c.6.2.B** (C_{2h}, ^{2}B$_u$), being 0.14 eV higher in energy than **c.6.2.A**, is generated by substituting two Si atoms in bicapped octahedral shape of neutral Si_8[13] by two Mg atoms.

vii) **Si_7Mg_2**. The structure of the lowest-lying neutral isomer Si_7Mg_2 **n.7.2.A** (C_{2v}, ^{1}A$_1$) can be considered as the result of a change of two Si-atoms of the pentagonal bipyramid Si_7 framework by both Mg-atoms, whereas two Si atoms adsorb to pentagonal faces. The next isomer, **n.7.2.B**, being 0.33 eV higher in energy than **n.7.2.A**, possesses the bicapped octahedral shape of neutral Si_8 in which one Si position is substituted by a Mg-atom, whereas the remaining Mg-atom makes a bridge between two other Si atoms. The isomer **n.7.2.C**, being only 0.01 eV above **n.7.2.B**, is the third stable structure. This isomer keeps the pentagonal bipyramid Si_7 and both Mg atoms cap on it. In other words, **n.7.2.C** is characterized by the edge-capped pentagonal bipyramid of the cation Si_8^+ [14] where the first Mg atom takes the capping position and the remaining Mg adds on its face. However, in the cationic states, **c.7.2.A**, the corresponding cation of **n.7.2.C**, becomes the most stable structure lying 0.17 eV below the second isomer.

viii) **Si_8Mg_2**. The most stable structure of neutral Si_8Mg_2 is the high symmetry isomer **n.8.2.A** (D_{2d}, ^{1}A$_1$) in which both Mg atoms add on two opposite faces of the anion Si_8^- framework.[13] The next isomer, **n.8.2.B**, being 0.21 eV higher in energy than **n.8.2.A**, also has Si_8^- counterpart in which a Mg caps on a face and the other Mg adds on an edge of it. On the other hand, both **n.8.2.A** and **n.8.2.B** can be formed by replacing a Si atom in bicapped pentagonal bipyramid Si_9[13] by a Mg atom whereas the remaining Mg adds on a face or edge of it. The remaining isomer are less stable.

In the cationic states, **c.8.2.A**, the corresponding cation of **n.8.2.A**, is also the lowest-lying isomer. However, our G4 calculations indicate that the isomers **c.8.2.A** and **c.8.2.B** are degenerate with an energy gap of only 0.06 eV. This isomer can be generated by substitution of both Si atoms into the pentagonal bipyramid Si_7 by two Mg in which three other Si atoms cap on different positions. The corresponding cation of **n.8.2.B**, namely **c.8.2.C,** is also stable being 0.12 eV above **c.8.2.A**.

ix) **Si_9Mg_2.** Four lower-lying isomers of Si_9Mg_2 have the tetra-capped trigonal prism framework of Si_{10} in which a Mg atom replaces one of Si atoms whereas the other Mg caps at different positions. The isomer **n.9.2.A** (C_s, $^1A'$), being 0.15 eV more stable than the second isomer possessing higher symmetry **n.9.2.B** (D_{3h}, $^1A_1'$), becomes the lowest-lying structure.

However, in the positively charged state, **c.9.2.A**, which is the corresponding cation of **n.9.2.B**, turns into the most stable isomer. Again, our G4 results indicate a near degeneracy of both **c.9.2.A** and **c.9.2.B** with an energy gap of only 0.08 eV.

x) **$Si_{10}Mg_2$.** According to G4 calculations, the four isomers of $Si_{10}Mg_2$ **n10.2.A**, **n10.2.B**, **n10.2.C** and **n10.2.D** are energetically degenerate within an energy range of only 0.08 eV. A reason for such a close energy is that these low-lying isomers can be formed by replacement of two Si atoms of the same hexa-capped trigonal prism Si_{12} cage[15] by two Mg dopants even though their geometric structures are significantly distorted. In the cationic state, the high symmetry isomer **c.10.2.A** (C_{2h}, ^2B_u), being 0.10 eV lower in energy than **c.10.2.B**, is the most stable structure. **c.10.2.A** also exhibits the hexa-capped trigonal prism Si_{12} framework in which both Mg dopants substitute two Si atoms whereas **c.10.2.B** is formed by adding both Mg atoms on the faces of tetra-capped trigonal prism Si_{10} framework.

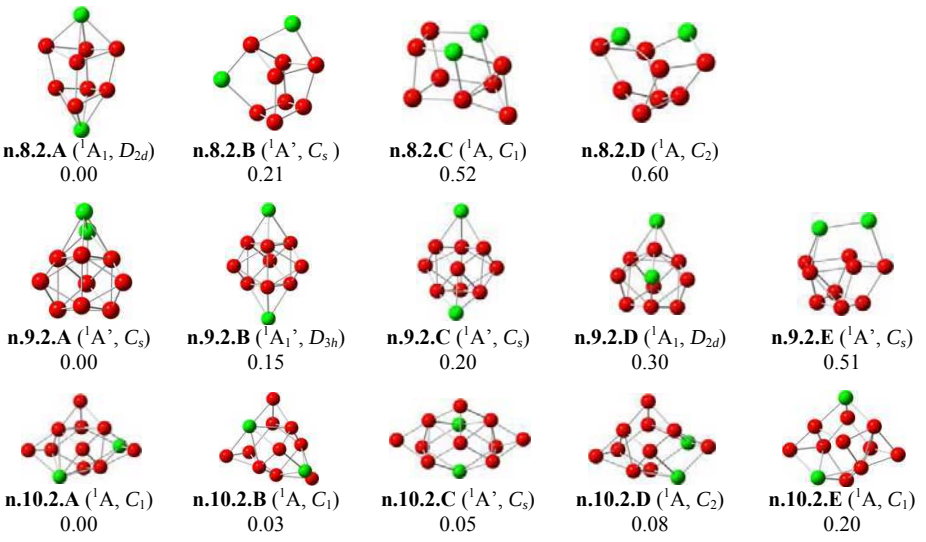

a) The neutral Si_nMg_2 clusters

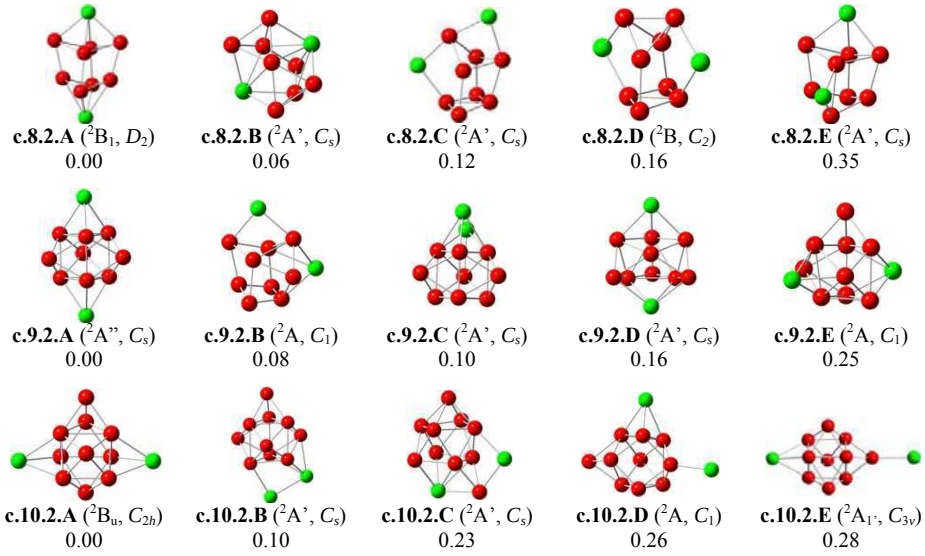

b) The cationic $Si_nMg_2^+$ clusters

Figure 6.4 Shapes, electronic states, point groups, and relative energies (G4 values, eV) of lower-ling isomers of neutral Si_nMg_m and cationic $Si_nMg_m^+$ with n = 8-10 and m = 2

6.3 GROWTH PATTERN OF THE EQUILIBRIUM Si_nMg_m CLUSTERS

On the basis of the structural features of the most stable isomers identified above, the growth pattern of the clusters Si_nMg_m with n = 1-10 and m = 1-2 can be established considering the following findings:

The growth sequence of the singly doped neutral Si_nMg is similar to that of the singly doped neutral Si_nLi clusters (Chapter 3). In Si_nMg structures, the Mg atom tends to favour addition on either an edge or a face of the anionic ground state structure Si_n^- framework. However, both energetically degenerate lowest-lying isomers of Si_8Mg have a Mg dopant which substitutes a Si atom in the anion Si_8^- counterpart, whereas it replaces a Si atom adds on its face. In other words, both structures can be considered to be formed by replacing a Si atom in the Si_9 framework by a Mg atom.

For the cations Si_nMg^+, surprisingly, there is a difference between the behaviour of Mg and Li. The Mg atom seems to cap on one of edge or face of the cationic Si_n^+ instead of the neutral bare Si_n like as in the case of Li. No exception on this rule can be observed in the size range n = 1-10.

The doubly magnesium doped neutral Si_nMg_2 clusters grow up following the same way as the doubly doped neutral Si_nX_2 with X = Li, Al reported in previous chapters. Their growth pattern is that one Mg atom substitutes into a position of Si_{n+1}, whereas the other Mg atom is usually added on an edge, or a face, of the existing cluster. However, the most stable structures include Si_7Mg_2 which is formed by replacing two Si-atoms of the pentagonal bipyramid Si_7 framework by two Mg atoms, while two Si atoms adsorb in the faces of pentagon. The stable $Si_{10}Mg_2$ in which both Mg dopants replace two Si atoms of the same hexa-capped trigonal prism Si_{12} cage is another exceptions of this observation.

Similarly, for the positively charged state, it can be considered that $Si_nMg_2^+$ cations contain the cationic Si_{n+1}^+ frameworks in which one Mg atom actually substitutes into a Si position whereas the remaining Mg atom caps on an edge, or a face. Again, $Si_{10}Mg_2^+$ appears as an exception, due to the fact that it also possesses the

hexa-capped trigonal prism Si_{12} skeleton in which both Mg dopants substitute two Si atoms.

6.4 THERMOCHEMICAL PROPERTIES

The TAEs and enthalpies of formation at both 0 K and 298 K are summarized in Table 6.1. The calculated heats of formation at 0 K are used to evaluate the adiabatic ionization energies (IE), obtained from the energy difference between the neutrals Si_nMg_m and their corresponding $Si_nMg_m^+$ cations. The IE values are summarized in Table 6.2.

Table 6.1. TAE and heats of formation at 0K [ΔH_f (0 K)] and 298K [ΔH_f (298 K)] (kcal/mol) of Si_nMg_m(n = 1-10, m = 1-2) in both neutral and cationic states (G4)

Structure	TAE	ΔH_f (0 K)	ΔH_f (298 K)
n.1.1.A	25.5	116.6	117.0
c.1.1.A	-132.5	274.6	275.0
n.2.1.A	121.8	127.5	127.9
c.2.1.A	-44.1	293.4	293.8
n.3.1.A	215.4	141.1	141.7
c.3.1.A	41.8	314.7	315.3
n.4.1.A	296.7	167.0	168.0
c.4.1.A	134.2	329.5	330.6
n.5.1.A	418.2	152.7	153.6
c.5.1.A	256.6	314.2	315.1
n.6.1.A	503.1	174.9	176.0
c.6.1.A	345.0	333.1	334.0
n.7.1.A	593.1	192.2	193.7
c.7.1.A	448.3	336.9	338.4
n.8.1.A	682.7	209.8	211.3
c.8.1.A	523.5	360.0	370.6
n.9.1.A	788.4	211.3	213.0
c.9.1.A	629.5	370.2	372.2
n.10.1.A	900.4	206.5	208.5
c.10.1.A	744.2	362.7	364.6
n.1.2.A	50.6	126.4	126.5
c.1.2.A	-84.0	260.9	261.1
n.2.2.A	137.3	146.9	147.7
c.2.2.A	-10.1	294.2	294.8

n.3.2.A	227.1	164.3	165.0
c.3.2.A	87.8	303.6	303.8
n.4.2.A	348.9	149.6	150.3
c.4.2.A	186.8	311.8	312.7
n.5.2.A	441.4	164.3	165.4
c.5.2.A	290.8	314.9	315.9
n.6.2.A	534.3	178.6	179.8
c.6.2.A	382.7	330.3	331.5
n.7.2.A	622.7	197.5	198.8
c.7.2.A	469.3	350.8	352.4
n.8.2.A	722.2	205.1	206.6
c.8.2.A	564.3	363.0	364.7
n.9.2.A	841.8	192.8	194.4
c.9.2.A	676.3	358.2	360.2
n.10.2.A	900.8	241.0	242.6
c.10.2.A	774.4	367.4	369.6

Table 6.2 Adiabatic Ionization Energies (AIE, eV) of Si_nMg_m (n = 1-10, m = 1-2) (G4)

n	**Si_nMg**	**Si_nMg_2**
1	6.85	5.83
2	7.19	6.39
3	7.52	6.04
4	7.05	7.03
5	7.00	6.53
6	6.86	6.58
7	6.28	6.65
8	6.90	6.85
9	6.89	7.18
10	6.77	5.48

As far as we are aware, no experimental thermochemical parameters on these systems are actually available. Therefore they can be considered as predicted values, with an expected error margin of, or even better than, ± 0.2 eV.

6.5 THERMODYNAMIC STABILITY

The average binding energies (E_b) can conventionally be defined as follows (equations 6.1 - 6.4):

$$E_b(Si_nMg) = [nE(Si) + E(Mg) - E(Si_nMg)]/(n+1) \quad (6.1)$$

$$E_b(Si_nMg^+) = [(n-1)E(Si) + E(Si^+) + E(Mg) - E(Si_nMg^+)]/(n+1) \quad (6.2)$$

$$E_b(Si_nMg_2) = [nE(Si) + 2xE(Mg) - E(Si_nMg_2)]/(n+2) \quad (6.3)$$

$$E_b(Si_nMg_2^+) = [(n-1)E(Si) + E(Si^+) + 2xE(Mg) - E(Si_nMg_2^+)]/(n+2) \quad (6.4)$$

where E(Mg), E(Si), $E(Si^+)$ are the total energies of the Mg-atom, Si-atom and the cation Si^+, respectively. For their part, $E(Si_nMg)$, $E(Si_nMg^+)$, $E(Si_nMg_2)$, and $E(Si_nMg_2^+)$ are total energies of the neutral Si_nMg, cationic Si_nMg^+, neutral Si_nMg_2 and anionic $Si_nMg_2^+$ structures, respectively. All these energies are obtained from G4 calculations. While the E_b values are given in Table 6.3, plots illustrating their evolution are depicted in Figure 6.5.

Table 6.3. Average Binding Energies (E_b, eV) of Si_nMg_m (n = 1-10, m = 1-2) (G4)

n	**Si_nMg**	**Si_nMg^+**	**Si_nMg_2**	**$Si_nMg_2^+$**
1	0.55	1.20	0.73	1.50
2	1.76	2.08	1.49	1.93
3	2.33	2.49	1.97	2.39
4	2.57	2.79	2.52	2.71
5	3.02	3.21	2.73	2.96
6	3.12	3.30	2.90	3.09
7	3.21	3.45	3.00	3.17
8	3.29	3.43	3.13	3.26
9	3.42	3.54	3.32	3.41
10	3.55	3.67	3.26	3.48

The E_b values raise with increasing cluster sizes. For Si_nMg, the $Si_{10}Mg$ in both neutral and cationic states consistently reveal the highest E_b values as compared

to the smaller neutral and cationic singly doped species. For neutral Si_nMg_2 , the Si_9Mg_2 presents with the highest E_b value as compared to those of the remaining doubly doped species. In the series of cations considered, $Si_{10}Mg_2^+$ get a larger value peak in the E_b plot.

Figure 6.5 points out that binding energies of Mg-doped Si clusters are decreased with respect to the pure Si counterparts, irrespective of the charge state.

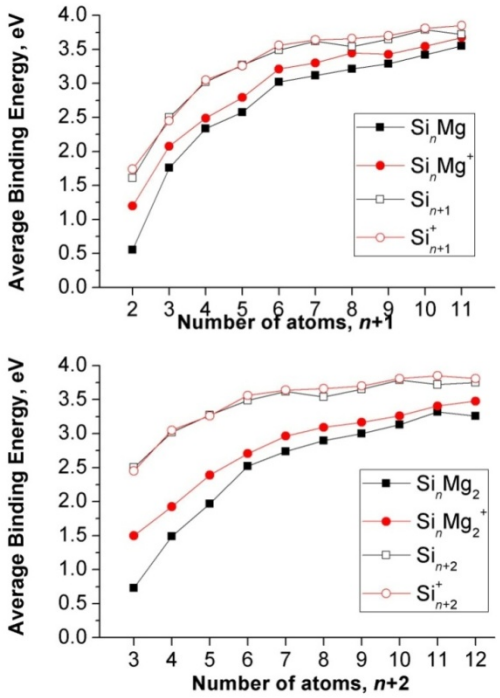

Figure 6.5. Binding energies of the Mg-doped silicon clusters (eV, G4) compared with cooresponding pure silicon clusters.

6.6 IN SEARCH OF SILICON NANOWIRES WITH MAGNESIUM LINKERS

After having carefully investigated the geometrical and energetic properties of small Si_nMg_m, we now carry out a search for a way of assembling some typical Si_n clusters, namely Si_5, Si_7, Si_8, and Si_{10}, with the Mg atoms as linkers between these building blocks. These pure silicon units are chosen due to their relatively high and

enhanced stabilities, and their unchanged geometrical shapes following attachment of Mg atoms. Our extensive calculated results reveal that addition of successive Si_n units in a symmetrical way leads to formation of potential Mg-doped Si nanowires.

In this strategy, we use different pure silicon clusters Si_k (k = 5, 7, 8, 10) as building blocks and Mg atoms as linkers to generate the magnesium-doped silicon nanowires $(Si_kMg)_l$ in different forms. However, it turns out that only two forms, that are either *linear* or *cyclic* structures, are of interest.

Geometrical optimizations of $(Si_kMg)_l$ structures are followed by harmonic vibrational frequency computations at the B3LYP/6-311G(d) level in order to characterize real local minima. Due to our computational resource limitation, however, we are not able to carry out optimizations for structures with $i > 6$ for $(Si_5Mg)_l$ and $l > 4$ for $(Si_7Mg)_l$, $(Si_8Mg)_l$, and $(Si_{10}Mg)_l$. The shapes of the equilibrium structures located for both linear and ring forms $(Si_5Mg)_l$, $(Si_7Mg)_l$, $(Si_8Mg)_l$ and $(Si_{10}Mg)_l$ are summarized in Figures 6.6, 6.7, 6.8 and 6.9, respectively. Let us briefly describe their characteristics:

i) **$(Si_5Mg)_l$.** The linear structures (Si_5Mg) are formed by assembling Si_5 units along the main axis of the trigonal bipyramids and the Mg atom operates here as a linker connecting two Si atoms that are two tops of adjacent bipyramids. In the cyclic forms of $(Si_5Mg)_l$, each Mg linker connects a top of bipyramid with an edge of another bipyramid (Figure 6.6).

Calculated results of the average assembling energy of $(Si_5Mg)_l$ show that silicon clusters tend to assemble in ring forms **R*l*** over the linear forms **L*l*** as the assembling energy of the **R*l*** are significantly larger than those of the **L*l*** counterparts (see results given hereunder).

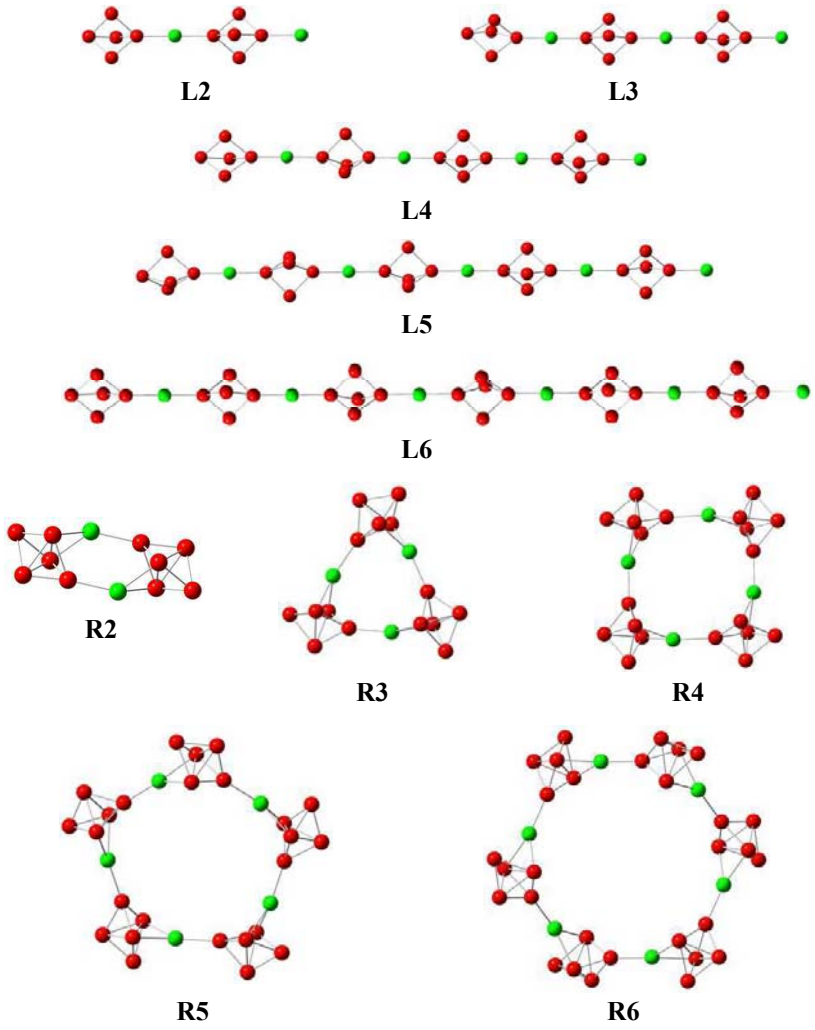

Figure 6.6 Linear (**L1-L6**) and cyclic (**R1-R6**) forms of $[(Si_5Mg)]_l$.

ii) **$(Si_7Mg)_l$**. Similar to $(Si_5Mg)_l$, the linear $(Si_7Mg)_l$ structures are created by assembling the pentagonal bipyramid Si_7 builing blocks in which each Mg atom link two Si atoms located at two tops of the bipyramid (Figure 6.7). In the cyclic forms, Mg atoms prefer to connect a Si atom located at the pentagonal planar of a Si_7 unit with one or two Si atoms which is (are) either a top or an edge of a pentagonal face of another one.

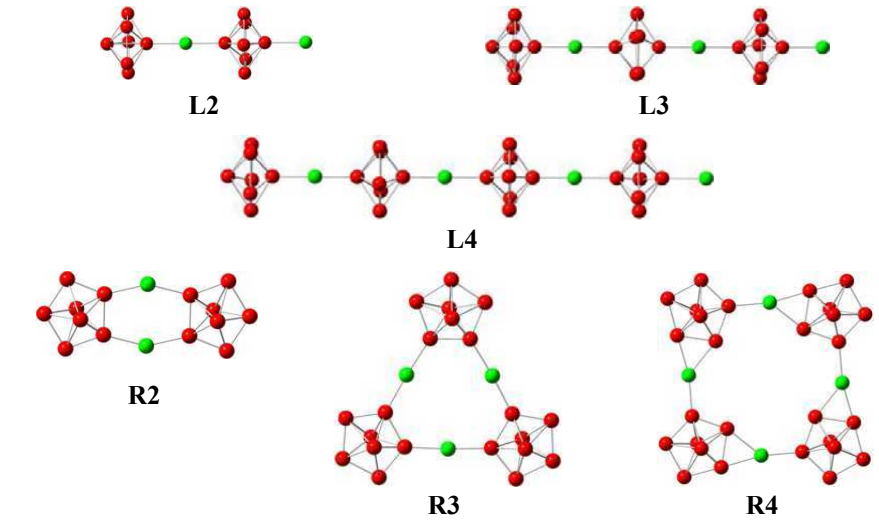

Figure 6.7 Linear (**L1-L4**) and cyclic (**R1-R3**) forms of $[(Si_7Mg)]_l$.

iii) **$(Si_8Mg)_l$**. The geometrical optimization reveals that the building block Si_8 possesses the shape of Si_8^-13 [13] for both linear and ring forms of $(Si_8Mg)_l$ and Mg atoms act as a bridge linking between two Si atoms of two different Si_8 units or connect one Si atom with an edge of another building block (Figure 6.8).

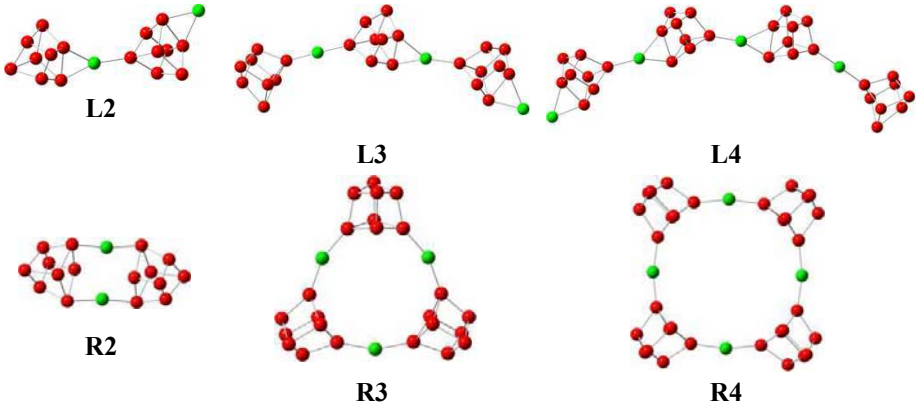

Figure 6.8 Linear (**L1-L4**) and cyclic (**R2-R4**) forms of $[(Si_8Mg)]_l$.

iv) **$(Si_{10}Mg)_l$.** The $(Si_{10}Mg)_l$ nanowires are formed by Si_{10} building blocks which are connected together by Mg linkers (Figure 6.9). These Si_{10} building blocks have the bicapped squared anti-prism cage of the pure Si_{10}^{2-} dianion,[16] except for the first Si_{10} unit in linear forms which is connected with only one Mg atom possesses the tetra-capped trigonal prism framework of Si_{10}.

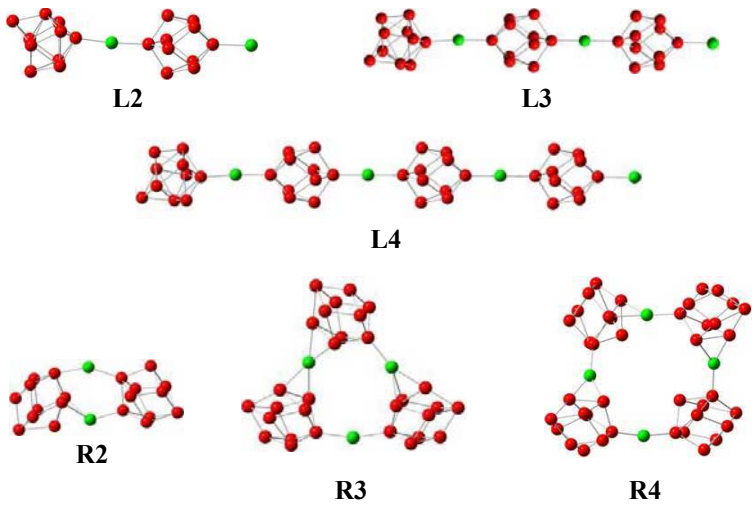

Figure 6.9 Linear (**L1-L4**) and cyclic (**R2-R4**) forms of $[(Si_{10}Mg)]_i$.

The average assembling energy E_A of $(Si_kMg)_l$ nanowires are also evaluated and shown in Table 6.4. The E_A is the energy release as the aggregate is formed from fragments per unit. This parameter gives us a trend of assembling the clusters. The E_A of $(Si_kMg)_l$ formed from the Si_k cluster and divalent linkers Mg can be computed as follows:

$$E_A[(Si_kMg)_l] = \{lE[Si_kMg] - E[(Si_kMg)_l]\}/l \qquad (6.5)$$

The calculated results of the E_A of $(Si_kMg)_l$ (k = 5, 7, 8, 10) show that silicon clusters Si_k tend to assemble in ring forms **R*l*** over the linear forms **L*l*** as the assembling energy of the **R*l*** are much higher than those of the **L*l***. However, a more important fact is that the average assembling energy of the linear form tends to

increase with the increasing size, implying that the nanowire can be considered as a plausible possibility as the length is extended.

Table 6.4. The average assembling energies for the linear and ring forms of $(Si_5Mg)_l$, $Si_7Mg)_l$, $(Si_8Mg)_l$, and $(Si_{10}Mg)_l$ calculated at B3LYP/6-311G(d) level.

	$(Si_5Mg)_l$		$(Si_7Mg)_l$		$(Si_8Mg)_l$		$(Si_{10}Mg)_l$	
l	**Linear**	**Ring**	**Linear**	**Ring**	**Linear**	**Ring**	**Linear**	**Ring**
2	0.51	2.01	0.27	0.41	0.39	1.61	0.08	1.11
3	0.90	2.30	0.51	0.53	0.65	1.36	0.41	1.41
4	1.14	2.39	0.69	0.87	0.89	1.43	0.62	1.45
5	1.29	2.40						
6	1.39	2.41						

6.7 CONCLUDING REMARKS

In summary, we investigated the structures of the singly and doubly magnesium doped silicon clusters in both neutral and cationic states Si_nMg_m with n = 1-10 and m = 1-2. The TAEs, heats of formation and binding energies were determined using the composite G4 method. As there is no experimental values available for these systems, the computed results can be regarded as predicted values, with an expected error margin of ± 3 kcal/mol (± 0.15 eV or ± 12 kJ/mol), due to the uncertainty of the experimental value of the heat of formation of the silicon atom.

The binding energies of the Mg-doped Si clusters are decreased with respect to the pure Si counterparts, irrespective of the charge state.

The growth sequence of the singly doped neutral Si_nMg is similar to that of the singly doped neutral Si_nLi clusters. In Si_nMg structures, the Mg atom tends to favour addition on either an edge or a face of the anionic ground state structure Si_n^- framework. Only in Si_8Mg, Mg substitutes a Si atom in the Si_9 framework.

For the cations Si_nMg^+, there is a difference between the behaviour of Mg and Li. The Mg atom seems to cap on one of edge or face of the cationic Si_n^+ instead of the neutral bare Si_n like as in the case of Li.

The doubly Mg-doped neutral Si_nMg_2 clusters grow up basically following a way comparable as the doubly doped neutral Si_nX_2 with X = Li, Al reported in previous chapters. Their growth pattern is that one Mg atom substitutes into a position of Si_{n+1}, whereas the other Mg atom is usually added on an edge, or a face, of the existing cluster. There are however a few exceptions of this observation such as $Si_{10}Mg_2$.

Similarly, $Si_nMg_2^+$ cations contain the cationic Si_{n+1}^+ frameworks in which one Mg atom actually substitutes into a Si position whereas the remaining Mg atom caps on an edge, or a face. Again, $Si_{10}Mg_2^+$ appears as an exception.

The most interesting result of this study is that the Mg dopant, due to its large electron transfer capacity, behaves as a cation $Mg^{\delta+}$ and thereby induces an ionic entity with the $Si_n^{\delta-}$ anionic partner. The resulting Mg cation can be served as a linker between $Si_k^{\delta-}$ blocks leading to stabilized linear and cyclic $[(Si_k)Mg]_l$ structures. In the systems with k = 5, 7, 8 and 10, the linear frameworks can be regarded as promising starting blocks for silicon assemblies. Further studies on these binary clusters are highly desirable to determine their properties as potential 1D-nanowire materials.

References

1) B. Mardsen, K. Sattler, Phys. Rev. B, 60 (1999) 11593.

2) U. Landman, R. N. Barnett, A. G. Scherbakov, P. Avouris, Phys. Rev. Lett. 85 (2000) 1958.

3) V. G. Kotlyar, A. V. Zotov, A. A. Saranin, T. V. Kasyanova, M. A. Cherevik, I. V. Pisarenko, V. G. Lifshits, Phys. Rev. B 66 (2002) 165401.

4) M. Paulose, C. A. Grimes, O. K. Varghese, E. C. Dickey, Appl. Phys. Lett. 81 (2002) 153.

5) T. Clark, J. Chandrasekhar, G. W. Spitznagel, P. V. R. Schleyer, J. Comput. Chem. 4 (1983) 294.

6) A. D. McLean, G. S. Chandler, J. Chem. Phys. 72 (1980) 5639.

7) M. J. Frisch, J. A. Pople, J. S. Binkley, J. Chem. Phys. 80 (1984) 3265.

8) K. A. Peterson, S. S. Xantheas, D. A. Dixon, T. H. Dunning, J. Phys. Chem. A 102 (1998) 2449.

9) L. A. Curtiss, P. C. Redfern, K. Raghavachari, J. Chem. Phys. 126 (2007) 084108.

10) A. Karton, J. M. L. Martin, J. Phys. Chem. A 111 (2007) 5936.

11) L. A. Curtiss, K. Raghavachari, P. C. Redfern, J. A. Pople, J. Chem. Phys. 106 (1997) 1063.

12) H. Fan, Z. Ren, J. Yang, D. Hao, Q. Zhang, J. Mol. Struct. THEOCHEM 958 (2010) 26.

13) J. C. Yang, W. G. Xu, W. S. Xiao, J. Mol. Struct. 719 (2005) 89.

14) (a) J. T. Lyon, P. Gruene, A. Fielicke, G. Meijer, E. Janssens, P. Claes, P. Lievens, J. Am. Chem. Soc. 131 (2009) 1115; (b) A. Fielicke, J. T. Lyon, M. Haertelt, G. Meijer, P. Claes, J. De Haeck, P. Lievens, J. Chem. Phys. 131 (2009) 171105.

15) S. Nigam, C. Majumder, S. K. Kulshreshtha, J. Chem. Phys. 121 (2004) 7756.

16) Zdetsis, A. D. J. Chem. Phys. 127 (2007) 244308.

Chapter 7

Chemical Bonding in Si_3, Si_4, Si_4^{2+}, Si_4C^{2+} and Si_9C

This chapter is adapted from the following articles:

- *Planar Tetracoordinate Carbon Stabilized by Heavier Congener Cages: The Si_9C and Ge_9C Clusters* by N. M. Tam, V. T. Ngan and M. T. Nguyen, *Chemical Physics Letters*, 595 - 596, 272 – 276 (2014).

- *Effects of Protonation and Attachment of Alkali Metal Cations on the Singlet - Triplet Gap and Bonding of Silicon Trimer* by N. M. Tam, T. D. Hang, H. T. Pham, M. P. Pham-Ho and M. T. Nguyen, *Journal of Computational Chemistry*, submitted (July 2014), and

- *Ring Currents in Silicon Tetramer (Si_4, Si_4^{2+}) and Planar Tetracoordinate Carbon Doped Cluster Si_4C^{2+}: σ versus π Aromaticity* by N. M. Tam, H. T. Pham and M. T. Nguyen, *Chemical Physics Letters*, 608, 255-263 (2014).

7.1 INTRODUCTION

In Chapter 2, it has been established that silicon clusters (Si_n) exhibit a diversity of three-dimensional shapes, and their geometrical shapes differ fundamentally from those of the carbon analogues. Similarly, the chemical bonding phenomena in the clusters containing C and Si, both lighter elements of the group IV, are basically different from each other.

The simplest clusters, namely the trimers X_3 and tetramers X_4 (X = C, Si), form a set of representative examples illustrating a sharp difference between the elements across the Periodic Table. Of the pair of trimers C_3/Si_3, C_3 exhibits a singlet linear structure ($X^1\Sigma^+_g$) which is located at 1.91 eV (16930 cm^{-1}) below the triplet linear $a^3\Pi_u$ state,[1] whereas Si_3 is strongly bent in two quasi degenerate low-spin $^1A_1$ (C_{2v}) and high-spin $^3A_2$' (D_{3h}) states[2,3,4,5]. Nevertheless, the reasons for such a difference, and the bonding of Si_3 have not been yet analyzed in depth.

An opposite situation holds for the pair of tetramers. The singlet state of the rhombic C_4 cycle (D_{4h}, ^1A_g) was found to be nearly isoenergetic with the corresponding triplet linear state ($D_{\infty h}$, $^3\Sigma^-_g$).[1] On the contrary, both lowest-lying singlet and triplet states of Si_4 have a rhombic shape, but the low-spin state is calculated to be ~0.9 eV lower in energy than the triplet counterpart, making it beyond any doubt the ground state of Si_4.[6] The chemical bonding of the silicon tetramer in different charge states has also been the subject of a previous theoretical study.[7] Using MOs, the authors[7] argued that the neutral rhombic Si_4, which has 16 valence electrons, is in the mean time a σ-anti-aromatic and π-aromatic system. The Si_4^{2+} dication, which possesses 14 valence electrons and is thus isoelectronic with the well known Al_4^{2-} dianion, was accordingly assigned to have multiple aromaticity with a π-aromaticity and a double σ-aromaticity. For its part, the 18 valence electrons Si_4^{2-} dianion was found to exist in either an anti-aromatic parallelogram or an aromatic butterfly structure, both having comparable energy content.[7]

There is however a continuing debate in the last decade about the nature of the aromaticity of Al_4^{2-}. Two main different points of view emerged on its

characteristics. The first view is that Al_4^{2-} has a three-fold (π and double σ) aromaticity,[8,9,10] whereas in the second view, such an aromatic character should solely be attributed to σ electrons.[11,12,13,14,15] The main argument for the former view is that when evaluating the aromaticity of a molecule, the contributions of all delocalized electrons should be considered. More than one independent delocalized electron type can simultaneously satisfy the electron counting rule, and thereby lead to multiple-fold aromaticity.[9] In the second point of view, consideration of all delocalized π and σ electrons is also put forward, but their presence, as indicated by canonical MOs, should only be regarded as a necessary condition and not a sufficient condition for aromaticity.[15] Accordingly, *the sufficient condition is an effective contribution of the relevant delocalized MOs to the molecular ring current, which is a magnetic response of the molecule considered.* The delocalized electrons should thus be able to contribute to the diamagnetic ring current,[15,16,17] which is usually considered as a condition for an aromatic character. Let us note that the moving direction of a diamagnetic ring current is anti-clockwise, and vice versa for the paramagnetic ring current.

The pentatomic dianion $[CAl_4]^{2-}$ is a well known representative of aromatic metallic clusters, which was experimentally identified having a typical structural unit in salt complexes.[18] This carbon-doped aluminum cluster dianion exhibits a squared planar shape (D_{4h}) with a central planar tetracoordinate carbon (ptC). A common view on the stability of these pentatomic clusters is that each contains 18 valence electrons completing the orbital shell formed by the highest occupied orbitals that arise from four-center peripheral ligand-ligand interactions.

In view of the fact that the dication Si_4^{2+} is not only isoelectronic with Al_4^{2-} but also has the same squared geometry, a legitimate question arises as to whether they also exhibit a similar bonding pattern, and the Si_4 framework can further be stabilized upon doping. As far as we are aware, the corresponding isoelectronic C-doped silicon cluster CSi_4^{2+} has not been investigated yet. It has recently demonstrated that it is possible to encapsulate a carbon dication at the center of a silicon cube. In the resulting CSi_8^{2+} cube **1**, the carbon element is obviously multi-

coordinated. However this cube can also be regarded as formed by a diagonal CSi_4^{2+} unit which contains a ptC, and is in the mean time stabilized by attachment of two Si_2 ligands.

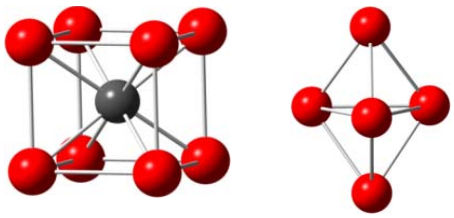

1 $\mathbf{CSi_8^{2+}}$ **2** $\mathbf{Si_5^{2-}}$

The Si_4C^{2+} dication, which is formed by doping a carbon atom at the centre of the squared Si ring, was found to be a stable structure containing a ptC atom. The cube CSi_8^{2+} **1**, which turns out the be a global minimum, has a peculiar feature of a cubic bonding.[19] We realize that it is possible to design small ptC clusters with enhanced stability by combining both electronic and mechanical stabilizing factors. Perhaps a more practical way of stabilizing a ptC is to combine the cation Si_4C^{2+} with a stable counterion such as the Zintl ion Si_5^{2-} **2** to yield a stable Si_9C cage in the neutral form.

We present in this chapter an analysis of the bonding in silicon trimer Si_3, tetramer Si_4 and its doubly charged derivatives Si_4^{2+}. Where possible, we perform a comparative analysis of the isoelectronic systems Si_4^{2+} and Al_4^{2-} that all have 14 valence electrons. The pentatomic carbon-doped clusters having 18 valence electrons systems including Si_4C^{2+} and Al_4C^{2-} are also examined. Finally we consider the Si_9C cluster which exhibits a ptC in a stable cage framework.

7.2 THE SILICON TRIMER

In this section, we first analyze some qualitative aspects of Si_3 using the well known Walsh diagrams. Subsequently, we consider its chemical bonding as derived

from a partition of the electron density using the ELF and ELI-D techniques,[20] and then probe its aromaticity using the ring current maps.[21]

7.2.1 A qualitative analysis of the electronic states: the Walsh diagrams of Si_3

Geometries and vibrational parameters of silicon trimer were well determined and abundantly discussed in the literature. The main geometrical characteristic of Si_3 is that it is cyclic in both low- and high-spin states, which basically differs from the linear homologue C_3. Let us briefly mention the optimized geometries of both states (values at CCSD(T)/aug-cc-pVQZ). The singlet state is an isoceles triangle (C_{2v}, $^1A_1$) with a distance of 2.19 Å and an apex angle $\alpha = 80.6^0$. The triplet state is an equilateral triangle (D_{3h}, $^3A_2'$) with a bond length of 2.29 Å. The singlet parameters are comparable to experimental microwave data.[2]

A qualitative analysis of electron distribution in both linear and cyclic forms of Si_3 is carried out in constructing the corresponding MO correlation which is well known as the Walsh diagram. Figure 7.1 displays the Walsh diagram of singlet Si_3 and Figure 7.2 that of triplet Si_3 (for the sake of simplicity, only the α spin MOs are shown).

The linear singlet $^1\Sigma^+_g$ of Si_3 is characterized as a second-order saddle point with a degenerate π_u bending mode. As in a linear triatomic structure X_3, upon angular motion each degenerate π orbital splits into two components. Accordingly, the doubly degenerate π_u orbital (in $D_{\infty h}$ point group) splits into one a_1 and one b_1 orbital (in C_{2v}), the former component being lower in energy.

As seen in Figure 7.1, in its linear state $^1\Sigma^+_g$ $[\ldots(7\sigma_g)^2\,(6\sigma_u)^2\,(3\pi_u)^4\,(2\pi_g)^0]$, the HOMO of Si_3 is the $3\pi_u$ orbital, and the low-energy location of its a_1 component upon bending appears to be a dominant stabilizing factor (cf. Figure 7.1). The b_1 component is also stabilized (becoming thus the $3b_1$ orbital of cyclic Si_3) but at a lesser extent. The resulting $10a_1$ orbital corresponds to a new cyclic σ-bond, whereas the $3b_1$ orbital is a cyclic π-bond.

The doubly degenerate π_g orbital is expected to split into one a_2 and one b_2 representation of C_{2v} point group, with the former component being lower in energy.

However, in Si_3 this orbital corresponds to its LUMO and as a consequence, its bending splitting is not important. Overall, as Si_3 bends, the singlet state $^1A_1$ [$\ldots(10a_1)^2\ (7b_2)^2\ (3b_1)^2\ (11a_1)^0$] is getting stabilized due to formation of new σ and π bonds (Figure 7.1). In the low-spin state, the linear $^1\Sigma^+_g$ is located at about 67 kJ/mol above the $^1A_1$ cycle (CCSD(T)/CBS value). In other words, the singlet state is strongly stabilized following a bending of the Si-Si-Si skeleton.

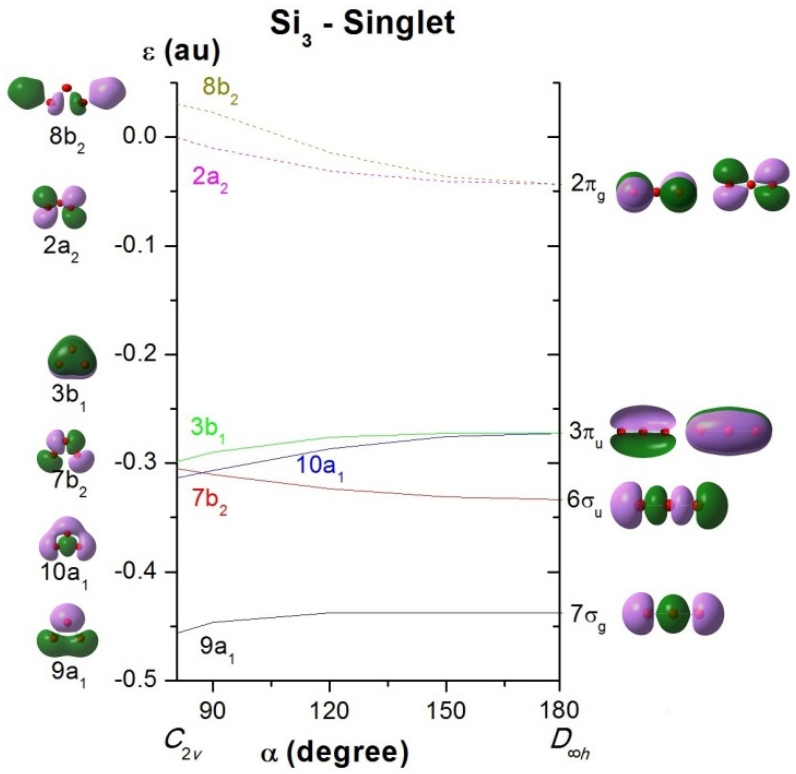

Figure 7.1 The Walsh diagram of the singlet Si_3. Orbital energies are obtained using HF/aug-cc-pvTZ wavefunctions.

In the triplet linear Si_3 whose orbital configuration is $^3\Pi_u$ [$\ldots(7\sigma_g)^2\ (3\pi_u)^4\ (6\sigma_u)^1\ (2\pi_g)^1$], the π_g orbital is now singly occupied, and its evolution upon angular motion implies a significant contribution. Following bending, the unpaired σ_u orbital is again destabilized, whereas the other unpaired π_g orbital is stabilized. The paired

orbitals σ_g and π_u, in particular the σ_g, turn out to significantly be stabilized following bending (Figure 7.2), and this likely constitutes the main contribution to the stabilization of the cyclic triplet Si_3. Let us note that as the linear Si_3 bends yielding a C_{2v} structure, a full occupation of either the b_1 (formed from π_u, leading to a $^3B_2$ state) or the b_2 orbital (formed from π_g, yielding a $^3B_1$ state) is the main event. The $^3B_2$ $[\ldots(3b_1)^2\,(7b_2)^1\,(11a_1)^1]$ state consistently becomes lower in energy and finally results in the $^3A_2'$ state $[\ldots(5a_1')^2\,(2a_2'')^2\,(6e')^2]$ under D_{3h} symmetry.

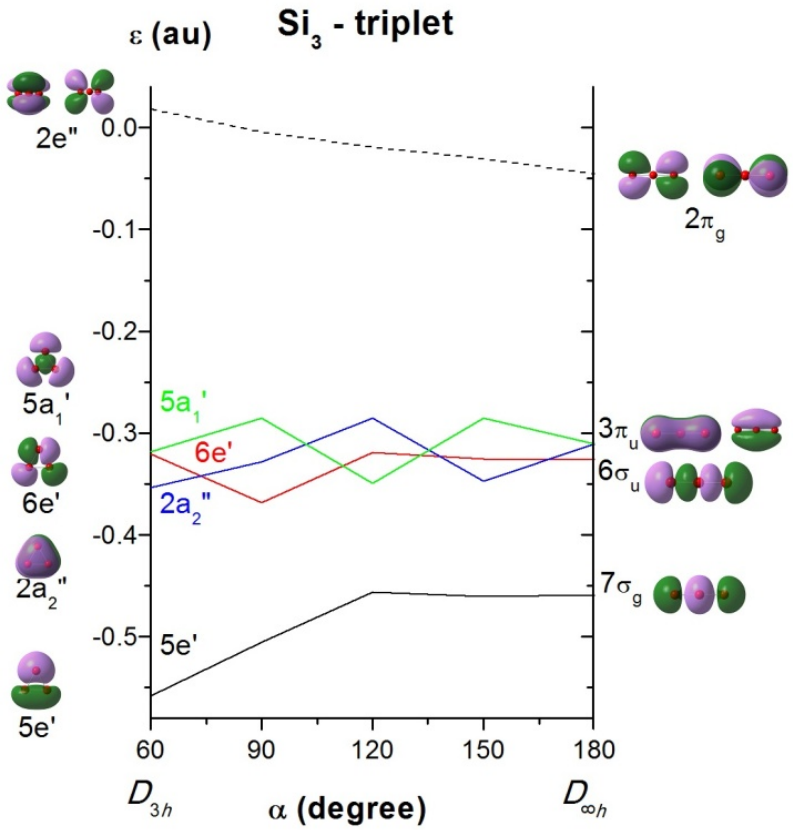

Figure 7.2 The Walsh diagram of the triplet Si_3. Energies of the α-electron orbitals are obtained using ROHF/aug-cc-pvTZ wavefunctions.

The linear $^3\Pi_u$ state is characterized as a first-order saddle point with an imaginary frequency for the π_u bending mode. It is much higher in energy than the corresponding singlet linear, as the relevant $^1\Sigma_g^+$ - $^3\Pi_u$ energy gap of linear Si_3 amounts to about 140 kJ/mol (CCSD(T)/CBS value). The linear $^3\Pi_u$ state is also much higher in energy than the cyclic $^3A_2'$ state (210 kJ/mol using CCSD(T)/CBS), thus suggesting that the triplet Si_3 is also not likely to undergo inversion process.

In summary, the bending mode of Si_3 splits the degenerate π MO of the linear form and lowers the energy of the resulting σ component, and thereby strongly stabilizes the cyclic form, in particular in its triplet state.

7.2.2 An analysis of the chemical bonding of Si_3

We use the electron localization function (ELF) technique in order to locate the whereabouts of electrons and thereby to identify the chemical bonds.

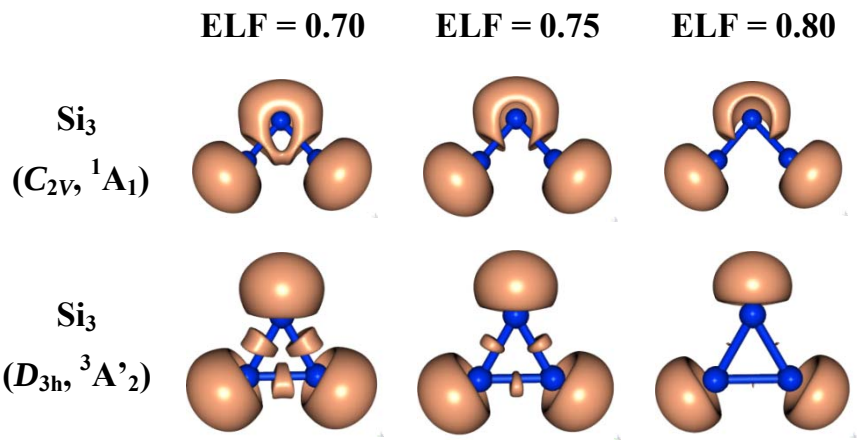

Figure 7.3 ELF isosurface plots of Si_3 in both singlet and triplet states (B3LYP/6-311+g(d)) at different bifurcation values.

Figure 7.3 displays the ELF plots of Si_3 in both electronic states. The ELF is a simple measure of the electron localization in a molecular system and thus gives information about the spaces of molecule, called basins, where electrons are likely to occupy. This method is useful to address localization domains which correspond to

bonding or lone pairs. The bifurcation ELF values are always in a range of [0,1] and are relatively large when the electrons are unpaired or formed into pairs with anti-parallel spins. The zero flux surfaces of the ELF separate the electron density into basins, and thus help us to identify the core, bond and lone pairs. The valence basins are characterized by their synaptic order, i. e., the number of the core basins that share a common boundary surface with the valence basin. Monosynaptic basin represents lone pair, whereas disynaptic basin belongs to two-centre covalent bond, and trisynaptic basin three-centre bond. The number of electrons in a basin is determined by integration of electron distribution function over its region. Figure 7.3 thus displays localization domains given at high bifurcation values of 0.70 - 0.90 of Si_3 in both low and high spin states. This allows us to have a view on the electron concentrations.

Accordingly, the electron distribution in both states of the Si_3 cluster differs somewhat from each other. In the triplet, three monosynaptic domains V(Si) and three disynaptic domains V(Si,Si) can clearly be identified. Each of the lone pairs is occupied by ~2.5 electrons, and each Si-Si bond by 1.5 electrons. In the singlet Si_3, two monosynaptic basins V(Si) are present corresponding to lone pairs of the two terminal Si atoms, each being occupied by 2.4 electrons. One monosynaptic V(Si) and two disynaptic basins V(Si,Si) are all centred around the central Si and practically form a large domain having ~5.0 electrons. In particular, a trisynaptic basin V(Si,Si,Si) with a population of ~2.2 electrons is located indicating a certain three-centre bond covering Si atoms.

7.2.3 Ring current and aromaticity

As the silicon trimer has a cyclic form, an issue of interest concerns its eventual aromaticity. For this purpose, the ipsocentric model is an effective model which was used to evaluate aromaticity of planar compounds.[22]

In the framework of this model, an excitation from an occupied to an unoccupied molecular orbital can result in a contribution to the ring current which can be either diatropic, paratropic or null. Accordingly, a diatropic current arises if the product of irreducible representations of both occupied and unoccupied orbitals

involved in the excitation contains that of an in-plane translational symmetry ($T_{x,y,z}$). In an opposite case, a paratropic current results when the product of symmetries of both occupied and unoccupied orbitals contains the in-plane rotational symmetry ($R_{x,y,z}$). This rule is relatively simple for planar species.

The calculated ring current plots of the singlet Si_3 are displayed in Figure 7.4. Calculations of the ring current are carried out using the SYSMO program.[23] The electron densities can be partitioned in terms of σ and π MOs. Only one delocalized σ MO is effective for the ring current, and the total current includes all core, π and σ MOs. The π electrons bring in small contribution to the total ring current. The σ electrons of singlet Si_3 induces a current around each Si nucleus, and a relatively weak total paratropic ring current (Figure 7.4).

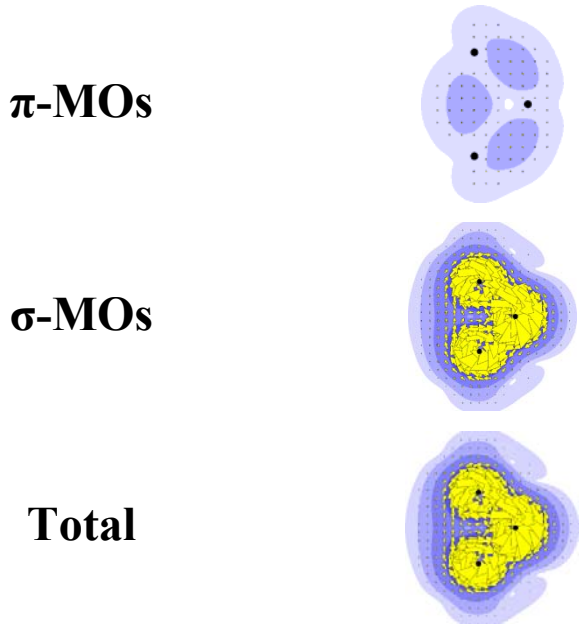

Figure 7.4 The maps of the π, σ and total ring currents of Si_3.

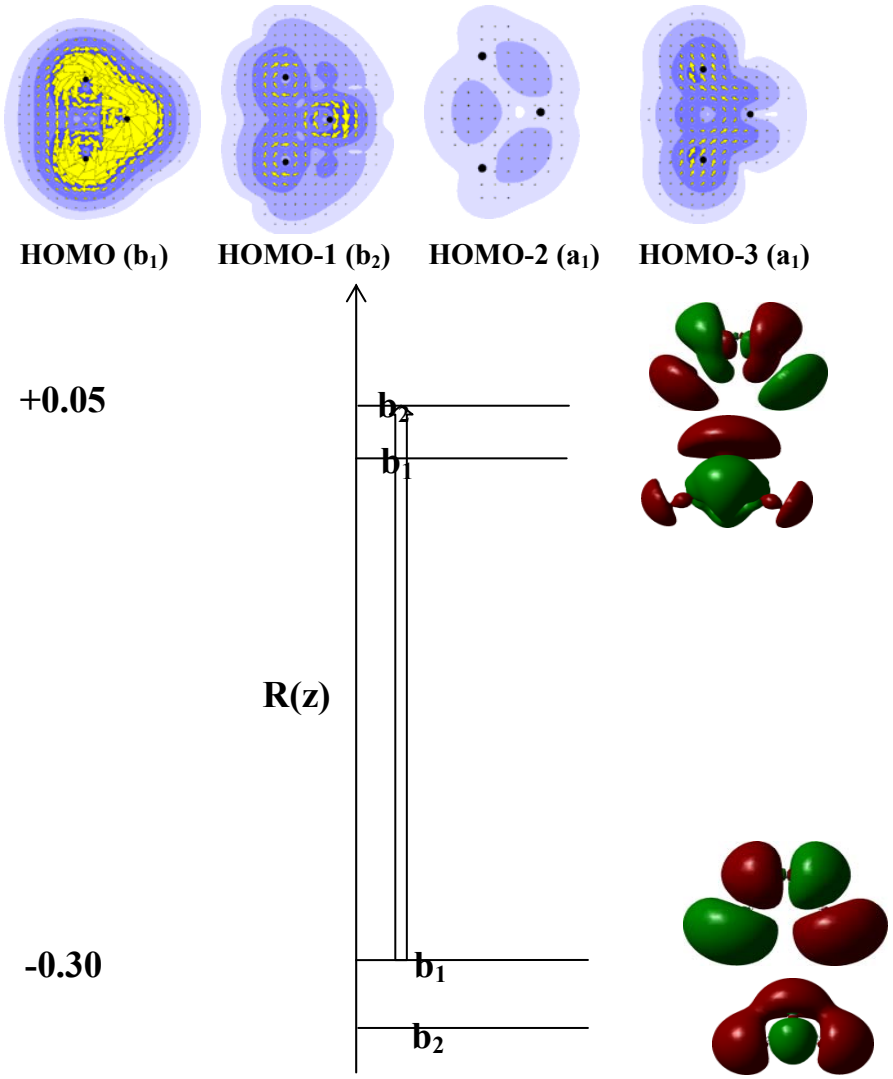

Figure 7.5 Contributions of the HOMOs to the ring currents of Si_3, and the electronic transitions (rotational) responsible for magnetic responses of Si_3.

Figure 7.5 schematically displays the contributions of the HOMOs, and electron excitations responsible for the ring current in Si_3. As stated above, the model based on electronic excitation and orbital contributions gives a plausible explanation

for the magnetic responses in both situations. In Si_3, the main excitation from HOMO (b_1) to LUMO+1 (b_2) which has the same symmetry representation (a_2) of a rotational transition R(z), thus produces a paramagnetic current density (Figure 7.5). This view is in line with the results depicted in Figure 7.5 that point out the contributions of the HOMOs to the ring currents. These yield in fact dominant contributions in accordance with the symmetry selection rules (rotational transition).

In summary, the singlet trimer Si_3 can best be considered, at best, as a basically non-aromatic (if not antiaromatic) species.

7.3. THE SILICON TETRAMER: Si_4, Si_4^{2+} AND Si_4C^{2+}

7.3.1 Structure of the tetramer Si_4 and its dication Si_4^{2+}

Preparation and spectroscopic characterization of Si_4 were carried out in a number of experimental studies. Infrared,[24] Raman,[25,26] and electronic absorption[25] spectra of the neutral tetramer were recorded and well interpreted. Thermochemical parameters including the total atomization energy and heat of formation of Si_4 were also determined (see Chapter 2).[4,6,27]

Geometries and vibrational parameters of silicon tetramer were well determined and abundantly discussed in the literature.[4,6,7] As stated above, the main geometrical characteristic of Si_4 is that it has a rhombic shape (D_{2h}) in both singlet and triplet states, which basically differs from the linear homologue C_4. For the purpose of comprehension, let us briefly describe again its geometric features.

Si_4 could a priori have a squared form. However, a squared Si_4 with optimized Si-Si bond distances is not a stationary point in the singlet potential energy surface. In the triplet state [$^3A_{1g}$: ...$(6e_u)^2$] the squared form becomes a first-order saddle point with one imaginary vibrational frequency (b_{2u} mode). The squared singlet state $^1A_{1g}$ is obviously unstable due to the fact that the degenerate frontier orbital is only occupied by two electrons $(6e_u)^2$, and therefore its structure is subjected to a Jahn-Teller effect. This effect is operative in splitting the D_{4h} e_u orbital to give rise to an energetically more stable rhombic form. The resulting D_{2h} structure has Si-

Si bond distances of 2.33 Å. The D_{2h} HOMO $(b_{1u})^2$, whose shape is similar to that of the D_{4h} e_u orbital, is now stabilized by ~1.7 eV upon geometry relaxation.

The rhombic D_{2h} form remains the lowest-lying in the Si_4 triplet state $^3B_{3u}$: $[....(b_{1u})^1(b_{2g})^1]$. The Si-Si distances are slightly shortened upon excitation (being now 2.29 Å). The singlet-triplet separation gap of Si_4 is calculated at ~20 kcal/mol (~83 kJ/mol) (B3LYP/6-311+G(d) + ZPE). Such a gap is large as compared to the degeneracy of both states of Si_3 (see above).

Removal of one electron from, or addition of one electron to Si_4, is expected to keep the rhombic structure, yielding the ground state $^2B_{1u}$ for Si_4^+ and $^2B_{2g}$ for Si_4^-.[4] Removal of two electrons from the D_{4h} Si_4 yields the dication Si_4^{2+} in which the degenerate $6e_u$ orbital becomes empty. As a consequence, the squared planar structure is no longer affected by a Jahn-Teller distortion, and the $^1A_{1g}$ (D_{4h}) becomes now the lowest-lying structure of the dication, having comparable Si-Si bond lengths of 2.31Å.

Due to the fact that the $6e_u$ orbital becomes now the LUMO of Si_4^{2+}, excitation to the triplet manifold induces a Jahn-Teller stabilization to a rhombic form. The resulting triplet state $^3B_{2g}$ $[....(b_{3u})^1(b_{1u})^1]$ of the dication has longer Si-Si distances of 2.45 Å. The singlet-triplet energy gap of Si_4^{2+} amounts now to ~16 kcal/mol (~67 kJ/mol by B3LYP/6-311+G(d) + ZPE).

Let us now analyze the electron distribution in both Si_4 and Si_4^{2+}. Figure 7.6 displays the ELI-D plots for both species. Similar to the ELF technique, the ELI-D is a simple measure of the electron localization in a molecular system and thus gives information about the molecular spaces, called basins, where electrons are likely to occupy. It is useful to address localization domains which correspond to bonds or lone pairs. The ELI-D description of the bonding is quite comparable to the picture given by the electron localization function (ELF). Both localization approaches of the electron density basically assign a lone pair at each Si centre. Integration of the electron densities over the basins leads to the corresponding populations (V). Populations of the bonds V(Si,Si) are rather comparable in both species, being around 1.5 - 1.7 electrons. It is clear that in order to generate the dication, populations are

mainly removed from Si lone pairs, V(Si), by up to ~0.5 electron by centre. Let us note that in Si_4 there is a population of ~0.8 electron for the shorter diagonal Si-Si bond.

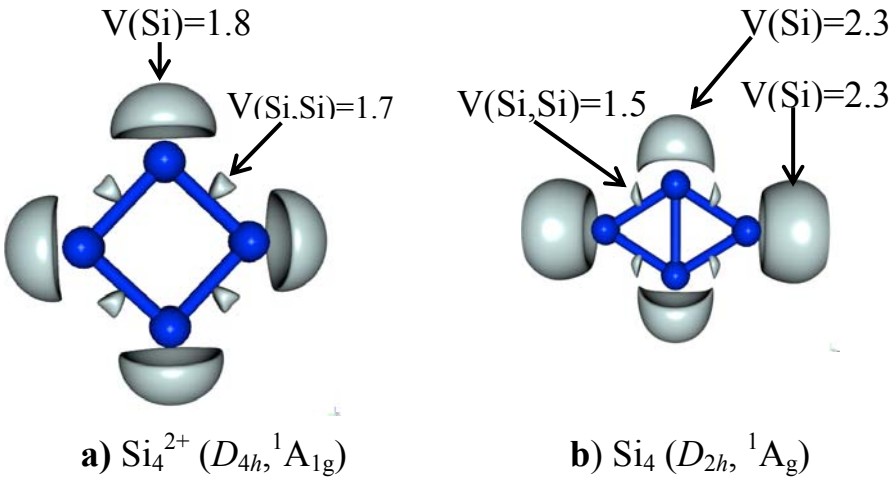

Figure 7.6 The ELI-D plots (at isosurface = 1.5) of both **a**) Si_4^{2+} (D_{4h}, $^1A_{1g}$) and **b**) Si_4 (D_{2h}, ^1A_g) . Electron populations are computed using B3LYP/6-311+G(d) densities.

As both the geometry and electronic structure of Si_4^{2+} are similar to those of Al_4^{2-}, let us now compare their ring currents. Figure 7.7 displays the current density maps of the neutral Si_4, dication Si_4^{2+} and dianion Al_4^{2-}. The ring current of the dianion has extensively been examined in previous reports.[11,12,13,14,15] We just reproduce it here for purpose of comparison.

Again, the electron density can be decomposed in terms of σ and π electron contributions. Figure 7.7 points out that the magnetic response of Si_4^{2+} is basically similar to that of Al_4^{2-}, in terms of electron contributions. The main difference between the ring current in both charged species resides in the intensities of the displacement. In both squared molecules, π electrons marginally contribute to the ring current, even though they are delocalized over the whole molecule. The total current

density turns out to be diatropic, and mainly arises from contributions of delocalized σ electrons.

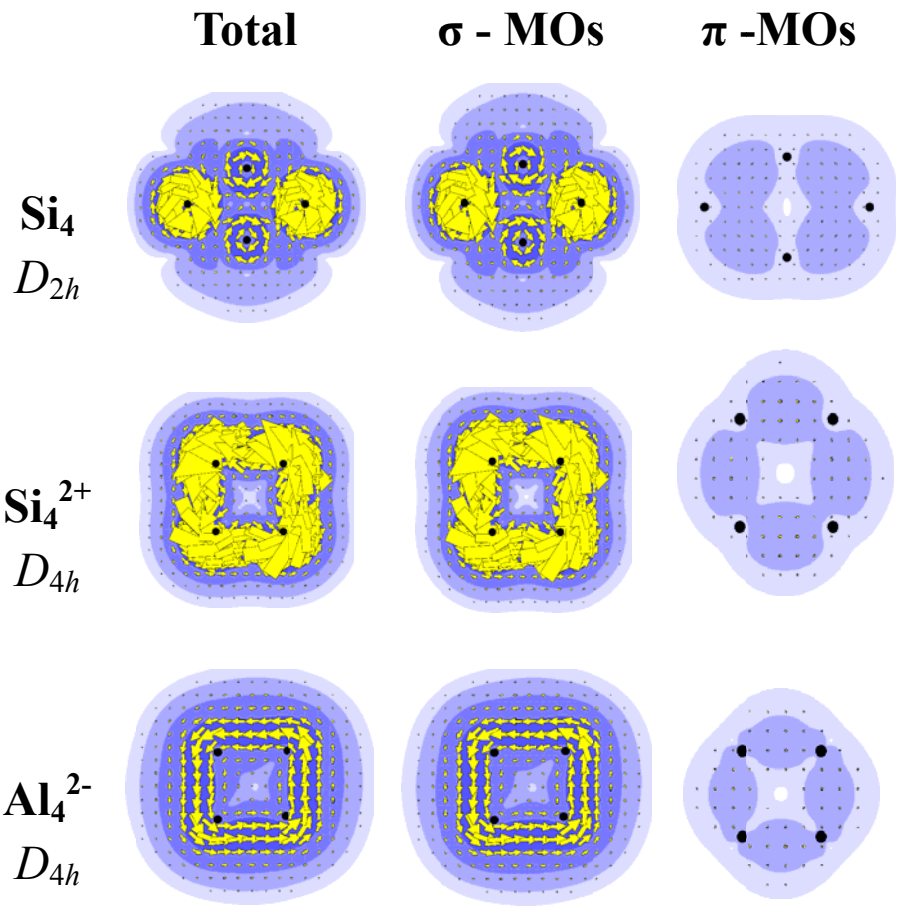

Figure 7.7 Current density maps of Si_4, Si_4^{2+} and Al_4^{2-} (HF/cc-pVTZ).

The individual contributions of MOs can be computed which shows the magnetic responses arising from all 14 valence electrons of Si_4^{2+} (not showed here), The π-MO a_{2u} has no contribution to total current density. The σ MOs e_u and a_{1g} (lower) also do not take part in the current. Only the three σ-MOs b_{1g}, b_{2g} and a_{1g} have characteristic contributions to diatropic current density. Contributions of the a_{1g} MO are mainly located in the central position. For its part, orbital contributions point out

that the diatropic magnetic response in the 16 valence electron Si_4 comes from contributions of σ electrons, again without significant contributions from π electrons.

Figure 7.8 schematically illustrates the electron excitations responsible for the ring currents in Si_4 and Si_4^{2+}. The model based on orbital contributions gives a plausible explanation for magnetic responses in both situations. In Si_4, three excitations are allowed as their symmetry representations are associated with a translational transition T(x,y). There is also one rotational transition. The ion Si_4^{2+} has three allowed translational transitions from the HOMOs to the LUMO. In both cases the translationally associated excitations lead to a total diamagnetic current density.

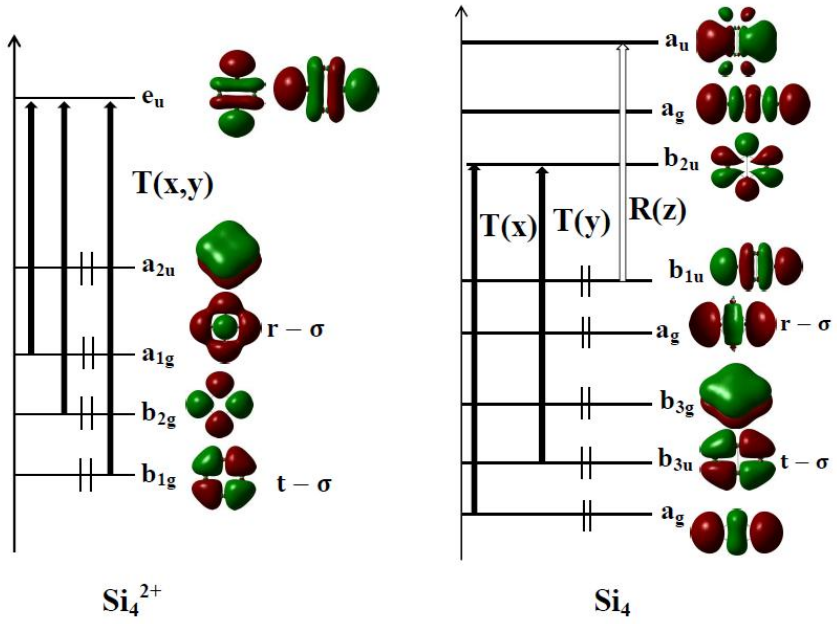

Figure 7.8 Excitation responsible for the ring current of Si_4^{2+} and Si_4. Black arrow: translational transition forming diatropic current, white arrow: rotational transition forming paratropic current.

In the magnetic ring current method,[21] the energy gap between both occupied and unoccupied MOs involved in the allowed transition appears in the denominator of

the main wavefunctions. Therefore, the smaller this energy gap, the stronger the current intensity. The energy separation between both a_{1g} (occupied) and e_u (unoccupied) of Si_4^{2+} (Figure 7.8) is calculated to be ~7 eV (HF/cc-pVTZ). The gap between both transition-allowed orbitals a_g (occupied) and b_{2u} (unoccupied) of Si_4 (Figure 7.8) amounts to ~4 eV at the same level.

7.3.2 Structure of the doped dication Si_4C^{2+}

We find that the doped dication Si_4C^{2+} exhibits in its most stable configuration a squared planar form in which the carbon dopant is simply inserted at the centre of the Si_4 square. This again gives rise to a typical structure for a ptC. It is therefore of interest to compare the bonding in some doped systems generated from the tetratomic framework. In addition to Si_4C^{2+}, we also consider the dianion Al_4C^{2-}. Both species are isoelectronic with the dianion Si_4^{2-}.

Our explorations on the CSi_4 system in different charge states point out that the systems having more than 18 electrons (CSi_4^{2-}, CSi_4^{-}, CSi_4, CSi_4^{+}) are not planar. The HOMOs of Si derivatives are basically different from that of the C_5^{2+} dication (see figure given below). In the former, the central ptC atom interacts with the all four-atomic framework so that the dications can be stable in a high symmetrical form while that is not the case for the latter.

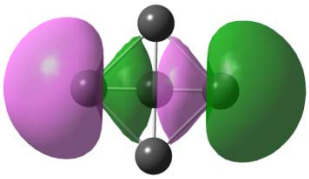

HOMO of C_5^{2+}

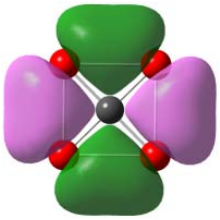

HOMO of Si_4C^{2+}

Our calculations point out that the squared planar D_{4h} structure is the true global minimum of the dication CSi_4^{2+}. The Si-Si and C-Si bond distances amount to

2.67 and 1.89 Å, respectively (B3LYP/6-311+G(d)). The dication Si_4C^{2+} has 18 valence electrons with the electron shell configuration:

Si_4C^{2+}: $[1S^2\ 1P_{x,y}{}^4\ 2S^2\ 1D^2\ 1P_z{}^2\ 2P_{x,y}{}^4\ 1D^2]$.

The HOMO of Si_4C^{2+} differs much from that of the similar $C_5{}^{2+}$ (see below). In the former, the central ptC atom interacts with the all four-atomic framework so that the dications can be stable in a high symmetrical form while that is not the case for the latter. This confirms the important role of the ligand-ligand interaction for the planarity (cf. HOMO of Si_4C^{2+} above).

However, the factors stabilizing both dications considered in squared planar form need to be investigated further. Figure 7.9 displays the total and partial densities of states (DOS) of the ground state of Si_4C^{2+} (B3LYP/6-311+G(d)). This plot shows a clear picture of electron shells and the large HOMO-LUMO gap which indicates a stable species.

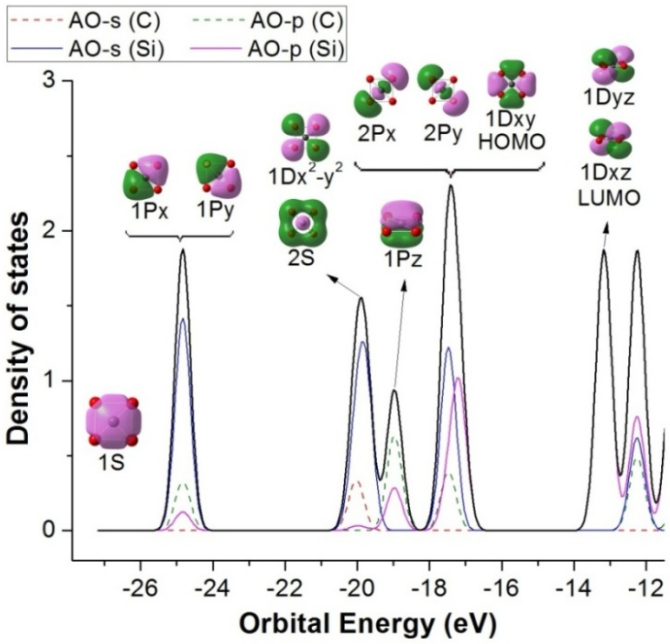

Figure 7.9. Total and partial densities of states of the ground state of the dication $CSi_4{}^{2+}$ (B3LYP/6-311+G(d)).

It also emphasizes the contributions of different atomic orbitals to the MOs. We also use the ELF to further probe the chemical bonding of these systems.[28,29] A topological analysis of the ELF shows that a structure whose ELF isosurface has high bifurcation value is aromatic, whereas a structure possessing low bifurcation value is non-aromatic.

Figure 7.10 displays the plots of the ELF of Si_4C^{2+}. The electrons are largely delocalized over the entire structure of the dication Si_4C^{2+} with a high bifurcation value of the ELF isosurface. Note that a complete separation of basins is only observed at $ELF_\pi = 0.90$ which is the value of $ELF_\pi = 0.91$ of benzene.

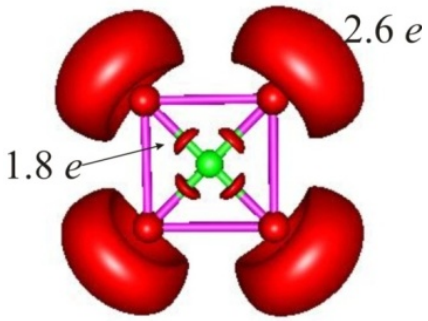

Figure 7.10: Plot of the electron localization function of the dication Si_4C^{2+} at the bifurcation ELF = 0.82. The values stand for the average integrated numbers of electrons (*e*) in the corresponding C-Si and Si lone pair basins (B3LYP/6-311+G(d)).

Integration of the electron densities of different basins points out that the electrons are localized within the C-Si bonds and around the Si atoms. While the C-Si basins correspond well to single bond (1.8 electrons), the Si lone pair regions have a larger concentration of electrons (2.6 electrons on each Si lone pair, Figure 7.10). This implier that the stability of the dication as the global minimum, and thereby the ptC characteristic, is significantly contributed by C-Si bonding. Therefore, besides the ligand-ligand (Si-Si) interaction as found in previous studies,[19] the center-ligand (C-Si) bonds also play important role in maintaining the planarity in the Si_4C^{2+} dication.

The dianion Al_4C^{2-} also has a D_{4h} shape enclosing a ptC. For the sake of comparison, Si_4^{2-} is considered here in a hypothetical D_{4h} geometry. Figure 7.11 displays the ring current maps of three 18-electrons species considered. The hypothetical squared dianion Si_4^{2-} results in a paratropic ring current in both σ electrons and total current densities (computed using HF/cc-pVTZ). Its electrons occupying the π MOs do not take part in the magnetic response. Addition of a C atom at the center of a D_{4h} Si_4^{2+} or Al_4^{2-} ring induces a clear-cut diatropic ring current in both resulting pentatomic clusters Si_4C^{2+} and Al_4C^{2-}. Again, only σ electrons are magnetically active, and no significant current density is detected from delocalized π MOs.

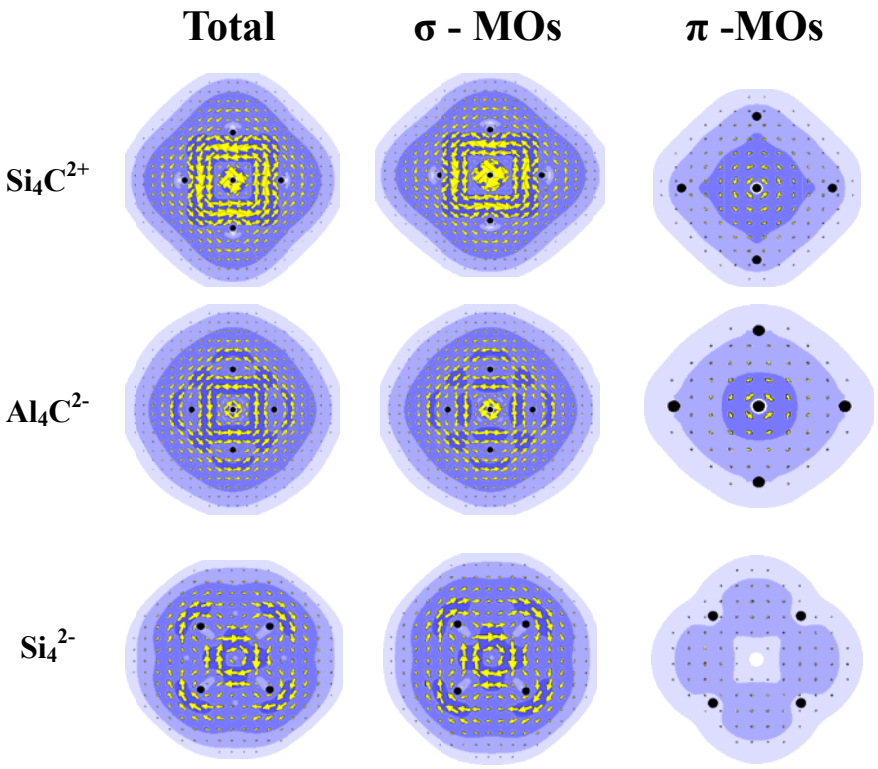

Figure 7.11. The current density maps of Si_4C^{2+}, Al_4C^{2-} and Si_4^{2-} having 18 valence electrons (HF/cc-pVTZ). Si_4^{2-} has a hypothetical D_{4h} geometry (see text).

The excitations responsible for the magnetic response is illustrated in Figure 7.12. The two allowed translational transitions from b_{1g} and b_{2g} to e_u and a rotational transition from e_u to e_u lead to diatropic and paratropic current densities, respectively. Accordingly, the total current density could be either diatropic or paratropic. In this case, the diatropic current becomes dominant. Both pentatomic ions have thus a σ aromatic character.

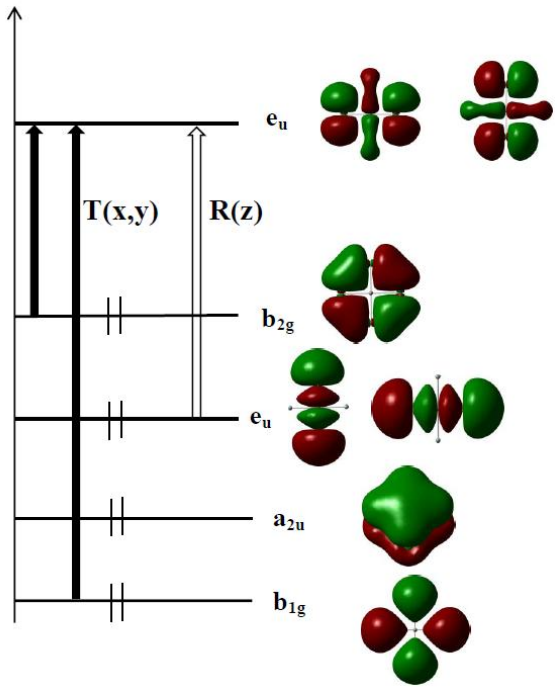

Figure 7.12 Excitation from occupied to vacant MOs of Si_4C^{2+}. Black arrow: transition associated with a translation; white arrow: transition associated with a rotation.

7.4 Si_9C: A STABLE C-DOPED SILICON CLUSTER

Let us now consider some larger doped clusters. Figure 7.13 displays the shapes and relative energies of the global minima and the ptC structure of the CSi_6^{2-} and CSi_6^{2+} systems. In each of the doubly charged species, a local minimum structure

having a ptC atom has been located but is calculated to lie higher in energy than the corresponding lowest-lying isomer.

We found that the ptC structure of the Si_6C^{2-} dianion that looks like a part of the cube containing two fragments (Si_2-Si_4C) lies 1.84 eV higher than the ground state. In the dication, the ptC-containing structure corresponds rather to an interaction between C^{2+} with two Si_3 moieties (Figure 7.5) and is only 0.66 eV higher in energy than its ground state. Note that the Si_8C^{2+} dication **1** which was analyzed in detail in a previous study,[19] has a centro-cubic form with a multi-coordinate carbon center.

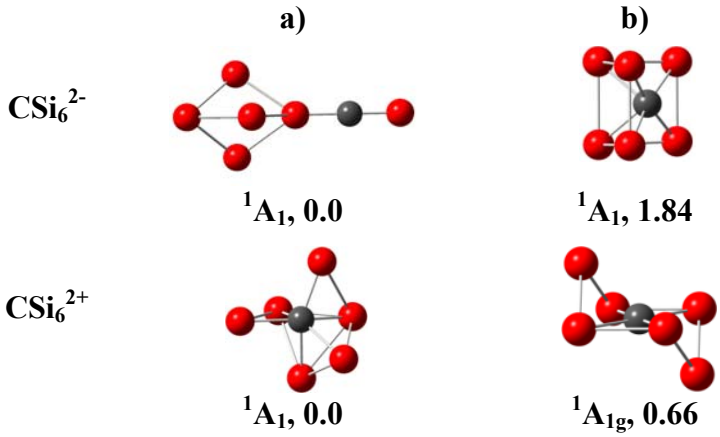

Figure 7.13 Some lower-lying isomers of Si_6C^{2-} and Si_6C^{2+}: **a**) global minimum and **b**) ptC containing structure. Relative energies given in eV are obtained from the B3LYP/6-311+G(d) computations.

We now examine a larger cluster, CSi_9. As mentioned above, this size can formally be generated upon interaction of an ion pair [Si_4C^{2+} + Si_5^{2-}]. Fusing the squared planar dication CSi_4^{2+} with the dianion Si_5^{2-} whose shape is shown in **2** (D_{3h}, see above) on a face leads to the global minimum structure of the neutral CSi_9 isomer shown in Figure 7.14a).

In order to investigate the charge effects, the NBO charges are calculated at the B3LYP/6-311+G(d) level. The carbon dopant bears a large negative charge of 1.85 electrons for CSi_9. On the squared plane, the Si atoms have a positive charge of 0.5 electrons. Thus, a net charge of +0.15 electrons is computed for the CSi_4 moiety

in both clusters and -0.15 for the Si_5 moiety. Therefore, upon fusing the Si_4C^{2+} dication and Si_5^{2-} dianion, a large charge transfer (1.85 electrons) occurs from the dianion to the dication. A certain electrostatic attraction between the ptC atom and the heavier congeners is apparently induced within the molecular plane rather than with the rest of the cage. The electrostatic attraction in the large clusters is comparable to that in the Si_4C^{2+} cluster as the NBO charge of the ptC center in Si_4C^{2+} is 2.5 electrons. However, the Si_9C cluster enjoys further geometrical constraint, a kind of mechanical stabilization, upon fusion.

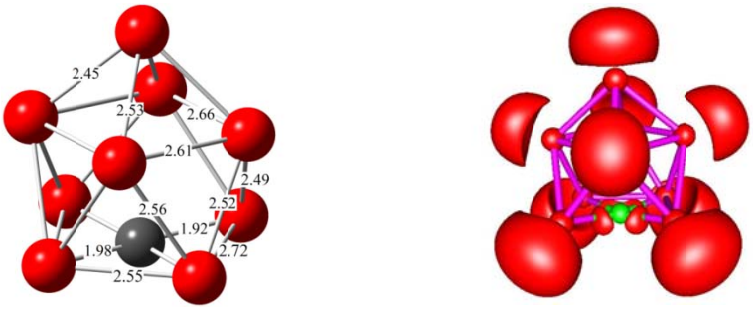

CSi_9 (C_s, ^{1}A')

a) **b)**

Figure 7.14. a) Lowest-lying structures of CSi_9. Selected bond distances given in Å are obtained from the B3LYP/6-311+G(d) computations; b) Plot of the ELF of the neutral CSi_9 at the bifurcation ELF = 0.82 (B3LYP/6-311+G(d)).

Figure 7.14b shows a plot of the ELF of CSi_9 at the bifurcation ELF = 0.82. The average integrated electron population of each of the Si atoms on the planar face is 2.6 electron, and 1.6 electron on each Si-C bond of the quasi-squared plane. The values are not much different from those of the Si_4C^{2+} dication shown in Figure 7.10.

7.5 CONCLUDING REMARKS

In this chapter, we rationalized the chemical bonding phenomena in a few simple silicon clusters, that can be summarized as follows:

i) **Si_3.** In both the singlet and triplet states of Si_3, that can be considered as basically degenerate, the bending mode splits the degenerate π MO of the linear form,

and lowers the resulting σ component, and thereby strongly stabilizes the cyclic form, in particular in its triplet state. The singlet trimer Si_3 can be considered as a basically non-aromatic species.

ii) **Si_4**. We have performed an analysis of Si_4 which has the 16 valence electrons and comparison between the dication Si_4^{2+} and the prototypical metallic cluster Al_4^{2-} (14 valence electron species), between the carbon doped Si_4C^{2+} and Al_4C^{2-} (18 valence electron systems). A consistent picture which emerges from our results is that the 14, 16 and 18 electrons systems exhibit an aromatic character, but this is essentially determined by contribution of σ electrons. The electrons located in π orbitals do not significantly take part in the magnetic response. Accordingly, the four-membered squared Si_4^{2+} and the doped Si_4C^{2+} cluster can best be regarded σ-aromatic species. Our analysis has thus not detected a multiple-fold aromaticity in these species. For its part, the singlet tetramer Si_4, having 16 valence electrons, is equally a σ-aromatic four-membered ring. This phenomenon does not obey the classical Hückel (4N+2) electron counting rule.

The present study provides a further support for the point of view that the existence of delocalized occupied molecular orbitals in a planar molecule is a necessary but not sufficient condition to assign a certain aromatic character (aromatic, non-aromatic or anti-aromatic) to that specific type of electrons. Different criteria, such as the magnetic response, need to be considered for a more consistent evaluation of this popular but intriguing molecular property.

iii) **Si_9C.** We found that the Si_4C^{2+} dication and the SiC_9 neutral both have a planar tetracoordinate carbon atom in their lowest-lying isomer. In the small dication, the driving force for the C-planarization includes not only the electron delocalization on the square frame as found before but also the bonding between dopant and the frame. In the larger neutral cluster cages, the Si_5 group tends to stabilize the cage by large electron transfer in maintaining a ptC configuration. Overall, it appears possible to achieve a stabilized planar tetrahedral carbon within a relatively small neutral Si cluster using both electronic effects and mechanical constraints. Due to the fact that

the Si_9C with a ptC represents the lowest-lying isomer, its stability could eventually lead to its experimental detection.

References

1) A. Van Orden, R. J. Saykally, Chem. Rev. 98 (1998) 2313.

2) M. C. McCarthy, P. Thaddeus, Phys. Rev. Lett. 90 (2003) 213003.

3) N. J. Reilly, D. L. Kokkin, X. Zhuang, V. Gupta, R. Nagarajan, R. C. Fortenberry, J.P. Maier, T. C. Steimle, J. F. Stanton, M. C. McCarthy, J. Chem. Phys. 136 (2012) 194307.

4) N. M. Tam, M. T. Nguyen, Chem. Phys. Lett. 584 (2013) 147, and references therein.

5) N. M. Tam, T. D. Hang, H. T. Pham, M. P. Pham-Ho, M. T. Nguyen, J. Comput. Chem. (2014) submitted.

6) K. Raghavachari, L. A. Curtius, in Quantum Mechanical Electronic Structure Calculations With Chemical Accuracy, Ed: S. R. Langhoff, Kluwer, The Netherlands (1995).

7) H. J. Zhai, . E. Kuznetsov, A. I. Boldyrev, L. S. Wang, ChemPhysChem 5 (2004)1885.

8) A. E. Kuznetzov, J. D. Corbett, L. S. Wang, A. I. Boldyrev, Angew. Chem. Int. Ed. 40 (2001) 3369.

9) C. G. Zhan, F. Zheng, D. A. Dixon, J. Am. Chem. Soc. 124 (2002) 14795.

10) P. Gonzalez, J. Poater, G. Merino, T. Heine, M. Sola, J. Robles, in Theoretical Aspects of Chemical Reactivity, edited by A. Toro-Labbe, Elsevier, The Netherlands (2007).

11) P. W. Fowler , R. W. A. Havenith, E. Steiner, Chem. Phys. Lett. 342 (2001) 85.

12) P. W. Fowler , R. W. A. Havenith, E. Steiner, Chem. Phys. Lett. 359 (2002) 530.

13) R. W. A. Havenith, P. W. Fowler , Phys. Chem. Chem. Phys. 8 (2006) 3383.

14) R. W. A. Havenith, P. W. Fowler , Chem. Phys. Lett. 449 (2007) 347.

15) P. Bultinck, S. Fias, M. Mandado, R. Ponec, in Aromaticity and Metal Clusters, edited by P. K. Chattarij, CRC Press, London, UK (2012) Chapter 13, pp. 245-270, and references therein.

16) J. A. Pople, J. Chem. Phys. 24 (1956) 1111.

17) Z. Badri, S. Pathak, H. Fliegl, P. Rashidi-Ranjbar, R. Bast, R. Marek, C. Foroutan-Nejad, K. Ruud, J. Chem. Theor. Comput. 9 (2013) 4789.

18) X. Li, H. F. Zhang, L. S. Wang, G. D. Geske and A. I. Boldyrev, Angew. Chem. Int. Ed. 39 (2000) 3630.

19) V. T. Ngan, M. T. Nguyen, J. Phys. Chem. A 114 (2010) 7609.

20) M. Kohut, F. R. Wagner, Int. J. Quant. Chem. 106 (2002) 1499.

21) P. Lazzeretti, M. Malagoli, R. Zanasi, Chem. Phys. Lett. 220 (1994) 299.

22) R. W. A. Havenith, P. W. Fowler, Phys. Chem. Chem. Phys. 8 (2006) 3383.

23) P. Lazzeretti, R. Zanasi, SYSMO package, University of Modena, Italy (1980).

24) S. Li, R. J. Van Zee, W. Weltner Jr., K. Raghavachari, Chem Phys. Lett. 243 (1995) 275.

25) E. C. Honea, A. Ogura, C. A. Murray, K. Raghavachari, W. O. Sprenger, M. F. Jarrold, W. L. Brown, Nature, 366 (1993) 42.

26) J. Fulara, P. Freivogel, M. Grutter, J. P. Maier, J. Phys. Chem. 100 (1996) 18042.

27) P. Rocabois, C. Chatillon, C. Bernard, F. Genet, High Temp. High. Press. 27 (1995) 25.

28) J. C. Santos, W. Tiznado, R. Contreras, P. Fuentealba, J. Chem. Phys. 120 (2004) 1670. (could be 48 in text)

29) T. Holtzl, T. Veszpremi, P. Lievens and M. T. Nguyen, in Aromaticity and Metal Clusters, edited by P. K. Chattaraj, CRC Press, Boca Raton (2010), Chapter 14, pp. 271-295.

Chapter 8

General Conclusions and Perspectives

Silicon still plays a pivotal role in the semiconductor industries. In these widespread applications that profoundly affect our daily life, silicon is often used in its bulk solid state. However bulk silicon can no longer satisfy the current needs of miniaturization of electronic devices. In the current intensive search for devices of the future, bare silicon clusters and silicon clusters doped by other elements have emerged as a potential alternative. Such a perspective has been stimulating a wealth of studies of the binary clusters of the elements in general, and silicon-based clusters in particular, as they feature a wide range of potentials for development of nanoscaled materials.

In this context, we carried out this doctoral study theoretical investigations on the geometrical and electronic structures of small silicon clusters doped with some representative main group elements, including Li, Mg, B, Al and also C by using quantum chemical calculations. Deep understanding of their geometric and electronic structures, energetics and bonding phenomena constitutes a necessary step in the extensive and intensive search for promising clusters that could be considered as building blocks for further assemblies.

Our searches for minima on the potential energy surfaces were performed using two different approaches. In the first, we used a stochastic genetic algorithm to generate as many guess structures as possible. Equilibrium structures that were initially detected using low-level computations, were then reoptimized using higher level methods. In the second approach, we made use of a chemical intuition, in that initial structures of clusters Si_nX_m were manually constructed by either substituting Si-atoms of the corresponding silicon frameworks by other element atoms, or adding dopant-atoms at various positions on surfaces of the Si_n clusters. The use of the genetic algorithm is less effective for producing singly doped-clusters having small sizes because most of relevant structures in Si clusters are relatively well known. On the contrary, the multi-doped and larger size clusters imply a huge number of initial guess structures and thus make the genetic search necessary and more effective, even though such a search is often tedious and computationally demanding. Nevertheless, only a combination of different search approaches allows a consistent set of lower-energy structures to be obtained. We are confident that the isomers reported in this

thesis at least correspond to the lower-energy equilibrium structures. However, not only a careful search is required, but the accuracy of the computational methods used is equally crucial in the determination of global minima.

The low-lying isomers of the clusters were identified on the basis of theoretical results obtained by hybrid (U)B3LYP functional in conjunction with the 6-311+G(d) basis set (d polarization plus sp diffuse functions), and then the ground states are assigned by high accuracy computational methods such as the composite G3B3 and G4 methods and when possible also the coupled-cluster theory extrapolated to the complete basis set CCSD(T)/CBS protocol.

Concerning the energetics, different basic thermochemical parameters of the clusters considered including total atomization energies (TAE), standard enthalpies of formation (ΔH_f), ionization energies (IE), electron affinities (EA), binding energies (E_b), embedded energy (EE) and dissociation energies (D_e) were determined using the G*n* (G3B3 and G4) and CCSD(T)/CBS approaches. For bare silicon clusters, a uniform set of standard heats of formation for the cationic and anionic Si_n clusters were determined for up to n = 13. In some cases, variations between G4 and CBS TAE values are relatively large. The differences of energetic properties between both G4 and CBS methods can be understood from the ways of computing single point electronic energies, as well as the geometries of clusters used. Geometry is beyond any doubt an important factor in the thermochemical evaluation.

For these systems, experimental results in the current literature were also characterized by large uncertainties, including the actual uncertainty of the standard heat of formation of the Si atom. For other parameters such as IEs and EAs, they were better predicted, in part due to a certain mutual cancellation of errors in the evaluation of relative energies. The corresponding G4 results are expected to be accurate to, or even better than, ± 0.15 eV (Chapter 2).

For lithium doped silicon clusters, the adiabatic (AIEs) and vertical (VIEs) ionization energies of the Si_nLi_m clusters were evaluated. Calculated AIE and VIE values at the B3LYP/6/311+G(d) and CCSD(T)/aug-cc-pVDZ levels for Si_6Li_2, Si_7Li,

$Si_{10}Li$, $Si_{11}Li$ compare quite well with the corresponding experimental results obtained using the photo-ionization efficiency measurements (Chapter 3).

For boron doped silicon clusters, heats of formation calculated by both G4 and CCSD(T)/CBS methods showed good agreement with available experimental data (Chapter 4).

Overall, it appears that an accurate evaluation of the TAEs and thereby the standard heats of formation of silicon-based clusters remains a great challenge for quantum chemical computations in order to attain the chemical accuracy of ± 1.0 kcal/mol. Due to the non-classical bonding of clusters, the use of other thermochemical approaches (such as bond separation reactions) and more economic computational methods could not be applied. The only option left is to increase the quality of the wavefunctions in going beyond the CCSD(T) level. However, our preliminary computations using the full CCSDT treatment pointed out that it is much more computer-demanding than the CCSD(T) method, which goes beyond our actual computing resources.

Based on the geometrical characteristics of the ground states, a growth mechanism for each series of binary silicon clusters Si_nX_m can now be established.

Generally, alkali (Li) or earth-alkali (Mg) dopants prefers add on an edge or a face of Si_n frameworks, whereas the boron group 13 element (B, Al) favors substitution into one of the Si positions in Si_{n+1} counterparts. Due to the shorter B-Si bond lengths, as compared with the Al-Si counterparts, the B impurity can intrude inside the corresponding Si_n cage (for up to $n \geq 8$). In particular, the neutral structures of doubly impurities doped silicon clusters Si_nX_2, (X = Li, Mg, Al) have similar way of growing up: one dopant atom substitutes into a position of Si_{n+1}, whereas the other is usually added on an edge, or a face, of the existing cluster.

Concerning the thermodynamic stabilities, Figure 8.1 displays a comparison of the binding energies of the neutral Si_n, Si_nLi, Si_nMg, Si_nB and Si_nAl using G4 results. It appears that while Li, Mg, and Al tend to decrease the cluster stability with respect to fragmentations, B marginally increases it.

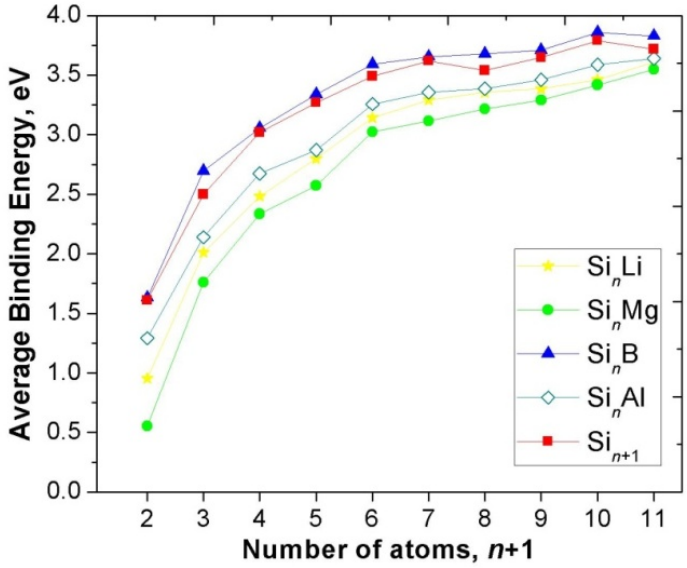

Figure 8.1. Average binding energy (E_b, eV) of Si_nX with n = 1-10, X = Li, Mg, B, Al clusters using the composite G4 method.

Our theoretical results also predicted that some closed-shell systems such as Si_9B^-, $Si_{10}B^+$ (Chapter 4), Si_9Al^- (Chapter 5), and Si_4C^{2+} (Chapter 7) are characterized by enhanced stabilities. Their higher thermodynamic stabilities can be understood by the Jellium shell model (JSM). According to JSM, the valence electrons are supposed to be freely itinerant in a simple mean-field potential formed by the nuclei of atoms and core electrons, the valence electrons fill the hydrogen-like orbitals following the pattern of orbitals as $[1S^21P^61D^{10}2S^21F^{14}2P^61G^{18}2D^{10}\ldots]$ etc… Within this model, the numbers of valence electrons of 8, 20, 34, 40, 56 and 68… emerge as the *magic numbers* that actually correspond to a complete filling of the successive shell electrons.

Typically, both anionic structures Si_9B^- and Si_9Al^- contain the same silicon Si_9 cage in which the B dopant is encapsulated but the Al dopant caps on its face. Each of them also has 40 valence electrons and their DOS features are quite similar. For example, the electronic structure of both anions Si_9Al^- and Si_9B^- satisfies the

electron shell configuration of $[1S^2 1P^6 1D^{10} 2S^2 2P^6 1F^{14}]$, and this basically makes them enhanced stability species with a magic number of 40 valence electrons.

Concerning the bonding phenomena, electron localization techniques (ELF and ELI-D) were used to locate the whereabouts of electrons, and thereby to identify the chemical bonds of some specific clusters such as Si_3, Si_4, Si_4^{2+}, Si_4C^{2+}, and Si_9C. Calculations of the ring current, which is the magnetic response of a molecule, were also carried out in order to probe their aromaticity (Chapter 7). This study provided a further support for the point of view that the existence of delocalized occupied molecular orbitals in a planar molecule is a necessary but not sufficient condition to assign a certain aromatic character (aromatic, non-aromatic or anti-aromatic) to that specific type of electrons. Different criteria (such as the magnetic ring current) need to be considered for a more consistent evaluation of this popular but intriguing molecular property.

In addition, both the Si_4C^{2+} dication and the SiC_9 neutral exhibit a planar tetracoordinate carbon atom (ptC) in their lowest-lying isomer. This is caused by a driving force for C-planarization which includes not only the electron delocalization on the square frame but also the bonding between C-dopant and the Si frame of the small dication. In the larger neutral cluster cage, the Si_5 group tends to stabilize electronically the cage by electron transfer but also mechanically by geometrical constraints in maintaining a ptC configuration (Chapter 7).

In silicon clusters doped by lithium and magnesium, alkali and alkali-earth atoms, the dopants tend to cap on faces or edges of silicon frameworks and they behave as electron donors. Such behaviour provide electrons for silicon cages to form stabilized anionic silicon blocks. Therefore, Li and Mg dopants are expected to become the promising linkers that can on the one hand stabilize the silicon building blocks, and on the other hand, connect them together to generate silicon cluster assemblies, including the nanowires. Contrary to Li and Mg, both B and Al atoms, that have only one valence electron less than Si, they prefers to substitute Si atoms in silicon framework rather than to donate electrons, and hence it is difficult for them to become charged linkers that can connect the building blocks. However, some boron

and aluminum doped silicon clusters, which follow the Jellium shell model rule, possess the enhanced thermodynamic stabilities and accordingly they can be considered as capable building blocks.

In this context, we attempted to search for potential linkers in making silicon nanowires. We found that the Mg dopant, due to its large electron transfer capacity, behaves as a cation $Mg^{\delta+}$ and thereby induces an ionic entity with the $Si_n^{\delta-}$ anionic partner. The resulting Mg cation can be served as a linker between Si_n blocks leading to stabilized linear $[(Si_k)Mg]_l$ structures in part due to electrostatic attraction forces. This allowed us to identify some suitable members that can further be used as superatoms for assemblies. We thus probed the five-, seven-, eight- and ten-atom Si building blocks, and the role of the Mg element as the linkers connecting them.

Calculated results of the average assembling energy which gave us an idea about the tendency of assembling the cluster of $(Si_kMg)_l$ with k = 5, 7, 8, 10, show that silicon clusters Si_k tend to assemble in ring forms (**R*l***) over the linear forms (**L*l***) as the assembling energy of the **R*l*** are larger than those of the **L*l***. However, a more important fact is that the average assembling energy of the linear form tends to increase with the increasing size (***l***), implying that a (longer) nanowire can be considered as a plausible possibility (Chapter 6).

In summary, theoretical investigations reported in this doctoral thesis revealed the structural formation and growth mechanism of small silicon clusters doped by some representative main group atoms. Calculated thermochemical parameters, reliably obtained by using high accuracy computational approaches, provide a set of consistent and useful predictions to be used for both experimental and theoretical studies in the future. Nevertheless, it remains a difficult task to predict with accuracy the shape, energetics and properties of clusters having larger sizes.

Atomic clusters and cluster-based nanostructures are expected to become pivotal for a new generation of materials and devices with tailored properties, due to the fact that clusters consistently exhibit novel properties which are not observed in atoms, molecules or bulk, and the cluster properties are depending on its size. We thus found a few doped Si clusters having enhanced stabilities and magic numbers

behavior which can be considered as *superatom* and thereby play as building blocks for cluster-assembled materials. Accordingly, this study suggests an avenue in cluster assemblies based on main group elements doped silicon clusters. In particular, building blocks that are based on alkali and earth-alkali metal atoms such as Li and Mg, respectively, can play a role of effective linkers connecting the Si cluster units, involving one or multiple dopant atoms and by electrostatic forces, appear to be promising in the construction of nano-assemblies (1D nanowires among others). It is our viewpoint, and our hope, that this avenue will be appropriately explored, both theoretically and experimentally, in future studies.